Immunomodulatory effect of specialised pro-resolving mediators in humans

Thesis presented for the degree of Doctor of Philosophy in the

Centre for Clinical Pharmacology,

Division of Medicine,

University College London

Madhur Parmanand Motwani

DECLARATION

"I, Madhur Motwani confirm that the work presented in this thesis is my own. Where information has been derived from other sources, I confirm that this has been indicated in the thesis."

Signed:

in vivo veritas

Abstract

Inflammation is a protective response but if dysregulated it can lead to chronic inflammatory conditions. Currently, these diseases are treated by inhibiting the factors that drive inflammation but such treatments can interfere with the tissue healing processes, e.g. NSAIDs or impair antimicrobial immunity, e.g. corticosteroids and biologics. Resolution is the other end of inflammatory spectrum and has been demonstrated to be an active process mediated by specific cellular events, soluble mediators and their receptors, that provide counter-regulatory signals to switch inflammation off. In this regard, specialised pro-resolving lipid mediators (SPMs), as effector molecules of resolution have shown promise as a novel therapeutic option to treat dysregulated inflammation. However, research supporting beneficial effect of SPMs has been largely conducted in murine models and there is a need to translate it for patient benefit. A human model of resolution of inflammation can facilitate investigation of the pharmacological action of SPM based therapies and their comparison with known anti-inflammatory agents. To attain this objective, I first performed a detailed characterisation of cantharidin skin blister model and learnt that neutrophil clearance, an important sign of resolution, can be affected by stromal scaffold around inflammatory contents. Therefore, I developed a novel model of self-resolving acute inflammation triggered by intradermal injection of UV killed *E. coli* bacteria (UVkEc), where local inflammatory exudate was acquired into a suction blister raised during onset and resolution phases of inflammatory response. UVkEc triggered self-resolving dermal inflammation model allowed appreciation of quantifiable indices of resolution such as clearance of neutrophils, reduction of inflammatory stimulus, pro-inflammatory cytokines and lipid mediators as well as vascular hyperaemia. In addition, I identified the presence of different classes of SPMs and their receptors at the junction between onset and resolution. Using this model, I showed that local therapeutic supplementation of SPMs, in physiological dose range, reduced neutrophil numbers during resolution but had modest effect on clearance of the inflammatory stimulus, reduction of pro-inflammatory cytokines or switch of macrophages to a pro-resolving phenotype. In another approach, I demonstrated that an oral, SPM inducing small molecule, JBT-101, a CB2 receptor agonist (chemical name: ajulemic acid) inhibited neutrophil numbers at onset coincident with enhanced clearance of inflammatory stimulus and reduction in levels of leukotriene B4, prostanoids and IL-8. It also increased the levels of the SPMs including lipoxin A_4, resolvin D1 and resolvin D3 during resolution. However, there was lack of correlation between the rise in SPMs and the effect of JBT-101 on resolution indices and there was no inverse correlation between levels of SPMs and neutrophil numbers during onset or resolution. Using UVkEc triggered self-resolving dermal inflammation model as a tool, this thesis demonstrates that in humans, effect of SPMs, at physiological doses, may be limited only to enhancing neutrophil clearance. It also shows that orally active SPM inducing molecule, JBT-101, at doses currently being employed in phase II clinical trials, has a potent anti-inflammatory effect and uncovers that its main mechanism is possibly via inhibiting the pro-inflammatory mediators than by inducing SPMs. Investigation of effect of pro-resolving therapies on resolution indices in humans can inform their future clinical development.

Acknowledgements

A supreme thanks to volunteers who trusted my abilities, tolerated the sharp scratches and dull aches and who accommodated the (often) inconvenient study time points. This research wouldn't have been possible without their patience and commitment.

Derek. Thank you. I am really grateful to you for putting me on this PhD wagon (well, you created one for me) despite all the odds. You taught me how to steer it, find new directions and taught me by example to persist despite the obstacles and failures. Thank you for having confidence in me.

Thanks to my secondary supervisor, Raymond, who provided the valuable ethical, pastoral (and financial) support for this PhD.

Members of Gilroy lab! You have been like a family. I would start by thanking Justine Newson (Lab Mum) who (very) patiently taught me the basics of research. You taught me to not fret over mistakes and rather see them as a learning experience. Julia Flint and Roel De Maeyer, for the great discussions and for helping me make sense of my brainwaves (and also for willingly helping me with lab experiments. James (Fullerton and Arrich), the first one for inspiring to see the bigger picture and the second one for helping me to appreciate the details. William Jenner, for patiently teaching me the basics of organising and managing research around healthy volunteers. Alex Maini, Frances Benett, Marc George, Daniel Marks and Alastair O'Brien. Thank you for helping me understand the clinical relevance of research observations and for being there as study clinicians. This research wouldn't be possible without your diligence and commitment.

Special thanks to Division of Medicine admin department: Liam, Tricia and Aisha. I always felt that you provided me (the international student) support above and beyond the normal to help me navigate the web of contracts, employment and graduate degree requirements.

Thanks to Andrew Smith and Milica Vukmanovic for providing the important training with the UV killed E. coli and suction blister technique.

Thanks to my collaborators. Angela Richard Londt for help with histology and Prof. Serhan, Dr Dalli and Dr Colas for help with lipid mediator analysis.

Finally, I would like to thank my parents and grandparents who offered me unwavering support and did not bother me too much to get married while I was doing this PhD.

TABLE OF CONTENTS

Publications, Conferences and Awards

Original articles

1. Jenner W[¶], **Motwani M[¶]**, Veighey K, Newson J, Audzevich T, Nicolaou A, et al. Characterisation of Leucocytes in a Human Skin Blister Model of Acute Inflammation and Resolution. PLoS ONE. 2014 Mar 6;9(3): e89375. (¶: Joint first author)

2. **Motwani, M. P**., Flint, J. D., De Maeyer, R. P., Fullerton, J. N., Smith, A. M., Marks, D. J. and Gilroy, D. W. (2016), Novel translational model of resolving inflammation triggered by UV-killed *E. coli*. J Path: Clin Res, 2: 154–165. doi:10.1002/cjp2.4

3. Madalli S, Beyrau M, Whiteford J, Duchene J, Singh Nandhra I, Patel NSA, **Motwani, M.P.,** Gilroy, D.W., Thiemermann, C., Nourshargh, S. et al. Sex-specific regulation of chemokine Cxcl5/6 controls neutrophil recruitment and tissue injury in acute inflammatory states. Biol Sex Differ. 2015; 6:27.

4. Maini AA, George MJ, **Motwani MP**, Day RM, Gilroy DW, O'Brien AJ. A Comparison of Human Neutrophils Acquired from Four Experimental Models of Inflammation. PLOS ONE. 2016 Oct 25;11(10): e0165502.

Reviews

1. **Motwani MP**, Gilroy DW. Macrophage development and polarization in chronic inflammation. Semin Immunol. 2015 Aug;27(4):257–66.

Conference abstracts

1. Jenner W, **Motwani M**, Veighey K, Nicolaou A, Murphy S, Macallister R, Gilroy D. Cantharidin skin blister: a novel model for the investigation of inflammatory resolution in skin. Immunology. 2013 Dec 1;140:208 (Poster presented at British Society of Immunology Conference, Liverpool, December 2013)

2. **Motwani M**, Maeyer RD, Fullerton J, Marks D, Smith A, Gilroy D. Exudate suction blister: a novel in vivo model of acute inflammation and resolution in humans. (CAM1P.145). J Immunol. 2015 May 1;194(1 Supplement):48.2-48.2. (Oral and poster presentation at American Association of Immunology annual conference IMMUNOLOGY 2015, New Orleans, May 2015)

Awards

1. American Association of Immunology Trainee Abstract Award for purpose of attending the American Association of Immunology annual conference IMMUNOLOGY 2015, New Orleans, May 2015, $500

2. BSI-ECI Travel grant for purpose of attending the European Congress of Immunology conference ECI 2015, September 2015, £410

3. Dean's Research Prize, UCL Faculty of Medical Sciences for best oral presentation (PhD) February 2017, £150

LIST OF FIGURES

LIST OF TABLES

LIST OF ABBREVIATIONS

7AAD	7-aminoactinomycin D
AA	Arachidonic acid
ACK	Ammonium chloride
ANOVA	Analysis of variance
AP-1	Activator protein 1
AT-	Aspirin triggered
ATP	Adenosine triphosphate
BAI1	Brain specific angiogenesis factor-1
BAK	Bcl-2 homologous antagonist/killer
BAX	Bcl-2-associated X protein
BCL-2	B-cell lymphoma-2
BMI	Body Mass Index
CAP	Cathelecidin antimicrobial peptides
CD	Cluster of differentiation
CGD	Chronic granulomatous disease
CLRs	C type lectin receptors
CO	Carbon monoxide
COPD	Chronic obstructive pulmonary disorder
COX	Cyclooxygenase
CRISS	Combined Response Index in Diffuse Systemic Sclerosis
CRP	C reactive protein
CRT	Calreticulin
DARC	Duffy antigen receptor complex
DHA	Docosahexaenoic acid
DMARD	Disease modifying anti-rheumatic drugs
DNA	Deoxyribonucleic acid
DPX	Distyrene, Plasticiser (tricresyl phosphate), and Xylene
DRY	Asp-Arg-Tyr
EDTA	Ethylenediaminetetraacetic acid
EET	Epoxy-5Z,8Z,11Z-eicosatrienoic acid
ELISA	Enzyme linked immunosorbent assay
ELR	Glu-Leu-Arg
eNOS	Endothelial nitric oxide synthase
EPA	Eicosapentaenoic acid
EU	Endotoxin units
FCS	Fetal calf serum
FITC	Fluorescein isothiocyanate
FPR	Formyl peptide receptors
FSC	forward scatter
Gas6	Growth arrest specific gene-6
GFP	Green fluorescent protein

GMP	Good Manufacturing Practice
GPCR	G-protein coupled receptor
GPR	G Protein receptor
H_2S	Hydrogen sulphide
HDHA	hydroperoxy-docosahexaenoic acid
HEPE	hydroxy-5Z,8Z,11Z,14Z,16E-eicosapentaenoic acid
HETE	hydroperoxy-5Z,8Z,11Z,13E-eicosatetraenoic acid
HGF	Hepatocyte growth factor
HLA	Human leucocyte antigen
HMGB	High mobility group box protein
hr	Hour
HSP	Heat shock proteins
ICAM	Intercellular cell adhesion molecule
IFN	Interferon
IL	Intereukin
IRFs	Interferon regulatory factors
JAM	Junctional adhesion molecules
LAL	Limulus amebocyte assay
LB	Luria- Bertani
LC	Liquid Chromatography
LDI	Laser Doppler Imager
LFA	Lymphocyte function associated antigen
LO	Lipoxygenase
LPC	Lysophosphatidylcholine
LPS	Lipopolysaccharide
LTA_4	Leukotriene A4
LXA4	Lipoxin A4
LXB4	Lipoxin B4
MCL-1	Myeloid leukaemia cell differentiation protein 1
MDP	Muramyl dipeptide
MFGE8	Milk fat globule EGF 8
MFI	Median Fluorescence unit
mg	Milligram
min	Minutes
ml	Millilitre
MLCK	Myosin light chain kinase
MMP	Matrix metallopeptidase
MPO	Myeloperoxidase
MS	Mass Spectrophotometry
mtDNA	Mitochondrial DNA
NADPH	Nicotinamide adenine dinucleotide phosphate
NCTC	National Collection of Type Cultures
NET	Neutrophil extracellular trap
NF-kB	Nuclear factor kB

NK	Natural killer
NO	Nitric oxide
PAF	Platelet activating factor
PBS	Phosphate buffered saline
PD	Protectin D1
PECAM	Platelet endothelial cell adhesion molecule
PG-	Prostaglandin
PPAR	Peroxisome proliferator-activated receptor
PS	Phosphatidylserine
PSGL-1	P-selectin glycoprotein ligand -1
PU	Perfusion units
RBC	Red Blood Cell
RLRs	Retinoic acid-inducible gene (RIG)-I-like receptors
RNA	Ribonucleic acid
ROS	Reactive oxygen species
RPM	Revolutions per minute
RT	Room temperature
Rv-	Resolvin
SLPI	Secretory leucocyte protease inhibitor
SPM	Specialised pro-resolving lipid mediators
SSC	Side scatter
TAM	Tyro3-Axl-Mer
TGF	Transforming growth factor
TNF	Tumour necrosis factor
TX	Thromboxane
UTP	Uridine triphosphate
UVkEc	UV killed *E. coli* bacteria
VCAM1	Vascular cell adhesion molecule-1
VEGF	Vascular endothelial growth factor
VLA	Very late antigen
μl	Microlitre

Chapter 1

Introduction

Inflammation is a defence response against noxious stimuli like microbes or tissue injury. A successful inflammatory response comprises an onset phase, during which immune cells migrate to the site and eradicate the offending pathogen. Clearance of the inciting stimulus is followed by a resolution phase, characterised by immune cell clearance and tissue repair. The process of resolution is tightly controlled to minimise bystander tissue damage by activated immune cells; however, its dysregulation can contribute to a state of persistent inflammation as seen in chronic inflammatory disorders [1]. For a long time, it was presumed that resolution is a passive process following removal of inflammatory stimulus and catabolism of pro-inflammatory mediators. However, in recent years' investigation of self-resolving inflammatory exudates have revealed that resolution is an active process mediated by specific cellular processes, receptors and an array of endogenous factors [2].

For my introduction, I will first describe the evolution of an inflammatory response with emphasis on the key events that mediate the active resolution of acute inflammatory response. Secondly, I will discuss the origin, mechanism and role of different classes of specialised pro-resolving mediators (SPMs), a novel genus of lipid mediators, in mediating resolution processes. Thirdly, I will highlight the potential benefits of SPM based therapies over the conventional anti-inflammatory agents. Finally, I will describe the need for translating research on SPMs in humans to justify my PhD aims.

1.1 Onset

1.1.2 Recognition of inflammatory stimulus

At steady state, the tissue comprises resident immune cells are interspersed amongst the parenchyma, connective tissue as well as the vascular and lymphatic networks of the organ. The resident immune cell compartment is comprised of macrophages, dendritic cells, mast cells, memory $CD4^+$ and $CD8^+$ T cells and the recently identified innate lymphoid cells [3].

An important function of resident immune cells is immunosurveillance i.e. the sensing of microbes or tissue injury associated products. This is facilitated by the presence of germline encoded receptors called pattern recognition receptors (PRRs) on immune cells. Different PRRs are present on the immune cells which either sense the pathogen associated molecular patterns (PAMPs) derived from the microbes or damage associated molecular pattern (DAMPs) produced during tissue injury. PRRs are classified into multiple families including Toll like receptors (TLRs), e.g. TLR4 which binds to bacterial lipopolysaccharide (LPS), TLR2 which detects tissue injury derived heat shock proteins (HSP) and high mobility group box protein (HMGB), nucleotide oligomerization domain like receptors (NLRs), e.g. NOD1 which detects bacterial products like muramyl dipeptide (MDP), C-type lectin receptors (CLRs), e.g. dectin-1 which detects β- glucan on fungi and retinoic acid-inducible gene (RIG)-I-like receptors (RLRs), e.g. RIG-1 which detects double stranded RNA of viruses [4].

Immunosurveillance is further enhanced by the strategic location of resident immune cells at sites of invasion in the tissue, e.g. Langerhans cells and $CD8^+$ resident memory T cells are located in the skin epidermis, tissue resident macrophages are located in the epithelial lining of serous cavities such as in peritoneum, pleural cavity and also occupy perivascular areas. In addition to resident immune cells, stromal cells such as fibroblasts and epithelial cells have also been shown to be involved in detection of inflammatory stimuli [5].

Activation of PRRs triggers nuclear translocation of transcription factors such as nuclear factor NF-κB, activator protein 1 (AP-1), interferon regulatory factors (IRF) which lead to transcription of inflammatory genes encoding for pro-inflammatory mediators including histamine, cytokines (TNFα, IL-6, etc.), Type 1 interferons and anti-microbial proteins. Together they activate the endothelium to facilitate extravasation of immune cells to the site [6].

1.1.3 Activation of the endothelium

Endothelial activation leads to an increase in blood flow, which underlies the major clinical signs of inflammation such as redness (rubor), heat (calor) and plasma leakage leading to tissue oedema (tumor).

Endothelial activation can be categorised into two types depending on the rate of activation. The Type 1 response is rapid and doesn't involve gene transcription as it is mediated by the release of pre-formed ligands within the endothelium. In contrast, the type 2 response is slower to evolve and requires the generation of inflammatory mediators by *de novo* gene transcription [7].

Type 1 activation is mediated by G-protein coupled receptor (GPCR) ligands such as mast cell derived histamine. It is rapid and short lived as signalling via the GPCR receptors lasts for 20-30 min before they get desensitised [8]. GPCR signalling leads to increase in levels of cytosolic Ca^{++} levels and activation of the myosin light chain kinase (MLCK). Increased Ca^{++} releases cytoplasmic phospholipase A2 (cPLA2) and also activates endothelial nitric oxide synthase (eNOS) [9]. cPLA2 releases arachidonic acid (AA) and lysophosphatidylcholine (LPC) from membrane phospholipids. AA is first oxidised then reduced by constitutionally expressed cyclooxygenase-1 (COX-1) to generate prostaglandin H_2 (PGH_2), which is further metabolised by prostacyclin synthase to prostacyclin (PGI_2). PGI_2 together with nitric oxide (NO) derived from eNOS act as potent vasodilators [10]. Activated MLCK results in contraction of actin that leads to opening of gap junctions between the endothelial cells [11]. In addition, MLCK and cytosolic Ca^{++} in combination result in the exocytosis of Weibel Palade bodies containing P-selectin onto the endothelial surface [12]. Simultaneously, LPC formed by the action of cPLA2, is acetylated in the endothelial cells to form PAF (platelet activating factor). Combined expression of P-selectin and PAF provide the first signal for adherence of neutrophils to the endothelial surface [13].

Type 2 activation supplements the transient stimulation provided by Type 1 activation and amplifies the leucocyte infiltration. Type 2 activation is classically mediated by TNFα and IL-1 family of cytokines produced by the first batch of neutrophil arriving at the site leading to a sustained endothelial activation. TNFα and IL-1 activate the NF-κB and AP-1 transcription factors that lead to the production of pro-inflammatory proteins, e.g. cyclooxygenase-

2(COX-2), interleukin (IL)-8 and adhesion molecules, e.g. E-selectin, intercellular cell adhesion molecule-1 (ICAM1), vascular cell adhesion molecule-1 (VCAM1) [14]. COX-2 increases the production of prostaglandins (PGE_2, PGI_2) causing further vasodilation [15]. IL-8 and E-selectin expression further enhance the neutrophil recruitment and adhesion to the endothelial surface. Together the above changes lead to increase in blood flow and extravascular leakage of plasma proteins, facilitating leucocyte migration into the tissues.

1.1.4 Migration of leucocytes

1.1.4.1 Neutrophil migration

Neutrophil migration from the endothelium to tissue comprises multiple steps: tethering and rolling, adhesion, crawling, transmigration. P-selectin and E-selectin on the activated endothelium bind to P-selectin glycoprotein ligand -1 (PSGL-1) on neutrophils causing them to tether to the endothelial surface [16]. Neutrophil L-selectin (also referred as CD62L) plays an additional role in tethering and rolling by binding to E- and P-selectin on the endothelium [17]. Subsequently, neutrophils start to slow down and adhere to the endothelial surface. This arrest of neutrophil rolling is facilitated by binding of endothelial ICAM-1 with neutrophil lymphocyte function associated antigen-1 (LFA-1) [18]. IL-8, acting via CXC chemokine receptor 2 (CXCR2/IL8RB) on neutrophils, also causes firm adhesion [19]. The next step is crawling, which is mediated by the interaction between neutrophil CD11b and endothelial ICAM-2 [20]. The final step is transmigration of the neutrophils through the endothelium which occurs either via a paracellular (between endothelial gap junctions) or

transcellular route (through the endothelial cells). This step involves binding of neutrophil LFA-1, macrophage antigen-1 (Mac-1), very late antigen- 4 (VLA-4) and platelet endothelial cell adhesion molecule (PECAM-1) correspondingly to the endothelial ICAM-1, ICAM-2, VCAM, PECAM-1 as well as junctional adhesion molecules (JAM) such as JAM-C [21].

Migration of neutrophils in the extravascular space is facilitated by a strong chemotactic gradient in tissue created by complement component 5a (C5a), and pathogen derived N-formyl-methionyl-leucyl-phenylalanine (fMLP) [22]. Once inside the tissue, neutrophils produce its own chemoattractants which provide a feedback loop to recruit more neutrophils. These chemoattractants include cytokines such as IL-17 [23] and lipid mediators such as leukotriene B_4 (LTB_4), formed by the action of 5-lipoxygenase 5-LO on AA [24]. The process of rolling and exposure to pro-inflammatory cytokines and growth factors cause neutrophil activation and subsequent engagement of their killing mechanisms.

1.1.4.2 Monocyte migration

Monocytes migrate sequentially after the neutrophil infiltration and follow a similar cascade of rolling and tethering, adhesion, crawling and transmigration. In the case of monocytes, rolling is facilitated by interaction of monocyte PSGL-1 with endothelial E-selectin, the adhesion by the interaction of VLA4 and Mac1 on monocytes with VCAM-1 and ICAM-1 on endothelium and transmigration is supported by binding of PECAM1 on monocytes and endothelium [25].

Activated neutrophils control sequential monocyte chemotaxis by modifying the monocyte chemoattractants and adhesion molecules. For instance, activated neutrophils lead to Type 2 endothelial activation causing it to release CC chemokine ligand 2 (CCL2), a classical monocyte chemoattractant protein that interacts with monocyte CC chemokine receptor 2 (CCR2) [26]. Type 2 endothelial activation by neutrophils is triggered by IL-6 trans-signalling. Neutrophils shed IL6R into the inflammatory milieu, which binds to IL-6 to form the IL6-s/IL6R complex. This complex binds to glycoprotein 130 (gp130) on the endothelium to initiate IL-6 trans-signalling and upregulate its expression of CCL2 and VCAM1 [27]. Neutrophil granule proteins further amplify monocyte migration. Azurocidin, derived from the secretory vesicles of neutrophils upregulates monocyte adhesion molecules on endothelium and also acts as a chemotactic signal to formyl peptide receptors (FPR) on monocytes. Neutrophil derived cathelicidin antimicrobial peptides (CAP) and alpha defensins also direct monocyte chemotaxis acting via its FPR receptors [28]. The role of neutrophil granule proteins in monocyte chemotaxis is also supported by the clinical observation where patients lacking CAP-18, a pro-form of cathelicidins show decreased monocyte accumulation at the site of infection or injury [29]. In addition to inducing the expression of adhesion molecules and acting as a chemotactic signal, neutrophil granule proteins have also been shown to increase the potency of monocyte chemoattractants. Serine protease causes amino-terminal modification of several monocyte chemokines like CCL-6, -19, -25. This results in a multi-fold increase in the ability of these ligands to bind to monocyte CCR1 and induce chemotaxis [30].

1.1.4.4 Removal of inflammatory stimulus: Tipping point of resolution

Migration along the endothelium and exposure to pro-inflammatory mediators causes activation of neutrophils and monocytes. Activated leucoytes eliminate the pathogen either via intracellular or extracellular killing mechanisms. The intracellular mechanism involves phagocytosis of the microbe and formation of a phagosome, which is exposed to reactive oxygen species (ROS) and anti-bacterial granules proteins, e.g. defensins, lactoferrin [31]. Extracellular mechanisms are mediated via neutrophil extracellular traps (NETs) or direct release of anti-bacterial proteins into the extracellular environment. NETs are composed of core DNA elements along with histones which trap the pathogen, limiting its spread and thus facilitating phagocytosis [32]. Defects in pathways regulating microbial killing can cause persistent inflammatory reaction and recurrent infections as seen in patients with chronic granulomatous disease (CGD) where ROS producing NADPH oxidase (nicotinamide adenine dinucleotide phosphate) system is either absent [33]. Another clinical example is of neutrophil specific granule deficiency characterised by lack of granule proteins such as lactoferrin, gelatinase-B and collagenase and marked deficiency of defensins [29].

1.2 Resolution

Eradication of the inflammatory stimulus by neutrophils and monocytes paves the way for resolution, characterised by clearance of immune cells from the site and tissue repair. Resolution was originally thought to be a passive process following catabolism of pro-inflammatory mediators and death of immune cells locally. However, it is now widely appreciated that resolution is

an active process and it involves distinct signalling and cellular processes aimed at inhibiting further recruitment of immune cells and promoting clearance of the leucocytes that have migrated to the site [34]. The section below describes the different processes involved in the resolution of inflammation.

1.2.1. Inhibition of chemokine signalling

Chemokines provide directional cues to leucocytes to migrate to the site of inflammation. Thus, to stop the continuous recruitment of neutrophils during resolution, it is important that the chemokine signalling networks be interrupted. A major mechanism by which body attenuates chemokine signalling is through sequestration and degradation of chemokines via decoy receptors. Decoy receptors are chemokine receptors that fail to initiate a signalling cascade. They are identified by the lack of DRY motif, an important component that couples the extracellular receptor loops of GPCR to G proteins. Two main members of this family are the D6 and DARC (Duffy antigen receptor complex) [35].

D6 receptor is highly expressed on the lymphatic endothelium [36]. It binds mainly to the inflammatory agonists of CCR1, CCR2 and CCR5 receptors but does not initiate the downstream signalling pathway [37]. It also clears their ligands by internalisation and endolysosomal degradation [38]. Compared to D6, DARC is expressed on the post capillary venular endothelium and has affinity for > 60% of pro-inflammatory cytokines including both CC and CXC chemokines, e.g. CCL5, CCL7, CCL2, CXCL8, CXCL5, CXCL11 [39]. By

binding to DARC, these inflammatory cytokines become inaccessible to bind to the functional chemokine receptors. DARC is also expressed on red blood cells, which can create a 'sink' for chemokines such as IL-8. This was evidenced by compartmentalization of IL-8 with RBCs when it was added to whole blood. IL8 bound to RBC was also unable to stimulate neutrophils [40]. The role of both these chemokine scavenger receptors as negative regulators of inflammation is further substantiated by receptor knockout studies in multiple murine models of inflammation, e.g. in a model of skin inflammation triggered by Freund's complete adjuvant D6-/- mice showed increased neutrophil migration and necrosis at site of inflammation along with increased cellular infiltrate and levels of CCL2 in the lymph node [41]. Similarly, DARC-/- mice showed hyper-inflammatory characterised by increased neutrophil infiltration in the liver and lung in response to intraperitoneal endotoxin [42].

The functional chemokine receptors like CCR5 and CCR2 can also act as decoy receptors and contribute to the resolution of inflammation. CCR5 on apoptotic neutrophils has been shown to sequester the chemokines CCL3 and CCL5. The levels of these chemokines increased in peritoneal exudates of CCR5 deficient mice and were scavenged by transfer of apoptotic neutrophils [43]. CCR2 receptor usually mediates monocyte trafficking but becomes insensitive by uncoupling itself from the G proteins under the simultaneous exposure of LPS-interferon-γ (IFN-γ) and IL-10. Monocytes treated this way show reduced migration in response to monocyte chemoattractants such as CCL-2, -3, -4 [44].

Another mechanism of inhibition of chemokine signalling is through chemokine proteolysis, which alters chemokine structure in a way that renders them ineffective on its receptor [45], e.g. matrix mettalopeptidase-12 (MMP-12) derived from macrophages truncates ELR motif from the CXC chemokines including CXCL-1,-2,-3,-5 and -8, which is critical for receptor binding. Accordingly, mice lacking MMP12 showed increased infiltration of neutrophils compared to wild-type mice in the bronchoalveolar lavage in response to LPS stimulation [46]. Another example is of stromal cell-derived gelatinase A which cleaves CCL-7, and thus renders it ineffective to signal via CCR-1, -2, -3 receptors. Moreover, gelatinase cleaved CCL-7 acts as an antagonist of these receptors. It was further shown in the murine model of acute zymosan peritonitis model, that gelatinase cleaved MCP-3 but not full length, attenuated trafficking of monocytes in the peritoneal cavity [47].

1.2.2 Neutrophil Apoptosis - Desired route of cell death for resolution

Neutrophil cell death at the site of inflammation occurs in many ways including autophagy, neutrophil extracellular trap (NET) osis, necrosis, necroptosis, and apoptosis [48]. The major mechanism of cell death in neutrophils is governed by the pathological state. For instance, autophagy, which involves breaking down and recycling of dispensable intracellular constituents occurs mainly in the low nutrient environment and during growth factor deprivation. Autophagy is a non-apoptotic form of cell death and serves to dampen inflammation by removing the endogenous inflammasome agonists like mitochondrial DNA (mtDNA) [49]. Another non-apoptotic form of cell death is NETosis which involves the release of nuclear chromatin and granule proteins in the extracellular environment (NETs) following the rupture of nuclear and plasma

membrane rupture [50]. While earlier it was proposed that NETs promote phagocytosis of bacteria and limit their spread [32], recent reports have cautioned that NETosis can cause exaggerated inflammation due to the release of autoantibodies to nuclear components [51][52]. Neutrophil death by necrosis can occur as a primary event in response to direct cellular insults such as heat shock and osmotic shock or in response to signalling via the TNF death receptor, Toll-like receptors, genotoxic stress. It can also occur as an event secondary to delayed apoptosis in which case it is referred as secondary necrosis such as in response to pathogen encoded caspase inhibitors [53]. A common feature of necrotic cell death is permeabilization of lysosomal and plasma membrane leading to release of toxic cellular components which can result in persistent inflammation [54].

Apoptosis is programmed cell death without loss of cell's membrane integrity and ensures safe disposal of neutrophil's toxic contents [55]. In addition, clearance of apoptotic cells by macrophages by the process of efferocytosis (discussed later) causes inhibition of inflammatory signalling. Neutrophil apoptosis is thus central event to mediate resolution. During resolution, neutrophil apoptosis is controlled by multiple regulatory mechanisms involving extrinsic and intrinsic apoptotic pathways. In an example of extrinsic pathway, neutrophils undergo apoptosis in response to ligation of surface death receptors to Fas ligand generated from macrophages [56] [57]. Reports have also shown that TNF-α at high concentrations can directly induce extrinsic apoptosis of neutrophils by increasing the turnover of an anti-apoptotic molecule myeloid leukaemia cell differentiation protein 1 (MCL-1) [58]. Neutrophils also regulate their own life span, e.g. cathepsin D, a protein

released from azurophilic granules of neutrophil causes independent activation of the pro-apoptotic caspase 8 pathway [59]. Another mechanism of neutrophil apoptosis involves phagocytosis induced cell death pathway. Phagocytosis of certain bacteria, e.g. *E. coli* results in an NADPH oxidase mediated production of ROS [60]. ROS thus generated induces apoptosis by a combination of extrinsic and intrinsic pathways, which involve direct activation of caspase-3 and increase in permeabilization of mitochondrial outer membrane leading to formation pro-apoptotic molecules of B-cell lymphoma-2 (BCL-2) family including Bcl-2 homologous antagonist/killer (BAK) and Bcl-2-associated X protein (BAX). The role of ROS in mediating neutrophil apoptosis is further substantiated from the clinical observation that neutrophils from CGD patients, who have a defective ROS system show delayed apoptosis compared to those from healthy donors [61].

Apoptotic neutrophils can also control other resolution processes through multiple mechanisms. Specifically, by secreting Annexin A1, which acts via FPR2/ALX, they can limit further recruitment of neutrophil during resolution. Annexin A1 also promotes neutrophil apoptosis in a paracrine manner and also promotes their clearance via macrophages [62] [63]. Apoptotic neutrophils also directly bind to LPS and aid in its removal [64].

1.2.3 Efferocytosis

Efferocytosis is the clearance of the apoptotic cells and is accomplished by professional phagocytes like macrophages with support from non-professional phagocytes, e.g. fibroblasts [65] and epithelial cells [66]. Although it resembles

phagocytosis which is classically defined as macrophage uptake of microbes, it involves the distinct family of receptors and downstream signalling pathways [67].

The process of efferocytosis can be subdivided into four steps: phagocyte attraction, apoptotic cell sensing, uptake and digestion [68]. The first step involves secretion of 'find me' signals by apoptotic neutrophils, e.g. nucleotides ATP and UTP, CXC3CL1, LPC. These “find-me” signals create a signalling gradient for the corresponding receptors on the macrophages namely purinergic receptor $P2Y_2$, CX3CR1, G2A which then migrate towards the apoptotic neutrophil [69]. The next step is apoptotic cell sensing by macrophages, facilitated by surface expression of the 'eat me' signals by apoptotic neutrophils, e.g. phosphatidylserine (PS) and calreticulin (CRT). These eat me signals on apoptotic neutrophils engage with the phagocyte in two ways. They either bind them directly, e.g. PS and CRT binding respectively to brain-specific angiogenesis factor-1 (BAI1) and CD91, the surface receptors on phagocyte. In another approach, the binding is facilitated by bridging molecules, e.g. PS bridges with $\alpha V\beta 3$ on phagocyte via milk fat globule EGF 8 (MFGE8), growth arrest specific gene-6 (Gas6) promotes the interaction between PS and TAM (Tyro3-Axl-Mer) receptor family on phagocytes [70]. Receptor engagement leads to rearrangement of cytoskeletal proteins within the phagocyte leading to engulfment of the apoptotic neutrophil in its entirety, a process which resembles macropinocytosis [71]. Engulfment of the apoptotic cells leads to the formation of a phagosome, a membrane bound compartment containing the apoptotic debris. Phagosome becomes increasingly acidic and then fuses with the lysosome to form a

phagolysosome, where it is degraded by the lysosomal enzymes like DNase, acidic proteases and nucleases into their basic cell materials i.e. amino acids, nucleotides, fats [72].

Timely clearance of apoptotic neutrophils avoids their death by secondary necrosis, which can lead to spillage of toxic cytoplasmic contents leading to a sustain inflammatory reaction or development of autoimmunity [73]. In addition, efferocytosis switches the phenotype of macrophage from pro-inflammatory to anti-inflammatory phenotype and is associated with the generation of anti-inflammatory mediators like IL-10, PGE_2 and TGF-β [74]. Efferocytosis also induces production of growth factors such as vascular endothelial growth factor (VEGF) and hepatocyte growth factor (HGF) from macrophages, which together with transforming growth factor- β (TGF-β) mediate the regeneration of tissue components, e.g. fibroblasts, endothelial and epithelial cells [75][76].

1.2.4 Lymphatic emigration

Lymphatic vessels have also been shown to provide an exit to inflammatory cells during resolution. Macrophages migrate via lymphatics to the local lymph node during resolution [77], which is in part controlled by efferocytosis induced expression of CXCR4 on macrophages [78]. CXCR4-CXCL12 axis is known to participate in lymphatic migration of dendritic cells, and it seems a similar mechanism is involved in macrophage lymphatic egress. Relatedly, the interaction of macrophages with apoptotic cells induces expression of the sphingosine-1-phosphate receptor (S1PR1) on macrophages, which primes them for lymphatic migration via the S1PR1-S1P axis [79]. Thus, efferocytosis

not only controls the clearance of neutrophils but also facilitates egress of macrophages from the site of inflammation.

Neutrophils have also been shown to leave the inflamed site via the lymphatics. However, this event is observed primarily in microbe triggered inflammation compared to tissue injury induced inflammation. Similar to macrophages, neutrophil lymphatic migration is controlled via CXCR4 on their surface [80]. CCR7, a chemokine receptor associated with dendritic cells and T cell migration to the lymph node also mediates neutrophil lymphatic egress [81]. In addition to reducing cellular burden at inflammation site, lymphatic migration of neutrophils facilitates shuttling of bacteria to the lymph node and modulates antigen presentation [82] [83].

1.2.5 Reverse transmigration

According to the classical view, neutrophils arrive at the site of inflammation via activated endothelium and are cleared at the site by efferocytosis during resolution. However, recent reports have identified a novel route for neutrophil clearance via the microvasculature called reverse transmigration. Reverse transmigration is the re-entry of neutrophils from the interstitial site into the vasculature and finally to the circulating compartment [84].

Re-entry of inflamed neutrophils back into circulation via microvasculature was first reported by Matthias et al in the zebrafish model of tissue injury using green fluorescent protein (GFP) expressing neutrophils [85]. These findings were later also confirmed in murine model of ischaemia reperfusion injury using real-time confocal imaging. In this murine study, Woodfin et al. identified that neutrophils exit across the endothelial sites which express low levels of

JAM-C, an adhesion molecule involved in neutrophil transmigration. Furthermore, they showed that reduction of JAM-C by pharmacological or genetic means enhanced reverse transmigration [86]. This process has also been replicated in vitro using primary human neutrophils on endothelial monolayer, and a similar phenotype of tissue experienced neutrophils have also been found in rheumatoid arthritis patients [87].

1.2.6 Post resolution

Classically, the hallmarks of resolution comprised removal of the inflammatory stimulus, reduction in levels of pro-inflammatory cytokines and clearance of inflammatory cells to restore tissue homoeostasis. However, recent studies have shown that the resolved tissue does not just return to its original state, but to a state of 'adapted homeostasis' and homes a diverse population of cells including monocyte-derived macrophages, monocyte-derived dendritic cells, regulatory T cells (T_{regs}) and myeloid derived suppressor cells (MDSCs) and other lymphocytes including B1, B2, NK and $\gamma\delta$ T cells [88] [89].

The cells occupying the site during post resolution serve two important functions. First, they maintain immune tolerance at the site by inhibiting proliferation of effector T cells. This function is mediated via immunosuppressive T_{regs} and MDSCs, which exert this regulatory function by producing cytokines like IL-10 and TGF-β [90,91]. Furthermore, MDSCs also suppress the effector T cells directly by producing iNOS and arginase at the site by cell-cell contact [92]. Second, the post resolution monocyte-derived cells regulate the lymphocyte activation in the lymph node in an iNOS

dependent manner leading to the effective generation of memory T and B lymphocytes in blood [88].

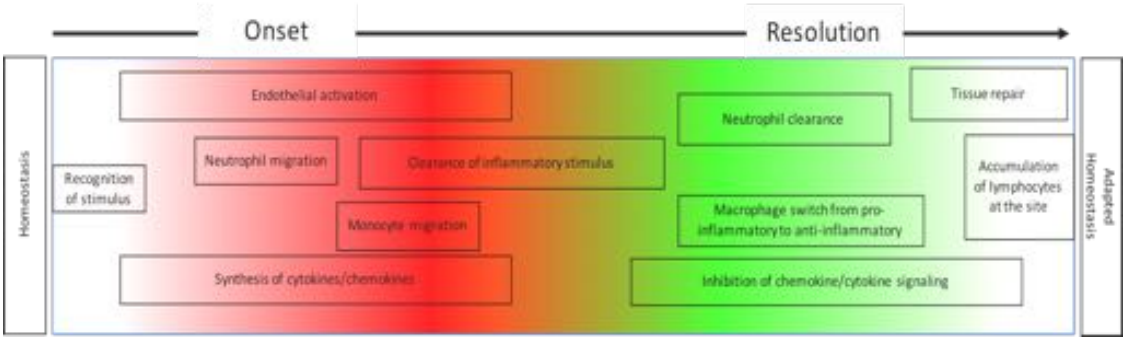

Figure 1.1 Events during onset and resolution of acute inflammation

1.3 Specialised pro-resolving mediators (SPMs)

SPMs are the novel genus of lipid mediators that serve as endogenous agonists of resolution of inflammation. Depending on the fatty acid substrate from which they are derived, SPMs are classified into multiple subsets. The section below describes each subset detailing their biosynthesis, the receptors through which they mediate their action and their effect on the resolution processes.

1.3.1 Lipoxins

Lipoxins are derived from arachidonic acid (AA) via two main routes, the 15S-hydroxyeicosatetranoic acid (15S-HETE) pathway and the leukotriene A_4 (LTA_4) pathway. In the 15S-HETE pathway, AA is first converted by 15-lipoxygenase (15-LO) into 15S-HETE. 15S-HETE is then further converted to

5(6)- epoxytetraene by 5-lipoxygenase (5-LO). In the second route, AA is first converted by the action of 5-LO into LTA_4 which is then further converted by 12 or 15-LO to 5(6)- epoxytetraene [93]. In both pathways, the 5(6)-epoxytetraene undergoes enzymatic hydrolysis to lead to the formation of lipoxin A4 (LXA_4) and its isomer lipoxin B_4 (LXB_4) [94] (Figure 1.2).

The lipoxin family also includes 15-epi-lipoxins, which are derived from AA in the presence of aspirin. Biosynthesis of 15-epi-lipoxins involves conversion of AA into 15R-HETE by the acetylated cyclooxygenase-2 (COX-2). Here, aspirin mediates the acetylation of COX-2. 15R-HETE is converted by 5-LO into 15-epi-LXA_4 or 15-epi-LXB_4 [95]. 15-epi-lipoxins can also be produced by the cytochrome p450 mediated oxygenation of AA [96] **(Figure 1.2)**.

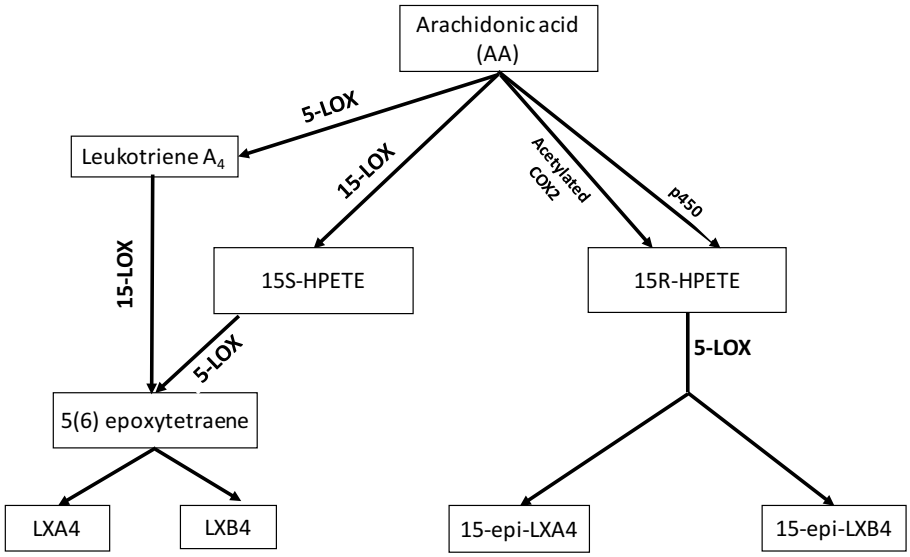

Figure 2.2 Biosynthesis lipoxins and 15-epi-lipoxins

LXA_4 and 15-epi-LXA_4 mediate their function primarily via a specific formyl peptide receptor, FPR2 (also called ALX), a member of FPR class of G-protein coupled receptor (GPCR) family. The receptor for LXB_4 or 15-epi-LXB4 is still

unknown [97]. In humans, FPR2/ALX has been identified on multiple immune cell types including neutrophils, monocytes, T cells as well as endothelial cells and epithelial cells [98].

1.3.2 Resolvins, Protectins and Maresins

Resolvins are a family of specialised pro-resolving mediators derived from omega-3 fatty acids. Depending on the omega 3 fatty acid, these mediators are broadly classified into two series: E-series resolvins, derived from eicosapentaenoic acid (EPA) and D-series resolvins, derived from docosahexaenoic acid (DHA). DHA gives rise to another family of SPMs called protectins and maresins [99].

Biosynthesis of E-series resolvins involves an aspirin dependent pathway and aspirin independent pathway. In the aspirin dependent pathway, acetylated COX-2 mediates the conversion of EPA to 18R-HEPE, and in the aspirin independent pathway, p450 enzymes convert EPA to 18-R-HEPE. Irrespective of the route, the 18R-HEPE intermediate is converted by the sequential action of leucocyte derived 5-LO into 5S-hydroperoxy-18R-HEPE and then into resolvin E1 (RvE1) or resolvin E2 (RvE2) [100]. 18R-HEPE can also be a substrate for 12/15-LO which leads to the formation of resolvin E3 (RvE3) [101] **(Figure 1.3).**

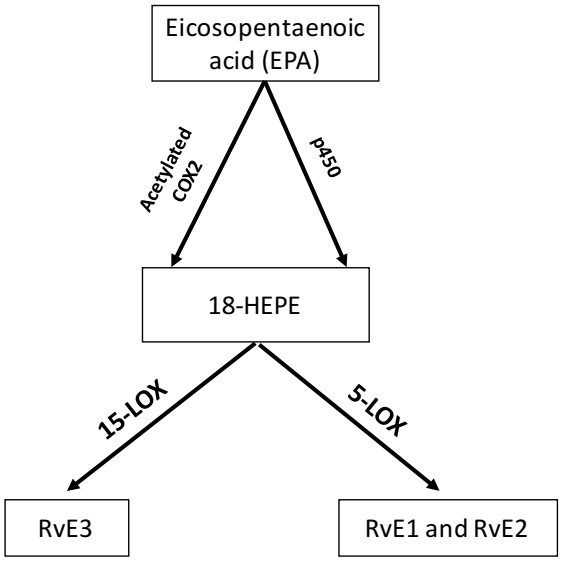

Figure 1.3 Biosynthesis of E-series Resolvins

DHA gives rise to three different types of SPM families: D-series resolvins, maresins and protectins. D- series resolvins involve the conversion of DHA by 15-LOX into 17S-hydroperoxy-DHA (17S-HDHA), which is then catalysed by the 5-LO to generate positional isomers including RvD1, RvD2, RvD3, RvD4, RvD5 and RvD6. The action of acetylated COX-2 on DHA yields 17R-hydroperoxy-DHA (17-R-HDHA), which is converted by 5-LO into aspirin-triggered D- resolvins including AT-RvD1, AT-RvD2, AT-RvD3, AT-RvD4. Similar to other aspirin-triggered SPMs, cytochrome P450 can also form aspirin-triggered D- resolvins [102]. 17-S-HDHA and 17-R-HDHA also give rise to protectin D1 and aspirin triggered-protectin D1 after undergoing enzymatic epoxidation and enzymatic hydrolysis [103]. Maresin synthesis involves the conversion of DHA by macrophage 12-LO into 14S-hydroperoxy-DHA in macrophages, followed by oxygenation [104] **(Figure 1.4).**

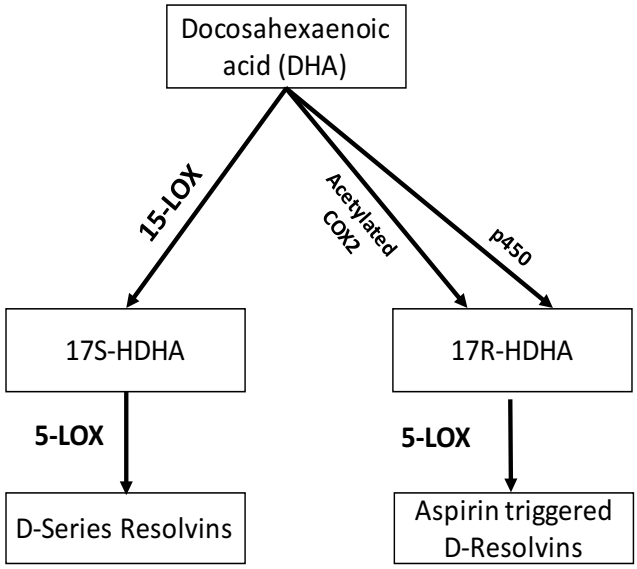

Figure 1.4 Biosynthesis of D-series Resolvins

RvE1 mediates its actions via two GPCR receptors: ChemR23 and BLT1[105]. RvE1 is a full agonist of ChemR23, which is primarily expressed on the monocytes, dendritic cells and also on the epithelial and endothelial cells [106] [107]. It also acts as a partial agonist on the BLT1 receptor. BLT1 is expressed on the granulocytes, monocytes and dendritic cells [108]. Receptors for RvE2 and RvE3 are not yet identified. Amongst the D-series resolvins, receptors have been determined for RvD1, RvD2, RvD3 and RvD5. RvD1 and its aspirin-triggered epimer AT-RvD1 activate two GPCR receptors, FPR2/ALX and GPR32 [109]. FPR2/ALX is primarily the LXA_4 receptor but is also activated by RvD1 at higher concentrations. GPR32 is also activated by RvD2 and RvD5, which are structurally similar to RvD1. GPR32 is primarily expressed on neutrophils, monocytes and monocyte-derived macrophages [109]. Resolvin D2 triggers GPR18, which is mainly expressed on neutrophils, monocytes [110].

1.3.4 Role of SPMs in promoting resolution processes

Through concerted action on different cell types, SPMs control the severity of inflammation and promote multiple resolution processes. SPMs inhibit neutrophil trafficking, e.g. LXA_4 and ATL-LXA_4 have been shown to exert their negative effects on neutrophil trafficking by preserving CD62L and downregulating CD11b on neutrophils, causing reduced adhesion on endothelium [111]. LXB_4 also inhibits neutrophil adhesion by downregulating expression of P-selectin on the endothelium [112]. RvE1 acts as a partial agonist of BLT1 receptor and interrupts the signalling via potent neutrophil chemoattractant LTB_4 [113]. Similar to lipoxins, RvD1 and AT-RvD1 also show inhibitory effect on neutrophil trafficking via FPR2/ALX [114][115].

In addition to inhibiting neutrophil migration, SPMs also promote neutrophil apoptosis and enhance their clearance by efferocytosis. RvE1 and 15-epi-LXA_4 increase neutrophil apoptosis by attenuating myeloperoxidase (MPO) induced expression of anti-apoptotic molecule MCL-1 [116][117]. LXA_4 and LXB_4 induce selective migration of monocytes and also reprogram these monocytes to increase efferocytosis [118][119]. In fact, the interaction between macrophages and apoptotic cells have been shown to enhance formation of SPMs like RvD1, RvE1 and PD1. Thus, efferocytosis and SPMs maintain a positive feedback loop to ensure resolution [120].

SPMs also downregulate the production of pro-inflammatory cytokines. One mechanism through which they mediate this action is by inhibiting the transcription of cytokines, e.g. LXA_4 reduces IL-8 transcription by activating the

repressors of the NF-κB [121][122]. RvD1 upregulates expression of mi-RNA 146b, which targets NF-κB signalling and reduces transcription of pro-inflammatory cytokines IL-8 and IL-1β [123]. In another mechanism, SPMs reduce the levels of chemokines by promoting their scavenging, e.g. LXA_4 increases the expression of CCR5 on apoptotic neutrophils, which scavenge the chemokines CCL3 and CCL5 [124].

In addition to their effect on immune cells, SPMs exert an effect on the stromal tissue to promote resolution. Lipoxins inhibit the fibroblast-derived metalloproteinases production. For instance, exposure of LXA_4 to human synovial expressing FPR2/ALX reduced their production of matrix metalloproteinase MMP-3, which otherwise can cause tissue destruction [125]. In another example, RvD2 was shown to promote revascularization in a model of ischaemic injury. Here it was shown that RvD2 enhances endothelial cell migration which promotes arteriogenesis and myocyte regeneration [126]. SPMs have also been shown to maintain epithelial barrier integrity. In a mouse model of dry eye, RvE1 not only decreased inflammation but also increased the density of corneal epithelial cells and improved tear production [127]. The effect on epithelial function was also seen in the model of colitis where RvE1 increased the expression of intestinal alkaline phosphatase and reduced the loss of epithelial barrier [128].

Another important characteristic of SPMs is their effect on promoting the clearance of microbes. In the cystic fibrosis model, LXA_4 administration directly reduced the lung burden of P. aeruginosa [129]. Likewise, RvE1 enhanced the clearance of *E. coli* in addition to decreasing neutrophil accumulation in an

acute lung injury model [130]. SPMs have also been shown to enhance the effects of antibiotics, e.g. 15-epi-LXA_4 in combination with the antibiotic ceftazidime reduced the bacterial load in a sepsis model triggered by *E. coli* induced peritonitis [131]. A similar effect has been shown in combination with ciprofloxacin for RvD1 and PD1. SPMs (RvD1, RvD5 and PD1) also enhance antibiotic effects of vancomycin in mouse model skin infection caused by *S. aureus* [132].

1.4 SPMs: A novel approach to treat inflammatory disorders

The current strategy to treat chronic inflammatory disorders is largely based on the 'anti-inflammatory' approach i.e. inhibiting the factors that drive inflammation. The anti-inflammatory tool kit comprises of three main classes. The most commonly used are NSAIDs, which function by inhibiting COX to reduce the levels of pro-inflammatory prostaglandins [133]. Second, corticosteroids, which act on multiple pathways including inhibition of NF-κB transcription, inhibition of phospholipase A2, downregulation of cell adhesion molecules, induction of anti-inflammatory proteins such as lipocortin, secretory leucocyte protease inhibitor (SLPI) [134]. And third, the disease modifying anti-rheumatic drugs (DMARDs) which can be further sub-classified into non-biologics for, e.g. methotrexate and biologics which are monoclonal antibodies against the cytokines or their receptors, e.g. anti-TNF and anti- IL1 [135].

While NSAIDs and corticosteroids are effective at relieving symptoms, they are associated with side effects in multiple organ systems including the immune system. NSAIDs can cause gastric ulcers, increase the risk myocardial infarction and stroke, and renal failure in patients with kidney disease

[136][137]. Furthermore, they directly interfere with the resolution processes and tissue repair [138][139]. The side effect profile of corticosteroids is more severe. They can predispose to diabetes mellitus, affect the nervous system and can cause mood disturbances and sleep disorders. Steroids also interfere with skin wound healing and have side effects on the skeletal system and can cause osteoporosis. Furthermore, they reactivate latent infections, e.g. cytomegalovirus (CMV) and tuberculosis (TB) and increase the risk of infections, e.g. candida infection [136]. Biologics, like corticosteroids, can also weaken the antimicrobial host defence of the body [140].

In recent years, evidence has accumulated that pathogenesis of chronic inflammatory disorders can in part be due to defects in the pro-resolution pathways [141], e.g. In a rat model of carrageenan-induced pleurisy, it was observed that decreased in the production of cyclopentenone prostaglandin 15d-PGJ_2, by COX-2 inhibition can lead to sustained inflammation [138]. In another example, mice deficient of 12/15 LO, a key enzyme involved in the generation of SPMs, showed exaggerated inflammation in a model of experimental arthritis [142]. These observations are also supported by clinical scenarios, e.g. levels of LXA_4 in the exhaled breath condensates and activated blood of asthmatic patients inversely correlated with disease severity [143].

Mounting evidence that 'failure to resolve' could contribute to the pathogenesis of chronic inflammatory disorders have given momentum to the novel 'pro-resolving approach, which involves enhancing the levels of endogenous mediators of resolution to correct the resolution deficit. While a diverse range of compounds such as lipid mediators, e.g. cyclopentenone prostaglandins

(15d-PGJ_2) [144], epoxy-oxylipins [145], gasses, e.g. hydrogen sulphide [146], purine nucleoside, e.g. adenosine [147], peptides, e.g. annexin A1, melanocortin and chemerin-derived peptides [148–150] have been shown to ameliorate inflammation, SPMs have been at the forefront of the pro-resolving approach.

The beneficial effect of SPMs has been proven in multiple models of chronic inflammatory disorders including arthritis [151], asthma [152], inflammatory bowel disease [153] and also in acute inflammatory conditions, e.g. sepsis [154]. In addition, SPMs actively promote tissue repair and in concert with antibiotics enhance the immune defence against microbial response [132] [155]. Furthermore, they have direct analgesic by modulating the central pain pathways and reducing pain hypersensitivity [156].

The promising results in animal models supported by correlation studies in patient populations make SPM based therapy an ideal candidate for drug development. Carefully designed human studies with validated biomarkers to confirm efficacy and support patient stratification will ensure they reach clinical practice in a timely manner.

1.5 Rationale for using human models of inflammation

Animal models have been indispensable for understanding disease mechanisms. By allowing genetic or pharmacologic manipulation, in vivo imaging and cell tracking, they have not only elucidated novel drug targets but have also allowed to investigate the pharmacology of novel compounds on

disease progression [157]. Despite the high quality of evidence from animal studies, the predictability of animal models to inform the success of clinical trials in humans has come into question [158]. The problem is worse in the case of inflammatory disorders exemplified by the failure of more than 100 clinical trials in sepsis [159].

An important factor that contributes to this problem could be differences within the immune systems of rodents and humans, e.g. in humans, the dominant immune cell type in circulating blood is neutrophils (50 - 70%), while in mice it is lymphocytes (75-90%) [160]. In addition to the quantitative differences, the immune cell types differ qualitatively. For instance, human neutrophils are rich in defensins, an antimicrobial peptide but it is absent in mouse neutrophils [161]. Another controversial example is a lack of inducible nitric oxide expression in human macrophages, which is otherwise clearly expressed by mouse macrophages in response to LPS and IFN-γ [162]. The differences are also evident in the adaptive immune components. For e.g. Fc receptors (FcR) which mediate the binding of antigen-antibody complexes are differently expressed between the two species. Mice lack the expression of FCαRI which is otherwise expressed in humans. Furthermore, there are species differences in the chemokines which partake in the movement of immune cells during the inflammatory response. The chemokines CXCL8, CXCL7, CCL13 are absent in mice, while CCL-6, -9 and -12 are absent in humans [163]. The non-immune cell components, like endothelial cells, are also different between two species. For instance, P-selectin, an integrin present on the endothelial cell to mediate trafficking of leucocytes is upregulated in response to LPS in mice but not in humans [164].

The variation in inflammatory response between mice and humans have also been highlighted at the systems level. Seok et al. showed that the genomic responses to different inflammatory stimuli including trauma, burns and endotoxin in humans poorly correlated with mice. Furthermore, they demonstrated that human model of intravenous endotoxin administration correlated highly with patients than any of the murine models of inflammation. In addition, they found that for same stimuli, the recovery time i.e. the time required for upregulated gene to decrease to half its maximum value, was significantly lower in murine models compared to the humans. This observation emphasises that the resolution of inflammatory signalling is variable in human and mice [165]. Humans are also 100,000-fold more responsive to intravenous LPS than mice, an effect which is in part due to differences in serum proteins between two species [166]. These differences are important to consider as LPS is one of the commonly used inflammatory stimulus in mice to model human inflammatory response [167].

Utilising human models is thus an important step towards understanding the pathogenesis of inflammatory diseases, particularly in cases where animal models fail to capture the characteristics of the disease in patients. Even though they lack the mechanistic rigour of animal models, humans can serve as a platform to validate the findings described in mice and understand their relevance and representativeness to human immunology [168]. They can also be used as proof of concept platform to validate mechanism of novel immune therapeutics and obtain data on their early clinical efficacy. Such proof of

concept studies also allows to discover new biomarkers or confirm the utility of existing ones for late stage clinical trials [169].

1.6 Human models of acute inflammation

Human models of acute inflammation are broadly classified into two groups, systemic and local. Systemic models, e.g. intravenous endotoxin mimic early sepsis [170]. In local models, inflammation is triggered in the tissue, either lung or skin to facilitate investigation of leucocyte migration and soluble mediators of inflammation [171]. Lung models of acute inflammation include endotoxin inhalation, ozone challenge and rhinovirus challenge models [169]. Skin is a preferred site as it allows the use of minimally invasive techniques, investigation of multiple sites and provides easy access to inflammatory contents. In the context of this thesis, I have described below the different types of skin inflammation models.

1.6.1 Cantharidin skin blister

Cantharidin is a blistering agent produced as a defence mechanism by a species of beetle collectively referred as Spanish fly or blister beetle [172]. On contact with skin, cantharidin causes the release of serine proteases within the epidermis, resulting in loss of cohesion between keratinocytes, a process called acantholysis [173]. Acantholysis induced tissue injury leads to sterile inflammation which gives rise to a skin blister. This blistering property of cantharidin is also exploited clinically for the treatment of plantar warts [174].

Cantharidin induced skin blister was first demonstrated by Day et al. to be a suitable in vivo model to investigate leucocyte migration and cytokines during onset phase of acute inflammation [175]. Their technique involved the application of cantharidin solution on a filter paper disc placed on the skin and then covering it using an adhesive dressing for 24h. After 24h, a skin blister is formed which can be aspirated to obtain the inflammatory exudate, which contains cells and soluble mediators. Morris et al. extended the use of cantharidin skin blister to study resolution biology in humans. In their study, two blisters were raised on the forearm of healthy volunteers; one was aspirated at 24h to study the onset of acute inflammation and the other one at 72h, to explore the resolution phase [176].

Cantharidin skin blister has been employed for multiple uses. For instance, Dinh et al. validated its use to study the effect of anti-inflammatory drugs, e.g. Anti-TNFα and corticosteroids on neutrophil migration at onset [177]. In another example, it was employed in patients undergoing cardiopulmonary bypass surgery, to understand dysfunction of leucocytes trafficking post-surgery [178].

1.6.2 Skin chamber technique

Skin chamber technique involves two steps. In the first step, a skin blister is generated by application of negative pressure on the skin followed by removal of the blister roof to form a denuded skin surface. In the second step, the denuded skin area is covered using a plastic collection chamber filled with autologous serum and kept for 4-24h. During this interval, the leucocytes and

soluble mediators accumulate in collection chamber fluid which can be sampled to investigate the different phases of inflammation.

Skin chamber technique has been primarily used to investigate defects in neutrophil migration in patient populations, e.g. cirrhosis patients [179] and renal failure[180].

1.6.3 Skin abrasion models

Skin abrasion models involve the creation of lesion on the superficial layer of skin with the use of either high-speed drill [181], tape stripping[182] or sandpaper [183]. The lesion provides a skin window for exudation of inflammatory contents on to the skin. The contents are either directly aspirated, or they are collected on a filter paper disc overlaid over the lesion. In the latter case, the cells are extracted by layering the filter paper disc on a glass slide which is then fixed and stained. The soluble mediators in the filter paper disc are eluted by incubating it in normal saline followed by centrifugation [183]. Skin abrasion models have also been employed to investigate defect in innate immune response in patients, e.g. Crohn's disease.

1.7 PhD aims and objectives

Studies demonstrating beneficial effects of SPMs in inflammatory diseases have been primarily conducted in animal models, and there is a need to investigate the SPM physiology and pharmacology in human models of inflammation that can lend themselves to delineating pro-resolution pathways and that are amenable to therapeutic intervention.

Keeping this aim mind, my PhD objectives were:

- To characterise an in vivo model of resolution of acute inflammation in healthy humans.

- To investigate SPM generation, SPM receptor expression and effect of SPMs on resolution indices using an in vivo model of resolution of acute inflammation in healthy humans.

- To investigate the effect of an SPM based drug on resolution indices and compare it to the conventional anti-inflammatory agent using an in vivo model of resolution of acute inflammation in healthy humans.

Chapter 2

METHODS

2.1 Cantharidin skin blister model

2.1.1 Ethics statement

Cantharidin skin blister study was approved by UCL Institutional Ethics Committee (Project ID: 2907/002). The procedures performed were in accordance with the ethical standards of the UCL Institutional Committee and Declaration of Helsinki. Written informed consent was obtained from all volunteers.

2.1.2 Volunteer recruitment

Healthy, young, non-smoking males (18-50 years) were recruited for this study. Volunteers were excluded if they had a history of any chronic inflammatory condition or allergies, recent history (< 1 month) of an acute inflammatory condition, immunisation in last three months, were taking regular medications or had taken any medication in the week before proposed study start date. Volunteers were advised to refrain from heavy exercise and alcohol for two days before study start date, during the study period and two days after the study period.

2.1.3 Application of cantharidin skin blister

Overall, the procedure involved three visits:

2.1.4.1 Visit 1: Blister induction

After obtaining written consent, two sites were marked over a forearm, 10-15 cm away from the elbow crease. The marked sites were cleaned using 70%

isopropyl alcohol and then dry shaved. Two filter paper discs (10mm diameter, Whatman grade 1) were placed over the marked sites, and 12.5 µl of 0.1% cantharidin solution (0.7% Cantharone, Dormer Laboratories Inc., Canada diluted 1:7 in acetone) was pipetted on to each of the filter paper disc **(Figure 2.1A)**. Each filter paper disc was then covered by laboratory film (16mm diameter; Parafilm) and further overlaid by two foam pads (30mm diameter, Activheal non-adhesive foam pad) **(Figure 2.1 B, C and D)**. The two sites were then secured by application of an adhesive dressing (Mepore, 10 x 14 cm) **(Figure 2.1 E, F)**. Participants were advised to keep the dressing dry and return the next day at the same time. A 5 ml sample of peripheral blood was also collected from the contralateral forearm before the application of cantharidin blister.

2.1.4.2 Visit 2: Dressing change and 24h blister exudate aspiration

At the 24h time point, the dressings were carefully removed. After ensuring that a patent blister has formed over both the sites, one of the blisters was pierced using a 26.5-gauge needle. The roof of the pierced blister was then gently squeezed using a sterile 1 ml syringe to push out the blister exudate, which was aspirated using a sterile pipette **(Figure 2.2 A, B)**. The blister exudate was mixed with 50 µl of 3% sodium citrate in a sterile 1.5 ml micro-centrifuge tube to prevent coagulation. The tube was then centrifuged at 1000 x *g* for 5 min at 4^0 C, and the resulting cell pellet was suspended in 1 ml of FACS buffer (PBS with 5% FCS + 0.1% sodium azide). Leucocytes were first enumerated as described in section 2.3 and then processed for flow cytometry

as described in section 2.6. The supernatant was aliquoted and stored at -80 ^{0}C.

The aspirated blister was cleaned using an aseptic solution (0.1 % Cetrimide, Savlon) and was covered with a protective dressing pad (9 x 10 cm, Mepore). The unaspirated blister was protected for another 48h using a cap dressing **(Figure 2.2 C, D)**. The cap dressing involved fitting a concentrically cut ulcer dressing (Comfeel Plus, Ulcer Dressing 10 x10cm) around the blister and then securing a blister cap over it. The blister cap was prepared by coating a plastic cap [the cap of a 50 ml specimen tube (Sterilin)] with an ulcer dressing along the rim. The blister cap and ulcer dressing were further secured by support bandage. The volunteer was asked to return after two days for 72h blister aspiration.

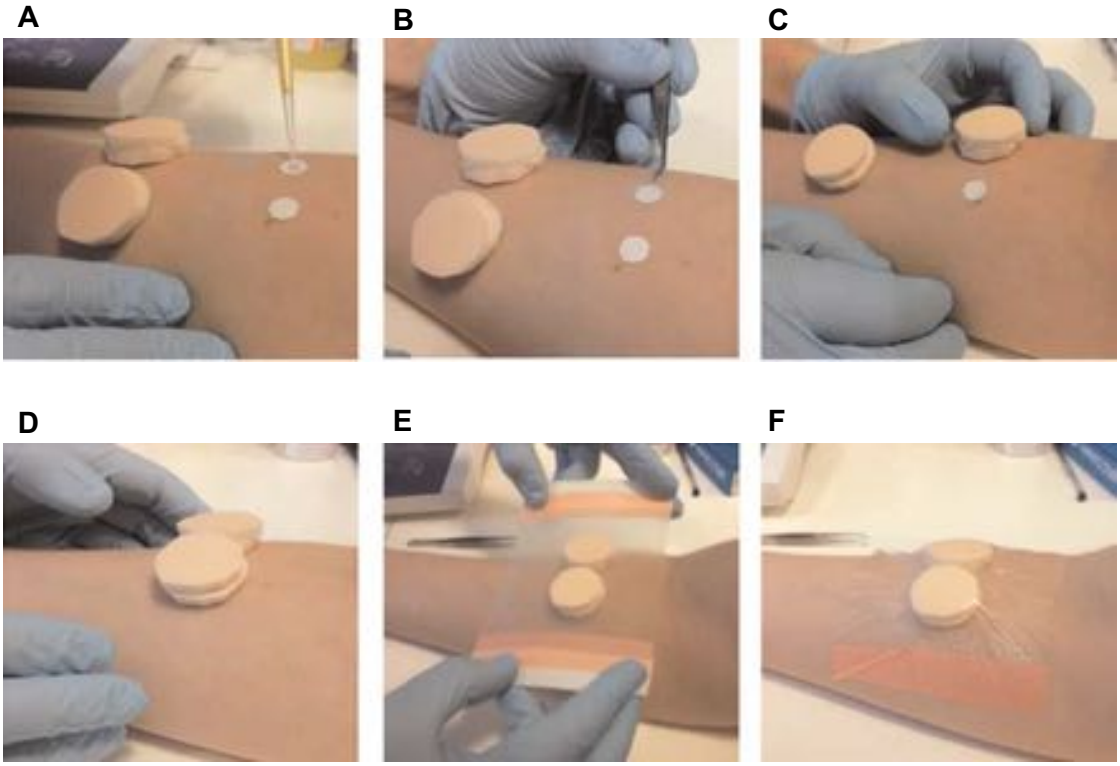

Figure 2.1 Application of cantharidin skin blister

0.1 % Cantharidin is pipetted over a filter paper disc **(A).** Filter paper disc is then covered by a parafilm and a foam pad **(B, C and D).** Foam pads are covered by an adhesive dressing **(E and F).** (Image reproduced from Jenner WJ, G. D. (2012). Assessment of leukocyte trafficking in humans using the cantharidin blister model. J R Soc Med Cardio, 1 no. 1 4)

2.1.4.3 Visit 3: 72h blister exudate aspiration

At this visit, the blister cap dressing was carefully removed, and the blister fluid was aspirated and processed in the manner described above for the 24h time point. The aspirated blister area was cleaned using an aseptic solution and covered with a protective dressing (Mepore). Volunteers were asked to keep the site dry until a visible scab formed over both the aspirated blister sites.

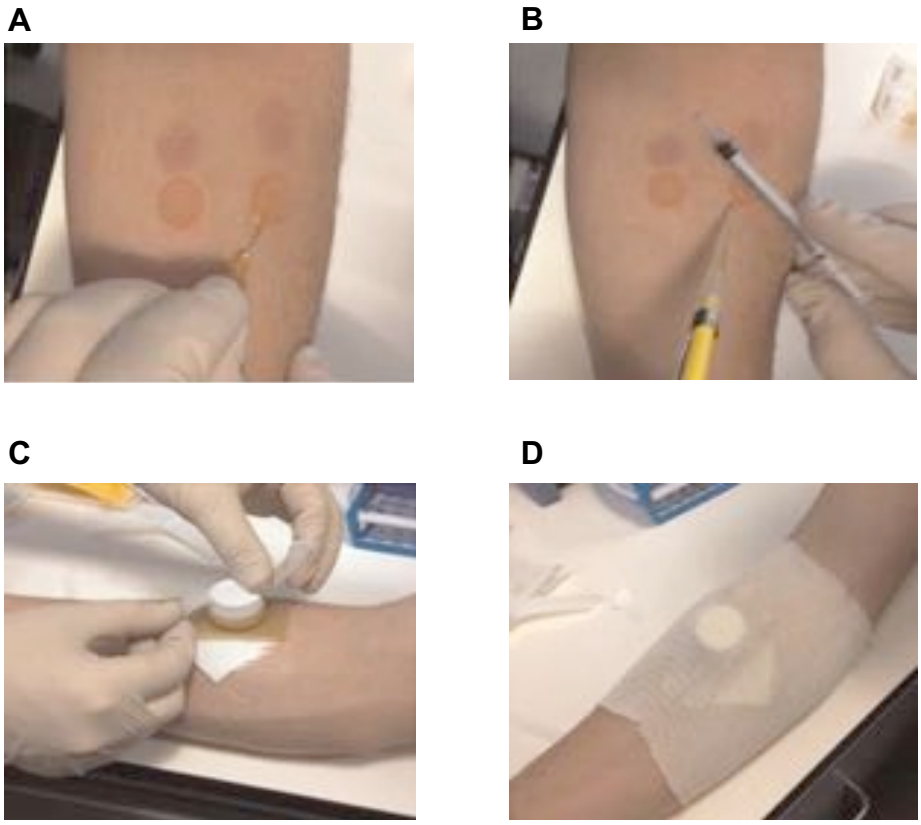

Figure 2.2 Aspiration of cantharidin blister exudate and application of cap dressing for 72hr time-point

Blister roof is pierced along the lateral border using a needle and fluid is rolled out using a 1 ml syringe which is then collected by a pipette **(A and B).** 72hr cantharidin blister is secured using a cap dressing made of hard plastic cap and ulcer dressing **(C and D)**. (Image reproduced from Jenner WJ, G. D. (2012). Assessment of leukocyte trafficking in humans using the cantharidin blister model. J R Soc Med Cardio, 1 no. 1 4)

2.2 UV killed *E. coli* (UVkEc) triggered self-resolving dermal inflammation model

2.2.1 Ethics statement

The study characterising the UVkEc triggered self-resolving dermal inflammation model was approved by UCL Institutional Ethics Committee (Project ID: 5051/001). All procedures performed were in accordance with the ethical standards of the UCL Institutional Committee and Declaration of Helsinki. Written informed consent was obtained from all volunteers.

2.2.2 Volunteer recruitment

Healthy, young, non-smoking males (18-50 years) were recruited in this study. Volunteer exclusion criteria included: a history of any chronic inflammatory condition or allergies, recent history (< 1 month) of an acute inflammatory condition, immunisation in last three months, were taking regular medications or had taken any medication in the week before proposed study start date. Volunteers were advised to refrain from heavy exercise and alcohol for two days prior to study start date, during the study period and two days after the study period. Volunteers were also asked to refrain from high concentration tasks, e.g. driving for the first 24h after UVkEc injection.

2.2.3 Preparation and injection UV-killed *E. coli* (UVkEc)

E. coli bacteria (Strain: NCTC 10418, Source: Public Health England, UK) were a kind gift from Dr Andrew Smith (UCL Division of Medicine). Using a wire loop, an aliquot of bacteria was transferred into Luria- Bertani broth (LB broth) (LB broth was prepared by mixing LB broth powder (Sigma) at 20 gm/L in distilled water followed by autoclaving). *E. coli* bacteria were incubated overnight at 37^0 C in LB broth. Next morning the LB broth was centrifuged (2500 x *g*, 20 min, 4^0 C) to pellet the bacteria. The bacterial pellet was washed twice (2500 x *g*, 5 min, 4^0 C) using sterile PBS and was then suspended in sterile saline (Braun). Bacteria in saline were transferred to a petri dish and were killed by exposure to ultraviolet light (UV) source (302 nm, ChemiDoc, trans-UV mode) for 60 min. The UV exposed bacteria were washed again using sterile saline. The non-viability of bacteria was confirmed by the testing absence of culture on the LB agar plate. Bacterial count was estimated using a spectrophotometer using the formula: OD_{600} = 0.365 equates to 10^8*E. coli*/ml (derived by Dr Andrew Smith, Division of Medicine). The final aliquots were prepared in sterile saline to contain 1.5 x 10^8 bacteria per ml of saline and were stored at -80 ^{0} C. The non-viability of frozen sample was again confirmed by UCLH (University College London Hospitals, UK) Microbiology department.

On the day of the study, the aliquot of frozen UVkEc in saline was thawed 30 min before volunteer arrival. The thawed tube was vortexed, and the bacteria were aspirated in 1 ml syringe. The skin on the volar aspect of forearm not overlying the subcutaneous veins was marked. The marked site was

disinfected and dry shaved and 1.5 x 10^7 UVkEc in 100 µl of sterile saline were injected intradermally where the site was marked **(Figure 2.4 A).**

2.2.4 Laser Doppler Imaging.

Laser Doppler Imager (moor LDI-HIR, Moor Instruments Ltd, Axminster, Devon, UK) was used to quantify the vascular hyperaemia (blood flow) at the site of inflammation. It is based on the principle of Doppler shift. The frequency of a monochromatic light source is broadened (shifted) after it is scattered by moving red blood cells (RBCs) [184].

To assess vascular hyperaemia, the inflamed site on the forearm was placed under the scanner at a fixed distance. The laser beam emitted by the scanner head of the imager is scattered by RBCs in the inflamed area. The reflected light rays with broadened frequency are then detected by a photo detector of the imager. The scatter (Doppler frequency shift) is proportional to velocity and number of red blood cells at the site and is measured as a photocurrent signal. The strength of this signal from different parts of the inflamed site is represented by an image. This image called a flux image is composed of a colour spectrum, where each colour indicates the degree of vascular hyperaemia. The flux images were analysed by moorLDI software (Version 5.2) and the vascular hyperaemia (measured in perfusion units) was obtained by multiplying the number of valid pixels in the flux image above the background signal (Cut-off = 300 perfusion units) with the mean signal over the valid pixels [182, 183] **(Figure 2.4 B)**

2.2.5 Suction Blister Technique

Suction blister was raised directly above the UVkEc triggered site to obtain the inflammatory exudate from the site (**Figure 2.3)**. This procedure is modified version of the procedure described previously [187]. To raise a suction blister, a suction chamber was placed over the marked injection site and then strapped on the forearm. The chamber was made of three parts: an aluminium plate with 10 mm aperture, a nylon cup, and a transparent glass lid, all secured by a detachable air-tight seal. The suction chamber was connected to negative pressure instrument (NP-4, Electronic diversities Ltd., MD, USA). After ensuring the position of the suction chamber to the forearm, the negative pressure was applied gradually at a rate of 1 inch of mercury (in of Hg) every 5 min until a bleb was observed. At this point, the pressure was kept constant until a uniloculated blister covering the surface area within the aperture was formed. After a complete blister had been formed, the pressure was lowered gradually at the rate of 1 in of Hg per min. The suction chamber was unstrapped carefully without disturbing the formed blister. The duration of suction blister induction process varied from 1.5-2h depending on the volunteer and phase of inflammation **(Figure 2.4 C).**

Suction blister was aspirated immediately after formation. Firstly, the blister roof was pierced along its lateral border using a 26.5 gauge needle. The blister exudate was then gently pushed out on the skin by rolling a 1 ml syringe over the blister surface and was simultaneously aspirated using a 200 µl pipette. **(Figure 2.4 D)** The aspirated blister site was cleaned using an aseptic solution

(0.1% Cetrimide), and the site was covered with a protective dressing. Volunteers were asked to keep the site dry until a scab formed.

The fluid was collected into a 96 well plate containing 50 µl of 3% sodium citrate. The plate was then centrifuged at 1000 x *g* for 5 min at 4^0 C to separate the cells from the supernatant. After centrifugation, the resulting cell pellet obtained was suspended in 200 µl of RBC lysis buffer (Lonza) to lyse the RBCs. RBC deplete cell pellet was suspended in 100 µl of FACS buffer and processed for cell counting as described in section 2.5 and for flow cytometry as described in section 2.6. The supernatant was aliquoted and stored at -80 ^{0}C.

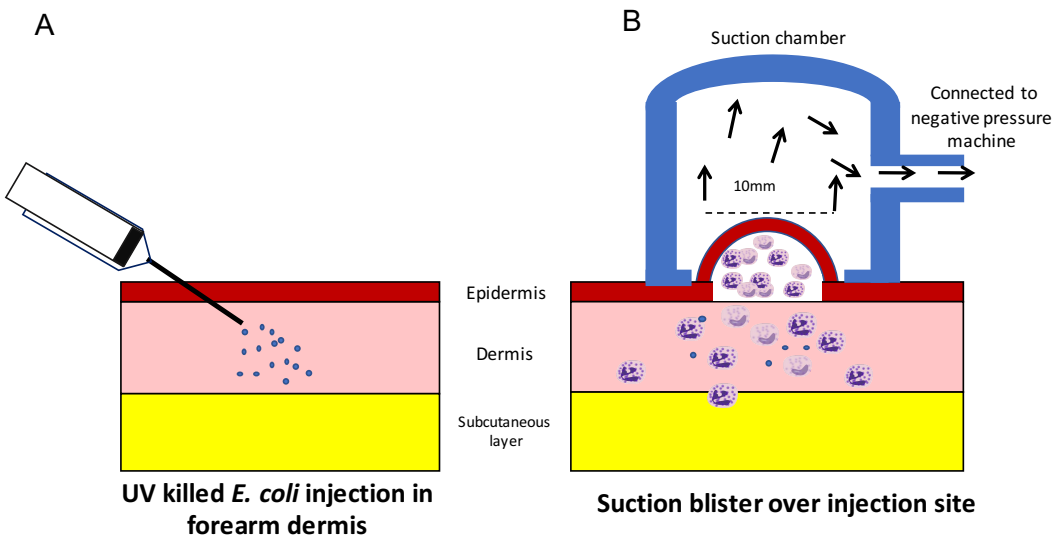

Figure 2.3 Graphic showing the technique of intradermal injection of UV killed *E. coli* (A) and acquisition of inflammatory exudate using suction blister (B)

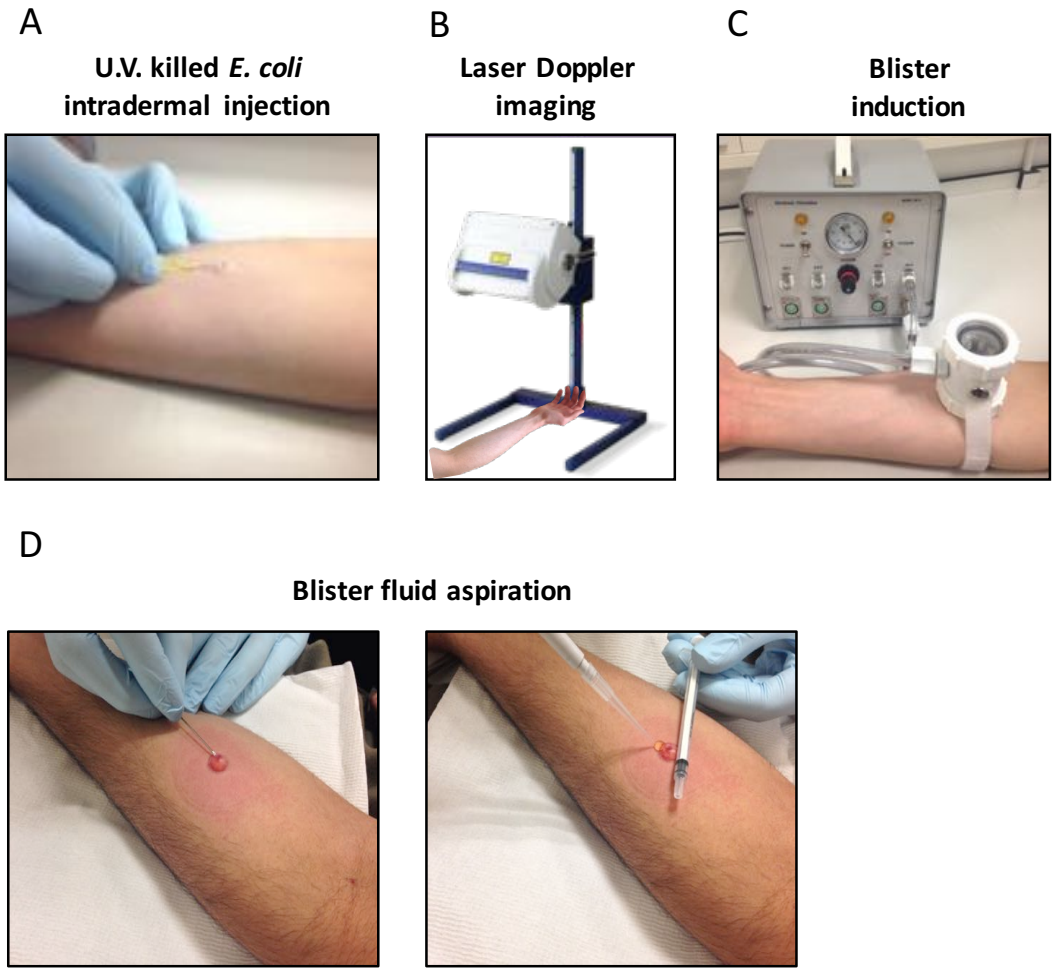

Figure 2.4 Study procedures involved in the UVkEc triggered self resolving dermal inflammation

Acute inflammation was triggered in the ventral aspect of the forearm of healthy volunteers by the intradermal injection of 1.5 x 10^7 UV killed *E. coli* (UVKEc) suspended in 100ul of sterile saline (A). After a certain interval, depending on phase of acute inflammation being investigated, the injected site was scanned by a laser Doppler imager to quantify local blood flow (B). Subsequently, a suction chamber connected to a negative pressure instrument was placed over the injection site to raise a 10mm blister to acquire the inflammatory exudate present at the site (C). Immediately after formation of the the blister, its roof was pierced using a sterile needle and the inflammatory exudate were aspirated by a pipette (D).

2.2.6 Volunteer feedback on the tolerability of UVkEc triggered self-resolving dermal inflammation model.

Volunteer feedback on the discomfort associated acute inflammation symptoms and due to research procedures employed in UVkEc triggered self-

resolving dermal inflammation model was obtained using an online questionnaire. The online questionnaire was prepared on the https://www.surveymonkey.com, and the link to the feedback form was sent to volunteers. Responses from the volunteers were anonymised.

2.3 Cell counting

Blister exudate was centrifuged to separate cells from the supernatant. Cells were suspended in FACS buffer and supernatant was transferred to a 1.5 ml microcentrifuge tube (Eppendorf) tube. Cell count was obtained using a manual haemocytometer. 10 µl of this cell suspension was mixed 1:1 with 0.4% trypan blue and 10 µl of this mixture was loaded on to the haemocytometer (C-chip, Digital-Bio Ltd.) and placed on a light microscope (Olympus). Total cell count, blister fluid volume and cell count/ml were obtained as below:

-Total cell count = Cell count in $1mm^2$ square (average numbers of cells in four corner squares of haemocytometer) x 10^4 x 2 x cell suspension volume (ml).

-Blister fluid volume = (Weight of microcentrifuge tube with blister supernatant) - (weight of microcentrifuge tube).

-Cell count/ml = Total cell count/ blister fluid volume

The leucocyte count in inflammatory exudate obtained in Chapter 6, was obtained using an automatic cell counter (ADAM MC 2000, Nanoetek).

2.4 Flow cytometry

Immune cell subsets in the blister fluid were phenotyped by multicolour flow cytometry. For cell surface marker staining, blister cells in 100 µl of FACS buffer were incubated for 30 min with an antibody cocktail (Flow cytometry antibodies specific for each study are described in Table 2.1, Table 2.2 and

Table 2.3 below). Stained samples were washed twice with wash buffer (1% FCS in PBS + 2 mM EDTA) at 1000 x *g* for 5 min, 4^0 C. The washed cell pellet was then suspended in 150µl of wash buffer followed by 150µl of 1% formaldehyde (Thermo Fischer) to fix the cells, and the mixture was transferred to 1 ml FACS tubes. Fixed samples were stored in the dark at 4^0 C and analysed within 24h on BD LSR Fortessa flow cytometer. Spectral overlap between fluorochromes was corrected by running single fluorochrome stained compensation beads (BD) before main samples. For apoptotic cell staining, cells were incubated with AnnexinV-FITC and 7AAD (BD apoptosis detection kit) and were acquired on flow cytometer without fixation and within 15 min. Flow cytometry data was analysed using FlowJo 7.6.1. The dilution of antibody used here was obtained after titration on peripheral blood leucocytes. Here, the positive events were identified by using fluorescent minus one (FMO) control, which contains all antibodies except the one of interest. The gating strategy to identify leucocyte subpopulations was first characterised on peripheral blood leucocytes (described in Chapter 3, Figure 3.1 and 3.2).

Table 2.1 Flow cytometry antibodies used for identification of leukocytes in the study characterising cantharidin skin blister model (Chapter 3)					
Serial no.	**Cell surface marker**	**Antibody clone**	**Fluorescent conjugate**	**Dilution**	**Manufacturer**
1	CD3	UCHT1	APC	1:10	BD Biosciecnes
2	CD14	M5E2	AF400	1:40	BD Biosciecnes
3	CD16	3G8	FITC	1:5	BD Biosciecnes
4	CD19	SJ25C1	PE-Cy7	1:40	BD Biosciecnes
5	CD56	B159	PerCP-Cy5.5	1:40	BD Biosciecnes
6	Siglec-8	7C9	PE	1:20	Biolegend
7	HLA-DR	L243	V450	1:40	BD Biosciecnes
8	CD163	GHI/61	PE	1:20	BD Biosciecnes

Table 2.2 Flow cytometry antibodies used for identification of leukocytes in the study characterising UVkEc triggered self resolving dermal inflammation model and in the study investigating effects of SPMs using this model. (Chapter 4 and Chapter 5)

Serial no.	Cell surface marker	Antibody clone	Fluorescent conjugate	Dilution	Manufacturer
1	CD3	HIT3a	FITC	1:80	Biolegend
2	CD4	RPA-T4	AF400	1:80	Biolegend
3	CD8	RPA-T8	BV510	1:80	Biolegend
4	CD14	M5E2	BV605	1:80	Biolegend
5	CD16	3G8	APC	1:100	Biolegend
6	CD45	HI30	BV785	1:80	Biolegend
7	CD19	HIB19	FITC	1:80	Biolegend
8	CD56	HCD56	PerCP-Cy5.5	1:80	Biolegend
9	HLA-DR	G46-6	APC-H7	1:40	BD Pharmingen
10	CD62L	MEL-14	PE-Cy7	1:80	Biolegend
11	CD1c	L161	BV421	1:80	Biolegend
12	CD163	M80	PE	1:100	Biolegend

Table 2.3 Flow cytometry antibodies used for identification of leukocytes in the study investigating pro-resolving effect of JBT-101 in UVkEc triggered self resolving dermal inflammation model (Chapter 6)					
Serial no.	**Cell surface marker**	**Antibody clone**	**Fluorescent conjugate**	**Dilution**	**Manufacturer**
1	CD3	HIT3a	FITC	1:80	Biolegend
2	CD14	M5E2	BV605	1:80	Biolegend
3	CD16	3G8	APC	1:100	Biolegend
4	CD19	HIB19	FITC	1:80	Biolegend
5	CD45	HI30	BV785	1:80	Biolegend
6	CD56	HCD56	FITC	1:80	Biolegend
7	CD62L	MEL-14	PE-Cy7	1:80	Biolegend
8	CD86	IT2.2	PerCP-Cy5.5	1:50	Biolegend
9	HLA-DR	L243	BV510	1:50	Biolegend
10	CD163	M80	BV421	1:80	Biolegend

2.5 Peripheral blood analysis

Peripheral blood was obtained from the volunteer's antecubital vein using a 21-gauge butterfly needle (BD). Depending on the downstream application, blood was drawn into different anticoagulant vacutainers.

For flow cytometry on peripheral blood leucocytes, blood was drawn into ethylenediaminetetraacetic acid (EDTA) vacutainer. For this application, red blood cells (RBC) in the blood were first lysed by incubating EDTA anticoagulated blood 1:10 in RBC lysis buffer (Lonza) for 5-10 min until the solution turned translucent. The solution was then centrifuged at 300 x *g* for 5

min at room temperature. The supernatant containing plasma and lysed RBCs was discarded, and the leucocyte pellet was washed using 5 ml of wash buffer. Washed pellet was suspended in 1 ml of FACS buffer and processed for flow cytometry.

For peripheral blood differential count analysis, the vacutainer containing EDTA anticoagulated blood was sent to TDL (The Doctor's Laboratory, UK) pathology lab.

For measurement of systemic CRP, a serum sample was sent to TDL pathology lab. To prepare serum sample, blood was collected in BD Vacutainer SST tubes and first allowed to clot for 30 min. After 30 min, the tubes were centrifuged at 1300 x *g* for 10 min at RT.

For systemic cytokine response, multiplex ELISA was performed on the plasma sample. To prepare plasma, blood was collected in lithium heparin vacutainer (BD) and centrifuged immediately at 2500 x *g*, 10 min at RT. Separated plasma was aliquoted and stored at -80^0 C until analysed.

2.6 Skin biopsy and immunohistochemistry

Skin biopsy procedure was performed by the clinicians in the Gilroy Laboratory (Dr Julia Flint, Dr Marc George, Dr Daniel Marks). Acu-Punch 3 mm kit (Schuco) kit, containing the 3mm punch biopsy needle was used. Skin was cleaned using alcohol and povidone-iodine. It was then anaesthetized using 1% lignocaine. After ensuring that the site is numb, a 3mm skin punch biopsy

needle was inserted, and the biopsy was collected using disposable forceps. The skin biopsy was irrigated with saline and then transferred in neutral buffered formalin. The biopsied site was compressed using sterile gauze and then protected using a water proof dressing. Aseptic technique was followed throughout all steps. Volunteers were advised to keep the site dry and maintain the dressing for at least 72h.

Formalin-fixed biopsies were transferred to UCL Institute of Neurology for immunohistochemistry. The antibodies used for immunohistochemistry are as follows: rabbit anti-human FPR2 (Novus Biologicals), rabbit anti-human ChemR23 (Thermo Scientific), rabbit anti-human GPR32 (Thermo Scientific), rabbit anti-human GPR18 (Lifespan Biosciences). Negative controls were stained for a corresponding isotype control. The digital images of the stained slides were obtained on a Nanozoomer (Hamamatsu) at UCL Rayne Institute.

2.7 Cytology

The cell populations of interest were first sorted on BD FACS Aria. For cell sorting, blister cells were suspended in 500 µl of FACS buffer in FACS tubes (BD). Cells were sorted in FACS buffer and after a wash step (1000 x *g* for 5 min, 4^0 C) they were suspended in 150 µl of PBS.

Cells in PBS were centrifuged on poly-lysine glass slides (Thermo Scientific) using a cytospin (Thermo Shandon) at 800 RPM (revolutions per minute), 8 min. Cell smear on the slide was allowed to air dry for 10 min and followed by fixation in methanol. After methanol fixation, the slides were stained by

Modified Wright-Giemsa staining (Kwik-Diff Method, Thermo Shandon). The staining procedure involved incubation of slides for 10 seconds in eosin solution followed by 5 seconds on methylene blue solution at room temperature. Stained slides were washed in distilled water and then air dried. Immediately after drying, the slides were dipped in xylene solution for 5 min. Xylene coated slides were mounted using a DPX mounting media (Sigma Aldrich) followed by placement of a cover slip on the smear area. Images were obtained using Optimus BX41 microscope and processed using Image Pro 6.3.

2.8 Lipid mediator profiling

Lipid mediator analysis by liquid chromatography- mass spectrophotometry (LC-MS) on the inflammatory exudate was performed by external collaborators. Prof. Anna Nicolaou (University of Bradford) performed lipidomics of cantharidin blister exudate. Prof Charles Serhan (Harvard University) performed lipidomics of UVkEc triggered inflammatory exudate. Data was analysed at UCL.

2.9 Preparation of SPM cocktail for injection

SPM cocktail (comprising LXB_4, RvE1, RvD2 and AT-RVD1) was prepared in sterile saline and validated for purity by Dr Jesmond Dalli, Queen Mary University of London (QMUL). Dr Dalli also ensured that the purity was >98% and the endotoxin content was below detection limits (< 0.1 EU/ml). The final concentration of each SPM in the cocktail was as follows: LXB_4 (570 pM = 200

pg/ml), RvE1 (115 pM = 40 pg/ml), RvD2 (450 pM = 170 pg/ml), AT-RvD1 (3.2 nM = 1200 pg/ml).100 µl of this cocktail solution was used for intradermal injection. The cocktail was prepared fresh by Dr Dalli and collected from QMUL University on the morning of the day of the injection.

2.10 Multiplex ELISA

Cytokines in the blister fluid were measured by V-PLEX Proinflammatory multiplex ELISA kit (Meso Scale Discovery, USA).

MSD multiplex ELISA is based on an electro-chemiluminescence principle. Each well in the 96-well plate had ten spots, each spot specific for a cytokine and coated with a cytokine specific capture antibody. After addition of test sample, the capture antibody binds to the analyte in the sample. The bound analyte is then sandwiched by the addition of a cytokine specific detection antibody. The detection antibody is tagged to an electro-chemiluminescent label (MSD SULFO-TAG™). The plate is read on an MSD reader that quantifies the intensity of light emitted from each spot in the well and the intensity is directly proportional to the amount of analyte present in the sample [188].

The ELISA protocol consisted four main steps

1) Preparation of standards
2) In-well dilution addition of cell free blister exudate sample
3) Addition of detection antibody

4) Signal acquisition on MSD reader

The highest concentration standard was prepared by adding 1000 µl of dilution reagent 2 in multi-analyte lyophilized calibrator vial (both supplied by MSD). The highest standard was diluted down 1:4, six times to generate seven tubes representing seven standard points for the standard curve. A final eight standard point consisted of the tube containing diluent 2 only. 50µl volume from each standard point tube was added to the standard curve column of the plate in duplicate.

The blister fluid sample was diluted 1:10 with diluent 2 directly in the plate to get a final volume of 50 µl. The 96-well plate containing standards and samples was sealed using an adhesive film and incubated at room temperature on a shaker at 1000 RPM for 2h. After the incubation period, the plate was washed 3 times with 150 µl of ELISA wash buffer (0.05 % Tween 20 in PBS) to remove the unbound analyte.

After the final wash above, 25 µl of detection antibody mix was added to each well of the plate. Detection antibody mix contained detection antibody for each cytokine or chemokine in dilution reagent 3 (both supplied by MSD). The plate was sealed again incubated at room temperature on a shaker at 1000 RPM for 2h. After the incubation period, the plate was washed three times with 150 µl of ELISA wash buffer (0.05 % Tween 20 in PBS) to remove unbound detection antibody.

After the final wash in above step, 50 µl of read buffer (diluted 1:2 in PBS) was added to each well of the plate. The plate was read immediately on the MSD Sector Imager 6000 to acquire the analytical signal. The data file was analysed on MSD Discovery Workbench software.

2.11 Kinetic turbidimetric Limulus amebocyte lysate (LAL) assay for measuring endotoxin

Endotoxin in the blister exudate was measured using the Pyrogent-5000 endotoxin measurement kit (Lonza). The test is based on the principle that gram-negative endotoxin causes the formation of a clot upon contact with lysate from the amebocytes of horse shoe crab (Limulus polyphemus). The turbidity of clot is directly proportional to levels of endotoxin in the sample. By comparing a fixed level of clot turbidity between test samples and endotoxin standards, the levels of endotoxin in the samples can be obtained [189]. The above method of measuring endotoxin is termed as kinetic turbidimetric LAL (Limulus amebocyte lysate) assay.

For use with this kit, the cell-free blister exudate was first treated to denature proteins by diluting 1:20 in 0.1% tween 80 buffer (Sigma) to a final volume of 100 µl, followed by heating at 70^0 C for 15 min as recommended previously for human biological matrices [190]. Endotoxin standards were prepared by diluting the stock endotoxin solution 1:10, five times in 0.1% tween 80 buffer to a final volume of 100 µl. 50 µl of treated samples was plated on a 96 well flat bottom cell culture plate (COSTAR) along with the endotoxin standards. After this step, the plate was incubated for 10 min at 37^0 C. Following the incubation, 50 µl of LAL reagent was added to each well, and then the plate

was immediately transferred to the microplate reader (OmegaStar, Biorad). As per manufacturer's instructions, clot turbidity was measured by assessing the optical density at 340nm every 60 seconds for 2 h and increase in absorbance by 0.03 was set as the threshold for turbidity. The values relative to the endotoxin standard are reported here.

2.12 Statistical analysis

GraphPad Prism software (Version 7) was used for generating figures and for statistical analysis. Data are presented as individual values with the mean ± standard deviation (SD) on a linear scale, but in the case of skewed data sets, the data are presented on a logarithmic scale.

For statistical testing, data were first assessed for normal distribution using the normality tests recommended by the software. For normally distributed data, differences between two groups were tested for statistical significance by paired t test (if paired data) or unpaired t test (if unpaired data). For more than two groups, differences were detected by Ordinary one-way ANOVA (for unpaired data) followed by Bonferroni's test to correct for multiple comparisons.

For non-normally distributed data, differences between two groups were tested for statistical significance by Wilcoxon matched pairs signed rank test (if paired data) or Mann-Whitney test (if unpaired data). For more than two groups, differences were detected by Kruskal-Wallis test (for unpaired data) followed by Dunn's test to correct for multiple comparisons.

A p value < 0.05 was taken as threshold for significance. The p values are indicated as follows: < 0.05 = ' * ', <0.01 = ' ** ', <0.001 = ' *** '.

Chapter 3

Characterisation of onset and resolution phase in cantharidin induced skin blister model of acute inflammation

3.1 INTRODUCTION

Cantharidin induced skin blister model lends itself to investigate both the onset and the resolution phase of acute inflammation. For instance, it has been utilised to show that anti-TNFα antibody and corticosteroids inhibit neutrophil migration at onset [177] and has also been to demonstrate the effect of low dose aspirin on the formation of 15-epi-lipoxins and neutrophil clearance during resolution [176]. However, a detailed characterisation of leucocytes, cytokines and lipid mediators during onset as well as resolution in this model is lacking. In this chapter, I investigated the above three parameters and highlighted the uses and limitations of the cantharidin skin blister model for studying resolution in humans. This study was done in collaboration with Dr William Jenner.

3.2 STUDY DESIGN

Each volunteer was asked to the make three visits to the laboratory. On the first visit, cantharidin was applied on two sites on one of the forearms, and a 5 ml sample of peripheral blood was collected from the contralateral forearm. The second visit was 24h later, during which one of the blisters was aspirated to investigate the onset phase and the other blister was covered with a protective dressing. The third visit was 72h after cantharidin application, and at this time the remaining blister was aspirated to investigate the resolution phase. The technique is described in detail in methods section 2.1 **(Figure 2.1 and Figure 2.2)**.

3.3 RESULTS

3.3.1 Flow cytometric characterisation of peripheral blood leucocytes

The flow cytometric gating strategy was first validated on peripheral blood leucocytes. After exclusion of cell debris and doublets **(Figure 3.1 A)**, the remaining total leucocyte population was firstly gated for $CD3^+$ T cells and $CD19^+$ B cells **(Figure 3.1 C)**. Resulting $CD3^-/CD19^-$ cells were then gated on CD56 to identify $CD56^+$ NK cells **(Figure 3.1D)**. The remaining leucocytes

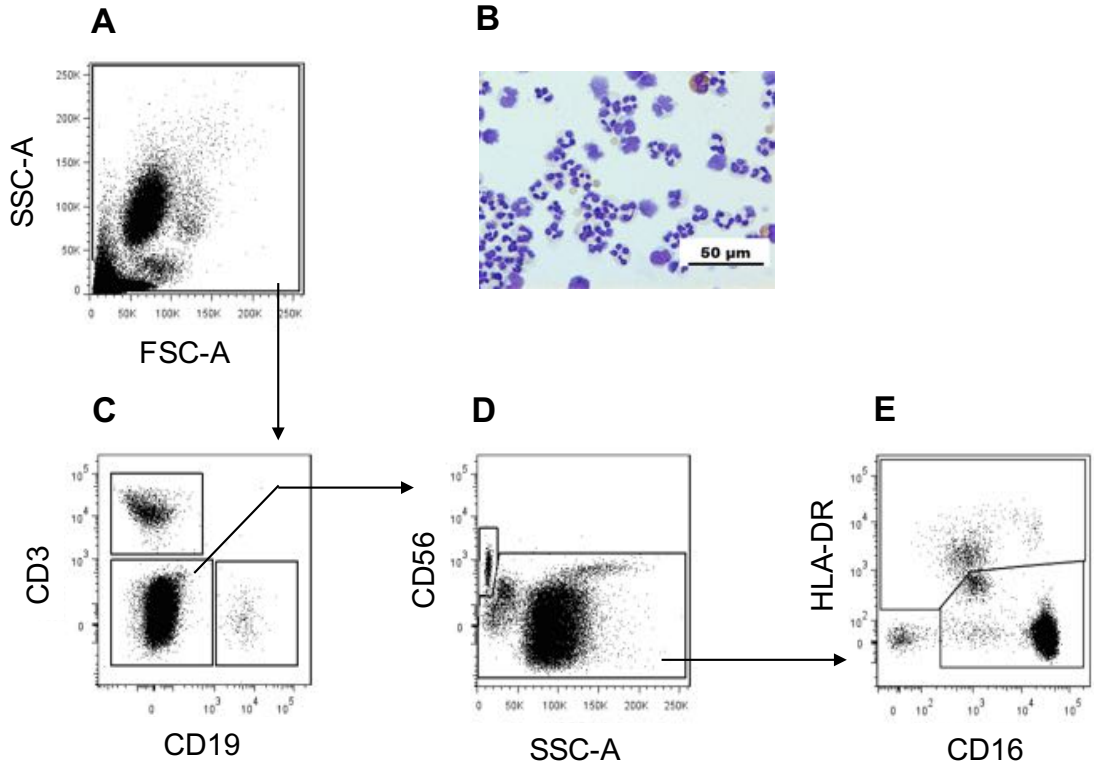

Figure 3.1 Polychromatic flow cytometric characterisation of peripheral blood leukocytes – I

Leucocytes from the peripheral blood of healthy volunteers were incubated with an antibody cocktail and phenotyped by flow cytometry. The FSC (size) vs SSC (granularity) plot of total leucocytes **(A)** and the modified Wright-Geimsa stained cytospin of total leucocytes **(B)** is shown. The FSC vs SSC plot was probed to first identify lymphocytes including $CD3^+$ T cells, $CD19^+$ B cells **(C)** and $CD56^+$ NK cells **(D)**. Remaining cells were divided into $HLA\text{-}DR^+$ and $HLA\text{-}DR^-$ cells **(E)** and characterised further in Figure 3.2. Representative gating plots are shown here

were then differentiated by HLA-DR expression **(Figure 3.1 E)**. This allowed for separate classification of HLA-DR^{+} mononuclear and HLA-DR^{-} granulocytic populations, as has been previously described [191].

Analysis of HLA-DR^{+} gate **(Figure 3.2 A)** revealed the expected distribution of classical CD14^{++}/CD16^{-}, intermediate CD14^{++}/CD16^{+}, and non-classical CD14^{+}/CD16^{+} monocytes **(Figure 3.2 B)** possessing varying degrees of the scavenger receptor marker, CD163 **(Figure 3.2 C, D, F)** [192]. Within this HLA-DR^{+} population we also identified CD14^{-} CD16^{-} dendritic cells, which upon extended characterisation were identified to be a mixture of CD141^{+} and CD11c^{+} dendritic cells **(Figure 3.2 E).**

The HLA-DR^{-} gate **(Figure 3.2 A)** comprised two sub-populations with varying degree of expression for CD16, labelled here as CD16^{hi} and CD16^{lo} **(Figure 3.2 G).** CD16^{hi} population was identified as neutrophils, confirmed by expression of CD66b **(Figure 3.2 H)**. On extended characterisation, the CD16^{lo} cells in blood were identified as Siglec-8^{+} eosinophils **(Figure 3.2 I, J).**

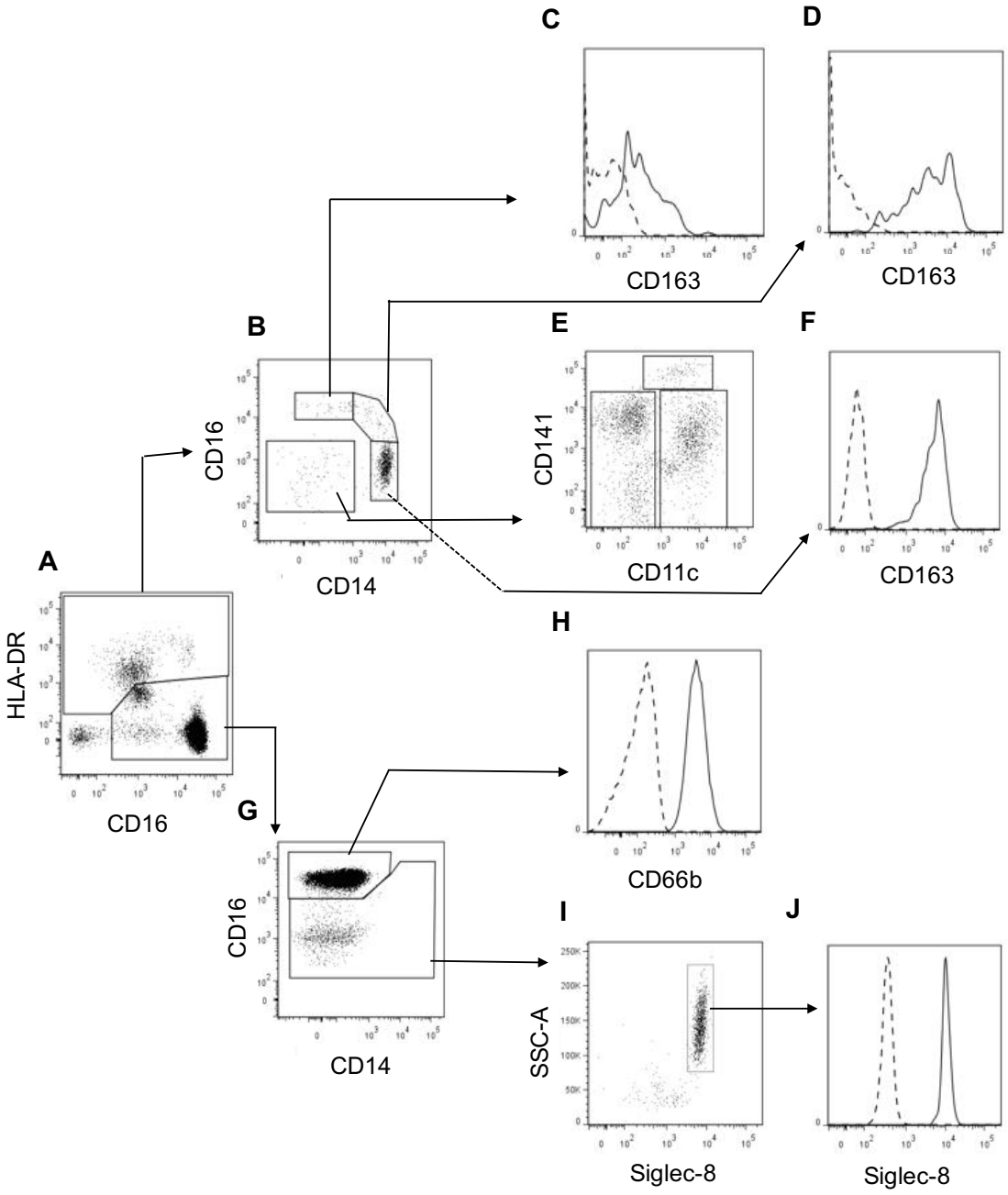

Figure 3.2 Polychromatic flow cytometric characterisation of peripheral blood leukocytes- II

HLA-DR$^+$ and HLA-DR$^-$ cells identified **in Figure 3.1E** were further analysed **(A)**. HLA-DR$^+$ cells were characterised into classical monocytes (CD14^{++}/CD16$^-$), intermediate monocytes (CD14^{++i}/ CD16$^+$) , non classical monocytes (CD14$^+$/CD16$^+$ monocytes) and dendritic cells (CD14$^-$/CD16$^-$) **(B)**. The expression of CD163 on classical monocytes **(C)**, intermediate monocytes **(D)** and non classical monocytes **(E)** is also shown. On extended characterisation, HLA-DR$^+$/CD14$^-$/CD16$^-$ dendritic cells comprised subpopulations of CD141$^+$ and CD11c$^+$ dendritic cells **(E)**. HLA-DR$^-$ cells comprised neutrophils (CD16^{hi}, CD66$^+$) **(H)** and a CD16^{lo} population which mainly comprised Siglec-8$^+$ eosinophils **(I, J).** Representative gating plots are shown here.

3.3.2 Flow cytometric characterisation of leucocytes in cantharidin skin blister at 24h and 72h

Skin blister aspirated 24h following cantharidin application showed a robust inflammatory cell infiltrate, also evident by cytology **(Figure 3.3 B)**. By utilising the gating strategy developed for peripheral blood leucocytes, 24h blister exudate revealed mainly $CD3^+$ T and $CD56^+$ NK cells **(Figure 3.3 C, D).** The remaining population was then probed for HLA-DR expression as for circulating leucocytes, and separated into the $HLA\text{-}DR^+$ and $HLA\text{-}DR^-$ cells **(Figure 3.3 E)**.

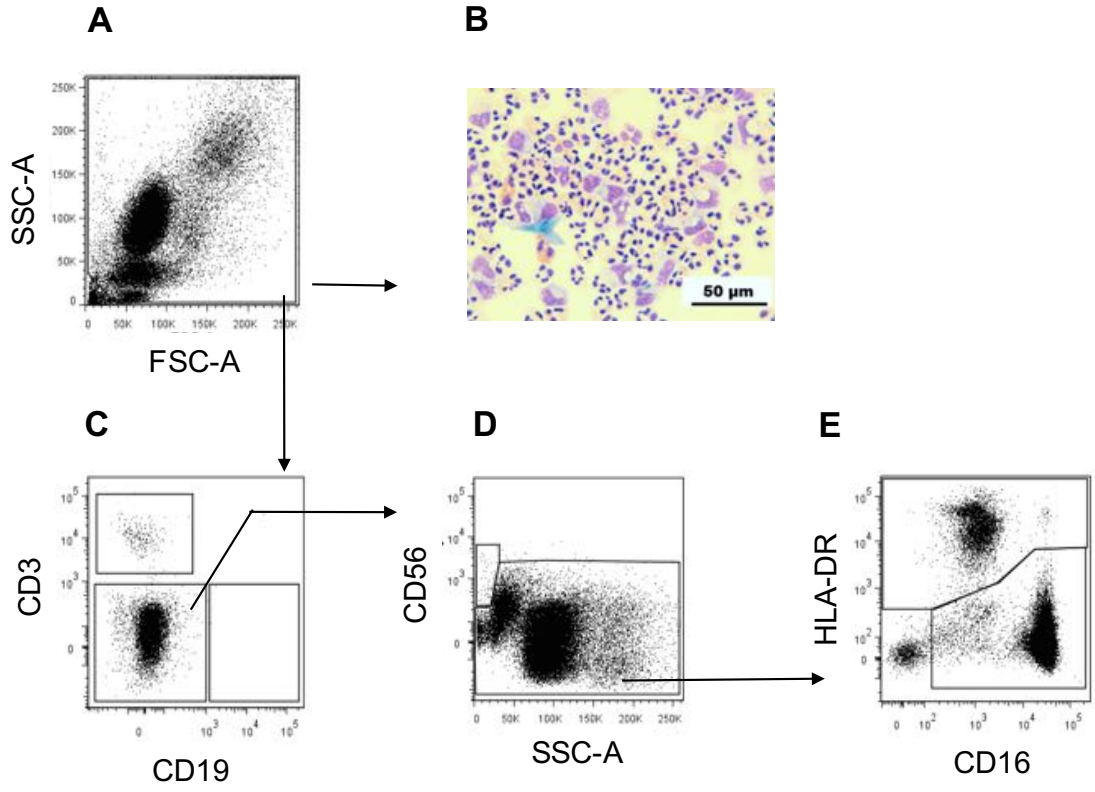

Figure 3.3 Polychromatic flow cytometric characterisation of leucocytes in cantharidin skin blister at 24hr (onset) – I

24hr after application of cantharidin, the blister was aspirated and the exudate was collected in 3% sodium citrate. Leukocytes in the blister were incubated with an antibody cocktail and phenotyped by flow cytometry. The FSC (size) vs SSC (granularity) plot of total leucocytes **(A)** and the modified Wright-Geimsa stained cytospin of total leucocytes **(B)** is shown here. Based on the gating strategy for peripheral blood described in Figure 3.1, $CD3^+$ T cells **(C)** and $CD56^+$ NK cells **(D)** were first identified and the remaining cells were divided into $HLA\text{-}DR^+$ and $HLA\text{-}DR^-$ cells **(E)**. Representative gating plots are shown here

The $HLA\text{-}DR^+$ population **(Figure 3.4 A)** comprised $CD14^+/CD16^-$ monocytes/macrophages expressing CD163 **(Figure 3.4 B, C)**, and a $CD14^-$ $CD16^-$ dendritic cell population, which upon extended characterisation, constituted three dendritic cell subpopulations: $CD11c^+$, $CD141^+$, and $CD11c^+/CD141^+$ **(Figure 3.4 D).**

The $HLA\text{-}DR^-$ population, included $CD16^{hi}$ and $CD16^{lo}$ cell populations **(Figure 3.4 E)**. $CD16^{hi}$ population labelled positive for CD66b and was identified as neutrophils **(Figure 3.4 F)**. The $CD16^{lo}$ cells comprised two different

populations with varying autofluorescence and side scatter. The autofluorescent $CD16^{lo}SSC^{hi}$ were identified as Siglec-8^{+} eosinophils **(Figure 3.4 H)**, whereas $CD16^{lo}SSC^{lo}$ population stained positive for apoptotic cell marker, Annexin-V/7AAD and were characterised as apoptotic neutrophils, as reported previously **(Figure 3.4 G)** [193]**.**

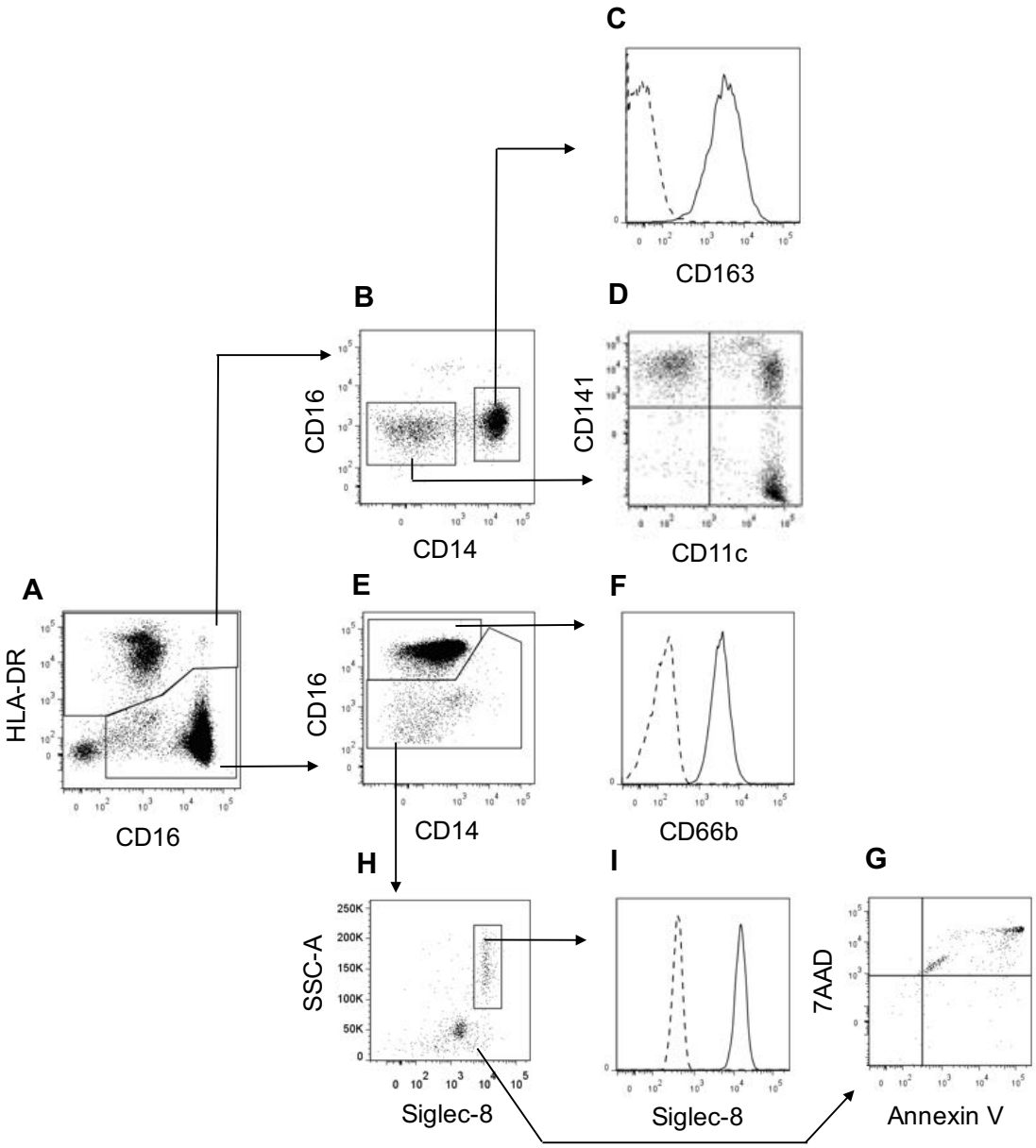

Figure 3.4 Polychromatic flow cytometric characterisation of leucocytes in cantharidin skin blister at 24hr (onset) – II

24hr after application of cantharidin, the blister was aspirated and the exudate was collected in 3% sodium citrate. HLA-DR$^+$ and HLA-DR$^-$ cells identified in Figure **3.3E** were further analysed **(A)**. HLA-DR$^+$ cells mainly comprised of CD14$^+$/CD16^{lo} monocytes/macrophages and HLA-DR$^+$/CD14$^-$/CD16$^-$ dendritic cells **(B)**. The expression of CD163 on CD14$^+$/CD16$^-$ monocytes/macrophages **(C)** is also shown. On extended characterisation, HLA-DR$^+$/CD14$^-$/CD16$^-$ dendritic cells comprised subpopulations of CD141$^+$ and CD11c$^+$ dendritic cells **(D)**. HLA-DR$^-$ cells comprised neutrophils (CD16^{hi}, CD66b$^+$) **(E,F)** and a population of CD16^{lo} cells which comprised of Siglec-8$^+$ eosinophils **(H, I)** and AnnexinV/7AAD$^+$ apoptotic/dead neutrophils **(G).** Representative gating plots are shown here.

Flow cytometric characterisation of the 72h blister is outlined in **Figure 3.5** and **Figure 3.6.** The gating strategy employed here is similar to one carried out for the 24h time point. In addition, the major 72h leucocyte subsets were sorted using flow cytometer and assessed for their morphological appearance to confirm the phenotype. HLA-DR^{-}CD16^{++} neutrophils revealed the classical polymorphonuclear appearance (**Figure 3.6 E)**, whilst HLA-DR^{+} CD14^{+} monocytes/macrophages were large mononuclear cells with a kidney shaped nucleus and vacuoles in the cytoplasm (**Figure 3.6 D)**. Siglec 8^{+} cells displayed a characteristic eosinophil morphology, namely a typical bi-lobed nucleus along with red cytoplasm (**Figure 3.6 I)**. CD16^{lo} AnnexinV/PI^{+} cells

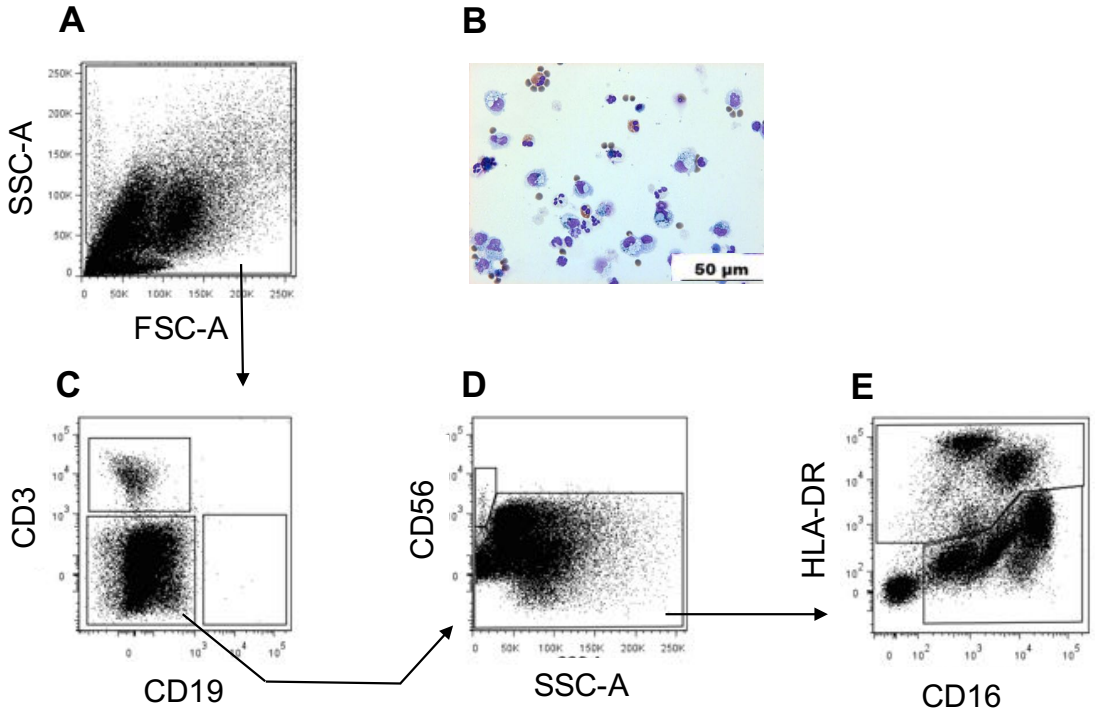

Figure 3.5 Polychromatic flow cytometric characterisation of leucocytes in cantharidin skin blister at 72hr (resolution) – I

72hr after application of cantharidin, the blister was aspirated and the exudate was collected in 3% sodium citrate. Leukocytes in the blister were incubated with an antibody cocktail and phenotyped by flow cytometry. The FSC (size) vs SSC (granularity) plot of total leucocytes **(A)** and the modified Wright-Geimsa stained cytospin of total leucocytes **(B)** is shown here. Based on the gating strategy for peripheral blood described in Figure 3.1, CD3^{+} T cells **(C)** and CD56^{+} NK cells **(D)** were first identified and the remaining cells were divided into HLA-DR^{+} and HLA-DR^{-} cells **(E)**. Representative gating plots are shown here.

appeared either as degranulated cells or cells with condensed nuclei **(Figure 3.6 G)** [194].

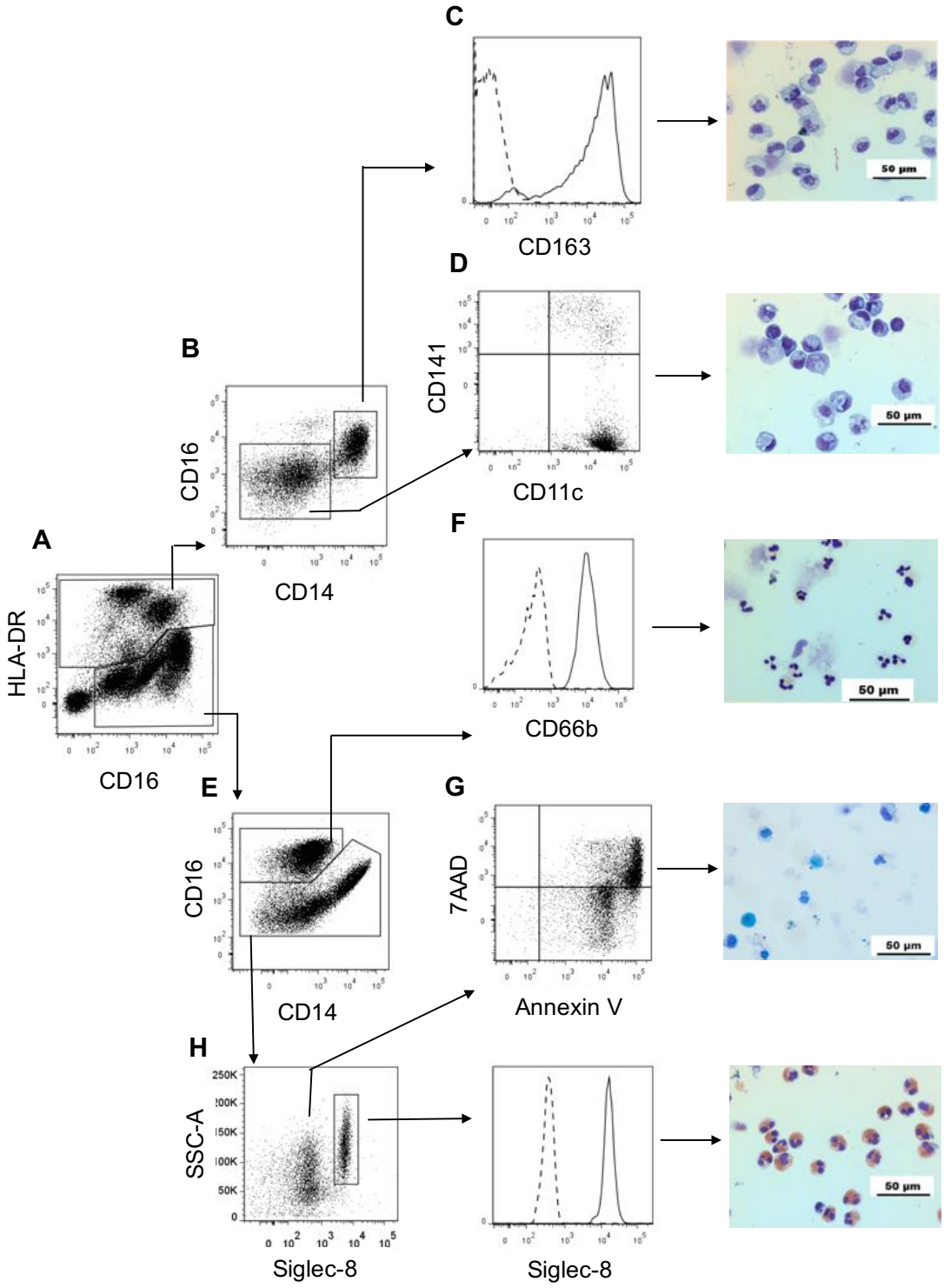

Figure 3.6 Polychromatic flow cytometric characterisation of leucocytes in cantharidin skin blister at 72hr (resolution) – II

72hr after application of cantharidin, the blister was aspirated and the exudate was collected in 3% sodium citrate. HLA-DR$^+$ and HLA-DR$^-$ cells identified in Figure **3.3E** were further analysed **(A)**. HLA-DR$^+$ cells mainly comprised of CD14$^+$/CD16^{lo} monocytes/macrophages and HLA-DR$^+$/CD14$^-$/CD16$^-$ dendritic cells **(B)**. The expression of CD163 on CD14^{++}/CD16$^+$ monocytes/macrophages **(C)** is also shown. On extended characterisation, HLA-DR$^+$/CD14$^-$/CD16$^-$ dendritic cells comprised subpopulations of CD141$^+$ and CD11c$^+$ dendritic cells **(D)**. HLA-DR$^-$ cells comprised of neutrophils (CD16^{hi}, CD66b$^+$) **(E,F)** and a population of CD16^{lo} cells which comprised Siglec-8$^+$ eosinophils **(H, I)** and AnnexinV/7AAD$^+$ apoptotic/dead neutrophils **(G).** Representative dot plots are shown here (n=17).

3.3.3 Temporal profile of leucocytes in cantharidin skin blister

The lymphocytes subsets identified in this model did not show significant differences in proportion or total count between 24h and 72h. $CD3^+$ T cells comprised 3.4 ± 1.75% and 4.3 ± 2.2% of total leucocytes at 24h and 72h respectively **(Figure 3.7 A)**. The total numbers of $CD3^+$ T cells at 24h and 72h are shown in **Figure 3.7 B.** The origin of these $CD3^+$ T cells in the blister is currently not known. They could either have trafficked from the peripheral blood or could represent a population of skin resident T cells. Further characterisation using CD69 and CLA, the resident T cell markers can elucidate their origin. The numbers of $CD56^+$ NK cell numbers were lower than $CD3^+$ T cells at both the time points. The proportion of $CD56^+$ NK cells was 0.13 ± 0.1% and 0.22 ± 0.19% at 24h and 72h respectively **(Figure 3.7 C)**. The total numbers of $CD56^+$ NK cells at 24h and 72h are shown in **Figure 3.7 D**. CD19+ B cells were present in < 0.01% at both the time points (not shown here).

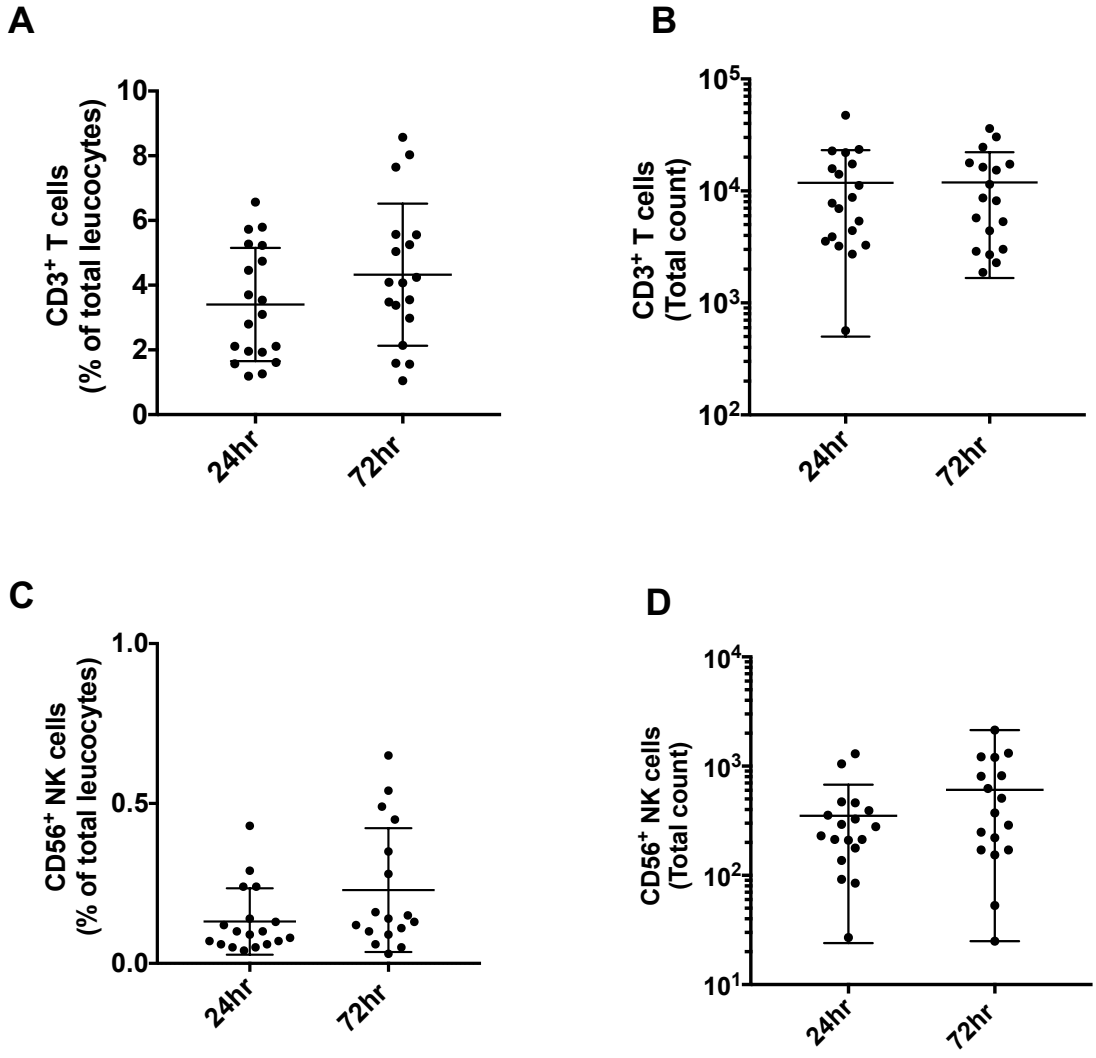

Figure 3.7 Profile of lymphocytes in cantharidin skin blister at 24hr and 72hr

The exudate from 24hr and 72hr cantharidin blister was centrifuged to pellet cells. Red blood cells were lysed and the remaining leukocytes counted by haemocytometer. Leukocytes were incubated with an antibody cocktail and processed for flow cytometry. For 24hr and 72hr time point, proportion of $CD3^+$ T cells of total leukocytes **(A)**, total numbers of $CD3^+$ T cells **(B)**, proportion CD56+ NK cells of total leukocytes **(C)** and total numbers of CD56+ NK cells **(D)** are shown here. Data expressed as individual values with mean ± SD (n=17).

Neutrophils were the dominant cell type at 24h comprising 57.97 ±18.57% of total leucocytes at 24h. By 72h the neutrophil proportion reduced significantly to 19.34 ± 8.54% **(Figure 3.8 A).** The total numbers of neutrophils at 24h and 72h are shown in **Figure 3.8 B.** Conversely, the numbers of $CD16^{lo}$ apoptotic neutrophils increased significantly from 24h to 72h **(Figure 3.8 D).** $CD16^{lo}$ cells increased from 4.94 ± 2.34% of the total leucocytes at 24h to 34.7 ± 12.06 % at 72h **(Figure 3.8 C)**. The total numbers of apoptotic neutrophils at 24h and 72h are shown in **Figure 3.8 D.** The difference in the proportion of eosinophils between 24h and 72h was insignificant. Eosinophils constituted 2.10 ± 2.96 % and 3.55 ± 4.59 % of total leucocytes at 24h and 72h **(Figure 3.8 E)**. However, the cell count of eosinophils increased significantly from 3,749 ± 4,243 at 24h to 11,208 ± 17,428 at 72h **(Figure 3.8 F)**.

The proportion of monocytes/macrophages did not change from 24h to 72h, but their numbers decreased significantly. Monocytes/macrophages constituted 18.41 ± 9.54% and 13.29 ± 6.26% of total leucocytes at 24h and at 72h, respectively **(Figure 3.8 G)**. The numbers of these cells decreased from 60,044 ± 51,001 at 24h to 34,363 ± 20,709 at 72h **(Figure 3.8 H).** Furthermore, the expression of CD163 did not change from 24h to 72h **(Figure 3.8 I).**

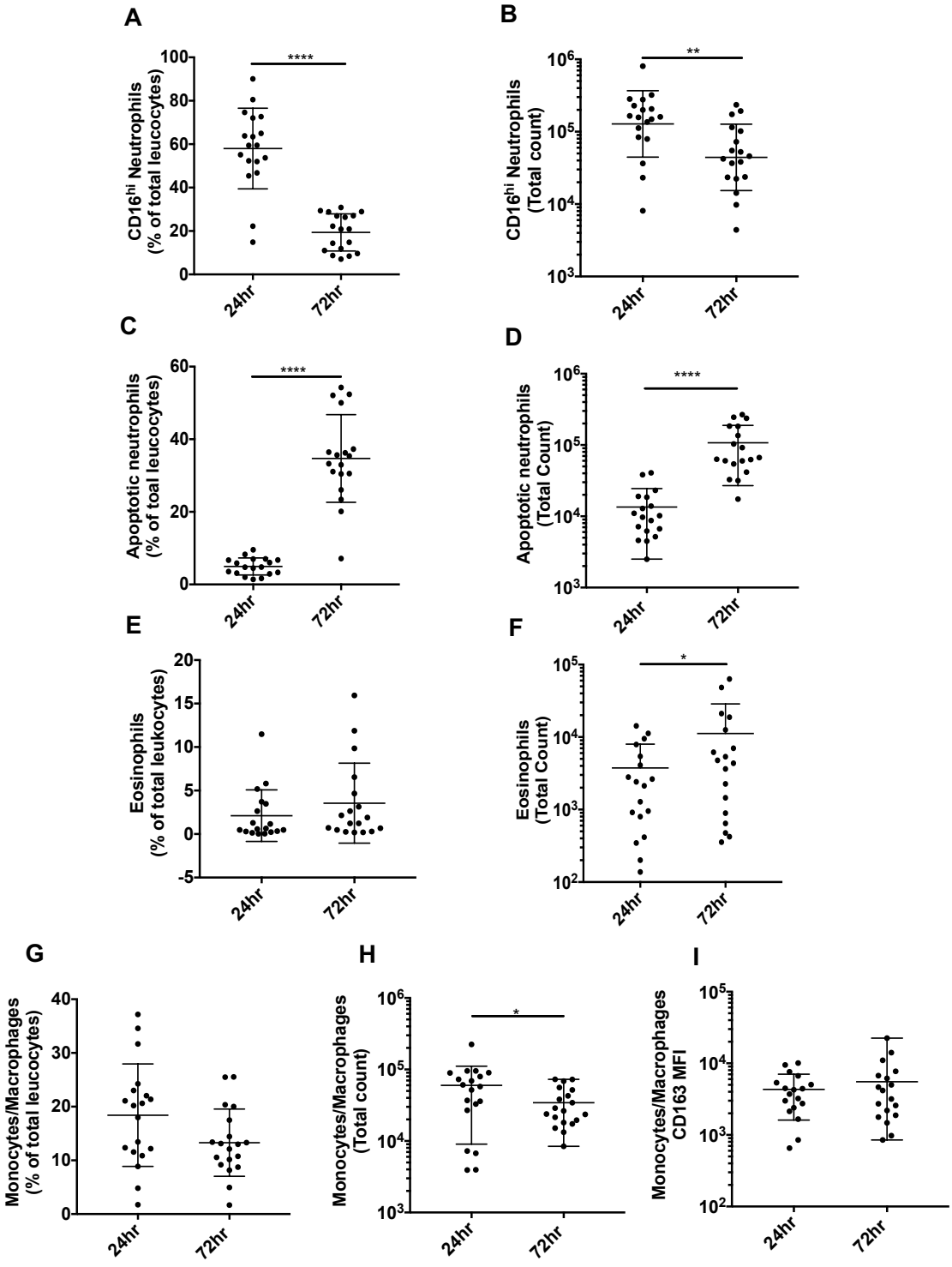

Figure 3.8 Profile of myeloid cells in cantharidin skin blister at 24hr and 72hr

The exudate from 24hr and 72hr cantharidin blister was centrifuged to pellet cells. Red blood cells were lysed and the remaining leukocytes were counted by haemocytometer. Leukocytes were then incubated with an antibody cocktail and processed for flow cytometry. For 24hr and 72hr time point, proportion of $CD16^{hi}$ neutrophils of total leukocytes **(A),** total count of $CD16^{hi}$ neutrophils **(B)**, proportion of $CD16^{lo}$ apoptotic neutrophils of total leukocytes **(C)**, total count of $CD16^{lo}$ apoptotic neutrophils **(D)**, proportion of Siglec-8^{+} eosinophils total leukocytes **(E)** and total numbers of Siglec-8^{+} eosinophils **(F),** proportion of monocytes/macrophages of total leukocytes **(G)** and total numbers of monocytes/macrophages **(H)** and CD163 expression on monocytes/macrophages **(I)** are shown here. Data expressed as individual values with mean± SD (n=17). p values are denoted as < 0.05 = ' * ', <0.01 = ' ** ', <0.001 = ' *** '.

At 24h, a noticeable spread was observed in numbers of neutrophils **(Figure 3.8 A, B)**. Subsequent comparison of 24h neutrophils with neutrophil clearance (calculated here as 72h neutrophils - 24h neutrophils) revealed that volunteers with the highest infiltration of neutrophils at onset showed highest neutrophil clearance at resolution **(Figure 3.9)**.

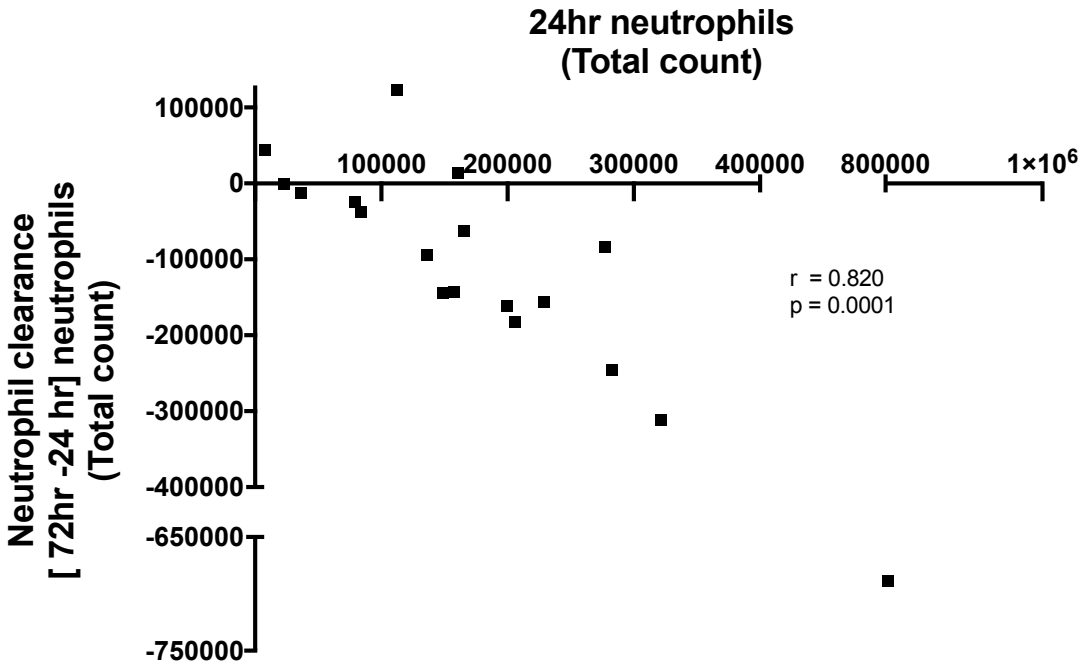

Figure 3.9 The correlation between neutrophils at onset (24hr) and neutrophil clearance (72hr-24hr neutrophil)

The exudate from 24hr and 72hr cantharidin blister was centrifuged to pellet cells. Red blood cells were lysed and the remaining leukocytes were counted by haemocytometer. Leukocytes were then incubated with an antibody cocktail and processed for flow cytometry. The correlation between neutrophil numbers at onset (24hr) and neutrophil clearance (defined as 72hr – 24hr neutrophils) is shown here (n=17).

3.3.4 Temporal profile of cytokines and lipid mediators in cantharidin skin blister

From 24h to 72h, the levels of pro-inflammatory cytokines TNF-α, IL-6 and IL-12p70 decreased significantly. At 24h, the concentration of TNF-α in the blister was 77.31 ± 41.61 pg/ml, and it declined to 31.32 ± 23.14 pg/ml **(Figure 3.10 A)**. The levels of IL-6 and IL-12p70 decreased from 665.7 ± 519.3 pg/ml and 12.21 ± 9.107 pg/ml at 24h to 309.3 ± 344.2 pg/ml and 10.73 ± 18.04 pg/ml at 72h respectively **(Figure 3.10 B, C)**. The difference in concentrations of other pro-inflammatory cytokines IL-1β and IL-8 between 24h and 72h were not found to be significant **(Figure 3.10 D, E)**. In contrast, the levels of IFN-γ showed an increasing trend from 24h to 72h **(Figure 3.10 F)**. Similarly, the levels of anti-inflammatory cytokine IL-10 showed an increasing trend from 24h to 72h **(Figure 3.10 G)**.

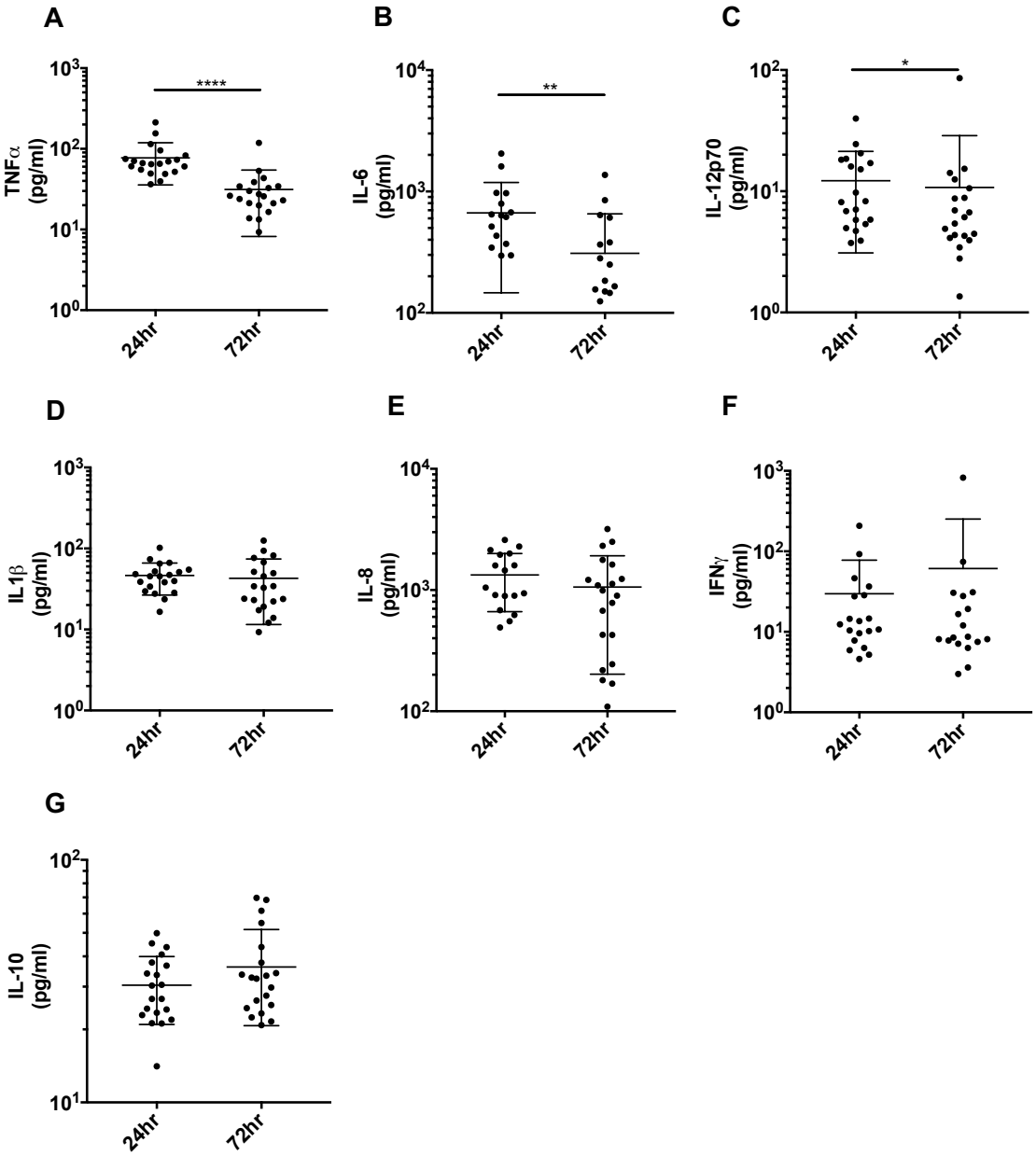

Figure 3.10 Cytokine/chemokine profile in cantharidin skin blister at 24hr and 72hr

The exudate from 24hr and 72hr cantharidin blister was centrifuged to pellet cells. The cell free exudate was analysed for cytokines by multiplex ELISA. The change in concentration of cytokines/chemokines from 24hr to 72hr is shown here **(A-G)**. Data expressed as individual values with mean ± SD (n=17). p values are denoted as < 0.05 = ' * ', <0.01 = ' ** ', <0.001 = ' *** '.

The levels of lipid mediators also decreased significantly from onset to resolution. At 24h, the level of PGE_2 in the blister was 4,752 ± 3,014 pg/ml, and it declined to 1,843 ± 1,090 pg/ml at 72h **(Figure 3.11A)**. The levels of TXB_2 declined from 6,377 ± 5,015 pg/ml at 24h to 6,377 ± 5,015 pg/ml at 72h while the levels of $PGF_{2\alpha}$ declined from 8,674 ± 14,008 pg/ml at 24h to 5,416 ± 7,907 pg/ml at 72h. **(Figure 3.11 B, C)**. Relative to other prostaglandins measured here, the levels of PGD_2 were lower at both time points but it declined significantly from 24h to 72h. At 24h, the concentration of PGD_2 in the blister fluid was 906 ± 550 pg/ml, and it declined to 544 ± 401 pg/ml at 72h **(Figure 3.11 D)**. The additional lipid mediators measured in this study are shown in the appendix (Figure 8.1).

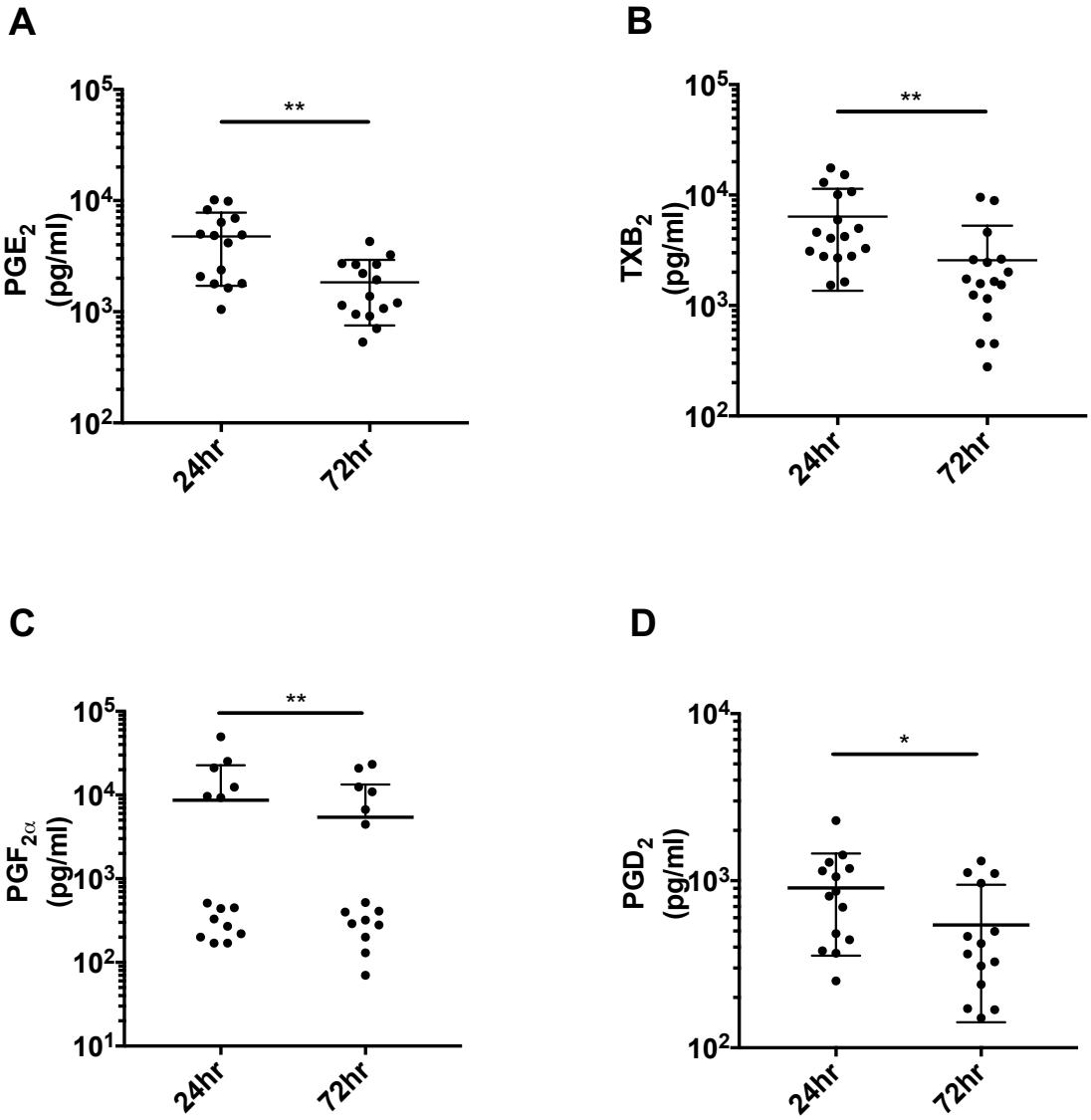

Figure 3.11 Prostanoid profile in cantharidin skin blister at 24hr and 72hr

The exudate from 24hr and 72hr cantharidin blister was centrifuged to pellet cells. Cell free exudate was subject to lipid mediator analysis by mass spectrophotometry by Dr A. Nicolaou at University of Bedford. The change in concentration of prostanoids from 24hr to 72hr is shown here. Data expressed as individual values with mean± SD (n=15). p values are denoted as < 0.05 = ' * ', <0.01 = ' ** ', <0.001 = ' *** '.

3.4 DISCUSSION

The current study presents an in-depth flow cytometric characterisation of leucocytes as well as cytokines and lipid mediators during the onset and resolution phases of cantharidin skin blister. The antibody panel and the gating strategy were first optimised to identify the major populations of peripheral blood leucocytes, and it was then employed to characterise the cantharidin skin blister leucocytes, which were further confirmed by cytology. The gating strategy serves as a template for future research to utilise the cantharidin blister model as a relatively non-invasive tool to quantify the human innate immune response *in vivo*.

One of the key observations from this model in terms of advancing our understanding of resolution in humans was that despite some volunteers generating strikingly greater numbers of neutrophils in their blisters at 24h than others; all volunteers had an approximately similar number of neutrophils remaining at resolution. This implies that despite the varying intensity of inflammatory response at onset, the resolution processes tune themselves to generate a consistent resolution phenotype.

Coincident with a significant decrease in neutrophil numbers from 24h to 72h, we saw the accumulation of apoptotic neutrophils at 72h. One explanation for this could be due to the absence of stromal scaffold in the blister. From 24h onwards the cells that have migrated in the blister are floating in a fluid sac, which is atypical when compared to the inflammatory responses in the tissue where a stromal scaffold is present. The absence of stromal support could

reduce cell-cell interaction and thus impede efficient efferocytosis of apoptotic cells by macrophages. In fact, monocytes/macrophages in this blister model did not upregulate the expression of CD163, a marker associated with efferocytosis [195]. As neutrophil clearance is one of the hallmarks of resolution, these data suggest that the 72h time point does not represent complete resolution.

Resolution of inflammation is associated with clearance of pro-inflammatory cytokines/chemokines and lipid mediators. The production of cytokines and chemokines is suppressed, and they are cleared either by scavenging by decoy receptors such as D6 leading to lysosomal degradation or proteolysis by metalloproteinases such as MMP-12 [196][38][46]. Prostaglandins which are involved in oedema, vasodilation and pain are degraded by 15-hyrdroxyprostaglandin dehydrogenase (15-PGDH), whereby they are first oxidised into their corresponding 15-keto compounds, then reduction by $\Delta^{13\text{-}15}$-ketoprostaglandin reductase and finally followed by their β-oxidation [197]. Correspondingly, we observed here that the concentration of pro-inflammatory cytokines, e.g. TNF-α, IL-6 and IL-12p70 decreased from 24h to 72h. In addition, the prostaglandins including PGE_2, $PGF_{2\alpha}$, TXB_2 and PGD_2 decreased significantly from 24h to 72h. Taken together, these data highlight that the cantharidin blister could be utilised to study to clearance of pro-inflammatory mediators, an important resolution biomarker, in humans.

Characterisation of eosinophils in this study by flow cytometry proved challenging due to the inherent auto-fluorescent nature of these cells. This was because of non-specific binding of fluorescein isothiocyanate (FITC)

fluorochrome to eosinophils. Eosinophils do not express CD16, but because they have an alkaline cytoplasm, they would have bound to FITC, an acidic dye. As a result, we got an erroneous impression that eosinophils express some CD16. Such non-specific interaction of eosinophils with acidic dyes has also been described previously [198]. Future studies should bear this in mind when trying to identify eosinophils within mixed cell populations using FITC-labelled antibodies. Use of Siglec-8 antibody to identify bona fide eosinophils can avoid such errors [199].

Increase in eosinophil numbers during resolution in this model is reminiscent of observations made in murine studies, e.g. it was shown in the model of acute zymosan-induced peritonitis, that eosinophils accumulate in the abdominal cavity during resolution. Furthermore, these animal studies attributed a pro-resolving function to eosinophils as they expressed high levels of 15-lipoxygenase and mediated formation of specialised pro-resolving mediator protectin D1 [200]. This is in contrast to the vast literature describing eosinophils as being pathogenic in allergic inflammatory diseases, e.g. asthma, dermatitis where eosinophil granule proteins exert cytotoxic effects on epithelial lining [201] [202]. It is unclear at this stage whether an increase in eosinophils during resolution in the cantharidin blister model is potentially pathogenic or pro-resolving.

The advantages of cantharidin blister model are that it is non-invasive, quick and easy to apply without the need of any special equipment. In addition, the materials required to induce a blister are inexpensive. Furthermore, the localised nature of blister allows induction of multiple blisters at the on the

same forearm that allows facilitates investigation of multiple time points of inflammation. Cantharidin blister is also devoid of side effects observed in skin abrasion models, e.g. bleeding [203]. Also, the skin roof of cantharidin blister provides a natural chamber for collection of leucocytes. In other skin abrasion models, an artificial collecting chamber has to be placed over the skin to facilitate leucocyte collection. These artificial chambers are difficult to maintain over skin and can leak if kept for the longer duration [204].

In conclusion, cantharidin skin blister is a model of tissue injury that allows investigation of multiple cell types of the innate immune system together with cytokines and lipid mediators during the onset and resolution of acute inflammation in healthy individuals. A major limitation is that the resolution time point in this model does not show complete clearance of apoptotic neutrophils.

Chapter 4

A novel human model of acute self-resolving dermal inflammation triggered by ultraviolet light killed *E. coli* (UVkEc)

4.1 INTRODUCTION

An ideal model of resolution of acute inflammation should allow investigation of biomarkers of resolution: neutrophil clearance, reduction of pro-inflammatory mediators and clearance of the inflammatory stimulus. It should be triggered by a uniform dose of inflammatory stimulus to ensure a consistent inflammatory response and should facilitate minimally invasive sampling of inflamed tissue. Furthermore, it will be advantageous if the model enables monitoring of the clinical signs of acute inflammation.

Acknowledging the above characteristics, I developed a novel model of resolution of acute inflammation in healthy humans by adapting two techniques. In the first step, acute inflammation was triggered by intradermal injection of ultraviolet light killed *Escherichia coli* bacteria (UVkEc) into the forearm. This technique was first employed by Smith *et al.* to study neutrophil trafficking in inflammatory bowel disease patients. In their study, patients were transfused with autologous radiolabelled neutrophils before the UvKEc injection, and neutrophil migration to the inflamed site was quantified by counting the radioactivity directly over the site [205]. While this method facilitated investigation of neutrophil kinetics and the inflammation-induced vascular hyperaemia, it did not provide information on other immune cell types or the soluble mediators of inflammation.

To investigate multiple immune cell subsets and local mediators, I induced a suction blister over the site of UvKEc injection to acquire the inflammatory exudate from the site. Immune cells in the exudate can be phenotyped by multicolour flow cytometry to characterise multiple immune cell populations

while the cell-free exudate can be used to measure the soluble mediators. The suction blister technique employed here is based on the approach adopted by Vukmanovic et al. who used it to assess the local T cell memory response to a vaccine antigen [206].

In this chapter, I characterised this novel UVkEc induced self-resolving dermal inflammation model encompassing the vascular hyperaemia, immune cell subsets and cytokines and chemokines at the inflamed site during the onset and resolution phases. In addition, I assessed the associated systemic immune response. Finally, I have described the tolerability of this approach amongst the study volunteers.

4.2 STUDY DESIGN

To characterise the different phases of inflammation, the UVkEc injected site was allowed to progress until one of the following time-points: 4h, 8h, 14h, 24h, 48h, 72h, and then a suction blister was raised over the injection site. Once the suction blister was formed, it was aspirated immediately. To assess vascular hyperaemia over the area of inflammation, the inflamed site on the forearm was scanned using laser Doppler imager. For the baseline time point, the blister was raised on the naive skin. In summary, each volunteer had two injection sites (one on each forearm) and contributed to two time points. Study time-points were discussed with the volunteer during recruitment and confirmed again before the consent procedure. The technique is described in detail in methods section 2.3 (**Figure 2.3 and Figure 2.4**).

4.3 RESULTS

4.3.1 Vascular hyperaemia at the site of UVkEc triggered self-resolving dermal inflammation.

UVkEc triggered acute inflammation became clinically apparent by 4h as a localised area of redness referred here as flare **(Figure 4.1 A)**. At 4h, the flare area was 12.18 ± 4.48 cm^2. It increased between 4h and 24h and reached its maximum size at 24h. At this time point, it was 23.42 ± 8.42 cm^2 in size. From 24h to 48h, the flare reduced significantly, and it disappeared by 72h. **(Figure 4.1 C).**

Vascular hyperaemia underlying the inflammation-induced redness was assessed by laser Doppler imager. The representative laser Doppler images at different phases of inflammation are shown in **Figure 4.1 B**. The laser Doppler images allows objective quantification of the inflammation induced redness in perfusion units. At 4h, the hyperaemia at the site was 1.72 x 10^6 ± 0.6 x 10^6 perfusion units. Similar to flare area, the hyperaemia increased between 4h and 24h and reached its peak at 24h to 3.19 x 10^6 ± 1.2 x 10^6 perfusion units. From 24h to 48h it declined significantly. At 48h, it was 0.74 x 10^6 ± 0.93 x 10^6 perfusion units. At 72h, the vascular hyperaemia over injection site was similar to baseline skin **(Figure 4.1 D).**

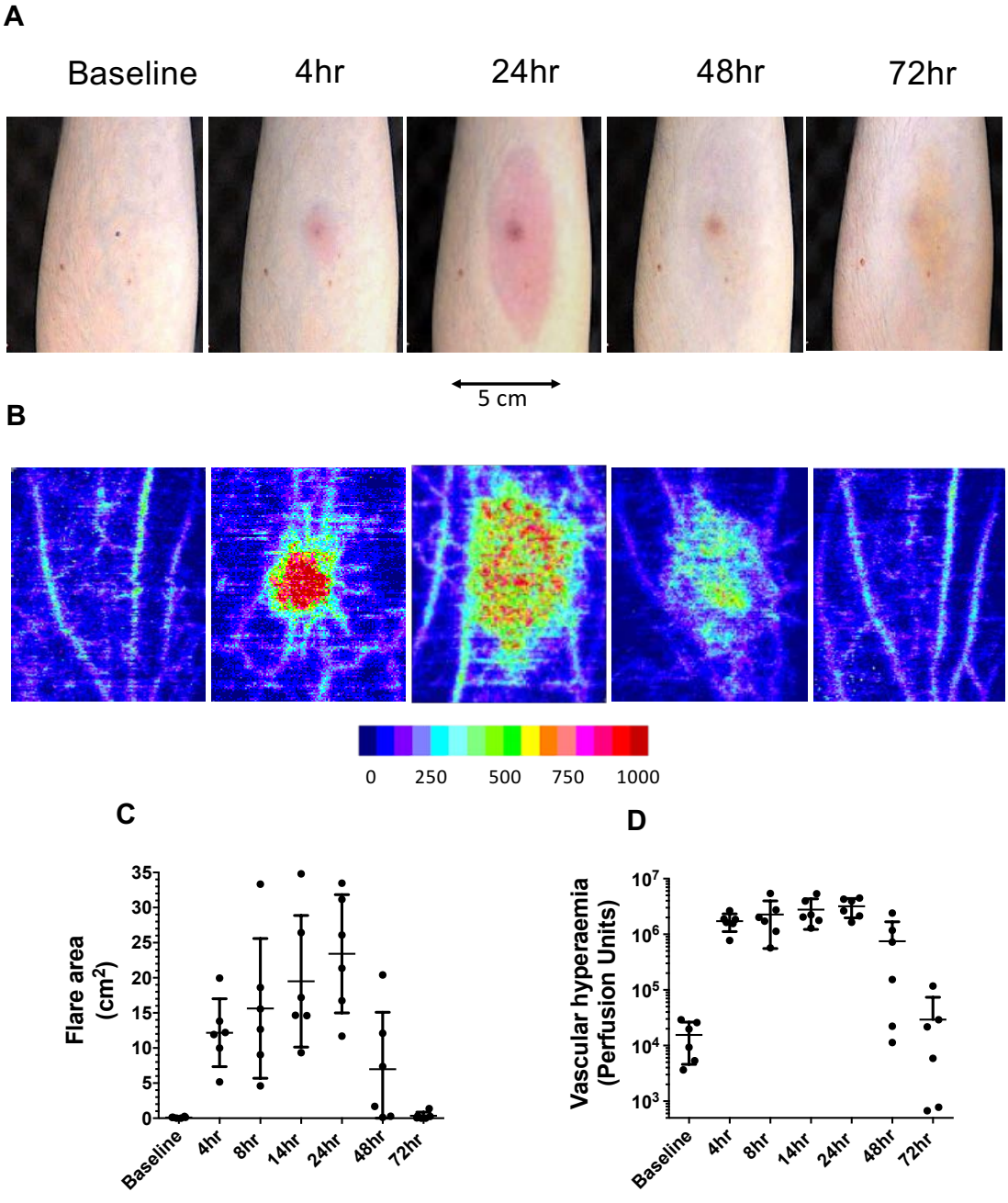

Figure 4.1 Vascular hyperaemia at the site of UV killed *E. coli* triggered self resolving dermal inflammation.

Acute inflammation was triggered in the ventral aspect of forearm of healthy volunteers by the intradermal injection of 1.5 x 10^7 UV killed *E. coli* (UVKEc) suspended in 100µl of sterile saline. Vascular hyperaemia at the site was assessed by laser Doppler imager. Representative camera images **(A)** and Doppler flux images **(B)** at baseline, 4hr, 24hr, 48hr and 72hr are shown here. Doppler flux images were analysed by moorLDI software to quantify the area of redness (flare area) **(C)** and the vascular hyperaemia **(D)**. Data expressed as individual values with mean ± SD; n=6 at each time point.

4.3.2 Characteristics of the inflammatory exudate at site of UVkEc triggered resolving dermal inflammation

To acquire the inflammatory exudate, the suction blister was raised over the injection site. It was immediately centrifuged to separate cells from soluble mediators. Total leucocyte count was enumerated using haemocytometer. The total leucocyte numbers peaked at 4h to 85,896 ± 55,508 cells. From 4h onwards, it declined and was significantly lower at 48h compared to 4h. At 48h, the total leucocyte count was 10,083 ± 4,521. The total leucocyte count of the suction blister exudate at different time points is shown in **Figure 4.2 A.** The suction blister volume, representing the volume of inflammatory exudate, is shown in **Figure 4.2 B.** The total leucocyte count/ml which represents the total leucocyte count adjusted for suction blister volume is shown in **Figure 4.2 C**.

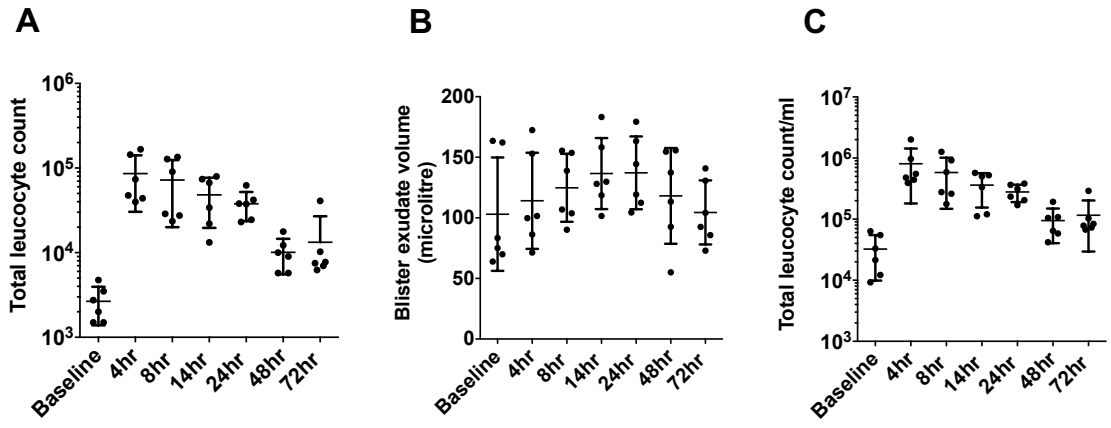

Figure 4.2 Characteristics of inflammatory exudate obtained from the site of UV killed *E. coli* triggered self resolving dermal inflammation.

Acute inflammation was triggered in the ventral aspect of forearm of healthy volunteers by the intradermal injection of 1.5 x 10^7 UV killed *E. coli* (UVKEc) suspended in 100µl of sterile saline. A suction blister was raised over the inflamed site at the specified interval to collect the inflammatory exudate. Exudate was centrifuged to separate cells from the supernatant. The cell pellet was suspended in FACS buffer and the cells were counted by haemocytometer. The total leucocyte count **(A)**, the volume of supernatant representing the blister exudate volume **(B)** and the total cell count adjusted per ml of exudate **(C)** is shown here. Data expressed as individual values with mean± SD; n=6 at each time point.

Total leucocytes were phenotyped by multicolour flow cytometry to characterise the immune cell subsets. The flow cytometry gating strategy was based on the strategy developed for cantharidin blister, described in Chapter 3 with some modifications. Briefly, after excluding cell debris **(Figure 4.3 A)**, total cells were plotted on $CD45^+$ to identify cells of haematopoietic origin **(Figure 4.3 B)**. $CD45^+$ cells were plotted on forward scatter height and width plots (FSC-H vs. FSC-W) to exclude the doublets **(Figure 4.3 C)**. CD45+ single cell events were plotted against CD3/CD19 **(Figure 4.3 D)**. $CD3^+/CD19^+$ were further probed to identify $CD4^+$ and $CD8^+$ T cells **(Figure 4.3 D and F)**. The $CD3^-/CD19^-$ compartment was interrogated further to identify $CD56^+$ NK cells **(Figure 4.3 E)**. After exclusion of major lymphocytes, the $CD3^-/CD19^-/CD56^-$ myeloid cell population was separated into mononuclear cells and granulocytes by HLA-DR **(Figure 4.3 G)**. The HLA-DR^+ population was plotted on CD14 and CD16, to identify a distinct population of HLA-$DR^+/CD14^+$ monocytes/macrophages (red gate) and HLA-$DR^+/CD14^-/CD16^-$ dendritic cells **(Figure 4.3 H)**, of which a major subset was $CD1c^+$ dendritic cells **(Figure 4.3 I)**. The HLA-DR^- gate comprised mainly $CD16^{++}$ neutrophils (blue gate) and at some time points it also contained the $CD16^{lo}$ apoptotic neutrophils (green gate) **(Figure 4.3 G).**

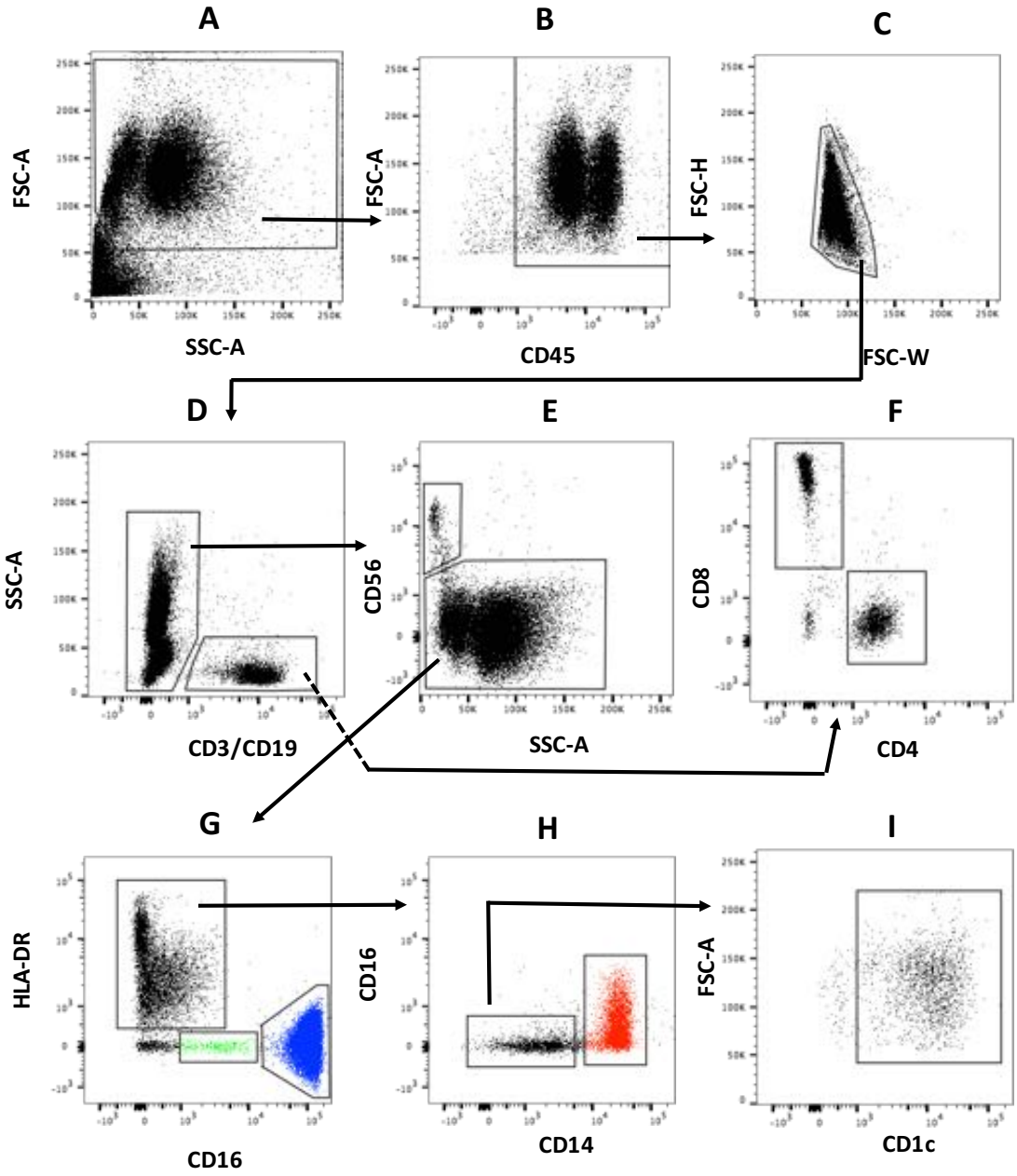

Figure 4.3 Polychromatic flow cytometric characterisation of leukocytes in the inflammatory exudate obtained from the site of UV killed *E. coli* triggered self resolving dermal inflammation.

Acute inflammation was triggered in the ventral aspect of forearm of healthy volunteers by the intradermal injection of 1.5 x 10^7 UV killed *E. coli* (UVKEc) suspended in 100µl of sterile saline. A suction blister was raised over the inflamed site to collect the inflammatory exudate. Exudate was centrifuged to separate cells from the supernatant. The immune cell subsets were identified by polychromatic flow cytometry. The gating strategy employed to identify neutrophils (blue gate) , monocytes/macrophages (red gate), $CD4^+$ and $CD8^+$ T lymphocytes, $CD56^+$ NK cells and $CD1c^+$ dendritic cells is illustrated here. Representative gating plots from the 14hr time point are shown here.

4.3.3 Cellular profile at the site of UVkEc triggered self-resolving dermal inflammation

At 4h, neutrophils were the dominant cell type comprising 79.8 ± 15.17 % of total leucocytes. From 4h onwards the neutrophil numbers declined, and at 48h they formed only 4.4 ± 5.2 % of total leucocytes. The neutrophil proportion and numbers at different points of inflammation are shown in **Figure 4.4 A and Figure 4.4 B** respectively. Consistent with reports shedding of CD62L during neutrophil activation [204], 4h neutrophils had a lower CD62L expression in this model. However, the CD62L expression on neutrophils increased gradually at later time points (**Figure 4.4 C).**

Monocytes/macrophages kinetics revealed two peaks. The first peak was observed at 8h when they comprised 23.38 ± 8.62 % of total leucocytes. Their proportion declined to 11.51 ± 5.72 % at 14h but rose again to 24.79 ± 8.62 % at 24h. However, From 24h onwards their numbers declined to form 8.45 ± 5.35 % of total leucocytes by 72h **(Figure 4.4 D)**. The total numbers of monocytes/macrophages during different phases of inflammation is shown in **Figure 4.4 E.** Further characterisation of these cells revealed that at 24h they had a higher expression of CD163 and CD16 compared to monocytes/macrophages population at 8h. The expression of CD163 and CD16 at different time points of inflammation is shown in **Figure 4.4 F and Figure 4.4 G** respectively.

Unlike neutrophils and monocytes/macrophages, $CD1c^+$ dendritic cells were present at baseline time point. These cells peaked at 24h and constituted 6.79

± 1.83 % of total leucocytes. From 24h to 48h their numbers declined and at 48h these cells comprised 1.1 ± 0.39 % of total leucocytes. The proportion and total numbers of $CD1c^+$ dendritic cells are shown in **Figure 4.4 H and Figure 4.4 I,** respectively.

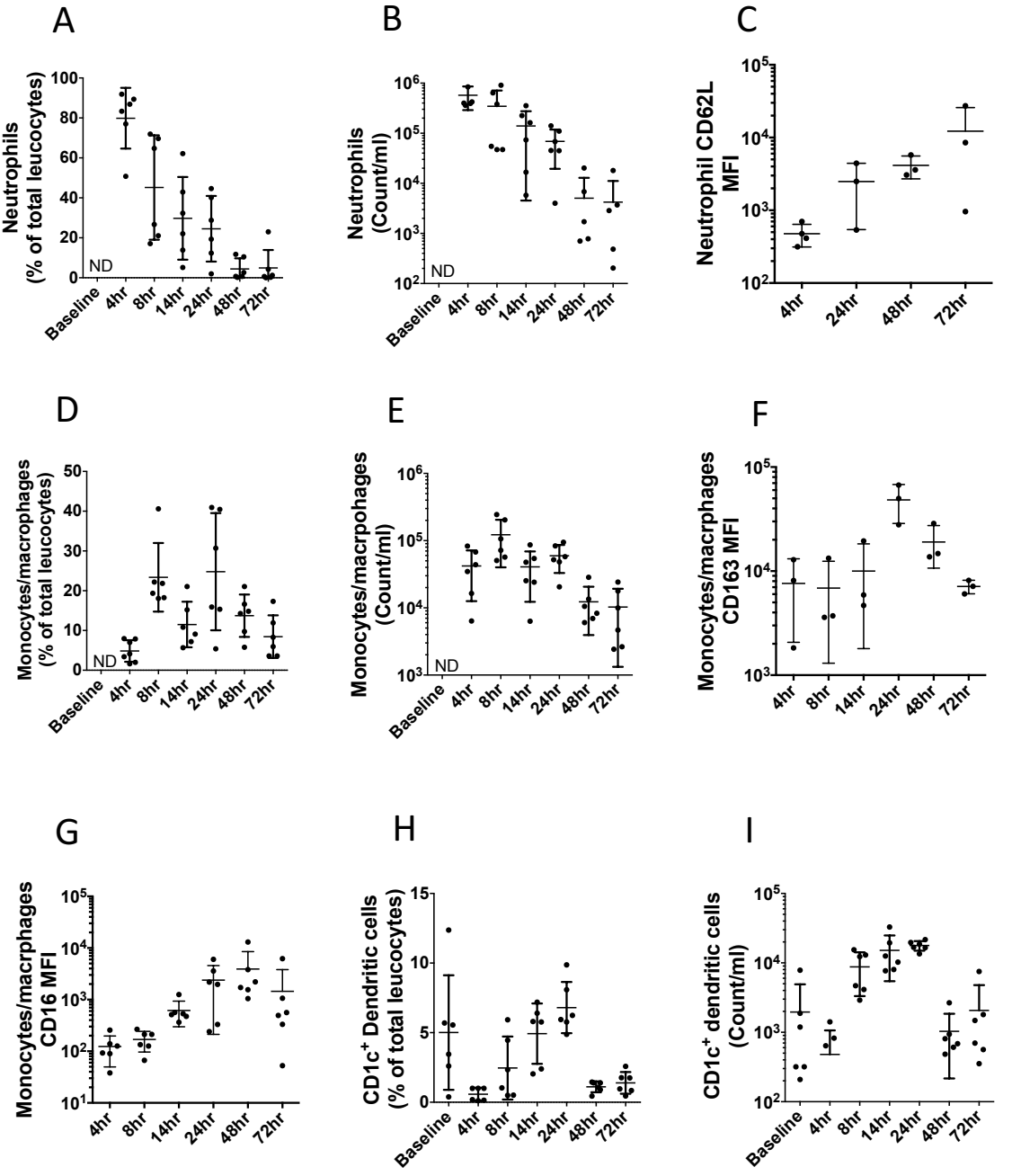

Figure 4.4 Profile of myeloid cells at site of UV killed *E. coli* triggered self resolving dermal inflammation.

Acute inflammation was triggered in the ventral aspect of forearm of healthy volunteers by the intradermal injection of 1.5 x 10^7 UV killed *E. coli* (UVKEc) suspended in 100µl of sterile saline. A suction blister was raised over the inflamed site at the specified interval to collect the inflammatory exudate. Exudate was centrifuged to separate cells from the supernatant. The cell pellet was suspended in FACS buffer and the cells were counted by haemocytometer. The immune cell subsets were identified by polychromatic flow cytometry. Proportion of neutrophils of total leukocytes **(A)**, total count/ml of neutrophils **(B),** neutrophil CD62L expression **(C)**, proportion of monocytes/macrophages of total leukocytes **(D)**, total count/ml of monocytes/macrophages **(E)**, expression of CD163 **(F)** and CD16 **(G)** on monocytes/macrophages**,** proportion of $CD1c^+$ dendritic cells of total leukocytes **(H)** and total count/ml of $CD1c^+$ dendritic cells **(I)** are shown here. Data expressed as individual values with mean ± SD; n=6 at each time point. n=3 for CD62L MFI and CD163 MFI. ND= not detectable.

To examine the effectiveness of neutrophil clearance in this model, I investigated $CD16^{lo}$ cells which were identified as a population of apoptotic neutrophils in cantharidin skin blister model. At 4h, $CD16^{lo}$ cells (green gate) comprised 5.4 ± 8.1 % of total leucocytes and increased up to 10.28 ± 12.46 % at 14h. From 14h to 72h they cleared, and by 72h their proportion was < 1% of total leucocytes. Thus, $CD16^{lo}$ cells were completely cleared from this model. The flow cytometric characterisation of these cells at different time points of inflammation is shown in **Figure 4.5 A,** and their temporal profile as a proportion of total leucocytes is shown in **Figure 4.5 B**.

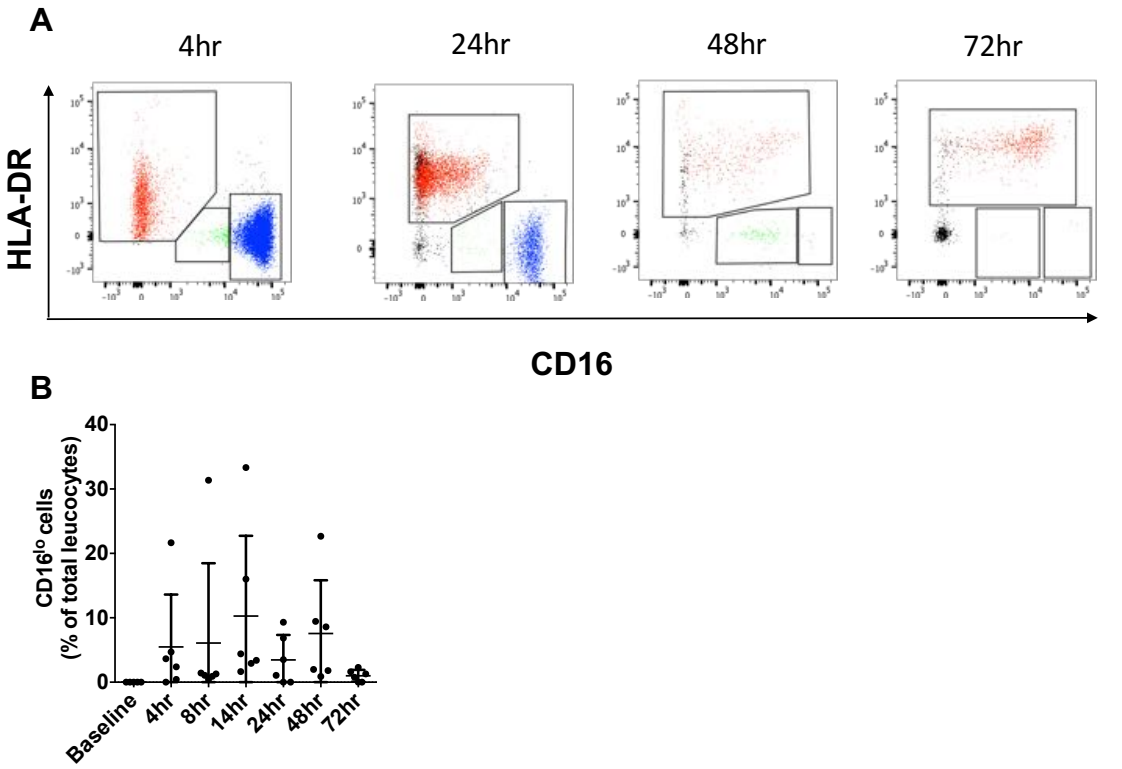

Figure 4.5 Profile of $CD16^{lo}$ cells at site of UV killed *E. coli* triggered self resolving dermal inflammation.

Acute inflammation was triggered in the ventral aspect of forearm of healthy volunteers by the intradermal injection of 1.5 x 10^7 UV killed *E. coli* (UVKEc) suspended in 100µl of sterile saline. A suction blister was raised over the inflamed site, at the specified interval, to collect the inflammatory exudate. Exudate was centrifuged to separate cells from the supernatant. The immune cell subsets were identified by polychromatic flow cytometry. Representative dot plots of $CD16^{lo}$ apoptotic neutrophils (green gate) at 4hr, 24hr, 48hr and 72hr time point relative to $CD16^{hi}$ neutrophils (blue gate) and HLA-DR^+ $CD14^+$ monocytes/macrophages (red gate) are shown here **(A)**. The proportion of $CD16^{lo}$ apoptotic neutrophils of total leukocytes at specified intervals is also shown **(B).** Data expressed as individual values with mean ± SD; n=6 at each time point.

Lymphocytes ($CD4^+$ and $CD8^+$ T cells) were the predominant cells types at the baseline time point. After UVkEc injection the proportion of $CD4^+$ T cells increased between 4hr and 14hr followed by a trend towards decline at 24hr. At 72hr, $CD4^+$ T cells were 16.02 ± 10.86 % of total leucocytes. The proportion and total numbers of $CD4^+$ T cells is shown in **Figure 4.6 A** and **Figure 4.6 B,** respectively. Proportion of $CD8^+$ T cells and $CD56^+$ NK cells also increased from 4hr to 72hr. At 72hr, $CD8^+$ T cells and CD56+ T cells comprised 25.87 ± 13.37 % and 13.13 ± 8.50 % of total leucocytes respectively. The proportion and total numbers of $CD8^+$ cells at the inflamed site is shown in **Figure 4.6 C** and **Figure 4.6 D** respectively**.** The proportion and total numbers of $CD56^+$ cells is shown is shown in **Figure 4.6 E** and **Figure 4.6 F** respectively**.** Thus, lymphocytes were the dominant cell type also at the 48hr and 72hr time points.

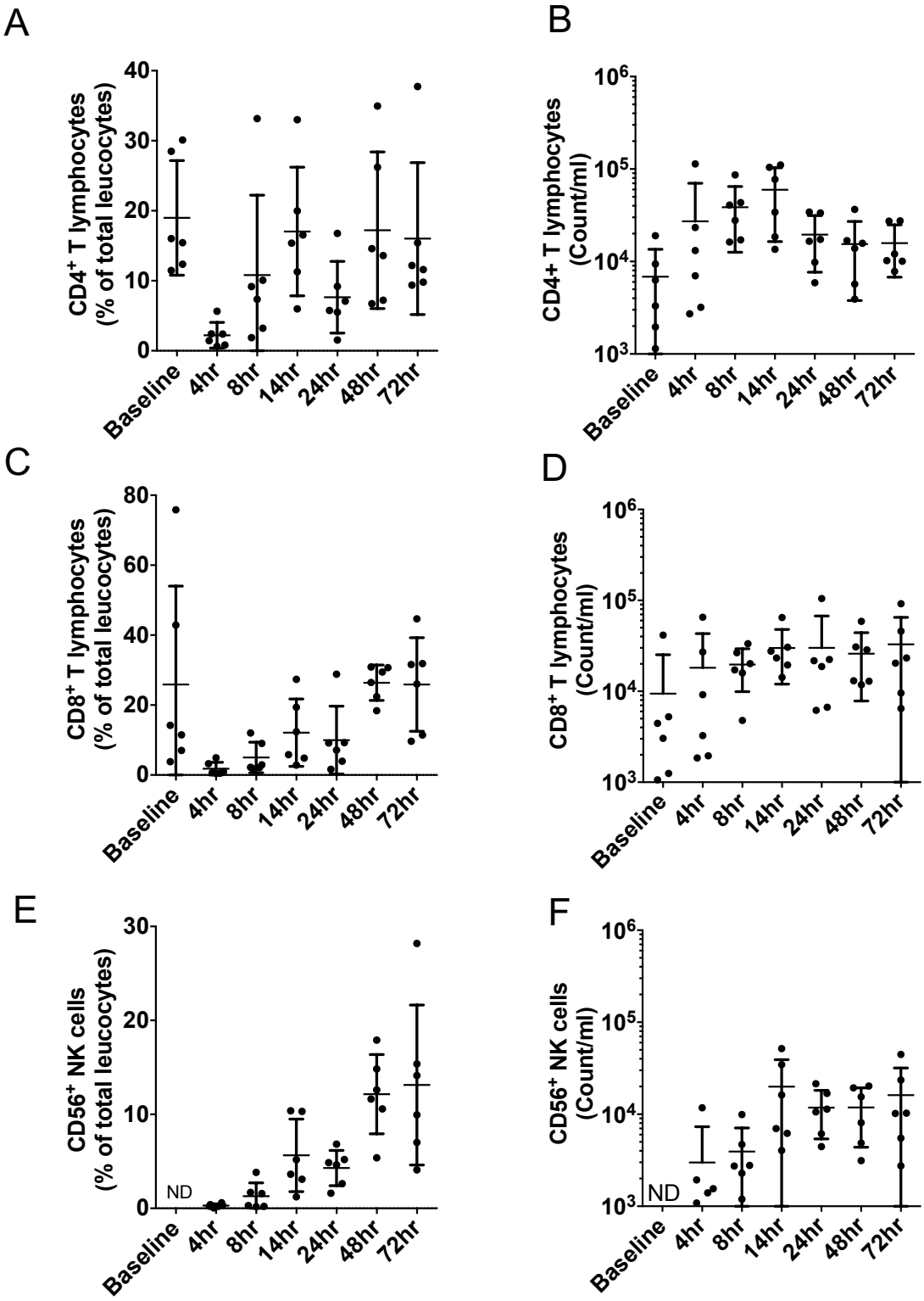

Figure 4.6 Profile of lymphoid cells at the site of UV killed *E. coli* triggered self resolving dermal inflammation.

Acute inflammation was triggered in the ventral aspect of forearm of healthy volunteers by the intradermal injection of 1.5 x 10^7 UV killed *E. coli* (UVKEc) suspended in 100µl of sterile saline. A suction blister was raised over the inflamed site at the specified interval to collect the inflammatory exudate. Exudate was centrifuged to separate cells from the supernatant. The cell pellet was suspended in FACS buffer and the cells were counted by haemocytometer. The immune cell subsets were identified by polychromatic flow cytometry. Proportion of $CD4^+$ T cells of total leukocytes **(A)**, total count/ml of $CD4^+$ T cells **(B) ,** proportion of $CD8^+$ T cells of total leukocytes **(C)**, total count/ml of $CD8^+$ T cells **(D),** proportion of $CD56^+$ NK cells of total leukocytes **(E)** and total count/ml **(F)** is shown here. Data expressed as individual values with mean ± SD ; n=6 at each time point. ND= not detectable.

4.3.4 Cytokine and chemokine profile at the site of UVkEc triggered self-resolving dermal inflammation

Cell-free inflammatory exudate was investigated by multiplex ELISA to measure the levels of soluble mediators. At 4h, when the numbers of neutrophils peaked at the inflamed site the levels of pro-inflammatory cytokines TNF-α, IL-1β and IL-8 were maximum **(Figure 4.7 A, B, C)**. At 4h, the levels of TNF-α were 1,568 ± 732 pg/ml, the levels of IL-1β were 509 ± 296 pg/ml and the levels of IL-8 were 3,556 ± 2232 pg/ml. Co-incidentally, the levels of anti-inflammatory cytokines IL-4, IL-10 and IL-13 also peaked **(Figure 4.7 D, E, F)**. IFN-γ, a macrophage activating cytokine peaked at 8h, coinciding with the peak of $CD163^{lo}$ pro-inflammatory macrophages **(Figure 4.7 G)**. The levels of IL-6 remained consistently high from 4h until 24h **(Figure 4.7 H)**. By 72h, concurrent with vascular and cellular resolution, the levels of these cytokines declined to be close to baseline levels. Additional cytokines and chemokines measured in this model are shown in the appendix (Figure 8.2 and Figure 8.3).

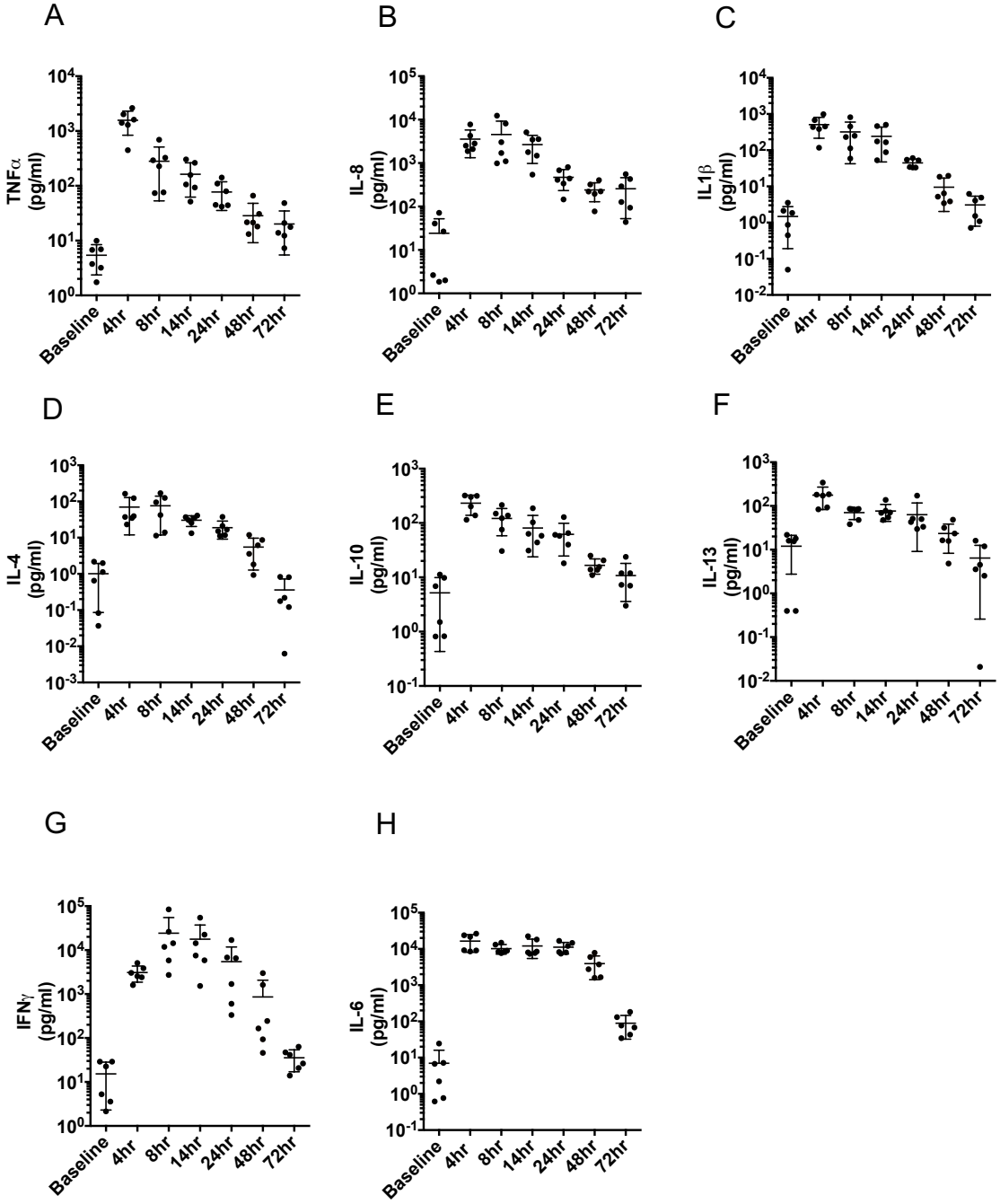

Figure 4.7 Profile of cytokines and chemokines at site of UV killed *E. coli* triggered self resolving dermal inflammation.

Acute inflammation was triggered in the ventral aspect of forearm of healthy volunteers by the intradermal injection of 1.5 x 10^7 UV killed *E. coli* (UVKEc) suspended in 100µl of sterile saline. A suction blister was raised over the inflamed site at the specified interval to collect the inflammatory exudate. Inflammatory exudate was centrifuged to separate cells from the supernatant containing soluble mediators. Cytokines and chemokines in the cell free exudate were measured using multiplex ELISA and their concentrations in the exudate obtained at the specified intervals are shown here. Data expressed as individual values with mean± SD; n=6 at each time point.

4.3.5 Systemic immune response to the UVkEc intradermal injection

Neutrophil and monocyte count in circulating blood and cytokine levels in plasma were measured to estimate the systemic immune response. Neutrophil numbers increased from 3.52 x 10^6 ± 1.49 x 10^6 cells/ml at baseline to 8.66 ± 0.64 x 10^6 cells/ml at 4h **(Figure 4.8 A)**. Peripheral blood monocytes showed a single peak at 4h compared to the biphasic monocyte kinetics seen at the site of inflammation. Their numbers increased from 0.39 x 10^6 ± 0.12 x 10^6 cells/ml at baseline to 0.69 x 10^6 ± 0.15 x 10^6 cells/ml at 4h **(Figure 4.8 B).** From 4h onwards, neutrophil and monocyte numbers declined gradually and reached baseline levels by 72h.

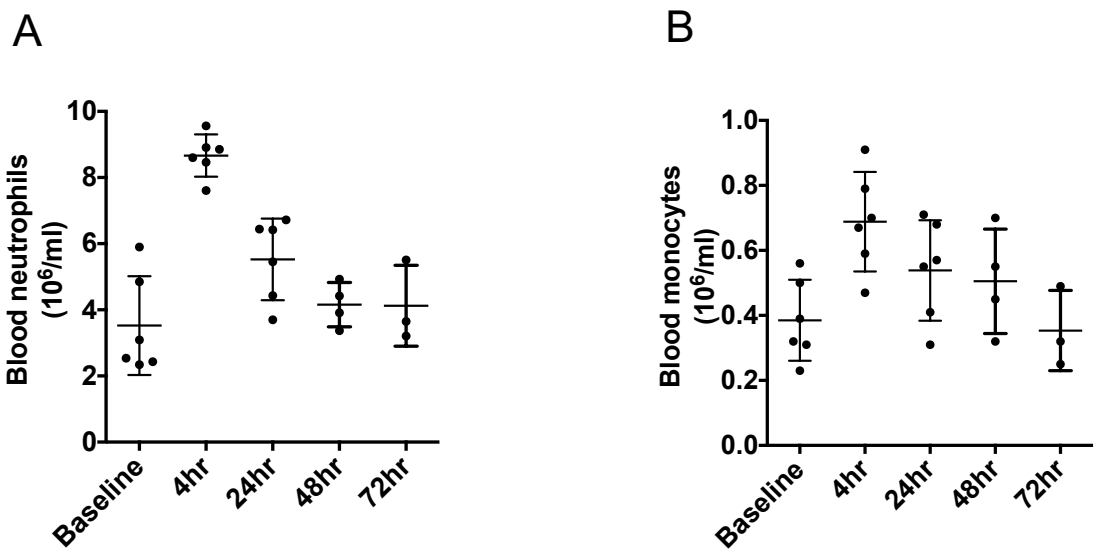

Figure 4.8 Profile of peripheral blood neutrophil and monocyte numbers in UV killed *E. coli* triggered self resolving dermal inflammation model.

Acute inflammation was triggered in the ventral aspect of forearm of healthy volunteers by the intradermal injection of 1.5 x 10^7 UV killed *E. coli* (UVKEc) suspended in 100µl of sterile saline. Peripheral blood was obtained by venepuncture at specified intervals and the anticoagulated blood was sent to The Doctor's Laboratory, Whitfield Street, London, UK for estimation of full blood count. Peripheral blood neutrophil count **(A)** and monocyte count **(B)** are shown here. Data expressed as individual values with mean ± SD; n=6 at baseline, 4hr and 24hr, n=4 at 48hr and n=3 at 72hr.

Plasma cytokines and chemokines did not show a temporal profile as observed in the local inflammatory exudate. From baseline to 4h, the plasma TNF-α levels unlike the blister exudate TNF-α levels did not rise significantly. At baseline, the levels of plasma TNF-α were 1.92 ± 0.94 pg/ml and increased to 2.933 ± 0.44 pg/ml at 4h **(Figure 4.9 A)**. Similarly, the plasma concentration of IL-8 did not rise at 4h or at the later time points of inflammation. Levels of IL-1β were undetectable **(Figure 4.9 B, C)**. Plasma IFN-γ increased above the baseline at 4h and peaked at 8h, coinciding with time point showing peak IFN-γ levels in the blister exudate. From 8h, its concentration declined and reached baseline levels at 72h **(Figure 4.9 D)**. Plasma concentration of IL-6 was consistently higher at 4h compared to baseline for the all the volunteers. Before UVkEc injection, it was 1.86 ± 1.13 pg/ml and increased to 18.6 ± 16.3 pg/ml at 4h **(Figure 4.9 E)**. By 48h, the concentration of plasma IL-6 returned to steady state levels.

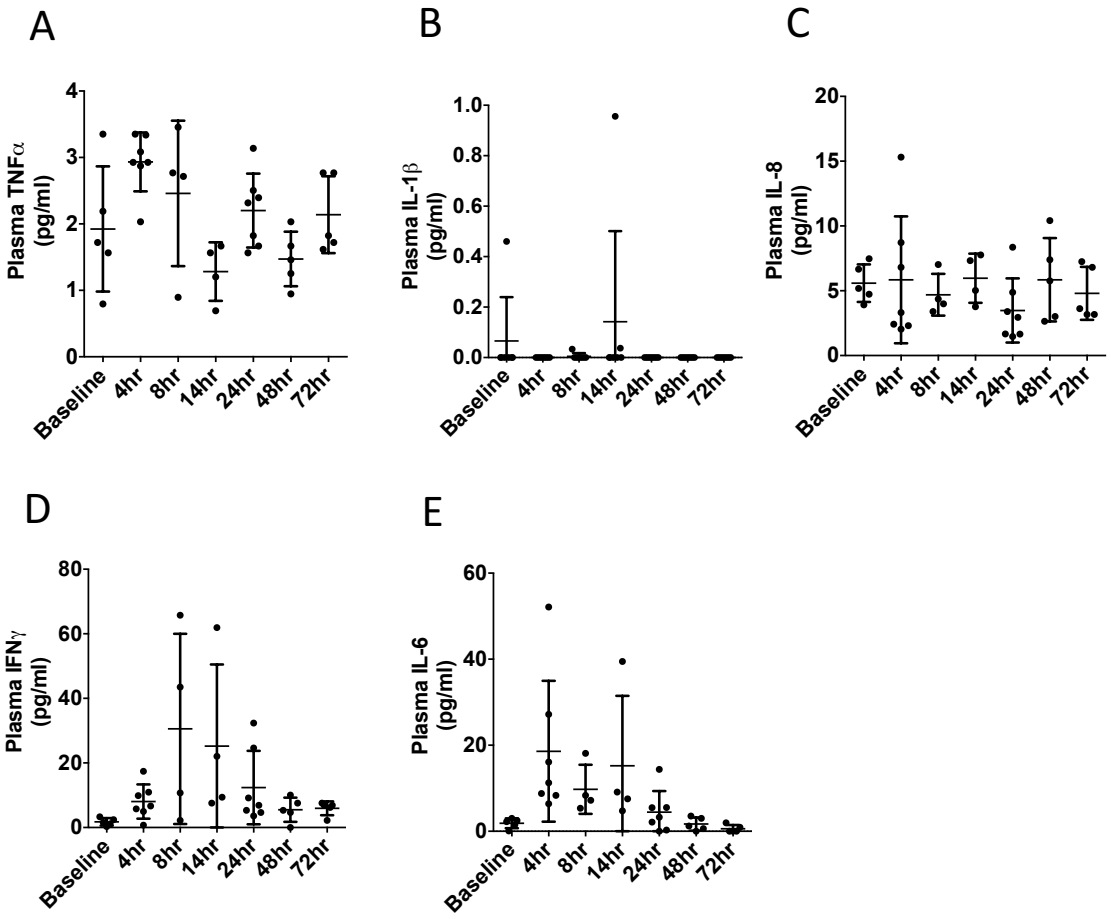

Figure 4.9 Profile of plasma cytokines and chemokines in the UV killed *E. coli* triggered self resolving dermal inflammation model.

Acute inflammation was triggered in the ventral aspect of forearm of healthy volunteers by the intradermal injection of 1.5 x 10^7 UV killed *E. coli* (UVKEc) suspended in 100µl of sterile saline. Peripheral blood was obtained by venepuncture at specified intervals and plasma was separated by centrifugation. The pro-inflammatory cytokines and chemokines in the plasma were analysed by multiplex ELISA and their concentration at specified intervals is shown here. Data expressed as individual values with mean ± SD; n=5 at baseline, 48hr and 72hr, n=4 at 8hr and 14hr, n=6 at 4hr and 24hr.

4.3.6 Tolerability of the UVkEc triggered self-resolving dermal inflammation model

To evaluate the tolerability of symptoms associated with UVkEc triggered acute inflammation and the study procedures, a post hoc survey was conducted for the volunteers who participated in the study. This survey was conducted in collaboration with Dr Julia Flint.

An anonymous online survey was emailed to volunteers asking them to report their experience. 13 out of the 24 volunteers who participated in this study responded to the survey. Results of the survey revealed that intradermal injection of UVkEc caused mild discomfort to 6 out of 13 volunteers. Laser Doppler Imaging was found to be very well tolerated. The blister induction process was reported to cause only mild discomfort by 9 out of 13 volunteers **(Figure 4.10 A)**. Amongst the inflammation associated local symptoms, mild pain at the injection site was a most common symptom and was reported by all the 13 volunteers. The second most common symptom was mild discomfort in the armpit region which was expected due to transient localised lymph node congestion and was reported by 6 volunteers. Three volunteers also reported arm heaviness which was expected due to localised oedema **(Figure 4.10 B).**

Systemic symptoms including headache, body ache, malaise and fever were less common than the local symptoms. Two volunteers reported headache, 5 reported body ache and 4 volunteers responded that they had a general feeling of illness (malaise). Fever was only reported by one volunteer **(Figure 4.10 B).** The survey results also revealed that 4 out of 13 volunteers did not

experience any symptoms and that by 48h all the symptoms had subsided **(Figure 4.10 C).** None of the volunteers withdrew from the study due to discomfort caused by study procedures or due to the acute inflammation associated symptoms.

A

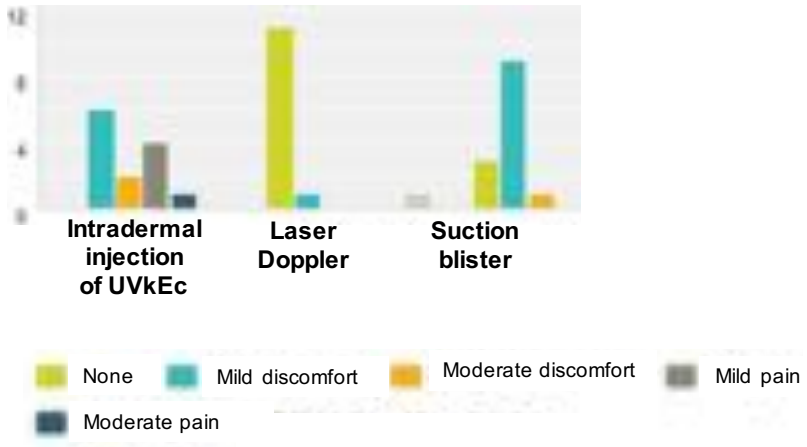

B

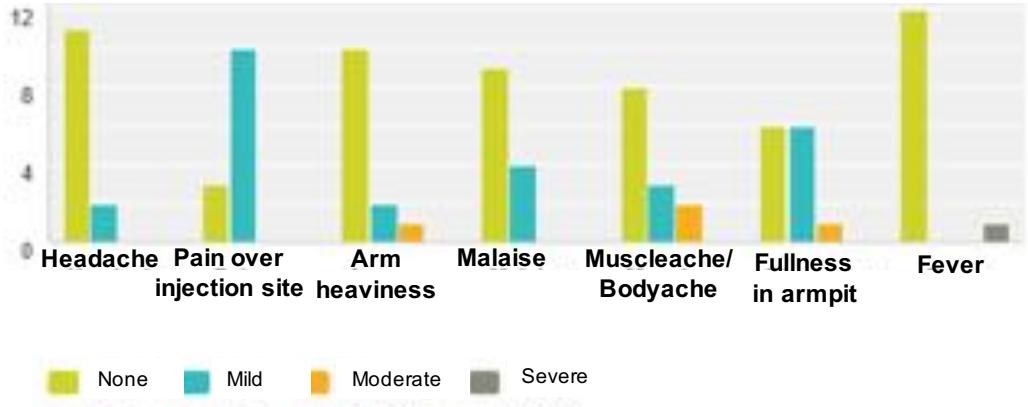

C

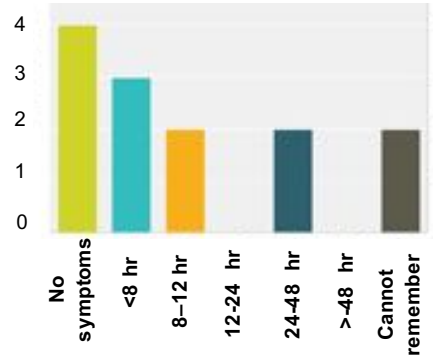

<u>Figure 4.10</u> Tolerability of UV killed *E. coli* triggered self resolving dermal inflammation model

To assess tolerability of acute inflammation associated symptoms and study procedures, volunteers were invited to take part in an online post hoc survey. Responses from the volunteers about the discomfort associated with study procedures **(A)**, symptoms of acute inflammation **(B)** and the duration for which of these symptom(s) lasted **(C)** are shown here. 24 volunteers were invited and 13 responded. Data from n=13.

4.4 DISCUSSION

This study describes a novel *in vivo* approach quantifying the vascular, cellular and soluble mediators elicited in response to UVkEc injection in healthy volunteers encompassing both the onset as well as the resolution phases of the inflammatory response.

The onset phase evident at 4h was characterised by an increase in blood blow, a maximal number of immune cells comprising mainly neutrophils, and the highest concentrations of classical pro-inflammatory cytokines. While the vascular response plateaued between 4h and 24h and started to resolve thereafter, the cellular resolution, classically defined by a reduction of neutrophil numbers [207], ensued gradually from 4h with > 90% of neutrophils cleared by 48h. During resolution, the expression of CD62L on neutrophils increased. These CD62L expressing tissue neutrophils may resemble a regulatory neutrophil phenotype that has been previously observed by Pillay et al during the resolution of systemic inflammation after intravenous LPS challenge in humans [208]. Regulatory neutrophils actively suppress $CD4^+$ T cell proliferation and could contribute to tolerance to self-antigens at the inflamed site [209]. Neutrophil clearance was also associated with monocytes/macrophages switching to a pro-resolution phenotype as evident from increase in CD163. CD163 is haemoglobin scavenger receptor which is upregulated on macrophages after efferocytosis [178]. Monocytes/macrophages also showed increased CD16 expression during resolution in this model, similar to the observations made in the cantharidin skin blister. The decline in neutrophils and monocytes/macrophages was

associated with an increase in lymphocytes, consistent with the results observed during resolution of acute peritonitis in the mice [88]. Taken together, the findings in this model are in agreement with our existing knowledge of the acute inflammatory response seen in patients and are also reminiscent of events characterising cellular resolution in mouse models, thus further validating the use of this model for investigating resolution processes and effect of pro-resolving therapies on resolution indices in humans.

Neutrophil clearance is one of the important hallmarks of resolution of acute inflammation. An important feature of a translational model of resolution should therefore be to allow investigation and quantification of the extent of neutrophil clearance. The UVkEc triggered dermal model of inflammation shows a clear temporal profile of neutrophils which were cleared completely from the inflamed site, indicating successful resolution. I speculate that complete neutrophil clearance is achieved in this model because of a stromal scaffold formed around the inflammation site by dermal components including fibroblasts, micro-capillaries and lymphatics. The stromal scaffold could increase macrophage-neutrophil interactions and enhance macrophage efferocytosis, a key process for neutrophil clearance [210]. Fibroblasts would further contribute to this process as they have been shown to directly phagocytose apoptotic cells [211]. In addition, the microvasculature and lymphatics would also facilitate neutrophil clearance by reverse migration and lymphatic emigration respectively [212][213]. This inflamed site of UVkEc induced dermal inflammation is in contrast to the fluid sac like structure of the cantharidin blister at resolution time point where the accumulation of apoptotic neutrophils is observed. Taken together, the UVkEc triggered model of dermal

inflammation allows investigation of neutrophil clearance, a key resolution index that can be used to validate and compare the effect of novel pro-resolving therapies in humans.

Peripheral blood monocytes are classified into three main subsets namely classical monocytes ($CD14^{++}$ $CD16^{-}$), intermediate monocytes ($CD14^{++}$ $CD16^{+}$) and non-classical monocytes ($CD14^{+}$ $CD16^{+}$) [214]. In this model, the monocytes/macrophages at 4h and 8h time point were mainly of the classical phenotype and at 24h and 48h, they had higher expression of CD16 resembling an intermediate monocyte phenotype. The origin of these $CD14^{+}$ $CD16^{+}$ monocytes/macrophages, during resolution, in this model is uncertain as they could be newly influxed intermediate monocytes from blood or classical monocytes at the site that gained CD16 expression or they could be a population derived from skin resident macrophages. Each monocyte subset has been attributed a specific function. For instance, classical monocytes are better at phagocytosis and production of reactive oxygen species compared to the intermediate monocytes. [215]. Resident macrophages also have a specialised function and are involved in clearance of apoptotic cells [216]. Understanding the origin of these monocytes can provide clues to how to modulate their numbers in vivo and thereby investigate their effect on the resolution indices. Conducting this model together with peripheral blood monocyte labelling and tracking techniques in humans, e.g. autologous transfusion of ex vivo technetium-99m radiolabelled monocytes [217] may help to investigate the origin of these $CD14^{+}$ $CD16^{+}$ monocytes/macrophages during resolution phase in this model.

The suction blister technique offers multiple advantages compared to skin biopsy technique for sampling of the inflamed tissue. Firstly, the suction blister technique is minimally invasive compared to skin biopsy. Unlike the acquisition of skin biopsy, induction of suction blister does not require local anaesthesia and has lower risk of bleeding. Secondly, the technique of negative pressure induced suction blister provides an inflammatory exudate which can be easily processed to obtain cell suspension for polychromatic flow cytometry and a cell-free supernatant that can be analysed for soluble mediators by multiplex ELISA. Comparatively, the inflamed skin biopsy tissue requires a time consuming process of ex vivo digestion to prepare cell suspensions for flow cytometry. Finally, compared to the skin biopsy, suction blister wound site heals quicker and does not leave a permanent scar. Taken together, suction blister is a safer and more productive sampling technique compared to skin biopsy. Also, according to the tolerability survey, the process of suction blister was reported to be only mild discomforting. One minor limitation is that it requires special negative pressure equipment and the process takes around 1-1.5 h.

Compared to other models of acute inflammation such as cantharidin blister or skin window technique, a unique feature of the UVkEc triggered self-resolving dermal inflammation model is that it allows monitoring of the clinical signs of inflammation. Vascular hyperaemia was investigated in this model, but pain could also be assessed by measuring pain threshold using algometer (a sensitive pressure application and measuring device) [218]. In addition, heat at the site could be measured using an infrared thermometer. Demonstration of both these techniques is shown in the appendix (Figure 8.4). By allowing

investigation of clinical signs of inflammation and established indices of resolution i.e. neutrophil clearance, pro-inflammatory cytokine reduction, pro-inflammatory to pro-resolving switch in macrophage phenotype, the UVkEc triggered self-resolving dermal inflammation model could serve as a robust, standardized platform to validate the mechanism and compare the efficacy of novel pro-resolving drugs and anti-inflammatory drugs in healthy humans. Furthermore, the model can also be employed chronic inflammatory disease patients to investigate whether defects in pro-resolution pathways contribute to their disease progression. In fact, studies are already ongoing in our laboratory to investigate resolution processes in patients with inflammatory bowel disease (by Dr Daniel Marks) and rheumatoid arthritis (by Dr Julia Flint) using this model.

The major limitations of this model are due to the local and systemic side effects caused by the acute inflammation associated symptoms and the study procedures. The most common symptoms were pain at the inflamed site on the forearm, headache and mild discomfort experienced during induction of suction blister. To assess the severity of these side effects a post hoc survey was conducted amongst the study volunteers. While the survey revealed that the acute inflammation associated symptoms were minimal and did not last longer than 24h in the majority of volunteers, it is advised to exercise extra caution during screening for volunteers. Specifically, volunteers should be screened for history of skin allergies to avoid the risk of a hyper-inflammatory response to UVkEc. During the screening, potential volunteers should also be counselled in detail about the expected side effects and to minimise these side effects they should be asked to refrain from strenuous physical activity and

high concentration tasks, e.g. driving during the study period The aspirated blister site also poses a risk of secondary infection and to minimise this volunteer should also be advised to keep the site covered and dry until a scab is formed. The volunteers should also be informed that a hyperpigmentation mark persists for 4-6 weeks at the aspirated blister site and that it can remain longer in darker skin types.

In conclusion, UVKEc induced self-resolving dermal inflammation model allows investigation of quantifiable indices of onset and resolution phases of acute inflammation in a minimally invasive way. It can serve as novel proof of concept platform to test the efficacy and investigate the mechanism of novel anti-inflammatory and pro-resolving drugs in healthy humans.

Chapter 5

Effect of SPMs on resolution indices in a human model of UVkEc triggered self-resolving dermal inflammation

5.1 INTRODUCTION

The beneficial effect of SPMs including lipoxins, maresins and protectins have been shown in multiple murine models of inflammation. However, evidence showing the direct pro-resolution effect of SPMs in humans is lacking.

The UVkEc induced self-resolving dermal inflammation is a novel human model that allows detailed investigation of cells and soluble mediators that drive the onset and resolution phases of inflammation. More importantly, the accessible nature of dermal inflammation lends itself to the local administration of immune modulatory agents at a desired time point.

In this chapter, using this novel model, I investigated the temporal profile of SPMs and prostanoids during onset and resolution phases of inflammation. In addition, I investigated the SPM receptors that transduce their pro-resolution effects on the microvascular endothelium and infiltrating leucocytes. Finally, I injected SPMs at the tipping point of resolution to investigate their effect on resolution biomarkers i.e. reduction of neutrophil numbers, the decline in levels of pro-inflammatory cytokines/chemokines and enhanced clearance of the inflammatory stimulus.

5.2 STUDY DESIGN

The temporal profile of SPMs and prostanoids was measured in the inflammatory exudate generated at baseline, 4h, 8h, 14h, 24h, 48h and at 72h during characterisation of UVkEc triggered dermal inflammation model. This was performed in collaboration with Prof Charles Serhan (Harvard University,

USA). SPM receptors including FPR2/ALX, ChemR23, GPR18 and GPR32 were investigated in the skin biopsy collected at baseline and 4h after injection of UVkEc. This was performed in collaboration with histologists at UCL Institute of Neurology.

I first validated the anti-inflammatory effect of naproxen, a dual COX-1/COX-2 inhibitor, in UVkEc triggered dermal inflammation model. For this, volunteers received 500mg naproxen twice daily for four days. On the morning of the fourth day, immediately after the naproxen administration, UVkEc were injected in the forearm, and after 4h, the suction blister was induced to study onset. Naproxen used in this study was bought over the counter from a local pharmacy.

To test the pro-resolution effect of SPMs, a SPM cocktail comprising LXB_4 (570 pM = 200 pg/ml), RvE1 (115 pM = 40 pg/ml), RvD2 (450 pM = 170 pg/ml), AT-RvD1 (3.2 nM = 1200 pg/ml) in 100 µl saline was injected in one of the forearm 4h after UvKEc injection and its effect on resolution biomarkers was investigated by raising a suction blister over the injection site at 10h. The doses of SPMs selected for intradermal injection reflect the highest concentration of these SPMs found at the inflamed site in this model. To serve as a control, an inflamed site on the contralateral forearm was injected at 4h time point with 100 µl saline only. SPM cocktail used in this study was prepared and validated by Dr Jesmond Dalli (The William Harvey Research Institute, Queen Mary University of London, UK).

5.3 RESULTS

5.3.1 Anti-inflammatory effect of naproxen in the UVkEc induced dermal inflammation model.

Naproxen significantly suppressed vascular hyperaemia at 4h compared to the control group. The mean blood flow in control group was 1.72 x 10^6 ± 0.61 x 10^6 perfusion units and it was decreased by naproxen to 0.6 x 10^6 ± 0.41 x 10^6 perfusion units **(Figure 5.1 A)**. The representative laser Doppler images of the control and naproxen treated arm are shown in **Figure 5.1 B.**

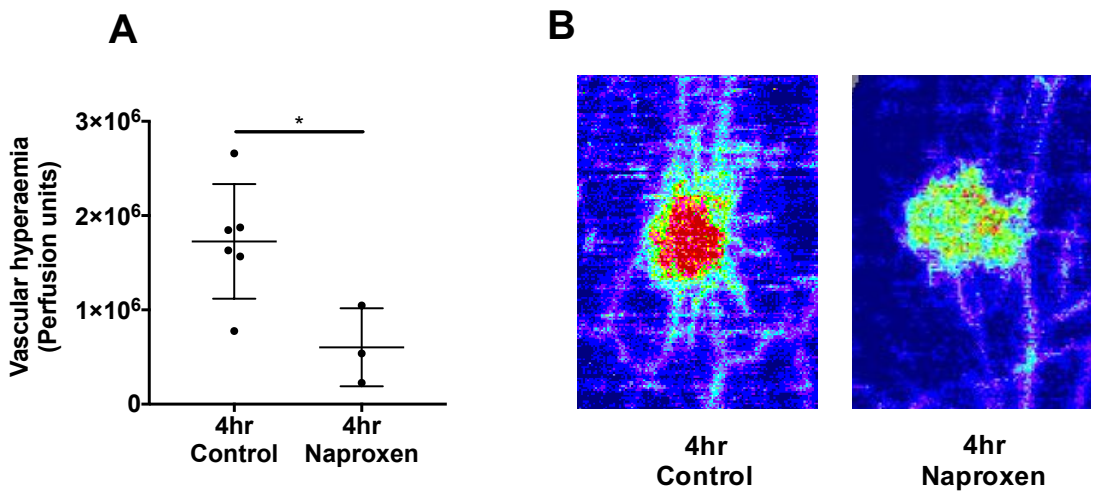

Figure 5.1 Effect of Naproxen on vascular hyperaemia during onset phase of UV killed *E. coli* triggered self resolving dermal inflammation

Healthy volunteers received Naproxen 500mg, twice daily for four days. On morning of fourth day, acute inflammation was triggered by intradermal injection of UV killed *E. coli (UVkEc)* in 100µl of saline. Vascular hyperaemia was assessed 4hr after bacterial injection using a Laser Doppler Imager. Vascular hyperaemia over the injection site at 4hr time point in the control arm vs naproxen arm **(A)** and the representative Doppler flux are shown here. Data expressed as individual values, mean ± SD. n= 6 for 4hr Control arm and n=3 for the 4hr naproxen arm. * p< 0.05.

In addition to suppressing vascular hyperaemia, naproxen significantly inhibited the migration of neutrophils and monocytes/macrophages in the inflamed site at 4h compared to the control group. Naproxen treatment

reduced neutrophil count at 4h from 573,455 ± 284,242/ml in control group to 206,835 ± 159,500/ml **(Figure 5.2 A)**. The proportion of neutrophils in naproxen vs. control group is highlighted in **Figure 5.2 B.** Monocyte/macrophage numbers decreased from 27,199 ± 43,129/ml in the control group to 990 ± 262 /ml following naproxen **(Figure 5.2 C).** The proportion of monocytes/macrophages in naproxen vs. control group is highlighted in **Figure 5.2 D.**

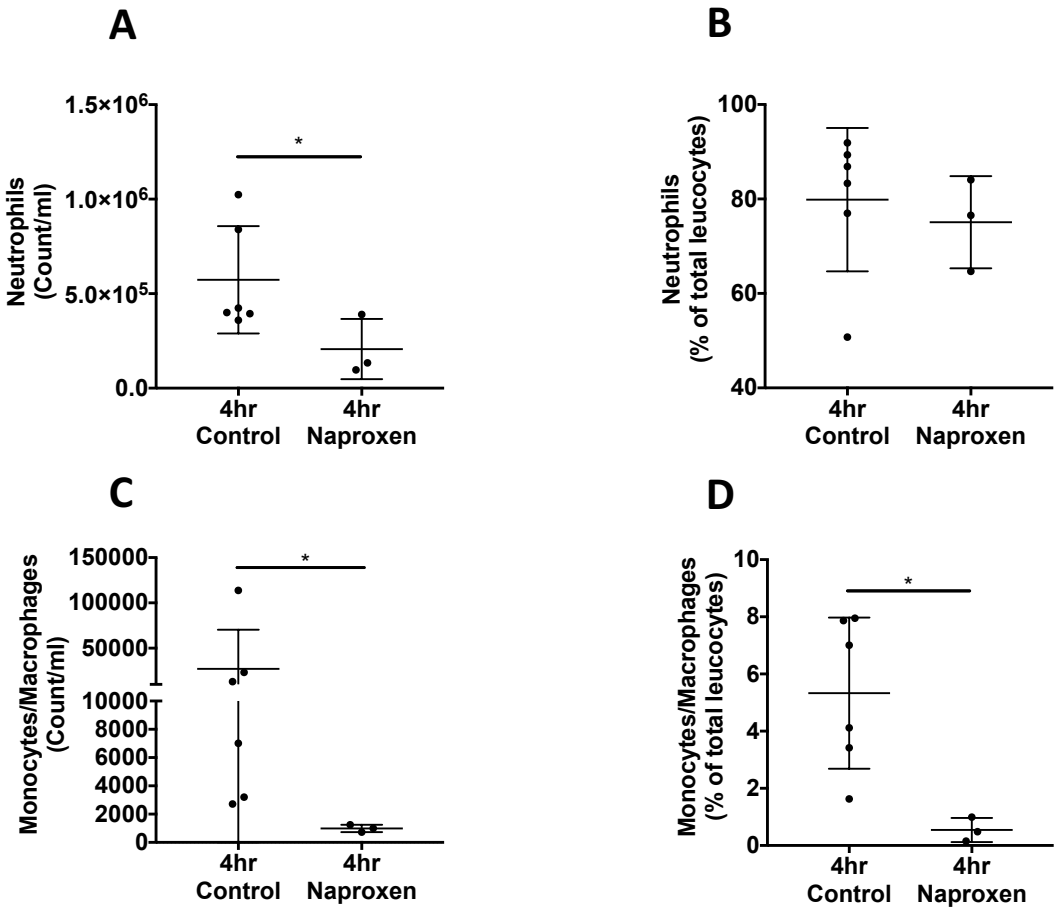

Figure 5.2 Effect of Naproxen on neutrophil and macrophage numbers during onset phase of UV killed *E. coli* triggered self resolving dermal inflammation

Healthy volunteers received Naproxen 500mg, twice daily for four days. On morning of fourth day, acute inflammation was triggered by intradermal injection of UV killed *E. coli (UVkEc)* in 100µl of saline. Suction blister was raised over the inflamed site 4hr after UVkEc injection to acquire inflammatory exudate. The immune cell subsets in cells in the exudate were identified by multi color flow cytometry. Neutrophil count/ml **(A)**, proportion of neutrophils of total leukocytes **(B)**, monocytes/macrophages count/ml **(C)** and proportion of monocytes/macrophages of total leukocytes **(D)** are shown here. Data expressed as individual values with mean ± SD. n= 6 for 4hr control arm and n=3 for the 4hr naproxen arm. * p< 0.05.

Unlike the reduction of vascular hyperaemia and neutrophil count, naproxen increased levels of pro-inflammatory cytokines TNF-α and IL-8 at 4h compared to the control group. TNF-α levels in placebo group were 1,568 pg/ml ± 732.5 and in naproxen group they were 7,608 ± 6,624 pg/ml **(Figure 5.3 A)**. Levels of IL-8 in the control group were 3,556 ± 2,232 pg/ml, and in the naproxen group, they were 9,601 ± 4,788 pg/ml **(Figure 5.3 B)**. Naproxen had on effect on other pro-inflammatory cytokines and chemokines including IL-1β **(Figure 5.3 C),** IFN-γ **(Figure 5.3 D)**, IL-6 **(Figure 5.3 E)** or IL-12p70 **(Figure 5.3 F)**.

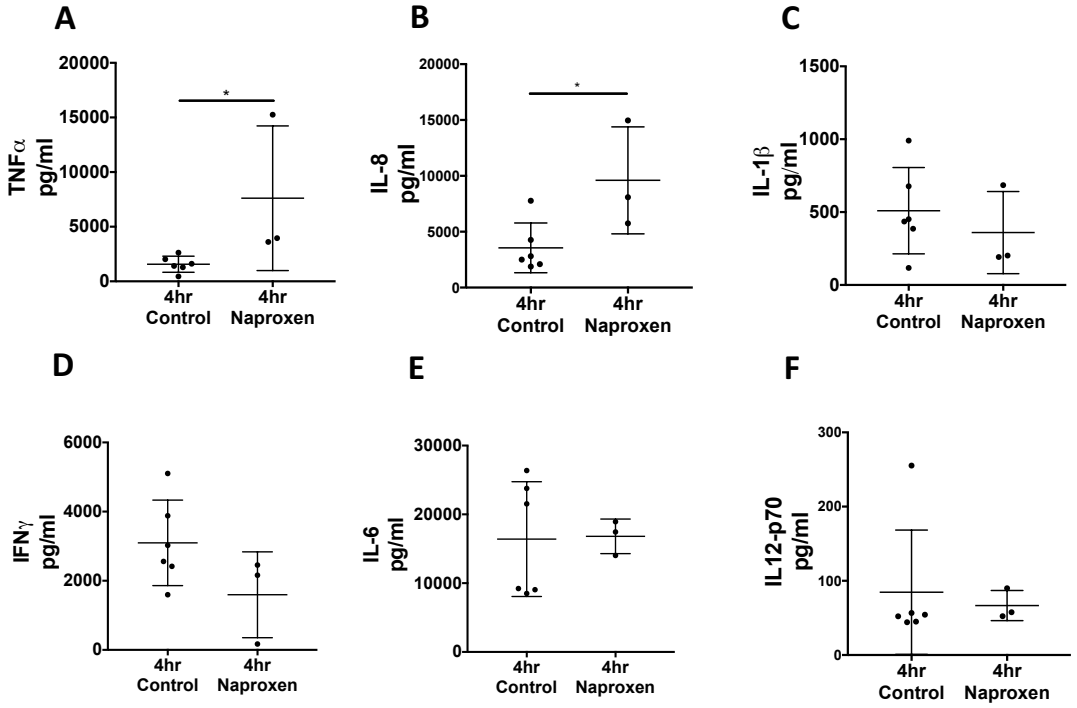

Figure 5.3 Effect of Naproxen on cytokine and chemokine profile during onset phase of UV killed *E. coli* triggered self resolving dermal inflammation

Healthy volunteers received Naproxen 500mg, twice daily for four days. On morning of fourth day, acute inflammation was triggered by intradermal injection of UV killed *E. coli (UVkEc)* in 100µl of saline. Suction blister was raised over the inflamed site 4hr after UVkEc injection to acquire inflammatory exudate. Cytokines and chemokines in the cell free exudate were measured by multiplex ELISA and their concentrations at 4hr time point in control vs naproxen arm are shown here. Data expressed as individual values with mean ± SD. n= 6 for 4hr Control arm and n=3 for the 4hr Naproxen arm. * $p < 0.05$.

5.3.2 Lipid mediator analysis of inflammatory exudate at the site of UVkEc triggered self-resolving dermal inflammation

LC-MS/MS (Liquid Chromatography tandem mass spectrophotometry) was used to quantify levels of arachidonic acid (AA), eicosapentaenoic acid (EPA) and docosahexaenoic acid (DHA) derived lipid mediators and was performed in collaboration with Dr Charles Serhan Lab (Harvard University, USA).

Levels of COX-derived products including PGE_2 (**Figure 5.4 A)**, TXB_2 (**Figure 5.4 B)** and $PGF_{2\alpha}$ (**Figure 5.4 C)** peaked at 4h. At this time point, the concentration of PGE_2 was 2,464 ± 947.8 pg/ml, $PGF_{2\alpha}$ was 3,237 ± 1511 pg/ml and TXB_2 was 1,051 ± 659.2 pg/ml. From 4h, levels of these lipid mediators declined gradually and reached baseline levels by 24h. There was a transient and mild second rise in these lipids at 48h that was nonetheless lower than that at 4h. At 48h, levels of PGE_2 were 1,420 ± 699.6 pg/ml, $PGF_{2\alpha}$ were 544.7 ± 362.1 pg/ml and TXB_2 were 528.4 ± 361.4 pg/ml. Compared to PGE_2, $PGF_{2\alpha}$ and TXB_2, levels of PGD_2 had high variance at all the investigated time points, and they also lacked a temporal profile **(Figure 5.4 D).**

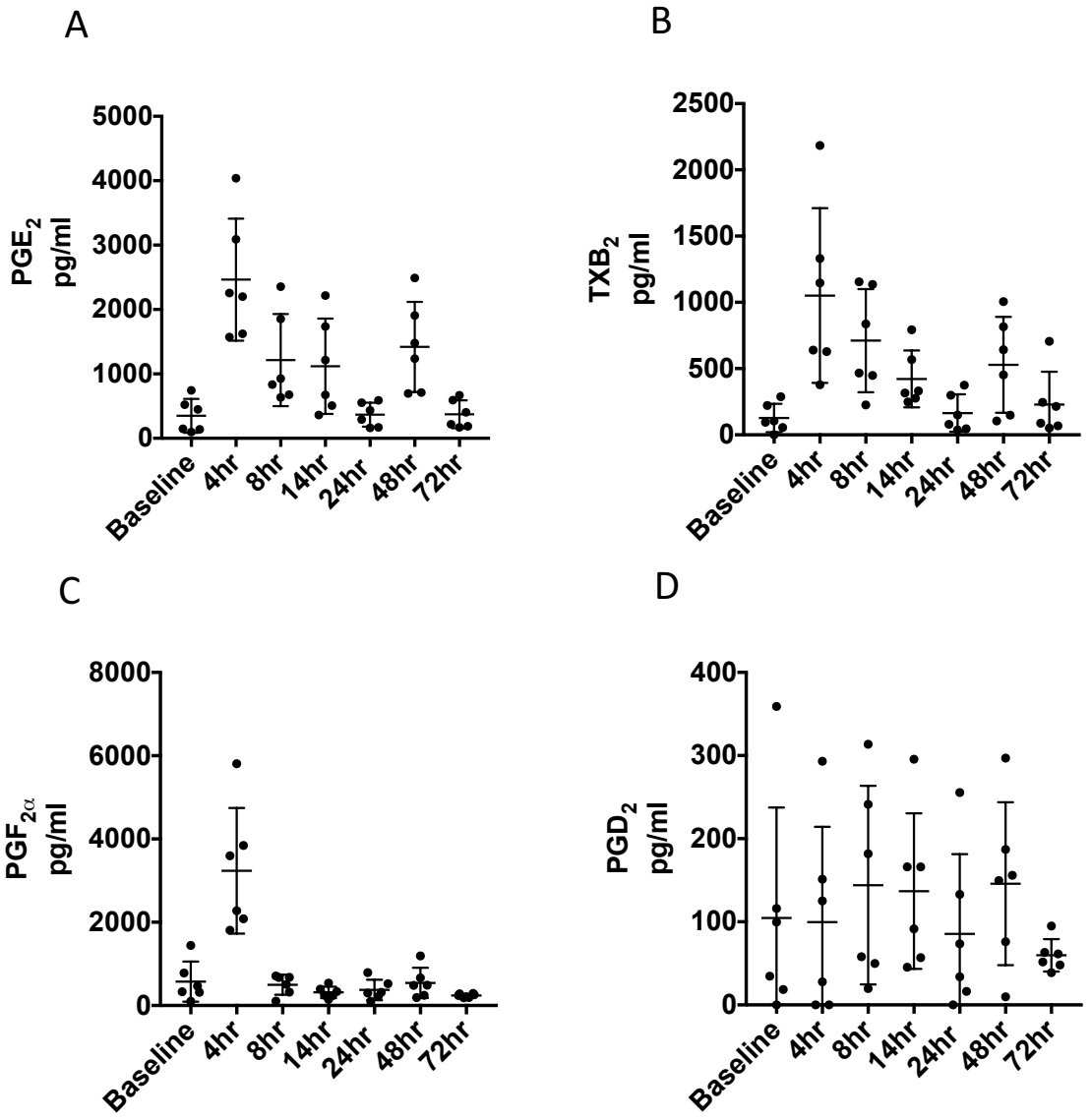

Figure 5.4 Profile of prostanoids at the site of UV killed *E. coli* triggered self resolving dermal inflammation

Acute inflammation was triggered in the ventral aspect of forearm of healthy volunteers by the intradermal injection of 1.5 x 10^7 UV killed *E. coli* (UVkEc) suspended in 100µl of sterile saline. A suction blister was raised over the inflamed site at the specified intervals to collect the inflammatory exudate. Lipid mediators in the cell free exudate were analysed by liquid chromatography mass spectrophotometry (LC-MS) by Prof. Serhan laboratory (Harvard University). Levels of PGE_2 (A), $PGF_{2\alpha}$ **(B)**, TXB_2 **(C)** and PGD_2 **(D)** in the inflammatory exudate at specified intervals are shown here. Data is expressed as individual values with mean ± SD. n=6 for each time point.

The concentration of LXA_4 and AT-LXA_4 did not change during different phases of inflammation, and the mean levels were < 40 pg/ml across all the time points **(Figure 5.5 A, C)**. In contrast, LXB_4 showed an increasing trend from baseline to 4h with levels increasing from 39.02 ± 26.08 pg/ml at baseline to 105.5 ± 30.97 pg/ml at 4h. Between 4h and 48h the levels of LXB_4 declined **(Figure 5.5 B).** Unlike LXB_4, the levels of AT-LXB_4 did not differ between the any of the time-points and the mean level was < 50pg/ml **(Figure 5.5 D)**.

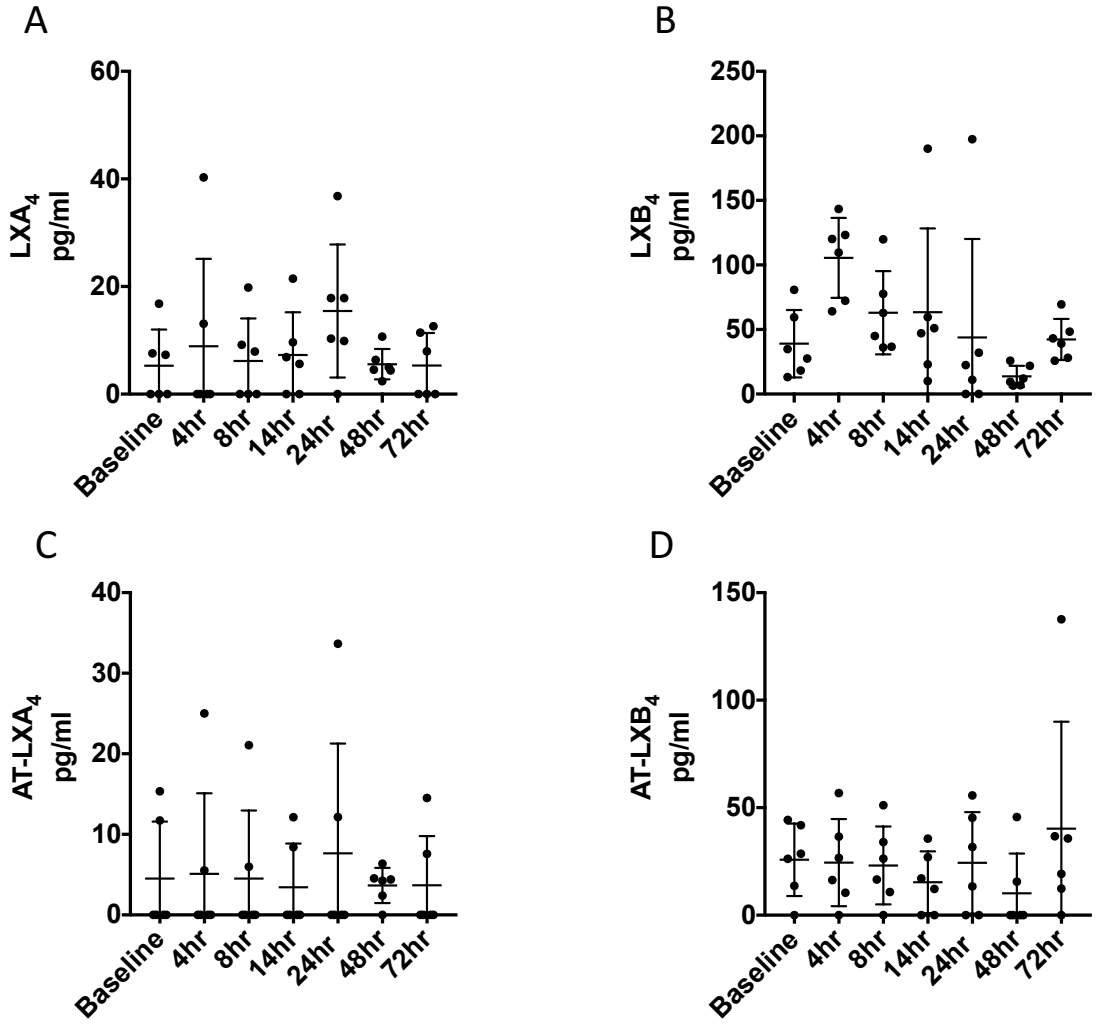

Figure 5.5 Profile of lipoxins and aspirin triggered-lipoxins at the site of UV killed *E. coli* triggered self resolving dermal inflammation

Acute inflammation was triggered in the ventral aspect of forearm of healthy volunteers by the intradermal injection of 1.5 x 10^7 UV killed *E. coli* (UVkEc) suspended in 100µl of sterile saline. A suction blister was raised over the inflamed site at the specified intervals to collect the inflammatory exudate. Lipid mediators in the cell free exudate were analysed by liquid chromatography mass spectrophotometry (LC-MS) by Prof. Serhan laboratory (Harvard University). Levels of LXA_4 **(A)**, LXB_4 **(B)**, AT-LXA_4 **(C)**, AT-LXB_4 **(D)** in the inflammatory exudate at specified intervals is shown here. Data is expressed as individual values with mean ± SD. n=6 for each time point.

The concentration of RvE1 and RvE2, the EPA derived lipid mediators did not increase during any specific phase of the inflammatory response **(Figure 5.6 A, B)**. However, the levels of RvE3 showed an increasing trend between baseline and 8h. At baseline, RvE3 levels were 160.2 ± 112.5 pg/ml, and at 8h they were 291.6 ± 50.97 pg/ml. The levels of RvE3 remained high until 14h, at which point they were 274.3 ± 29.06 pg/ml. **(Figure 5.6 C)**. From 14h onwards the concentration of RvE3 levels declined and reached baseline values at 72h.

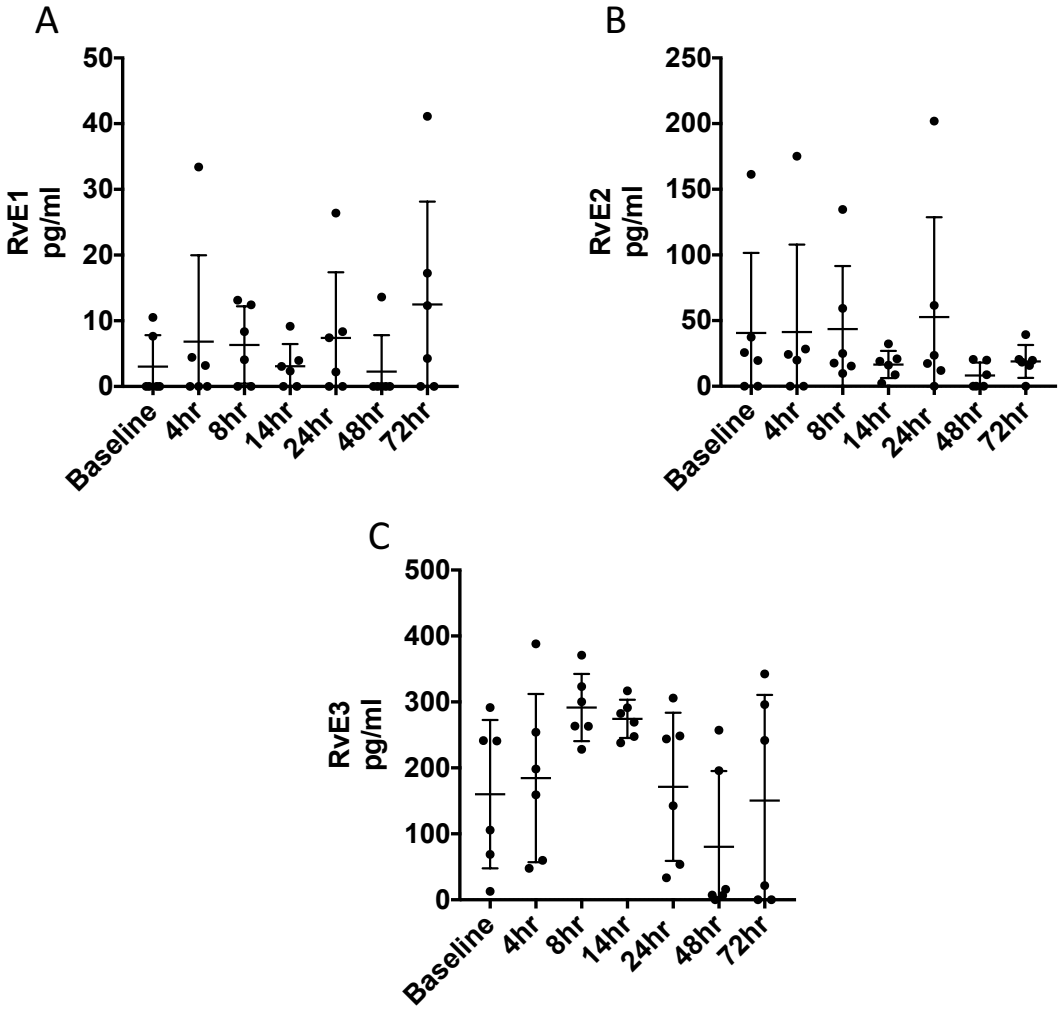

Figure 5.6 Profile of E-series resolvins at the site of UV killed *E. coli* triggered self resolving dermal inflammation

Acute inflammation was triggered in the ventral aspect of forearm of healthy volunteers by the intradermal injection of 1.5 x 10^7 UV killed *E. coli* (UVKEc) suspended in 100µl of sterile saline. A suction blister was raised over the inflamed site at the specified intervals to collect the inflammatory exudate. Lipid mediators in the cell free exudate were analysed by liquid chromatography mass spectrophotometry (LC-MS) by Prof. Serhan laboratory (Harvard University). Levels of RvE1 **(A)**, RvE2 **(B)**, and RvE3 **(C)** in the inflammatory exudate at specified intervals is shown here. Data is expressed as individual values with mean ± SD. n=6 for each time point.

The concentration of DHA derived metabolites including D- series resolvins and maresin 1 did not differ significantly from baseline during the onset or resolution time points. The mean levels of these metabolites were < 20pg/ml at all time points apart from RvD2 and AT-RvD1. At 4h, the levels of RvD2 and AT-RvD1 were 43.05 ± 62.42 pg/ml and 267.2 ± 449.9 pg/ml respectively **(Figure 5.7 B, F)**.

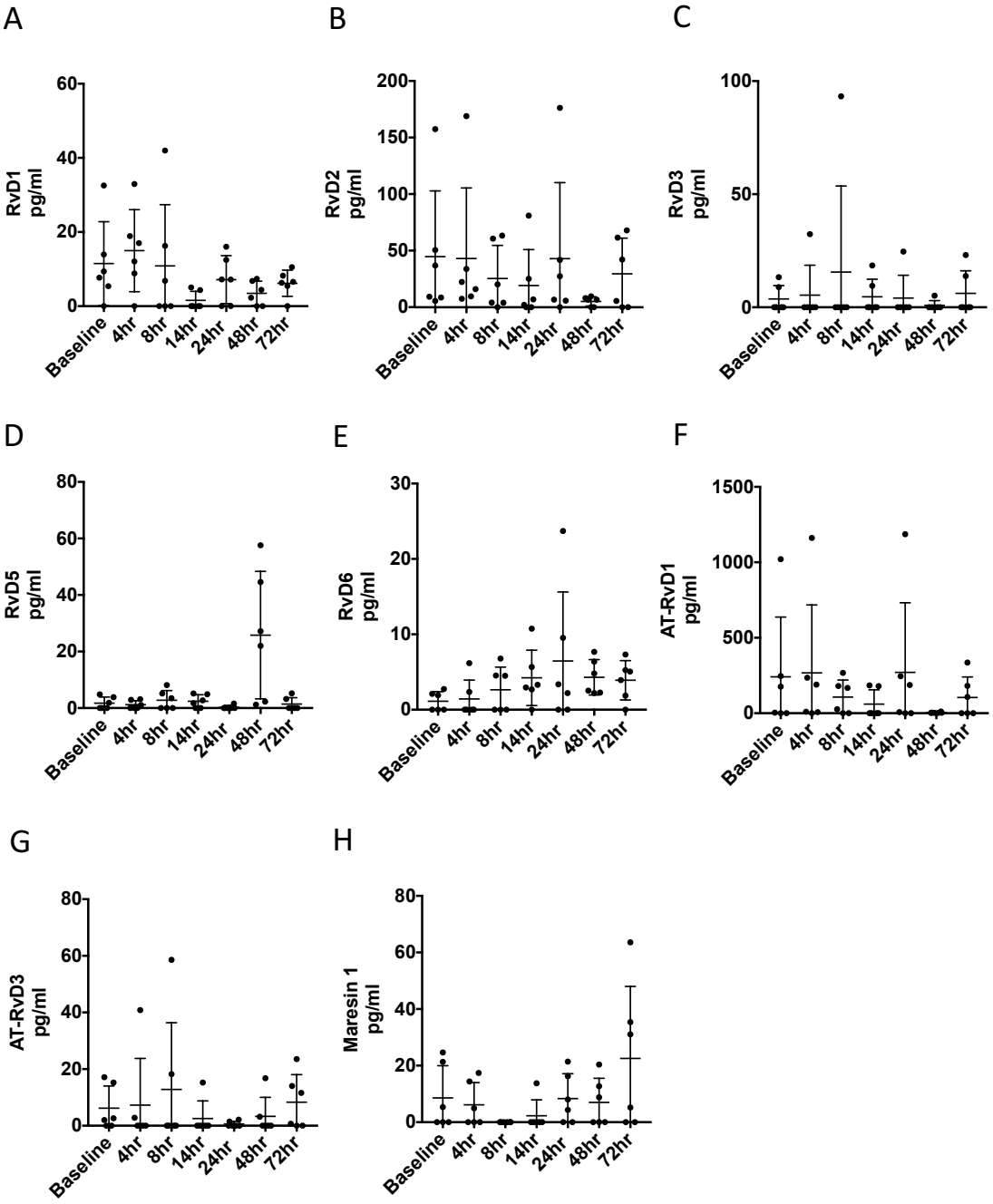

Figure 5.7 Profile of D-series resolvins and maresin 1 at the site of UV killed *E. coli* triggered self resolving dermal inflammation

Acute inflammation was triggered in the ventral aspect of forearm of healthy volunteers by the intradermal injection of 1.5 x 10^7 UV killed *E. coli* (UVKEc) suspended in 100µl of sterile saline. A suction blister was raised over the inflamed site at the specified intervals to collect the inflammatory exudate. Lipid mediators in the cell free exudate were analysed by liquid chromatography mass spectrophotometry (LC-MS) by Prof. Serhan laboratory (Harvard University). Levels of RvD1 **(A)**, RvD2 **(B)**, and RvD3 **(C),** RvD5 **(D),** RvD6 **(E),** AT-RvD1 **(F),** AT-RvD3 **(G)** and Maresin 1 **(H)** in the inflammatory exudate at specified intervals is shown here. Data is expressed as individual values with mean ± SD. n=6 for each time point.

5.3.3 Expression of SPM receptors at the site of UVkEc triggered self-resolving dermal inflammation

SPM receptors (FPR2/ALX, ChemR23, GPR18 and GPR32) were investigated in the skin biopsy by immunohistochemistry and was performed in collaboration with histologists at UCL Institute of Neurology. Skin biopsy was taken at baseline and at 4h, the time point when neutrophils start to clear from the site.

FPR2/ALX, the receptor for lipoxin A4, RvD1 and AT-RvD1 was detected at 4h mainly on the inflamed endothelium with no detectable expression on the endothelium of naïve skin (**Figure 5.8 A, B)**. The expression of ChemR23, the receptor for RvE1 was observed on the epithelium and endothelium in the naïve skin and was elevated mainly on the infiltrating leucocytes in the 4h inflamed skin (**Figure 5.8 C, D)**. GPR18, the receptor for RvD2 was observed on naive endothelium, and at 4h it was expressed on the endothelium and infiltrating leucocytes (**Figure 5.9 A, B)**. GPR32, the receptor for RvD1 and AT-RvD1 was observed mainly on the leucocytes in the 4h inflamed skin (**Figure 5.9 C, D)**.

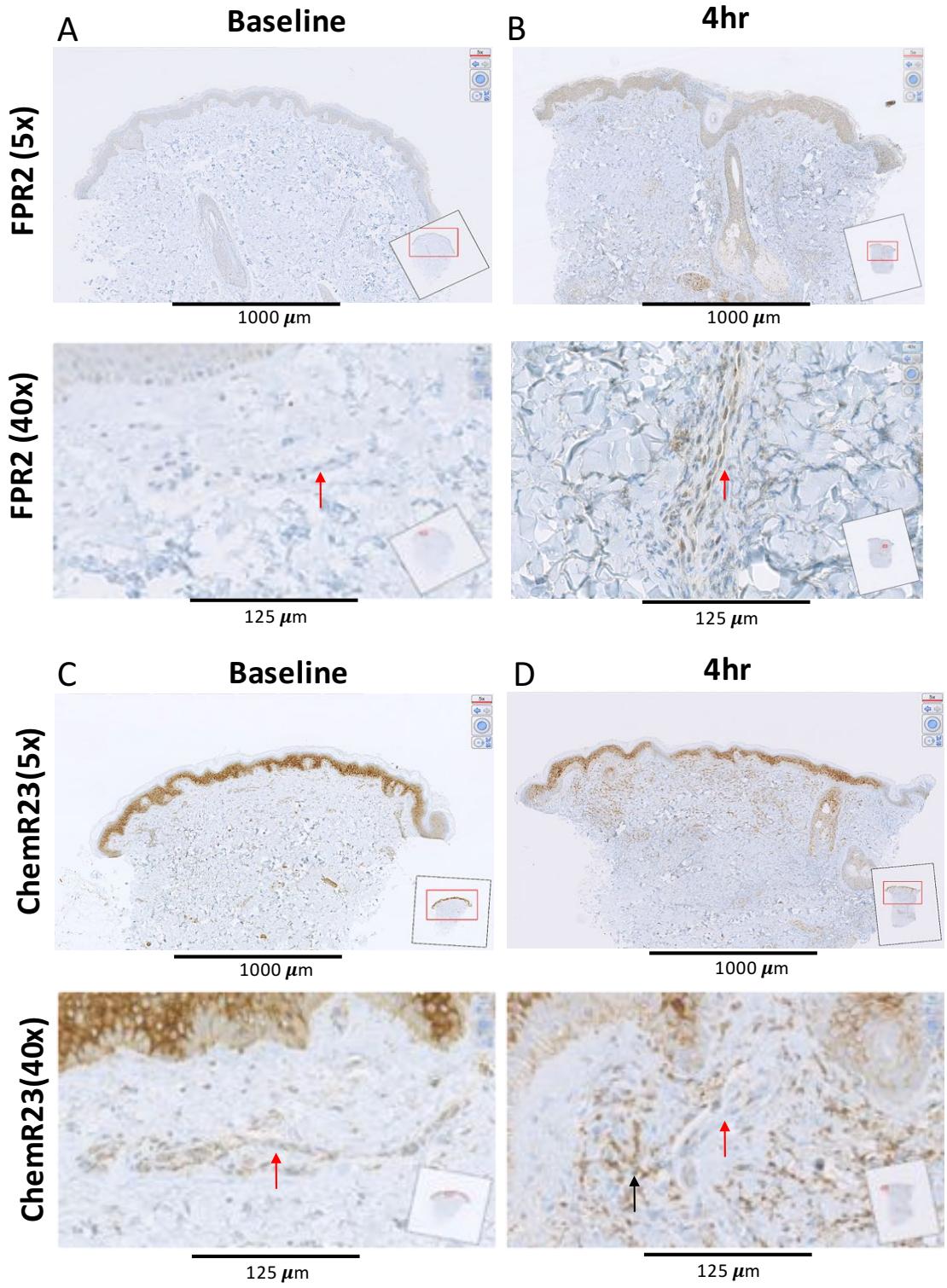

Figure 5.8 SPM receptor (FPR2 and ChemR23) expression on the endothelium and the infiltrating leucocytes.- at the baseline and 4hr in the UV killed *E. coli* triggered self resolving dermal inflammation model

Acute inflammation was triggered in the ventral aspect of forearm of healthy volunteers by the intradermal injection of 1.5 x 10^7 UV killed *E. coli* (UVKEc) suspended in 100µl of sterile saline. 4hr after injection a 3mm skin punch biopsy was taken from the inflamed site under local anaesthesia. Naive skin was treated as baseline. Formalin fixed paraffin embedded (FFPE) skin sections were probed by immunohistochemistry department at UCL Institute of Neurology for SPM receptor identification. Low magnification (5x) and high magnification (40x) images at baseline and at the 4hr time point are shown here for FPR2 **(A and B)** and ChemR23 **(C and D)**. Red arrow highlights endothelium and black arrow highlight the infiltrating leucocytes. Representative images from n=3.

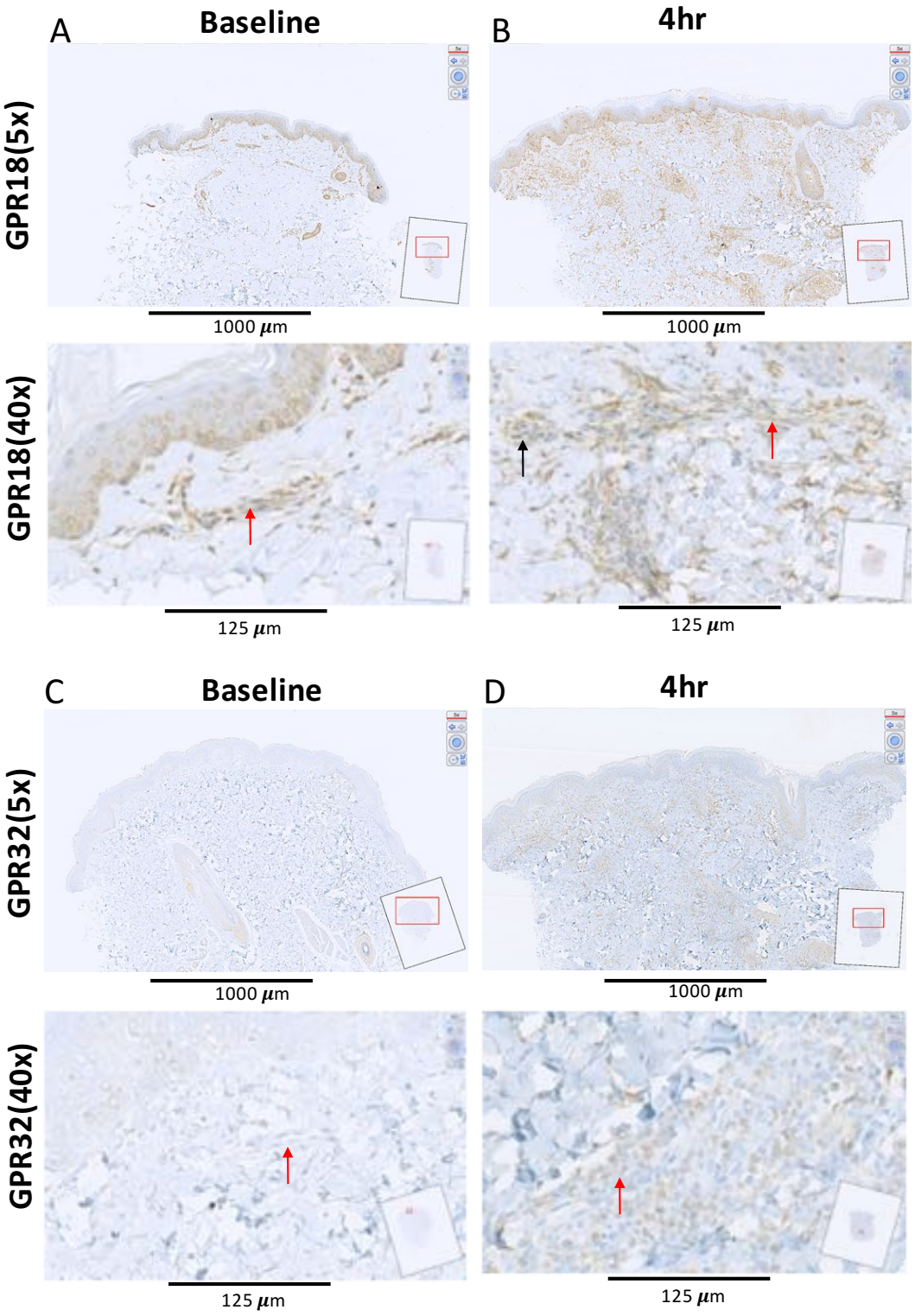

Figure 5.9 SPM receptor (GPR18 and GPR32) expression on the endothelium and the infiltrating leucocytes at the baseline and 4hr in the UV killed *E. coli* triggered self resolving dermal inflammation model

Acute inflammation was triggered in the ventral aspect of forearm of healthy volunteers by the intradermal injection of 1.5 x 10^7 UV killed *E. coli* (UVKEc) suspended in 100μl of sterile saline. 4hr after injection a 3mm skin punch biopsy was taken from the inflamed site under local anaesthesia. Naive skin was treated as baseline. Formalin fixed paraffin embedded (FFPE) skin sections were probed by immunohistochemistry department at UCL Institute of Neurology for SPM receptor identification. Low magnification (5x) and high magnification (40x) images at baseline and at 4hr time point are shown here for GPR18 **(A and B)** and GPR32 **(C and D)**. Red arrow highlights endothelium and black arrow highlight the infiltrating leucocytes. Representative images from n=3

5.3.4 Effect of SPMs on resolution biomarkers

5.3.4.1 Effect of SPMs on vascular hyperaemia during resolution

The injection of cocktail of SPMs into the inflamed site at 4h did not alter vascular hyperaemia at the site at 10h, compared to the saline arm. At 10h, the vascular hyperaemia at the saline-injected site was $0.93 \times 10^6 \pm 0.36 \times 10^6$ perfusion units, while at the SPM injected site it was $0.89 \times 10^6 \pm 0.42 \times 10^6$ perfusion units. However, at 48h the SPM arm had a decreasing trend in blood flow compared to the saline arm. At 48h, the total flux in saline injected arm was $1.08 \times 10^6 \pm 1.19 \times 10^6$ perfusion units and in SPM injected arm it was $0.68 \times 10^6 \pm 0.52 \times 10^6$ perfusion units **(Figure 5.10).**

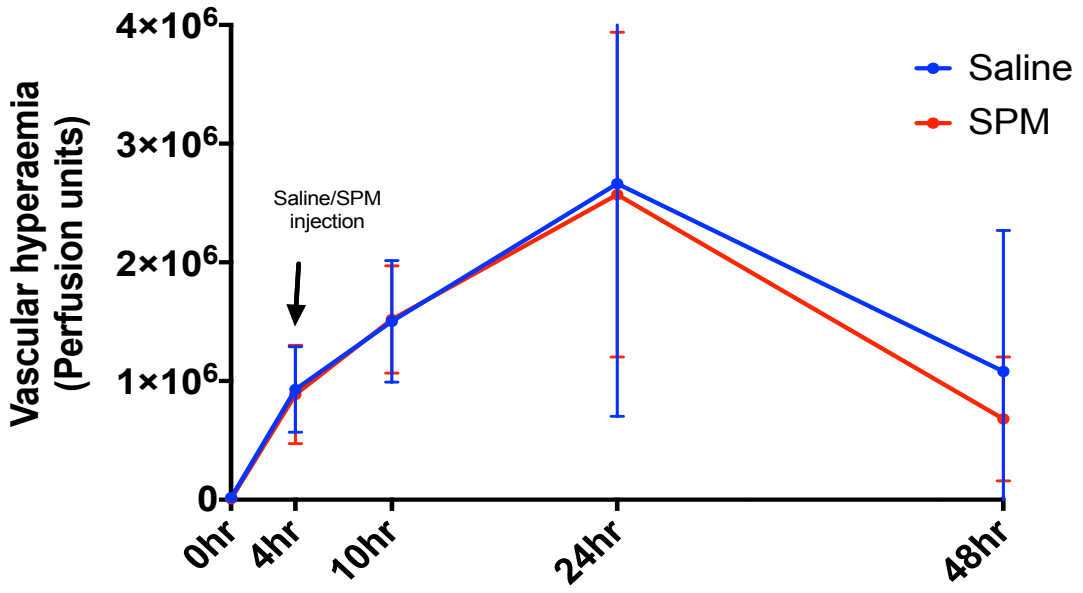

Figure 5.10 Effect of therapeutic administration of SPMs on vascular hyperemia at resolution time points in UV killed *E. coli* triggered self resolving dermal inflammation model

Acute inflammation was triggered by intradermal injection of UVkEc in both the forearms. 4hr after bacterial injection, SPM cocktail (570 pM LXB_4, 115 pM RvE1, 450 pM RvD2, 3.2 nM AT-RvD1 in 100µl saline) was injected into the inflamed site at 4hr in one forearm and 100µl of saline was injected into the contralateral forearm at same time to serve as a control . Vascular hyperaemia was assessed using a Laser Doppler Imager. The effects of SPM cocktail vs saline on vascular hyperaemia at specified intervals is shown here. Data is expressed mean ± SD. n=6 for each time point.

5.3.4.2 Effect of SPMs on neutrophil and monocytes/macrophages numbers during resolution.

SPMs significantly decreased the number of neutrophils at 10h. At this time point, the neutrophil count in saline injected arm was 22,885 ± 15,320 /ml, while in SPM injected arm it decreased to be 13,980 ± 8,424 /ml **(Figure 5.11 A)**. Compared to saline injected arm, there was no difference in neutrophil CD62L expression after SPM injection **(Figure 5.11 B)**.

The numbers of monocytes/macrophages and their expression of CD163 did not change significantly between saline and SPM injected arm. In the saline arm, the monocyte/macrophage count was 71,000 ± 36,255 and in the SPM injected arm it was 54,099 ± 27,516 (**Figure 5.11 C)**. The median fluorescence intensity of CD163 in saline injected arm was 5,499 ± 6,402 MFI units and in the SPM injected arm it was 6,416 ± 5,774 MFI units **(Figure 5.11 D)**.

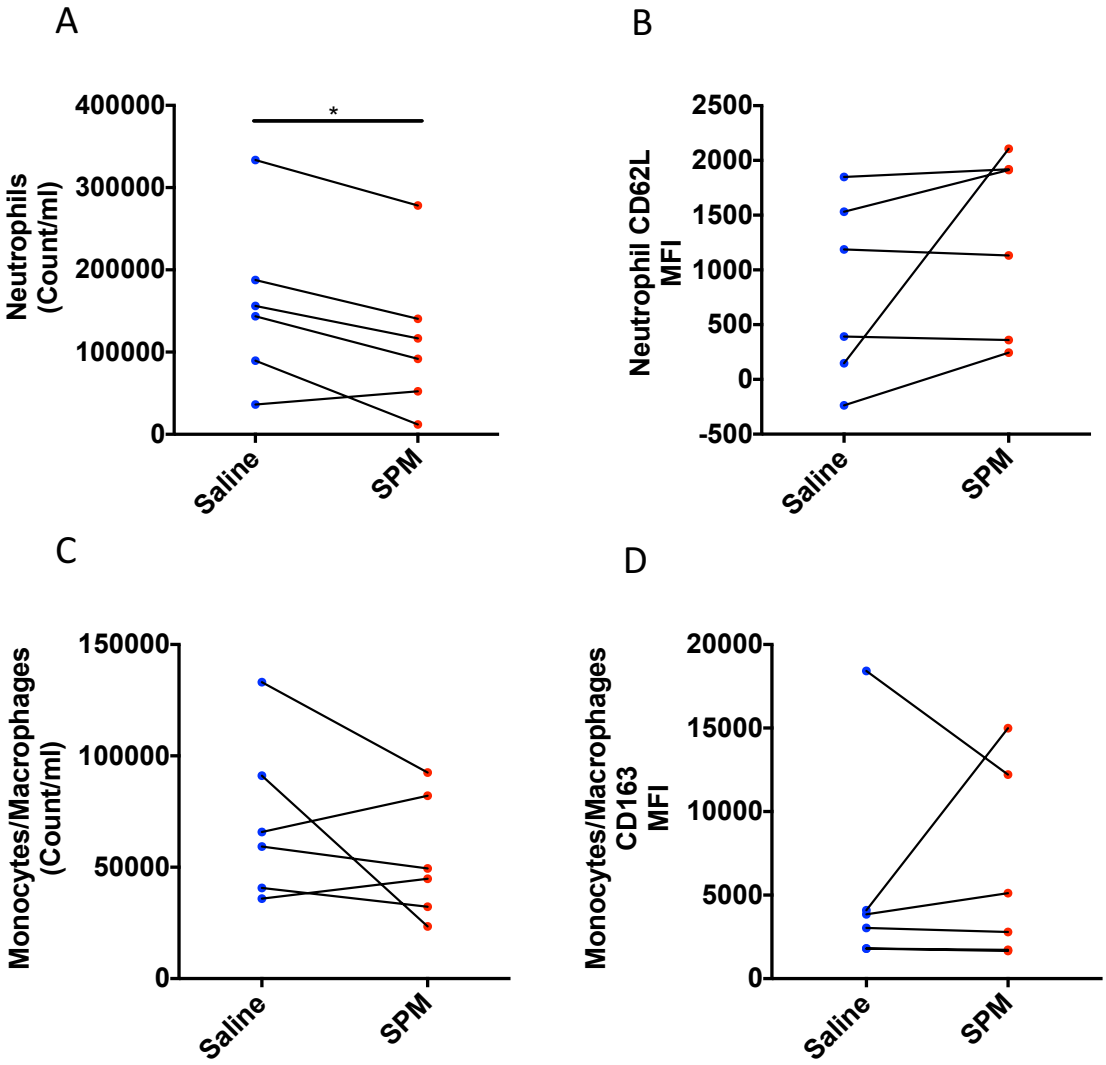

Figure 5.11 Effect of therapeutic administration of SPMs on neutrophil and monocyte/macrophage numbers at resolution time point in UV killed *E. coli* triggered self resolving dermal inflammation model

Acute inflammation was triggered by intradermal injection of 1.5 x 10^7 UV killed *E. coli* (UVKEc) suspended in 100µl of sterile saline in both the forearms. 4hr after bacterial injection, SPM cocktail (570 pM LXB_4, 115 pM RvE1, 450 pM RvD2, 3.2 nM AT-RvD1 in 100µl saline) was injected into the inflamed site at 4hr in one forearm and 100µl of saline was injected into the contralateral forearm at same time to serve as a control . 10hr after UVkEc injection (i.e. 6hr after SPM cocktail/saline injection) a suction blister was raised over the inflamed site on both forearm sites to acquire the inflammatory exudate. The immune cells in the exudate were identified by multi color flow cytometry. Neutrophil count/ml **(A)**, neutrophil CD62L MFI **(B)** monocytes/macrophages count/ml **(D)** and monocytes/macrophages CD163 expression **(D)** in saline vs SPM group at 10hr is shown here. Data is expressed as individual values. n=6 for each time point. * = $p < 0.05$

5.3.4.3 Effect of SPMs on pro-inflammatory cytokines/chemokines and endotoxin

The effect of SPMs on the reduction of pro-inflammatory cytokines or chemokines during resolution was not very evident in this model for any of the major pro-inflammatory cytokines including IL-8, TNF-α, IL-1β, IL-6, IL12-p70 and IFN-γ **(Figure 5.12 A, B, C, D, E, F).** Similarly, the mean levels of anti-inflammatory cytokines IL-4, IL10 and IL-13 were not significantly different between the SPM vs. saline injected arm. **(Figure 5.12 G, H, I)**.

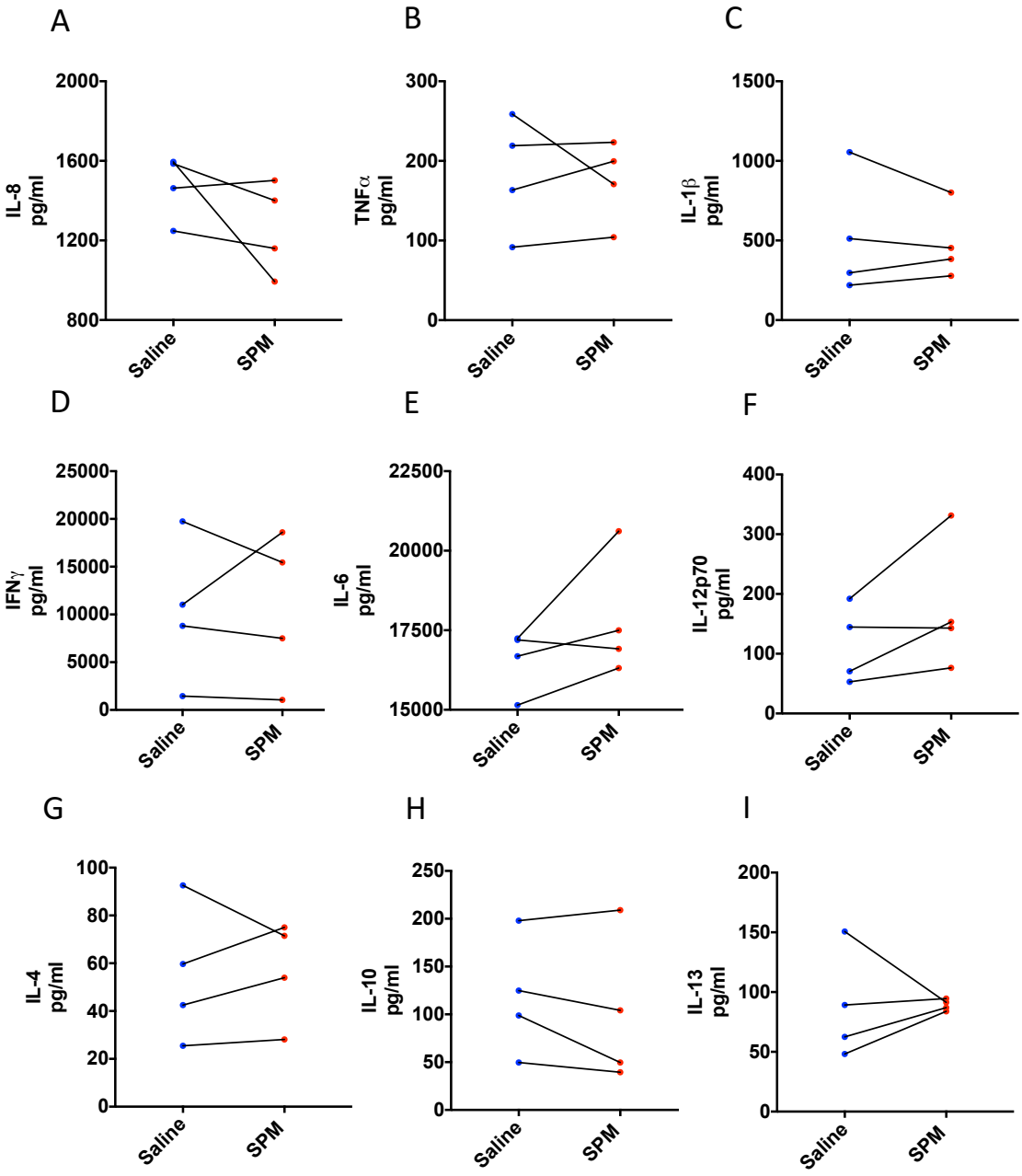

Figure 5.12 Effect of therapeutic administration of SPMs on cytokine and chemokine profile at resolution time point in UV killed *E. coli* triggered self resolving dermal inflammation

Acute inflammation was triggered by intradermal injection of 1.5 x 10^7 UV killed *E. coli* (UVKEc) suspended in 100µl of sterile saline in both the forearms. 4hr after bacterial injection, SPM cocktail (570 pM LXB_4, 115 pM RvE1, 450 pM RvD2, 3.2 nM AT-RvD1 in 100µl saline) was injected into the inflamed site at 4hr in one forearm and 100µl of saline was injected into the contralateral forearm at same time to serve as a control. 10hr after UVkEc injection (i.e. 6hr after SPM cocktail/saline injection) a suction blister was raised over the inflamed site on both forearm sites to acquire the inflammatory exudate. Cytokines/chemokines in the inflammatory exudate were measured by multiplex ELISA. The effect of SPM cocktail vs saline on cytokine and chemokine profile in the inflammatory exudate at 10hr is shown here. Data is expressed as individual values. n=4 for each time point.

In addition, SPMs did not increase the clearance of the inflammatory stimulus during resolution as evident from the levels of endotoxin, a component of gram negative bacterial wall in the 10h blister exudate. The endotoxin level in the saline arm was 2.42 ± 2.11 EU, and in the SPM group, it was 2.21 ± 2.67 EU **(Figure 5.13).**

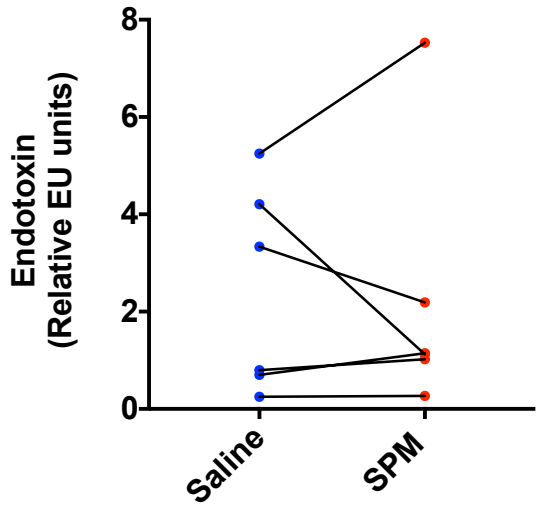

Figure 5.13 Effect of therapeutic administration of SPMs on endotoxin levels at resolution time point in UV killed *E. coli* triggered self resolving dermal inflammation

Acute inflammation was triggered by intradermal injection of 1.5 x 10^7 UV killed *E. coli* (UVKEc) suspended in 100µl of sterile saline in both the forearms. 4hr after bacterial injection, SPM cocktail (570 pM LXB_4, 115 pM RvE1, 450 pM RvD2, 3.2 nM AT-RvD1 in 100µl saline) was injected into the inflamed site at 4hr in one forearm and 100µl of saline was injected into the contralateral forearm at same time to serve as a control . 10hr after UVkEc injection (i.e. 6hr after SPM cocktail/saline injection) a suction blister was raised over the inflamed site on both forearm sites to acquire the inflammatory exudate. Endotoxin as a surrogate for inflammatory stimulus (UVkEc) was measured using kinetic turbidimetric limulus ameobocyte lysate test. The effect of SPM cocktail vs saline on endotoxin content in the inflammatory exudate at 10hr is shown here. Data is expressed as individual values. n=6 for each time point.

5.4 DISCUSSION

The beneficial effects of SPMs has been demonstrated in multiple mouse models of inflammatory diseases and in human *ex vivo* assays [117] [219][220]. Multiple studies have also validated SPM physiology in humans. For example, SPMs have been identified in plasma of healthy volunteers [221]. SPMs have also been identified in patient populations from sites of inflammation, including in joint effusions of rheumatoid arthritis patients [222] and bronchoalveolar lavage of asthma patients [223]. In addition, studies in sepsis patients have shown that SPM profiles in plasma can aid in stratification of disease severity and help in predicting their survival [224].

Taking this forward, we have now identified the presence of SPMs in a human model of self-resolving acute inflammation triggered by UV-killed *E. coli*. In addition, we determined the expression of the receptors that they work upon, and have shown that exogenously adding these local mediators into the established site of inflammation hastens the resolution cascade. Specifically, SPMs, when added therapeutically at the resolution tipping point, led to enhanced neutrophil clearance within the ensuing 6h. Increased expression of SPM receptors in the 4h inflamed skin supported the therapeutic administration of SPMs which is also consistent with the clinical scenario where patients interact with their doctors once inflammation is already established, and so it makes sense to attempt to facilitate the resolution of this inflammation instead of only preventing the onset of inflammation. Taken together, these data show, for the first time, the potential efficacy of SPMs in humans.

The mechanisms by which SPMs reduce neutrophil numbers in this model are not certain at this stage. The lack of increased CD163 on resolution-phase macrophages reduces the likelihood of increased efferocytosis. SPMs also failed to reduce the levels of classic neutrophil chemoattractants. Another possible mechanism could be through increase in production of nitric oxide that can lead to reduced adherence of neutrophils to endothelium [225]. This hypothesis garners support from two observations. First, the SPM receptors including FPR2/ALX and GPR18 are expressed abundantly on the inflamed endothelium in this model and second, from results of murine studies which show that SPMs such as RvD2 can increase the production of nitric oxide [154]. The action of SPMs on endothelium could also lead to reduced neutrophil transmigration. This could be through the action of RvD1 on FPR2/ALX on endothelial cells that prevents the IL-17 mediated downregulation of developmental endothelial locus-1 (del-1), an endothelial cell secreted anti-inflammatory protein that limits neutrophil transmigration [226]. Other mechanisms such as enhanced reverse transmigration back into systemic circulation or enhanced lymphatic drainage cannot be excluded as possible mechanisms through which SPMs are promoting neutrophil clearance during resolution in this human model [80] [86].

One of the principle concerns of promoting neutrophil clearance in the context of bacterial infection is that the host immune system might not efficiently clear the bacteria. This could result in continuous activation of the innate immune response leading to chronic inflammation. This is very well exemplified in chronic granulomatous disease, which results from a failure of the phagocytic NADPH oxidase enzyme system to produce superoxide and kill invading infections leading to a predisposition to recurrent bacterial and fungal

infections and the development of inflammatory granulomas [227]. According to murine studies, a distinctive feature of SPMs is that they not only promote neutrophil clearance but also enhance bacterial clearance. This has been demonstrated in multiple mouse models of bacterial infection including *E. coli* triggered sepsis [154], aspiration pneumonia [228], *P. aeruginosa* induced lung infection [129]. However, in this model, SPMs did not show a reduction in levels of endotoxin, a surrogate marker of gram negative bacterial load. While it is not known whether the effect of SPMs on different resolution biomarkers is dose dependent, it could be that dose of SPMs used here was low for exerting bacterial clearance. The total dose of SPMs added to the inflamed site here was around 150pg and the murine studies described above demonstrated the effect of SPMs on enhancing bacterial clearance when they were used at doses equivalent to 100 ng/mouse. Nonetheless, these data hint that supplementation with SPMs does not negatively affect the clearance of inflammatory stimulus by impairing the host antimicrobial defence.

In murine dorsal air pouch model of acute resolving inflammation, temporal analysis of exudate show appearance of prostaglandins during onset followed by SPMs during the resolution phase, a phenomenon referred as lipid mediator class switching [229]. However, in this model, we did not see this phenomenon, despite observing an expected increase in levels of prostaglandins during onset. It might be that these differences are due to site-specific local degradation of SPMs as similar loss of SPM signal was observed by Homman et al in murine model of oxalazone induced dermal inflammation, where they also showed that the recovery of SPMs as early as 2h after injecting them in healthy mouse skin was < 10 % [230]. Another explanation

for the loss of SPM signal could be due to the use of cell-free inflammatory exudate for lipid mediator analysis. Preparation of cell-free exudate involves centrifugation to separate the cells, and this process perhaps leads to the exclusion of membrane-derived microvesicles which have been shown to also contain SPMs [231]. Future studies using cell rich exudate or snap frozen skin biopsies from the inflamed site for lipidomic analysis can elucidate the extent to which SPM compartmentalization in cells contributes to loss of signal. In summary, in this model, we did not observe a rise in levels of SPMs specifically in the resolution phase as shown previously in murine models.

SPMs transduce their pro-resolving effect through a variety of GPCR receptors including FPR2/ALX (receptor for LXA_4, RvD1 and AT-RvD1), ChemR23 (receptor for RvE1), GPR18 (receptor for RvD2) and GPR32 (receptor for AT-RvD1) [232]. Murine studies have shown that deficiency of these SPM receptors heightens the inflammatory response. For instance, FPR2/ALX and GPR18 knockout mice showed increased leucocyte infiltration and reduced bacterial clearance in the peritoneum compared to wild-type mice in a model of caecal ligation and puncture (CLP) induced polymicrobial sepsis [233][234]. The expression of these receptors is upregulated during inflammation as evident from results of ex vivo studies using primary cells, e.g. stimulation with LPS was shown to upregulate the expression of FPR2/ALX on primary mouse microvascular endothelium [235]. In another example, expression of ChemR23 was found to selectively upregulated on pro-inflammatory monocytes/macrophages [236]. Extending these observations, we find in our model, which represents a dynamic in vivo inflammation setting, that the inflamed site at junction between onset and resolution is characterised by

increased expression of SPM receptors which could be either due to their upregulation on resident immune cells and endothelium or due to migration of leucocytes expressing these receptors. Two important implications of this observation are that the site is prepared to enhance pro-resolution signalling either by endogenously released SPMs and that it is also amenable to therapeutic manipulation by exogenous addition of SPMs. Another interesting observation made here was that SPM receptors such as ChemR23 and GPR18 were expressed on endothelium at baseline skin. Activation of GPR18 by RvD2 triggers formation of nitric oxide, which in addition to reducing leucocyte-endothelial adherence, also plays an important role in maintaining endothelial function by preventing platelet aggregation, regulating vasomotor tone and by acting as an antioxidant [237]. Constitutive expression of SPM receptors on endothelium suggest a possibility where SPMs can be used prophylactically to prevent endothelial dysfunction which underlies the development of cardiovascular disorders such as atherosclerosis and hypertension [238]. In summary, increased expression of SPM receptors at the tipping point of resolution in this model highlight that the inflamed site is primed to mediate the effects of SPMs. It also lays the foundation for future studies which can employ this model to investigate whether pharmacological agonists of these receptors can mimic the effect of SPMs on resolution indices in humans.

The rationale for using the cocktail of four SPMs (LXB_4, RvE1, RvD2 and AT-RvD1) was based on an ethical argument as it was thought that use of single SPM would decrease the likelihood of observing a pro-resolution effect and lead to exposing a large number of volunteers to the UVkEc challenge. The

choice of SPMs included in the cocktail was guided by receptor expression. A representative member of each receptor class was chosen. RvE1 for ChemR23 [239], RvD2 for GPR18 [240] and AT-RvD1 for FPR2/ALX and GPR32 [220]. LXB_4 was also included as it showed a consistent signal at 4h in all volunteers. Also for ethical reasons, the concentration of each of the SPMs included in the cocktail was at a concentration equivalent to the highest level found at the site of inflammation.

In summary, we identified local SPM biosynthesis as well as the receptors that transduce their actions at the junction of onset and resolution. In addition, we report that therapeutic supplementation of SPMs triggers reduction of neutrophils during resolution. Using the UVkEc model of self-resolving inflammation, these observations show for the first time in humans that harnessing body's own counter-regulatory signals can be used controlling inflammation. It also highlights a novel approach to investigate the effect of pro-resolving therapies on resolution biomarkers in humans.

Chapter 6

Effect of SPM inducing small molecule, JBT-101, a cannabinoid receptor 2 agonist, on resolution indices in UVkEc triggered self-resolving dermal inflammation model

6.1 INTRODUCTION

SPM based therapies can be broadly classified into three groups. The first group includes supplementation of their substrate, the n-3 fish oils, e.g. eicosapentaenoic acid (EPA), docosahexaenoic acid (DHA) [241], the second group involves direct administration of the synthetic stable SPM analogues which are currently under development, e.g. RvE_1 eye drops for dry eye [242] and LXA_4 mouth rinse for gingivitis [243]. The third group includes orally active small molecules that induce SPM generation by modifying the biosynthetic machinery, e.g. low dose aspirin (75mg), which acetylates COX-2 to trigger formation of family of aspiring triggered lipoxins (also called 15-epi-lipoxins) and resolvins [244] and statins, which cause nitrosylation of COX-2 to trigger formation of 15-epi-lipoxins [245].

JBT-101 is a cannabinoid receptor-2 (CB2) agonist (chemical name: ajulemic acid) and is a novel member of SPM inducing small molecules currently being tested in Phase II clinical trials by Corbus Pharmaceuticals (USA) for scleroderma, cystic fibrosis, dermatomyositis and systemic lupus erythematosus [246]. A murine study has shown that oral administration of JBT-101 enhances production of LXA_4 and reduces neutrophil migration to the peritoneal cavity in zymosan-induced peritonitis model [247]. In another murine study, JBT-101 treatment was shown to decrease the burden of *P. aeruginosa* bacteria in the lung [248]. Murine studies have proposed that by inducing SPM formation, JBT-101 exerts a positive effect on resolution indices. However, this effect of JBT-101 has not been explored in humans yet.

Using the UVkEc induced self-resolving dermal inflammation model, I

conducted an open-label, parallel group, placebo-controlled pilot study to investigate whether JBT-101 dose-dependently triggered SPM biosynthesis and whether it shows an effect on resolution indices in humans, at doses currently being studied in Phase II clinical trials. I also compared the effect of JBT-101 on resolution biomarkers with prednisone, a commonly used corticosteroid.

6.2 STUDY DESIGN

This study involved additional exclusion criteria and clinical monitoring, and therefore the design of the study is described here in detail. The study procedures for the UVkEc triggered self-resolving dermal inflammation model were conducted in a similar manner as described in methods section 2.3.

An open-label, randomised, parallel group, placebo-controlled pilot study was conducted in collaboration with Corbus Pharmaceuticals (UCL Ethics Project ID: 5051/002). The study was advertised to recruit healthy, young (18-45 years) male volunteers. Interested volunteers were first invited for a screening that was conducted by the study clinician. The following exclusion criteria were established for this particular study:

- Smokers (including nicotine, marijuana and other narcotics).
- Currently ill or were ill in last one week.
- History of any chronic medical condition (including skin and food allergies or diagnosed mental health disorder).
- Taking regularly prescribed or over-the-counter medication.

- Taken any oral corticosteroids or other immunosuppressive agents within the last 3 months.
- Recent vaccination (within 3 months) or take recreational drugs.
- Enrolled in another research study.
- Abnormal blood tests during screening
    - **Full Blood Count:** Haemoglobin, platelet count, total white count and differential.
    - **Urea and Electrolytes:** Urea, Creatinine, Potassium, Sodium, Chloride, Calcium.
    - **Liver Function Tests:** Total Protein, Albumin, Bilirubin, Alkaline Phosphatase, Alanine Aminotransferase.
- Abnormal findings on physical examination during screening.
- Screening blood pressure >160/100 mmHg or <90/60 mmHg.
- Screening heart rate >100 beats per minute (bpm) or <45 bpm.
- Body mass index (BMI) >30 kg/m^2
- Any other condition that, in the opinion of the study clinician or investigator, were clinically significant and may put the subject at greater safety risk, influence response to study product, or interfere with study assessments.

Volunteers who were eligible after the screening meeting were invited to take part in the study within one week of the meeting. The study was conducted in clinical procedures room, Rayne Institute, UCL.

The total study duration was seven days. The first day comprised two visits. During the first visit, the study clinician obtained the written informed consent from the volunteer after ensuring that volunteer's history or health has not

changed since screening. After the consent procedure, a blood sample was taken, and the volunteer was randomised to one of the four study groups:

Group A: Placebo, twice daily for four days, oral.

Group B: 5mg JBT-101, twice daily for four days, oral.

Group C: 20mg JBT-101, twice daily for four days, oral.

Group D: 15mg Prednisone, single morning dose for four days, oral.

GMP standard placebo, JBT-101 5mg and 20mg tablets were provided by Corbus Pharmaceuticals, USA. Prednisone 15mg was procured from UCL pharmacy by Dr Frances Bennett.

After taking the first dose of the investigational drug (depending on the group assigned), the volunteer was observed for any side effects in the clinical procedures room, Rayne Institute, UCL for 3h. At the end of this period, the volunteer was examined for vital signs by the study clinician. The second visit was in the evening, 8h after the first visit, during which the volunteer took the second dose of the drug. After taking the second dose, the volunteer was monitored for 30 min by the study clinician.

On day 2 and day 3 the volunteer was asked to come to clinical procedures room in the morning and in the evening to take the investigational drug under our observation. A 10ml blood sample was also drawn from the volunteer before the morning dose on both these days.

On day 4, immediately after volunteer took the morning dose of the investigational drug, acute inflammation was triggered in the forearm using UVkEc at two sites, one on each forearm. Inflammatory exudate was collected in a suction blister raised at 4h (onset time point) on one forearm and at 10h (resolution time point) on the contralateral forearm, after UVkEc injection. On this day, the forearm was also scanned by a laser Doppler imager to assess local vascular hyperaemia at baseline and then at 2h, 4h, 10h after UVkEc injection. A 10ml blood sample was also collected at the above time points to assess systemic immune response.

On day 5, 6 and 7, the volunteer was asked to visit once in the morning to assess the vascular hyperaemia over the inflamed site using laser Doppler measurement and to provide a 10ml blood sample to monitor the systemic immune response. This was to investigate the effects of JBT-101 on later time points of resolution and to ensure that volunteer is recovering without any complications.

The study protocol detailing drug administration and procedures conducted on each day is summarised in **Figure 6.1**

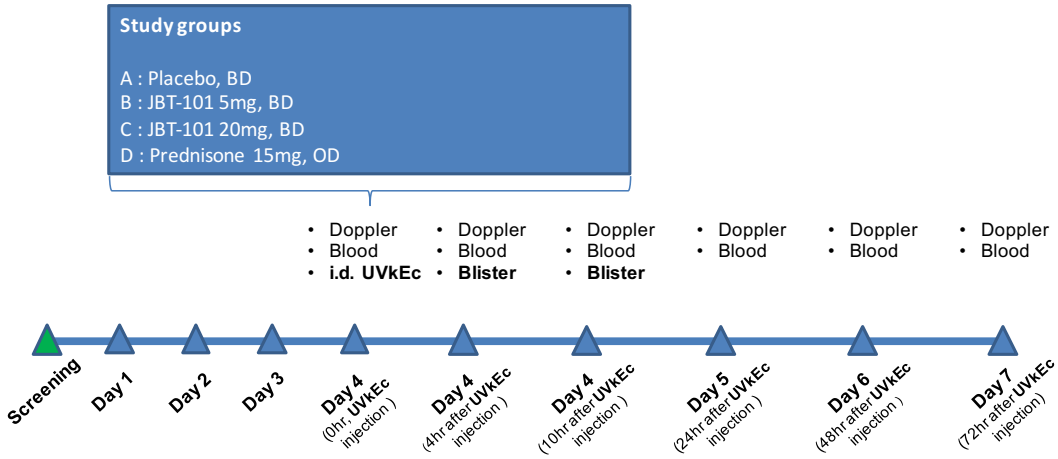

Figure 6.1 Protocol of the study investigating effect of 5mg JBT-101, 20mg JBT-101 and prednisone on resolution biomarkers in UVkEc triggered self resolving dermal inflammation model.

6.3 RESULTS

6.3.1 Volunteer recruitment

Twenty-eight volunteers were screened, and five volunteers were excluded. The reasons for exclusion were following: out of reference range blood counts (n=2), high BMI (n=1), needle phobia (n=1) and loss to follow-up (n=1). The remaining 23 volunteers were randomised into the four study groups. In the placebo group, two volunteers were excluded. The first volunteer was excluded on day 3 because his serum creatinine levels went above the reference range. Follow up investigation by study clinician revealed that it was due to dehydration. The other volunteer was excluded during analysis as he arrived an hour late for the scheduled 4h blister time point. In the 5mg JBT-101 group, one volunteer was excluded on day 3 as his platelet count was found to be below the reference range. Follow up investigation by study clinician indicated the low platelet count was not related to the drug. In total, data was collected from 20 volunteers, and each group had 5 volunteers **(Figure 6.2).**

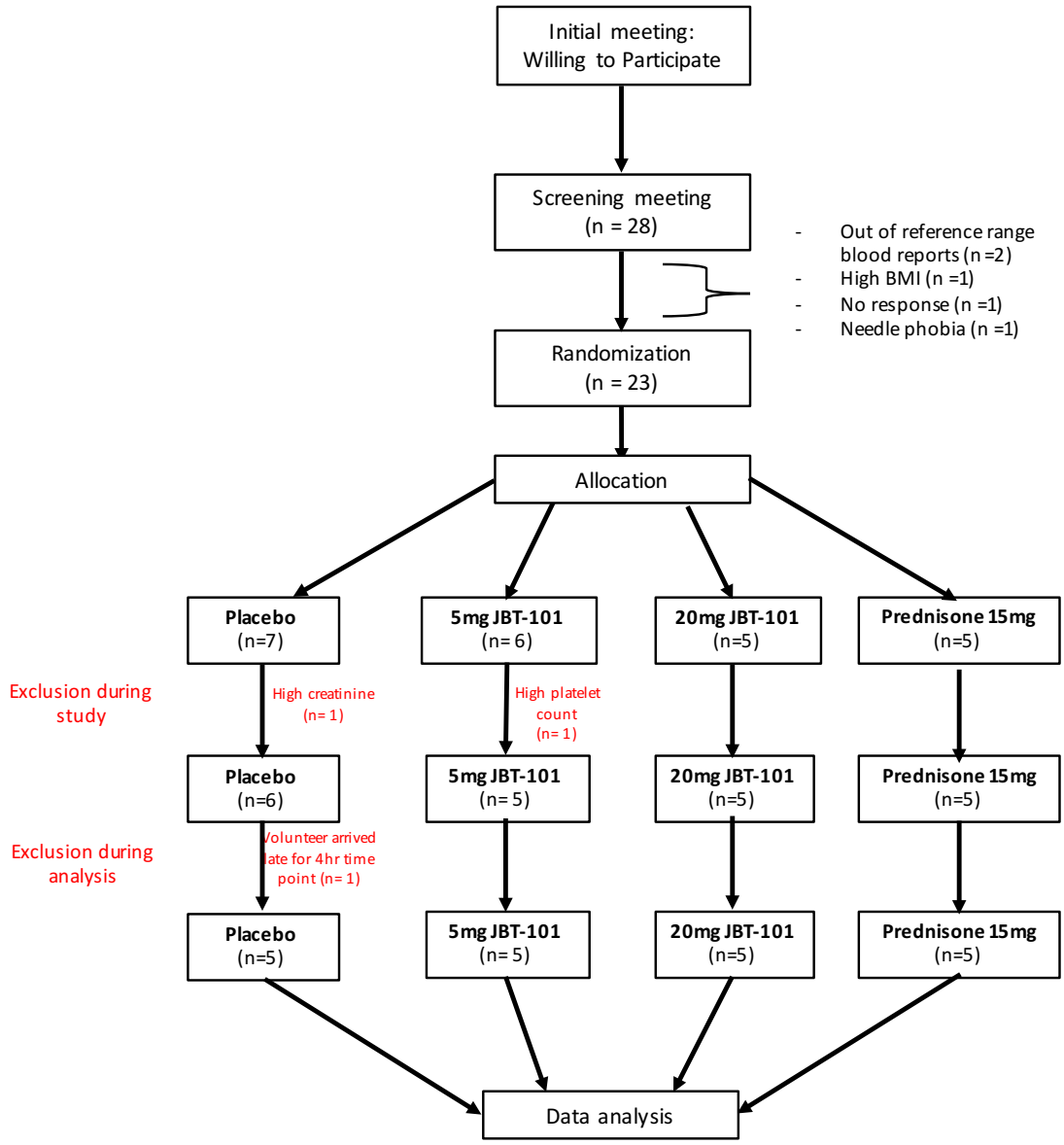

Figure 6.2 Consort diagram of the open label, randomised, parallel group, placebo controlled pilot study to test effect of 5mg JBT-101, 20mg JBT-101 and prednisone on resolution biomarkers in UVkEc triggered self resolving dermal inflammation model.

Volunteers interested to participate in the study were screened by the study clinician (Dr Alexander Maini, Dr Marc George and Dr Fran Bennett). If they were eligible as per the study criteria, they were randomized to one of the four study groups: placebo, 5mg JBT-101 , 20mg JBT-101, twice daily or 15mg Prednisone once daily for four days. In total, data was collected from 20 volunteers and each group had 5 volunteers

6.3.2 Effect of JBT-101 on vascular hyperaemia at the site of UVkEc triggered acute inflammation

Compared to placebo, JBT-101 dose-dependently increased vascular hyperaemia at the site of inflammation. The trend was established as early as 2h after UVkEc injection and became apparent at 24h. At 24h, the total flux in placebo arm was $1.73 \times 10^6 \pm 0.7 \times 10^6$ perfusion units, which was increased by 5mg and 20mg JBT-101 to $2.58 \times 10^6 \pm 1.19 \times 10^6$ and $5.88 \times 10^6 \pm 0.92 \times 10^6$ perfusion units respectively. The kinetics of vascular hyperaemia in prednisone group closely followed the placebo group. Between 24h and 48h, the vascular hyperaemia decreased in all the treatment groups but the average reduction in JBT-101 5mg and prednisone group was higher than the placebo group. The reduction from 24h to 48h in placebo group was 610,694 ± 640,780 perfusion units and in 5mg JBT-101 and prednisone group it was $1.75 \times 10^6 \pm 0.7 \times 10^6$ perfusion units and $1.68 \times 10^6 \pm 0.7 \times 10^6$ perfusion units. The vascular hyperaemia also declined in the 20mg JBT-101 group from 24h-48h however at 48h it remained higher in the placebo group. At 72h, the blood flow returned to baseline levels in all groups apart from 20mg (**Figure 6.3 A)**.

Vascular hyperaemia for each volunteer in the placebo group is shown in **Figure 6.3 B**, 5mg JBT-101 group in **Figure 6.3 C**, 20mg JBT-101 group in **Figure 6.3 D** and the prednisone group in **Figure 6.3 E.** The representative camera and laser Doppler images at 24h and 48h, from the above four groups is shown in **Figure 6.4**.

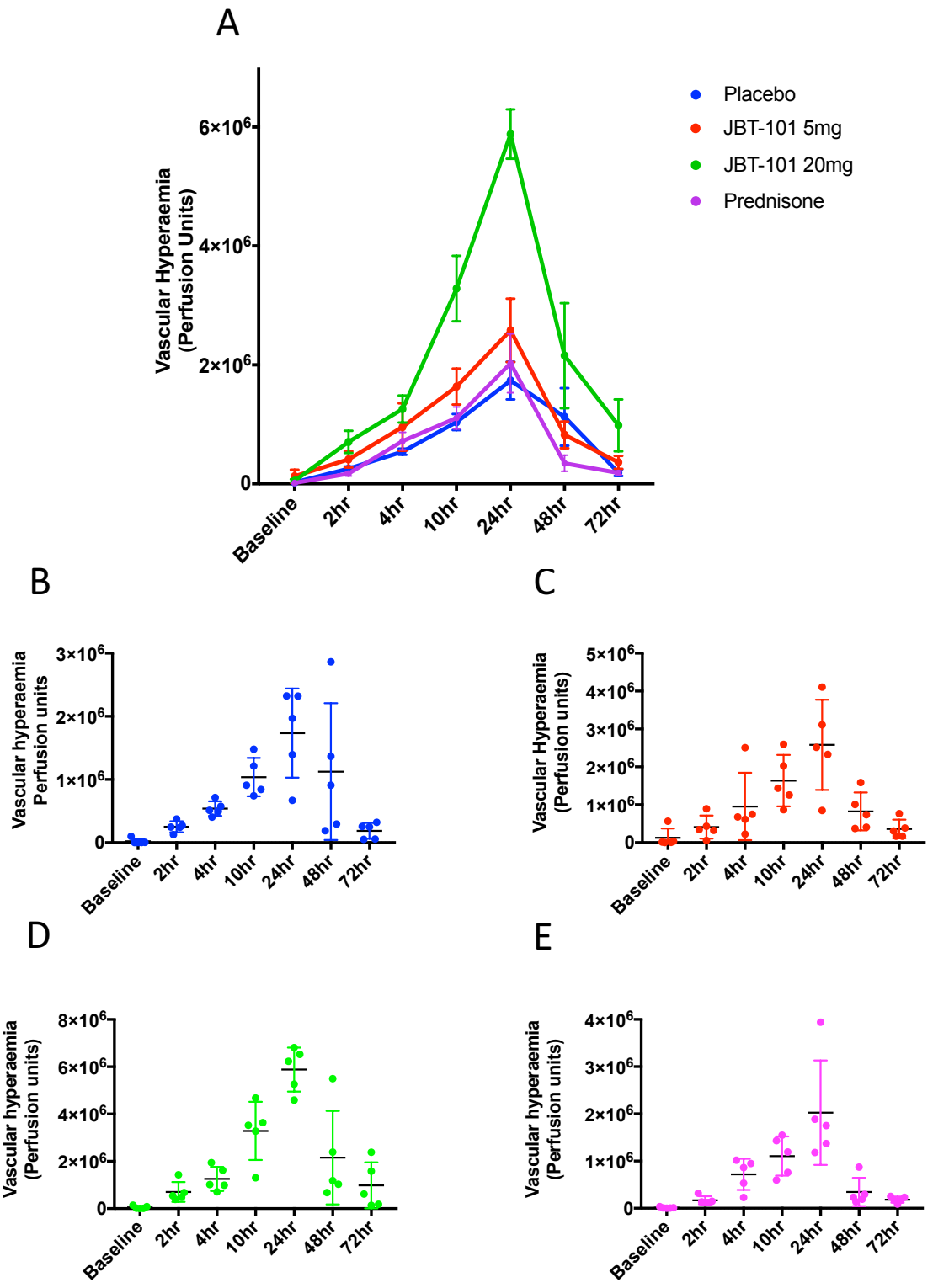

Figure 6.3 The effect of JBT-101 and prednisone on vascular hyperaemia at the site of UVkEc triggered self-resolving dermal inflammation.

Healthy male volunteers were randomized to receive either placebo, 5mg JBT-101 , 20mg JBT-101, twice daily or 15mg Prednisone once daily for four days. On fourth day, acute inflammation was triggered by intradermal injection of 1.5 x 10^7 UV killed *E. coli* (UVkEc) suspended in 100µl of saline in both the forearms. Vascular hyperaemia at the injection site was assessed at specified intervals by a laser Doppler imager. The comparison of vascular hyperaemia (mean ± SD) between the four treatment groups **(A)** and the vascular hyperaemia for each volunteer in placebo **(B)**, 5mg JBT-101 **(B)**, 20mg JBT-101 **(C)** and 15mg prednisone **(D)** group are shown here. Data expressed as individual values with mean ± SD. n=5/group.

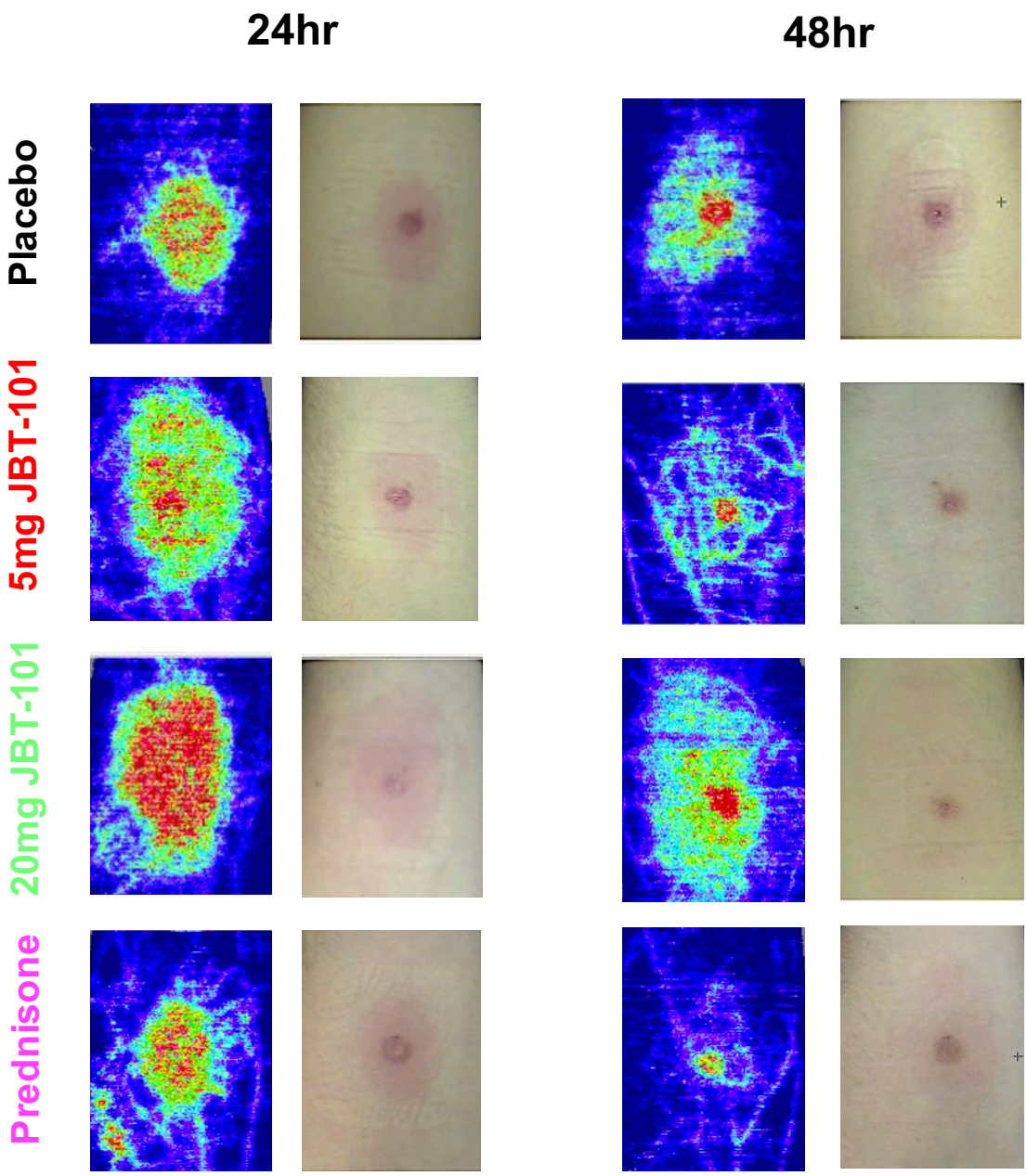

Figure 6.4 Representative camera images and laser Doppler images of the site of UVkEc triggered dermal inflammation at the 24hr and 48hr time point after JBT-101 and prednisone administration.

Healthy male volunteers were randomized to receive either placebo, 5mg JBT-101 , 20mg JBT-101, twice daily or 15mg prednisone once daily for four days. On fourth day, acute inflammation was triggered by intradermal injection of 1.5 x 10^7 UV killed *E. coli* (UVkEc) suspended in 100µl of saline in both the forearms. Vascular hyperaemia at the injection site was assessed by a laser Doppler imager. The representative laser Doppler images and camera images at 24hr and 48hr for each treatment group are shown here. Representative images from n=5/group.

6.3.3 Effect of JBT-101 on numbers and phenotype of neutrophils at the site of UVkEc triggered acute inflammation

In contrast to vascular hyperaemia, 5mg and 20mg of JBT-101 significantly reduced numbers of neutrophil, compared to the placebo at 4h. However, the reduction in neutrophils by JBT-101 was not dose-dependent. At 4h, in the placebo group, number of neutrophils were 261,820 ± 157,068 /ml decreasing to 55,067 ± 37,358 /ml in 5mg JBT-101 group and 65,580 ± 36,203 /ml in 20mg JBT-101 group. Prednisone also caused a significant reduction in neutrophils at 4h, equivalent to that of JBT-101. At 4h, the neutrophil count in prednisone group was 72,382 ± 54,805 /ml. At 10h, JBT-101 at both the doses maintained this reduction in neutrophil numbers, but the differences were not significant when compared to placebo. At 10h, in placebo group, the neutrophil count was 243,531 ± 225,022 /ml and it was reduced to 119,898 ± 117,045/ml in 5mg JBT-101 and to 72,066 ± 45,975/ml in 20mg JBT-101. **(Figure 6.5 A)**. The change in the proportion of neutrophils at 4h and 10h after JBT-101 and prednisone administration is detailed in **Figure 6.5 B**.

Previously in this model, I have identified that during resolution phase neutrophils express CD62L, which could indicate they acquire a regulatory phenotype. I therefore investigated whether JBT-101 promoted expression of CD62L on neutrophils during resolution in this study. The CD62L expression on neutrophils in the placebo group at 10h was 673 ± 289 MFI units, and it was reduced by 5mg and 20mg JBT-101 to 343 ± 717 MFI units and 340 ± 448 MFI units, respectively. At 10h, the CD62L expression on neutrophils in prednisone group was 1547 ± 827 MFI units **(Figure 6.5 C)**.

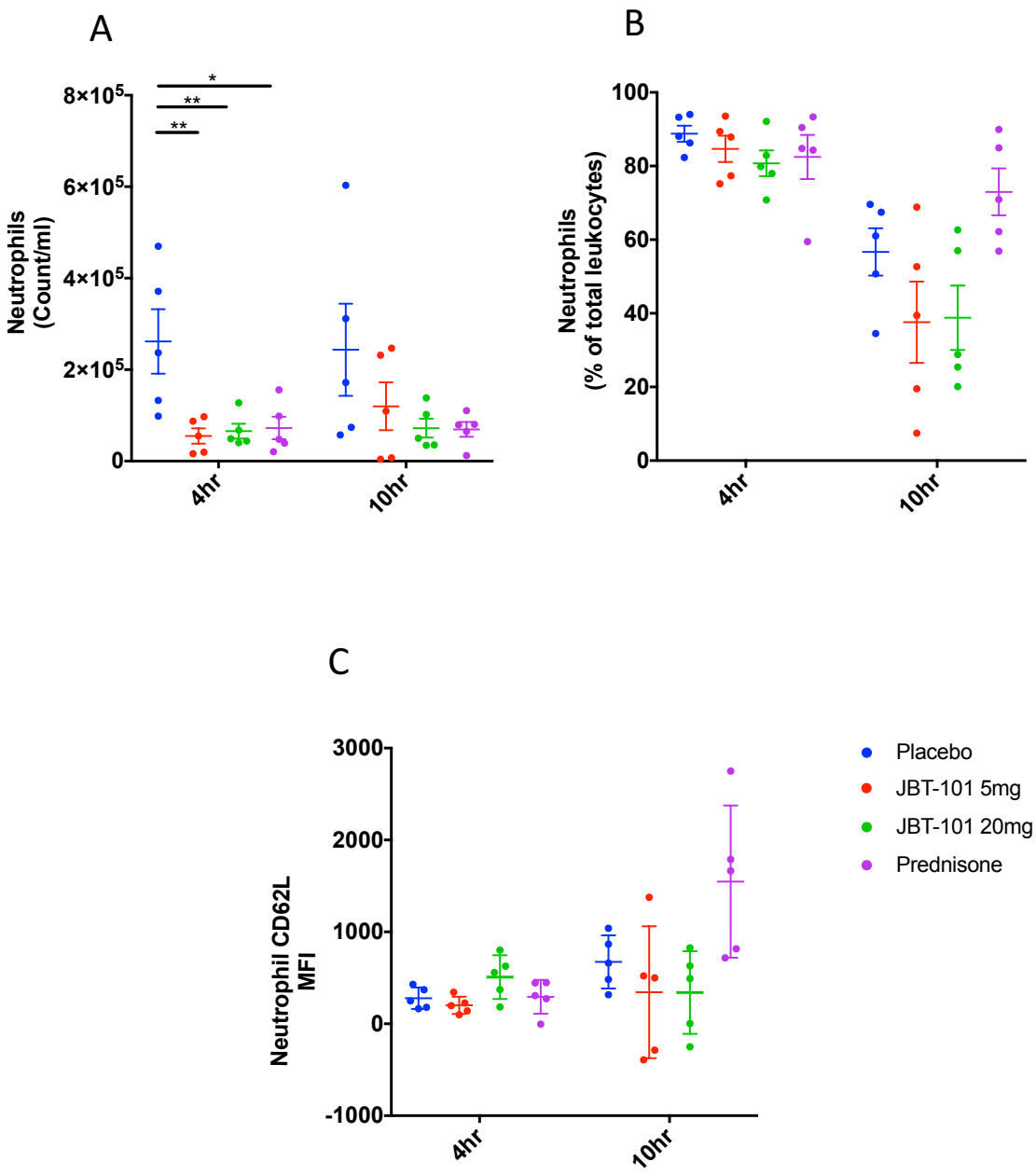

Figure 6.5 The effect of JBT-101 and prednisone on neutrophil numbers and neutrophil CD62L expression in the inflammatory exudate at the site of UVkEc triggered dermal inflammation.

Healthy male volunteers were randomized to receive either placebo, 5mg JBT-101 , 20mg JBT-101, twice daily or 15mg prednisone once daily for four days. On fourth day, acute inflammation was triggered by intradermal injection of 1.5 x 10^7 UV killed *E. coli* (UVkEc) suspended in100µl of saline in both the forearms. Inflammatory exudate at the injection site was acquired into a suction blister raised after 4hr (onset phase) on one forearm and after 10hr (resolution phase) on the contralateral forearm. Cells in the exudate were phenoytped by multi colour flow cytometry. The neutrophil count/ml **(A)**, proportion of neutrophils **(B)** and surface expression of CD62L on neutrophils **(C)** at 4hr and 10hr is shown here. Data expressed as individual values with mean± SD. n=5/group. p values are denoted as < 0.05 = ' * ', <0.01 = ' ** '

6.3.4 Effect of JBT-101 on numbers and phenotype of monocytes/macrophages at the site of UVkEc triggered acute inflammation

The effect of JBT-101 on monocytes/macrophages numbers was not evident either at 4h or 10h time point. However, in the prednisone group monocytes/macrophages numbers showed a decreasing trend at 4h, which reached significance at 10h, when compared to placebo **(Figure 6.6 A).** At 10h, the number of monocytes/macrophages in the placebo group were 71,711 ± 31,263/ml, and prednisone decreased it to 9,678 ± 4,940/ml. The change in the proportion of monocytes/macrophages at 4h and 10h after JBT-101 and prednisone administration is detailed in **Figure 6.6 B.**

CD163, a cell surface marker acquired my monocytes/macrophages when they phagocytose apoptotic neutrophils was assessed to investigate whether JBT-101 differentiated them to a pro-resolution phenotype. While CD163 expression on monocytes/macrophages was increased in all treatment groups from 4h to 10h, there was no difference between placebo and any of the two doses of JBT. Prednisone increased expression of monocyte/macrophage CD163 at both the time points. At 4h, CD163 expression in the placebo group was 704 ± 243 MFI units and it increased to 5,233 ± 2,144 MFI units in prednisone group. At 10h, CD163 expression in the placebo group was 2383 ± 477 MFI units and it increased to 5,233 ± 2,144 MFI units in prednisone group **(Figure 6.6 C).**

CD86 provides a co-stimulatory signal for T cell proliferation and is a marker for pro-inflammatory macrophages [249]. Here, CD86 expression was measured on monocytes/macrophages to assess whether JBT-101 influenced their phenotype [250]. At 4h, the differences in monocytes/macrophages CD86 expression between the investigation groups were insignificant. However, at 10h, compared to placebo there was a decreasing trend in CD86 expression in 5mg JBT-101, 20mg JBT-101 and prednisone group. In placebo, the monocytes/macrophages CD86 expression was 1856 ± 275 MFI units, and it decreased to 1514 ± 487 MFI units in 5mg JBT-101, 1758 ± 276 MFI units in 20mg JBT-101 and 1285 ± 202 MFI units in prednisone group **(Figure 6.6 D).**

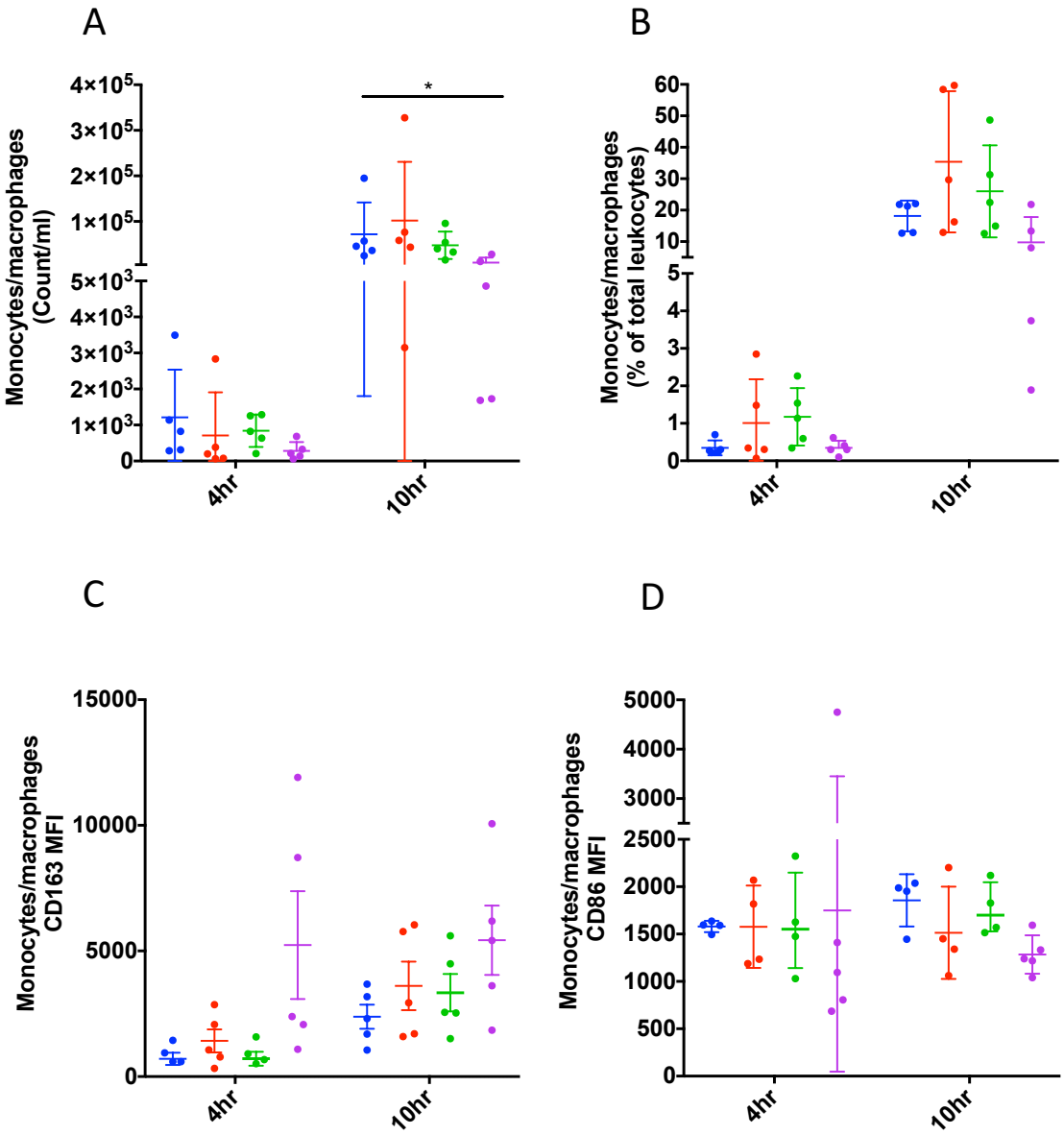

Figure 6.6 The effect of JBT-101 and prednisone on monocyte/macrophage numbers and monocyte/macrophage CD163 and CD86 expression in the inflammatory exudate at the site of UVkEc triggered dermal inflammation.

Healthy male volunteers were randomized to receive either placebo, 5mg JBT-101 , 20mg JBT-101, twice daily or 15mg prednisone once daily for four days. On fourth day, acute inflammation was triggered by intradermal injection of 1.5 x 10^7 UV killed *E. coli (*UVkEc) suspended in 100µl of saline in both the forearms. Inflammatory exudate at the injection site was acquired into a suction blister raised after 4hr (onset phase) on one forearm and after 10hr (resolution phase) on the contralateral forearm. Cells in the exudate were phenoytped by multi colour flow cytometry. The monocyte/macrophage count/ml **(A)**, proportion of monocytes/macrophages **(B)** and surface expression of CD163 **(C)** and CD86 **(D)** on monocytes/macrophages at 4hr and 10hr is shown here. Data expressed as individual values with mean± SD. n=5/group. p values are denoted as < 0.05 = ' * ', <0.01 = ' ** '

6.3.5 Effect of JBT-101 on cytokines and chemokines at the site of UVkEc triggered acute inflammation

Despite inhibiting neutrophil numbers at 4h, JBT-101 increased the levels of pro-inflammatory cytokines TNFα and IL-1β **(Figure 6.7 A, B)** with the exception of a trend towards a reduction in IL-8. JBT-101 dose-dependently decreased the levels of IL-8. At 4h, IL-8 levels in placebo group were 5,930 ± 2,062 pg/ml and 5mg JBT-101 and 20mg JBT-101 decreased it to 3,298 pg/ml ± 1,728 and 3,023 ± 2,762 pg/ml respectively. Prednisone also showed a decreasing trend for IL-8, but it was less apparent than either of the doses of JBT-101. At 4h IL-8 levels in prednisone group were 4,288 ±3,073 pg/ml **(Figure 6.7 C).** At 10h, both doses of JBT-101 maintained the reduction in levels of IL-8, but the differences were less apparent compared to placebo.

Interestingly, only 5mg JBT-101 and prednisone decreased levels of IFN-γ at 4h. IFN-γ was 3,249 ± 3,164 pg/ml in the placebo group and 5mg JBT-101 decreased it to 894 ± 331 pg/ml, and prednisone decreased it to 327 ± 157 pg/ml **(Figure 6.7 D)**. The levels of IL-4, IL-10 and IL-13, were not different between placebo, JBT-101 and prednisone groups **(Figure 6.7 E, F, H)**.

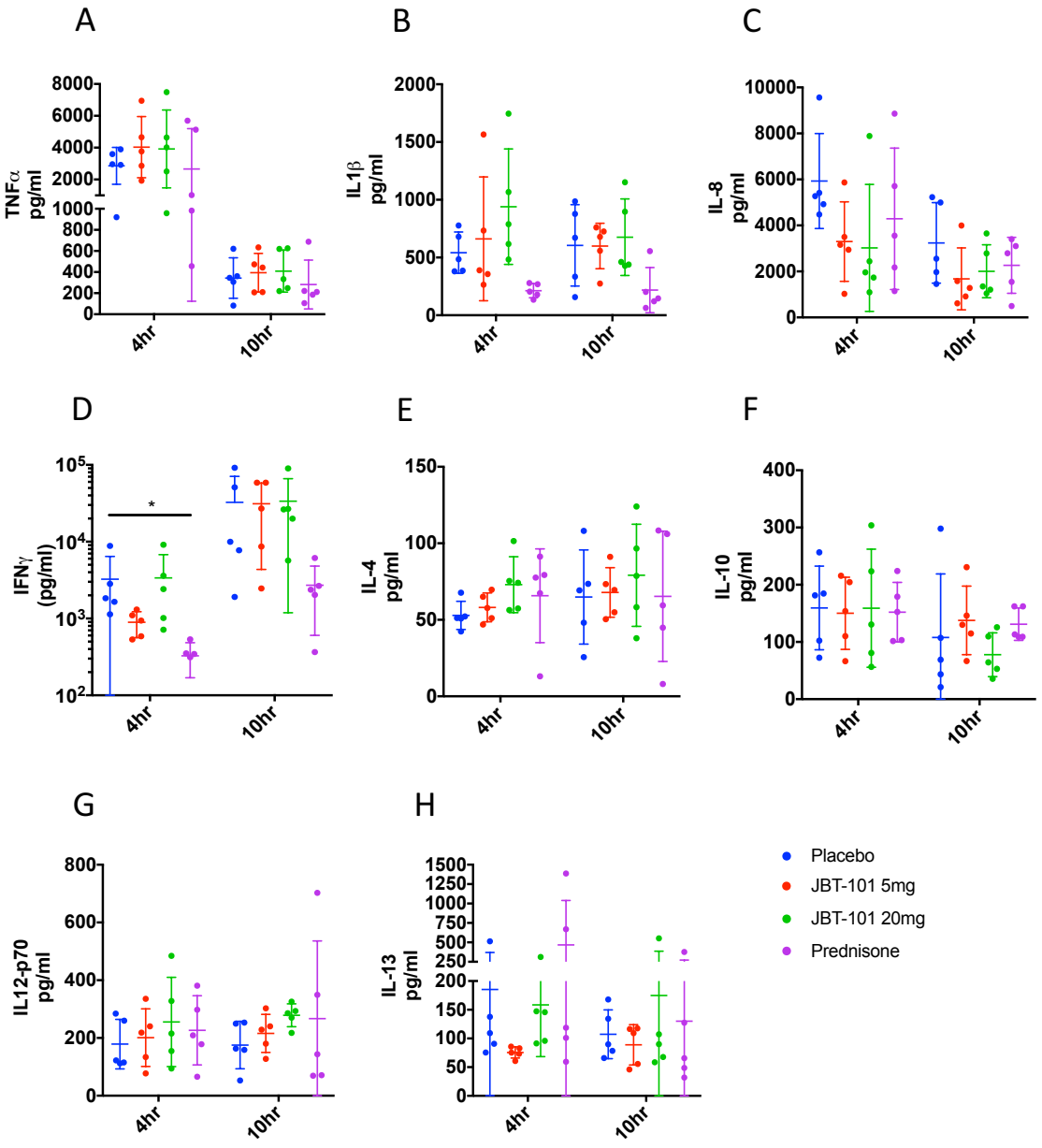

Figure 6.7 The effect of JBT-101 and prednisone on cytokines and chemokines in the inflammatory exudate at the site of UVkEc triggered dermal inflammation.

Healthy male volunteers were randomized to receive either placebo, 5mg JBT-101 , 20mg JBT-101, twice daily or 15mg prednisone once daily once daily for four days. On fourth day, acute inflammation was triggered by intradermal injection of 1.5 x 10^7 UV killed *E. coli* (UVkEc) suspended in 100µl of saline in both the forearms. Inflammatory exudate at the injection site was acquired into a suction blister raised after 4h (onset phase) on one forearm and after 10h (resolution phase) on the contralateral forearm. Cytokines and chemokines in the inflammatory exudate were measured by multiplex ELISA. The concentrations of cytokines and chemokines in the inflammatory exudate at 4hr and 10hr are shown here. Data expressed as individual values with mean± SD. n=5/group. p values are denoted as < 0.05 = ' * ', <0.01 = ' ** '

6.3.6 Effect of JBT-101 on the endotoxin levels at the site of UVkEc triggered acute inflammation

Removal of inflammatory stimulus from the site of inflammation is one of the hallmarks of resolution. Endotoxin is the component of gram-negative bacterial cell wall and has been used as a surrogate marker of bacterial load [251]. To assess whether JBT-101 promotes the removal of inflammatory stimulus, I measured endotoxin in the blister exudate. At 4h, compared to placebo, both doses of JBT-101 showed a dose-dependent decreasing trend in endotoxin. The relative endotoxin levels in the placebo group were 14.60 ± 4.22 EU and 5mg JBT-101 and 20mg JBT-101 decreased it to 5.26 ± 2.00 EU and to 6.78 ± 4.27 EU respectively. Prednisone did not alter endotoxin levels compared to placebo. At 4h, the endotoxin levels in prednisone group were 17.18 ± 5.25 EU. At 10h, the levels of endotoxin declined in the placebo group. However, at this time point, the decreasing trend in endotoxin levels between placebo and JBT group was less obvious **(Figure 6.8)**.

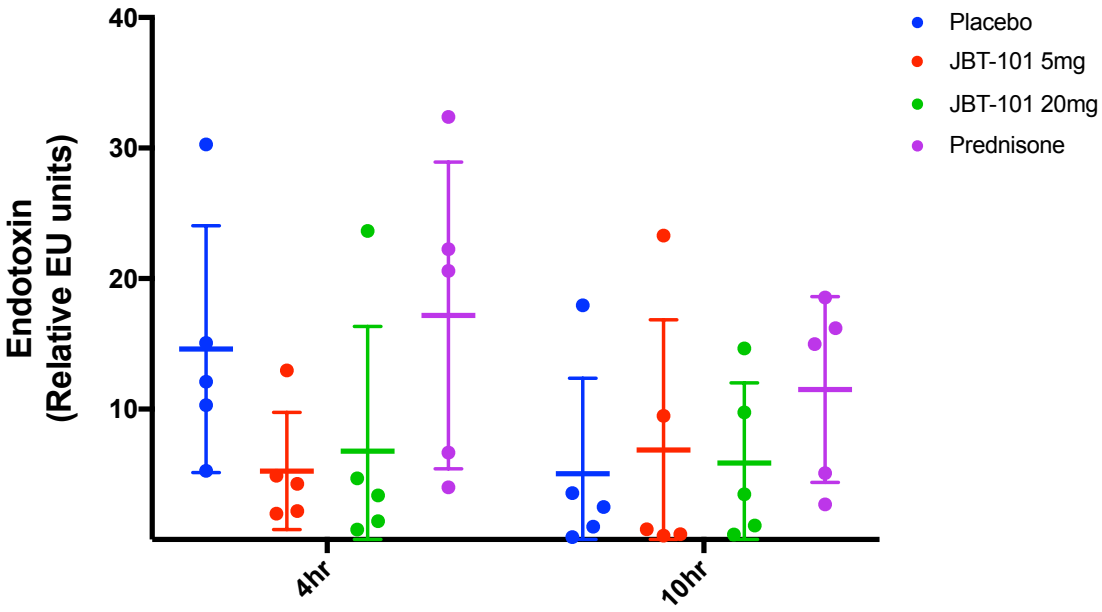

Figure 6.8 The effect of JBT-101 and prednisone on endotoxin content in the inflammatory exudate at the site of UVkEc triggered dermal inflammation.

Healthy male volunteers were randomized to receive either placebo, 5mg JBT-101 , 20mg JBT-101, twice daily or 15mg prednisone once daily for four days. On fourth day, acute inflammation was triggered by intradermal injection of 1.5 x 10^7 UV killed *E. coli* (UVkEc) suspended in 100µl of saline in both the forearms. Inflammatory exudate at the injection site was acquired into a suction blister raised after 4hr (onset phase) on one forearm and after 10hr (resolution phase) on the contralateral forearm. Endotoxin as a surrogate for inflammatory stimulus (UVkEc) was measured using kinetic turbidimetric limulus ameobocyte lysate test. The relative concentration of endotoxin in the inflammatory exudate at 4hr and 10hr is shown here. Data expressed as individual values with mean± SD. n=5/group.

6.3.7 Effect of JBT-101 on lipid mediators at the site of UVkEc triggered acute inflammation

JBT-101 decreased the levels of leukotriene LTB_4 and prostanoids including PGE_2, TXB_2, $PGF_{2\alpha}$ in a dose-dependent manner during onset and resolution phases. 20mg JBT-101 inhibited LTB_4 to a greater extent than prednisone at 4h and 10h. At 4h, the LTB_4 level in placebo was 126.17 ± 85.25 pg/ml and it decreased to 58.37 ± 23.86 pg/ml in 5mg JBT-101 group and further to 12.11 ± 2.32 pg/ml in 20mg JBT-101 group. At 4h, the levels of LTB_4 in prednisone group were 41.98 ± 28.24 pg/ml **(Figure 6.9 A)**. The levels of PGE_2, $PGF_{2\alpha}$ and TXB_2, are shown in **Figure 6.9 B, C, D.** The levels of PGD_2 were decreased only by the 20mg JBT-101 **(Figure 6.9 E).**

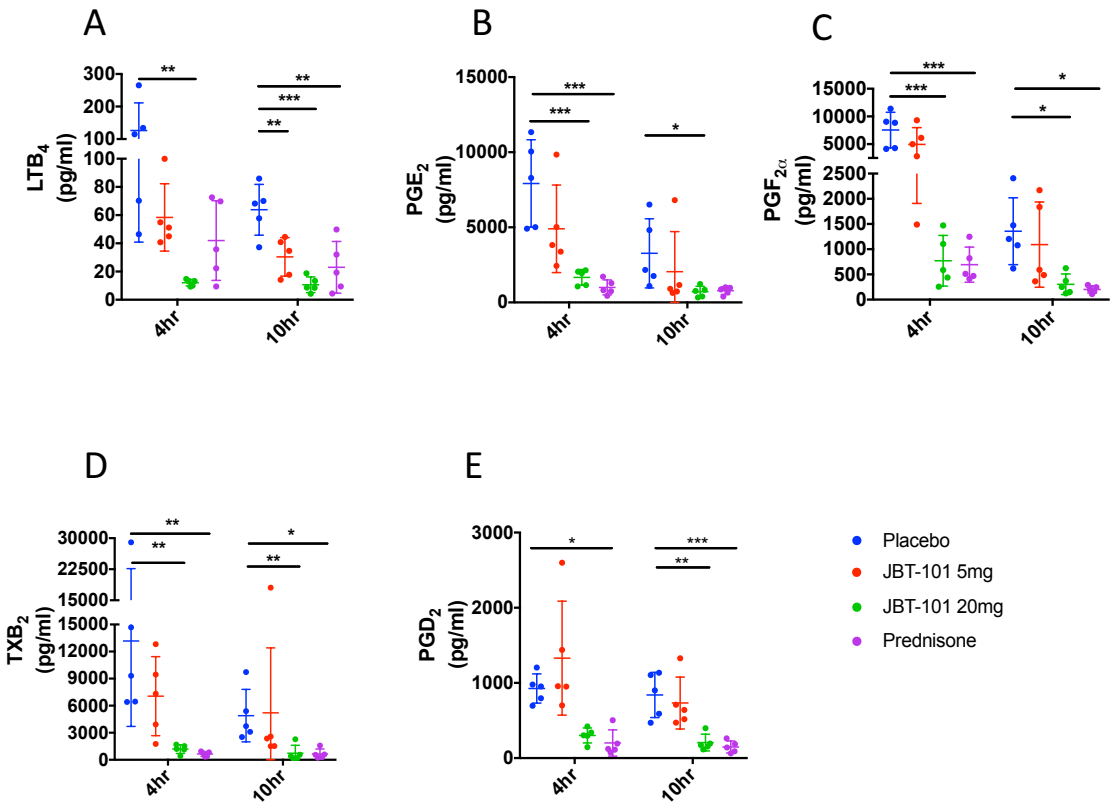

Figure 6.9 The effect of JBT-101 and prednisone on LTB_4 and prostanoids in the inflammatory exudate at the site of UVkEc triggered dermal inflammation

Healthy male volunteers were randomized to receive either placebo, 5mg JBT-101 , 20mg JBT-101, twice daily or 15mg prednisone once daily for four days. On fourth day, acute inflammation was triggered by intradermal injection of 1.5 x 10^7 UV killed *E. coli* (UVkEc) suspended in 100µl of saline in both the forearms. Inflammatory exudate at the injection site was acquired into a suction blister raised after 4hr (onset phase) on one forearm and after 10hr (resolution phase) on the contralateral forearm. Lipid mediators in the inflammatory exudate were analysed by liquid chromatography mass spectrophotometry (LC-MS) by Prof. Serhan laboratory (Harvard University). The concentrations of prostanoids in the inflammatory exudate at 4hr and 10hr are shown here. Data expressed as individual values with mean ± SD. n=5/group. p values are denoted as < 0.05 = ' * ', <0.01 = ' ** ', <0.001 = ' *** '. <0.0001 = '****'

In general terms, levels of SPMs were substantially lower than conventional prostaglandins. JBT-101 dose-dependently increased LXA_4 and more potently at the 10h time-point. At 10h, the levels of LXA_4 in the placebo group were 4.44 ± 0.2 pg/ml and 5mg JBT-101 raised it to 6.29 ± 2.45 pg/ml and 20mg JBT-101 increased it to 12.26 ± 2.23 pg/ml **(Figure 6.10 A)**. The levels LXB_4 levels showed a decreasing trend in the 5mg JBT- 101 group at 4h and 10h, while the 20mg JBT-101 showed an increasing trend **(Figure 6.10 B)**.

Of the DHA derived metabolites, the precursor of D-series resolvins 17-HDHA was dose-dependently reduced in the JBT and also by prednisone at onset and resolution phase **(Figure 6.10 C)**. The levels of D-series resolvins, RvD1 increased dose dependently by JBT-101 and the also by prednisone at both the time points. At 4h, RvD1 was undetectable in the placebo group while in the 5mg JBT-101 and 20mg JBT-101 it increased to 0.916 ± 2.048 pg/ml and 7.55 ± 2.178 pg/ml respectively. At 10h, the levels of RvD1 in the placebo group was 1.72 ± 2.37 pg/ml, and it was increased by 5mg JBT-101 to 2.72 ± 2.49 pg/ml and by 20mg JBT-101 to 6.04 ± 2.15 pg/ml **(Figure 6.10 D)**. The levels of RvD3 were detected only in the 20mg JBT-101 group, and it increased from 4h to 10h. At 4h, it was 8.48 ± 2.31 pg/ml, and at 10h it was 16.48 ± 5.47 pg/ml **(Figure 6.10 E)**. The levels of 14-HDHA, PD-1 and 18-HEPE, were not different between placebo, JBT-101 and prednisone groups and are shown in **Figure 6.10 F, G, H.**

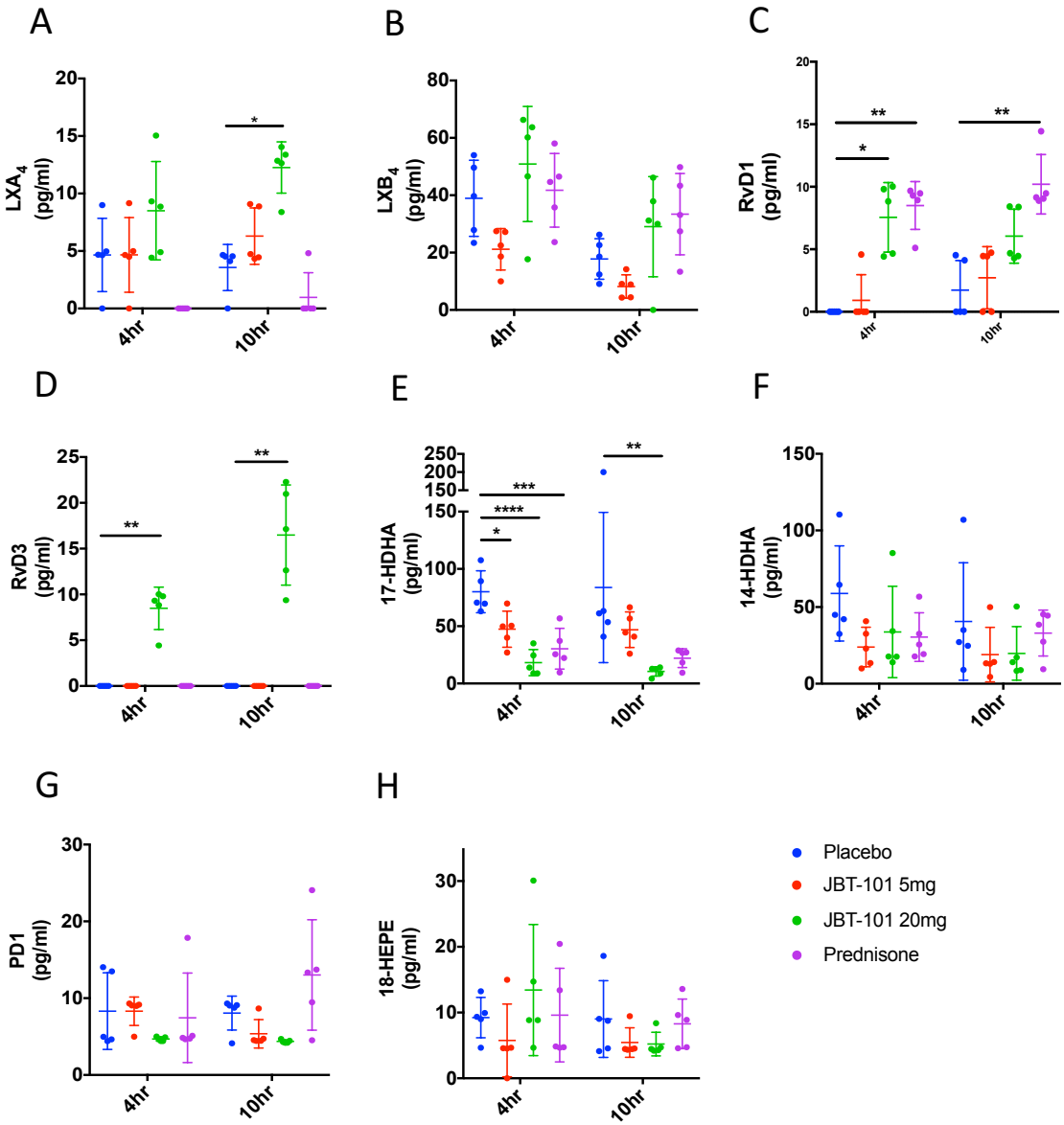

<u>Figure 6.10</u> The effect of JBT-101 and prednisone on specialised pro-resolving mediators (SPMs) in the inflammatory exudate at the site of UVkEc triggered acute inflammation

Healthy male volunteers were randomized to receive either placebo, 5mg JBT-101 , 20mg JBT-101, twice daily or 15mg Prednisone once daily for four days. On fourth day, acute inflammation was triggered by intradermal injection of UV killed *E. coli* (UVkEc) in 100µl of saline in both the forearms. Inflammatory exudate at the injection site was acquired into a suction blister raised after 4h (onset phase) on one forearm and after 10h (resolution phase) on the contralateral forearm. Lipid mediators in the inflammatory exudate were analysed by liquid chromatography mass spectrophotometry (LC-MS) by Prof. Serhan laboratory (Harvard University). The concentrations of SPMs in the inflammatory exudate at 4hr and 10hr are shown here. Data expressed as individual values with mean± SD. n=5/group. p values are denoted as < 0.05 = ' * ', <0.01 = ' ** ', <0.001 = ' *** '. <0.0001 = '****'

Correlation between the neutrophil numbers at the site with the soluble mediators measured in this study revealed a significant positive correlation only with LTB_4 in the 20mg group at 4h **(Table 6.1)**.

Neutrophil/ml vs	Placebo				5mg				20mg			
	4hr		10hr		4hr		10hr		4hr		10hr	
	r	p	r	p	r	p	r	p	r	p	r	p
IFNγ	0.9	0.0833	0.8	0.1333	-0.3	0.6833	-0.1	0.95	-0.3	0.6833	0.3	0.6833
IL-1β	-0.3	0.6833	0.9	0.0833	0.3	0.6833	-0.1	0.95	0.8	0.1333	0.5	0.45
IL-2	-0.5	0.45	0.9	0.0833	-0.1	0.95	-0.1	0.95	-0.8	0.1333	-0.9	0.0833
IL-4	0.6	0.35	0.1	0.95	-0.7	0.2333	-0.3	0.6833	-0.5	0.45	-0.8	0.1333
IL-6	-0.6	0.35	0.7	0.2333	0.2	0.7833	0.3	0.6833	0.1	0.95	-0.9	0.0833
IL-8	-0.9	0.0833	0.8	0.1333	0.1	0.95	0.4	0.5167	0	>0.9999	0.8	0.1333
IL-10	0.1	0.95	0.3	0.6833	-0.4	0.5167	0.5	0.45	-0.2	0.7833	-0.5	0.45
IL-12p70	0.4	0.5167	0.9	0.0833	-0.6	0.35	-0.4	0.5167	0	>0.9999	-0.6	0.35
IL-13	-0.6	0.35	0.8	0.1333	-0.1	0.95	-0.3	0.6833	0.1	0.95	-0.6	0.35
TNFα	0.5	0.45	0.9	0.0833	0.3	0.6833	-0.1	0.95	0.7	0.2333	0.4	0.5167
LTB4	0.3	0.6833	-0.1	0.95	0.5	0.45	-0.3	0.6833	1	0.0167	-0.7	0.2333
PGE2	0.6	0.35	0.5	0.45	0.1	0.95	-0.4	0.5167	0.2	0.7833	0.9	0.0833
PGF2α	0.6	0.35	0.9	0.0833	0.4	0.5167	-0.2	0.7833	-0.1	0.95	0.2	0.7833
TXB2	0.1	0.95	0.6	0.35	0	>0.9999	0.8	0.1333	0.1	0.95	0.9	0.0833
PGD2	0.1	0.95	-0.3	0.6833	0.6	0.35	0.3	0.6833	0.6	0.35	-0.3	0.6833
LXA4	0	>0.9999	0.3	0.6833	0.3	0.6833	0.9	0.0833	-0.6	0.35	-0.7	0.2333
LXB4	0.4	0.5167	0.6	0.35	-0.8	0.1333	0.3	0.6833	0.2	0.7833	0.9	0.0833
RvD1	NA	NA	-0.4472	0.5	-0.3536	0.8	0.0513	>0.9999	0	>0.9999	0.3	0.6833
RvD3	NA	NA	NA	NA	NA	NA	NA	NA	-0.2	0.7833	0.8	0.1333
17-HDHA	-0.8	0.1333	0.8	0.1333	0.2	0.7833	0.7	0.2333	-0.1	0.95	-0.6	0.35
PD1	-0.2	0.7833	0.6	0.35	0.1	0.95	-0.7	0.2333	-0.1	0.95	-0.7	0.2333
14-HDHA	0.1	0.95	0.9	0.0833	-0.4	0.5167	0.6	0.35	0.4	0.5167	0.2	0.7833
5,15-diHETE	NA	NA	NA	NA	NA	NA	NA	NA	-0.1	0.95	0.1	0.95
Endotoxin	-0.3	0.6833	0.6	0.35	0	>0.9999	-0.3	0.6833	0.3	0.6833	-0.1	0.95

Table 6.1 Correlation matrix between neutrophil count and the concentration of soluble mediators in the blister exudate

The table showing correlation matrix where neutrophil count per ml of exudate for each volunteer in placebo, 5mg JBT-101 and 20mg JBT-101 at 4hr and 10hr was correlated (spearman correlation) with the soluble mediators measured in the inflammatory exudate in this study. Data expressed as correlation co-efficient (r) with the corresponding p value. n=5 for each test. p values < 0.05 were chosen as significant.

6.3.8 Effect of JBT-101 on the systemic immune response at the site of UVkEc triggered acute inflammation

The systemic immune response was assessed by measuring peripheral blood neutrophil and monocyte count and the CRP levels.

At 4h, circulating neutrophil numbers showed an increasing trend in 5mg JBT-101 and prednisone group when compared to placebo **(Figure 6.11 A)**. At 4h, the neutrophil numbers per ml of blood in placebo group was $8.59 \times 10^6 \pm 2.78$ /ml, while in 5mg JBT-101, 20mg JBT-101 and prednisone group it was $10.4 \times 10^6 \pm 3.22$ /ml, $8.52 \times 10^6 \pm 2.02$ /ml, $11.29 \times 10^6 \pm 4.05$ /ml respectively. From 4h onwards, the neutrophil count started to decline, and the differences between groups were less apparent. Peripheral blood neutrophil count for each volunteer in the placebo group is shown in **Figure 6.11 B**, the 5mg JBT-101 group in **Figure 6.11 C**, the 20mg JBT-101 group in **Figure 6.11 D** and the prednisone group in **Figure 6.11 E.**

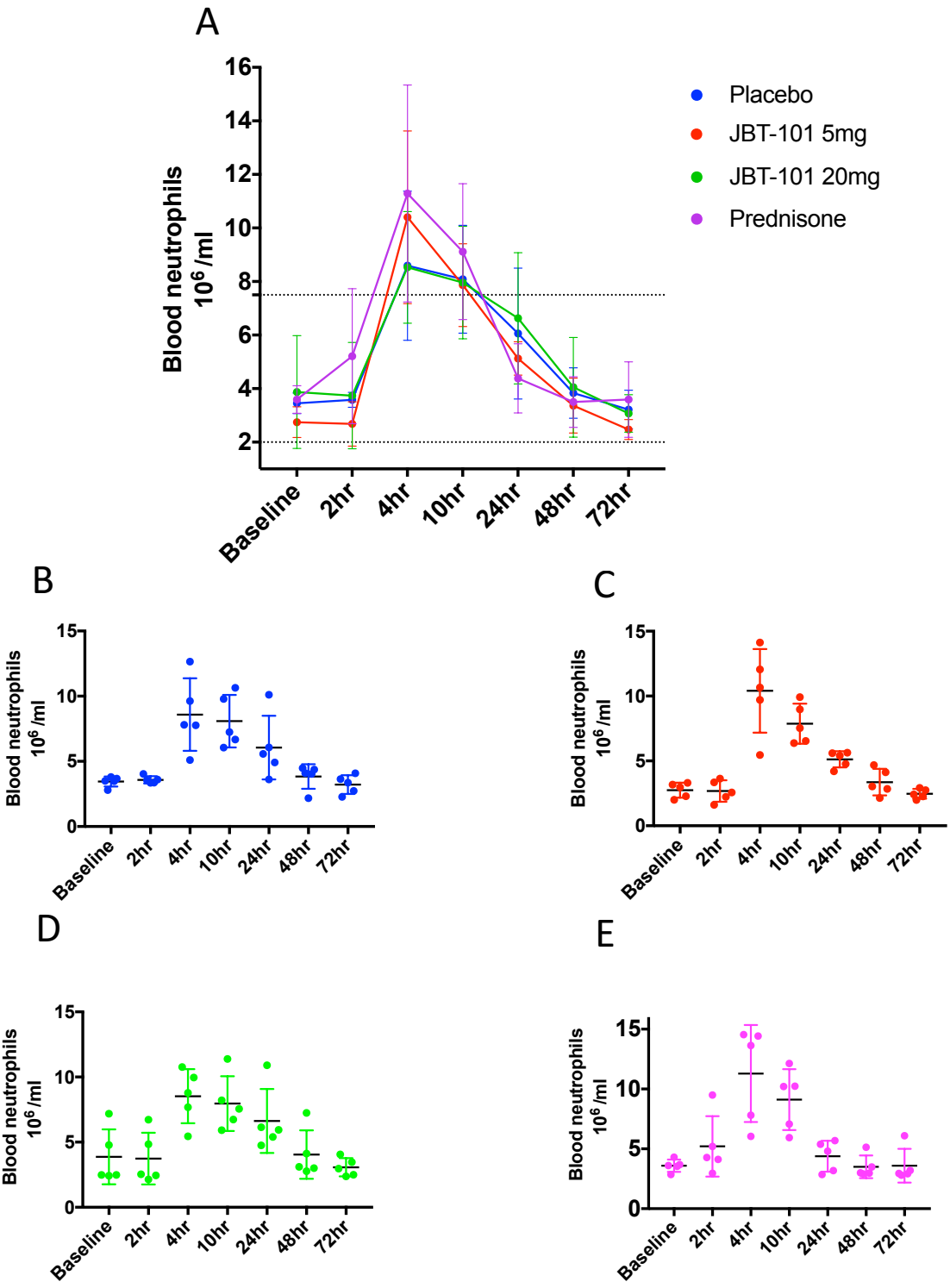

<u>Figure 6.11</u> The effect of JBT-101 and prednisone on peripheral blood neutrophil count in the UVkEc triggered self-resolving acute inflammation model

Healthy male volunteers were randomized to receive either placebo, 5mg JBT-101 , 20mg JBT-101, twice daily or 15mg Prednisone once daily for four days. On fourth day, acute inflammation was triggered by intradermal injection of UV killed *E. coli* (UVkEc) in both the forearms. Peripheral blood was taken at specified intervals after inflammation and full blood analysis was performed by an external pathology lab (The Doctor's laboratory, London, UK). The peripheral blood neutrophil count in placebo **(A)**, 5mg JBT-101 **(B)**, 20mg JBT-101 **(C)** and 15mg prednisone **(D)** and the comparison of peripheral blood neutrophil count (mean ± SD) between the four treatment groups **(E)** is shown here. Data expressed as individual values with mean± SD. n=5/group.

The numbers of peripheral monocyte per ml of blood were not different between any of the groups during the onset of inflammation. However, 20mg JBT-101 showed a trend towards during later time points of resolution, e.g. At 48h, monocyte count in the placebo group was 0.47 x 10^6 ± 0.19 /ml, and 20mg JBT-101 increased it to 0.81 x 10^6 ± 0.45 /ml (**Figure 6.12 A)**. Peripheral blood monocyte count for each volunteer in the placebo group is shown in **Figure 6.12 B**, the 5mg JBT-101 group in **Figure 6.12 C**, the 20mg JBT-101 group in **Figure 6.12 D** and prednisone group in **Figure 6.12 E** respectively. By 72h, the peripheral blood neutrophil and monocyte count returned to baseline levels.

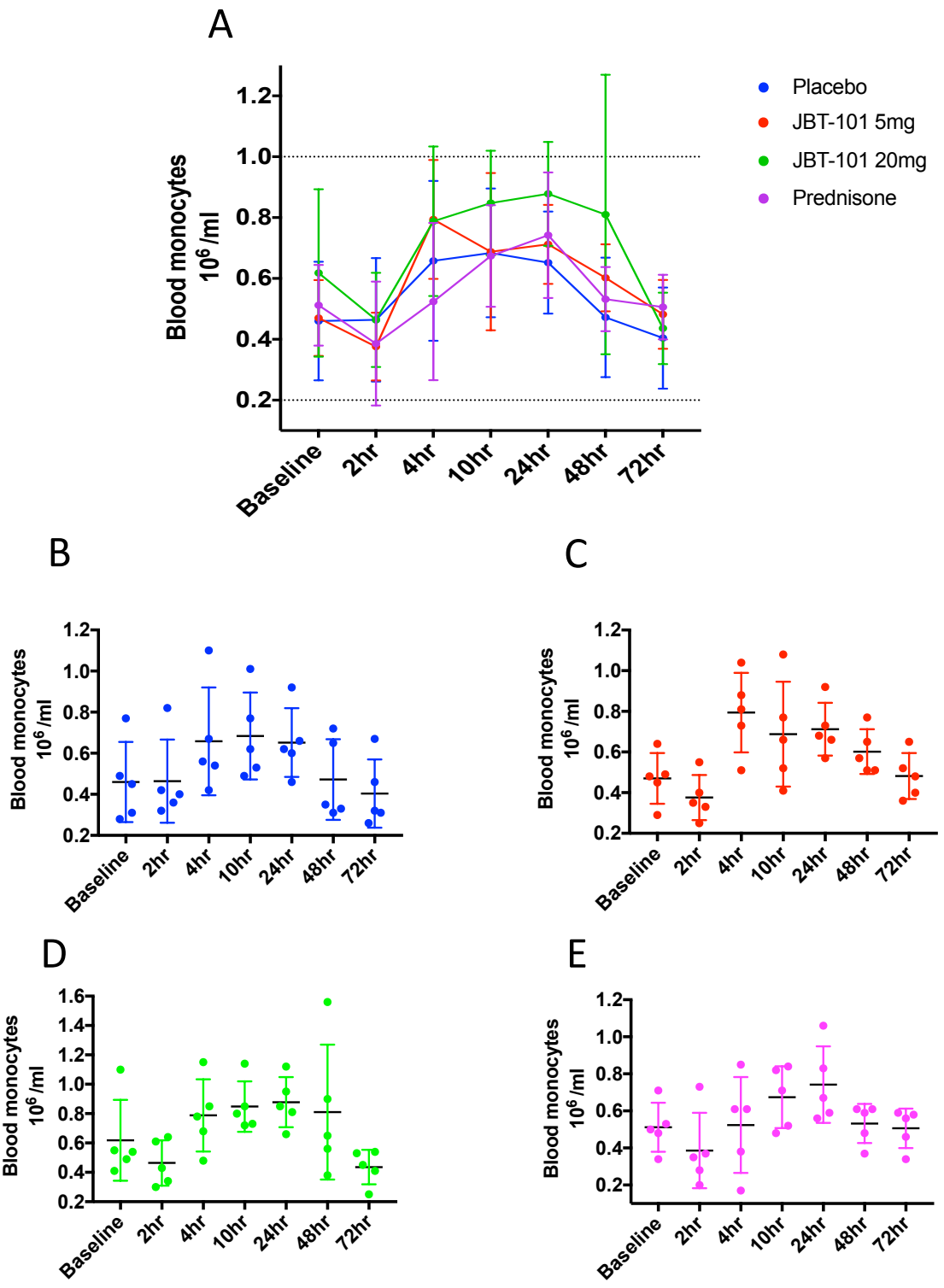

Figure 6.12 The effect of JBT-101 and prednisone on peripheral blood monocyte count in the UVkEc triggered self-resolving acute inflammation model

Healthy male volunteers were randomized to receive either placebo, 5mg JBT-101 , 20mg JBT-101, twice daily or 15mg Prednisone once daily for four days. On fourth day, acute inflammation was triggered by intradermal injection of UV killed *E. coli* (UVkEc) in both the forearms. Peripheral blood was taken specified intervals after inflammation and full blood analysis was performed by an external pathology lab (The Doctor's laboratory, London, UK). The peripheral blood monocyte count in placebo **(A)**, 5mg JBT-101 **(B)**, 20mg JBT-101 **(C)** and 15mg prednisone **(D)** and the comparison of peripheral blood monocyte count (mean ± SD) between the four treatment groups **(E)** is shown here Data expressed as individual values with mean± SD. n=5/group.

C-reactive protein (CRP) is an acute-phase protein produced from the liver in response to acute inflammation [252]. In placebo and both the JBT-101 dose groups, CRP levels began to rise from 10h and showed an increasing trend between 10h to 24h. However, between 24h and 48h, the 5mg JBT-101 showed a decreasing trend. At 48h, the CRP level in the placebo group was 10.98 ± 11.01 mg/L, and in the 5mg JBT-101 and 20mg JBT-101 group, it was 6.6 ± 3.43 mg/L and 13.44 ± 10.18 mg/L respectively. Volunteers in prednisone group inhibited the rise of CRP at all the time points **(Figure 6.13 A)**. Serum CRP levels for each volunteer in the placebo group is shown in **Figure 6.13 B**, the 5mg JBT-101 group in **Figure 6.13 C**, the 20mg JBT-101 group in **Figure 6.13 D** and the prednisone group in **Figure 6.13 E.**

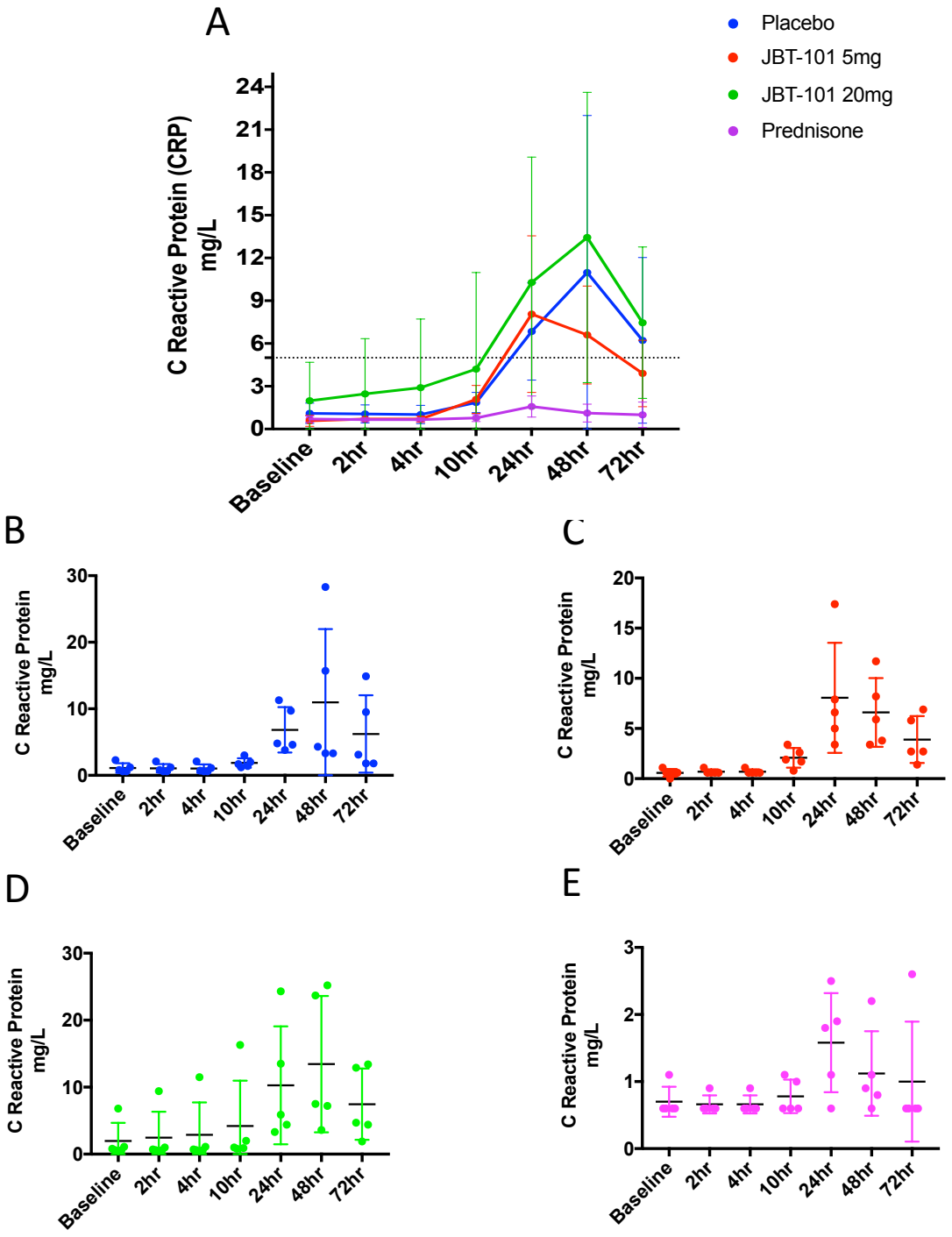

Figure 6.13 The effect of JBT-101 and prednisone on serum C- reactive protein levels in the UVkEc triggered self-resolving acute inflammation model

Healthy male volunteers were randomized to receive either placebo, 5mg JBT-101 , 20mg JBT-101, twice daily or 15mg Prednisone once daily for four days. On fourth day, acute inflammation was triggered by intradermal injection of UV killed *E. coli* (UVkEc) in both the forearms. Peripheral blood was taken at specified intervals after inflammation, serum was separated and analysed for C- reactive protein (The Doctor's laboratory, London, UK). The serum CRP in placebo **(A)**, 5mg JBT-101 **(B)**, 20mg JBT-101 **(C)** and 15mg prednisone **(D)** and the comparison of peripheral blood neutrophil (mean ± SD) between the four treatment groups **(E)** is shown here. Data expressed as individual values with mean± SD. n=5/group.

6.4 DISCUSSION

In this pilot study, we found that JBT-101 at both 5mg and 20mg doses was as effective as prednisone in decreasing neutrophil numbers during onset. This effect was co-incident with its dose-dependent reduction of IL-8 and endotoxin. In addition, JBT-101 dose-dependently decreased the levels of LTB_4 and prostanoids including PGE_2, $PGF_{2\alpha}$ and TXB_2 during onset and resolution. Furthermore, it was observed that JBT-101 increased the concentration of SPMs including LXA_4, RvD1 and RvD3 at the resolution time point but only at the higher 20mg dose.

Studies in mice using zymosan-induced peritonitis model have shown that JBT-101 increases the formation of LXA_4 and have further proposed that the mechanism through which JBT-101 exerts an effect on neutrophil reduction is via LXA_4 [247]. While our study validates the observation that JBT-101 induces the formation of LXA_4, it warrants a discussion as to whether this is the main mechanism through which JBT-101 mediates neutrophil reduction. Three observations made here discourage me from linking the rise in SPMs by JBT-101 with its effect on neutrophil reduction in this model. Firstly, the levels of LXA_4 were increased significantly only in the 20mg group and that too at the 10h time point. This suggests a lack of dose-dependent effect of JBT-101 on increasing SPMs. Secondly, JBT-101 reduced neutrophil numbers at both the lower 5mg and the higher 20mg dose and mainly at the 4h time point. This highlights the absence of concurrence as the effect of JBT-101 on inducing SPMs was at 10h while its effect on reducing neutrophil numbers was obvious at 4h. Thirdly, there was no inverse correlation observed between neutrophil

count and levels of any of the SPMs at either time points. It could be argued that these correlation studies include only five volunteers per group, nevertheless they provide a hint to question whether the rise in SPMs is associated with a reduction in neutrophil numbers. Also, JBT-101 counterintuitively decreased the levels of 17-HDHA, a DHA metabolite which has been shown to directly inhibit the production of pro-inflammatory cytokine TNFα [254]. Taken together, these observations suggest the need for further investigations in both mice and humans before SPMs could be associated as the main mechanism through which JBT-101 is mediating neutrophil reduction. One approach to investigate this would be to test the effect of JBT-101 using specific FPR2/ALX (LXA_4 receptor) knockout mice, which have been shown to abrogate the inhibitory effect of LXA_4 on neutrophil migration [151]. Another approach to test whether the levels of LXA_4 in the 10h blister fluid in this model can inhibit neutrophil migration could be accomplished by using the 10h blister fluid in an *in vitro* neutrophil migration assay with or without FPR2/ALX receptor antagonist such as BOC-2 [255]. It would be important to elucidate the main mechanism of JBT-101, so that correct disease indications are considered for future clinical trials using this potent anti-inflammatory drug.

The effect of JBT-101 on neutrophil reduction in this model may also be due to its inhibitory effect on other neutrophil chemoattractants measured in this model. For instance, JBT-101 dose-dependently and at both the 4h and the 10h time point reduced the levels of LTB_4, a potent neutrophil chemoattractant which acts via BLT1 receptor on neutrophils and mediates their extravasation to tissues [24], [256]. The likelihood of this mechanism is also supported by the observation that LTB_4 significantly correlated with the neutrophil count at 4h

albeit only in the 20mg group. Another mechanism could be through the effect of JBT-101 on inhibition of prostaglandins PGE_2 and $PGF_{2\alpha}$, both of which can induce the production of neutrophil chemoattractants such as IL-17 and IL-8 [257] [258]. The possible role of this mechanism is also supported by the observation in this model that JBT-101 caused a dose-dependent reduction in IL-8 levels at 4h. The reduction in IL-8 observed in this model could also be due to the effect of JBT-101 on reducing IL-8 transcription activity by its direct effect on activating PPARγ [259]. This could be another mechanism through which JBT-101 is reducing neutrophil numbers at 4h. Taken together, the observations in this model suggest that JBT-101 is inhibiting neutrophil migration possibly via its effect on inhibition of pro-inflammatory mediators.

JBT-101 at both low dose (5mg) and the high dose (20mg) showed equally potent inhibition of neutrophil count at 4h. This suggests that 5mg JBT-101 might be engaging additional mechanisms to reduce neutrophil numbers at 4h. One of them could be through inhibition of IFN-γ, which has been shown to directly induce neutrophil migration after intraperitoneal administration in rat peritoneal cavity [260] and was reduced only in the 5mg JBT-101 group in this model. Another mechanism could be via PGD_2 and/or its metabolite 15d-PGJ_2, both of which have been shown to reduce neutrophil trafficking in multiple murine models of acute inflammation [138,261–263]. The possibility of this mechanism operating in the 5mg JBT-101 group is suggested by the observation that the 5mg JBT-101 prevented the inhibition of PGD_2, which was alternatively decreased by 20mg JBT-101. Additionally, it has been shown that JBT-101 can induce the formation of 15d-PGJ2 from healthy human fibroblasts and it could be that at 5mg, JBT-101 specifically increases 15d-PGJ2 in this

model [264][253]. A definitive way to confirm this would be to compare the levels of 15d-PGJ2 in the blister fluid of volunteers in the 5mg and 20mg JBT-101 group at 4h. In summary, the observation that 5mg JBT-101 exerts a potent effect on neutrophil migration in combination with the knowledge obtained from Phase 1 safety and toxicology studies (reference: JBT-101 investigator brochure) that the 5mg has lower incidence of side effects compared to 20mg, suggest that the use of lower dose of JBT-101, depending on the clinical condition, could offer a better risk-benefit profile.

The effect of JBT-101 on some of the pro-inflammatory cytokines measured in this model are in the opposite direction to the results observed in *in vitro* studies. For instance, 5mg JBT-101 and 20mg JBT-101 showed an increasing trend for pro-inflammatory cytokines IL1-β and TNFα at 4h in this model. However, *in vitro* cytokine release assays using LPS stimulated synovial fluid monocytes show that pre-treatment with JBT-101 decreases both IL1-β and TNFα [265]. One reason for these divergent results could be due to the absence of endothelial cells in the *in vitro* systems described above. Selective activation of CB2 receptor on human umbilical venous endothelial cells (HUVECs) by 2-arachidonoylglycerol, an endogenous cannabinoid, has been shown that to increase the production of TNF-α in *in vitro* assays [266]. From this, it could be speculated that the activation of the CB2 receptor by JBT-101 on the endothelium at the inflamed is overriding the effect of JBT-101 on immune cells and thus leading to increase in levels of TNF-α and IL-1β. This hypothesis could be tested using an *in vitro* assay incorporating PBMC-endothelial cell co-culture [267], and could be further confirmed by in vivo murine studies. Taken together, this observation highlights the importance and

representativeness of *in vivo* models to predict the effect of novel drugs on inflammation biomarkers in humans.

In this model, JBT-101 dose-dependently increased vascular hyperaemia despite inhibiting COX activity as evident from the reduction of prostanoids. This is counterintuitive as previously it was shown in this model that naproxen, a conventional COX-1/2 inhibitor reduces blood flow at the site (Chapter 5, Figure 5.1 A). One likely explanation for increased vascular hyperaemia by JBT-101 could be due to its direct activation of PPARγ in endothelial cells which can lead to increased formation nitric oxide, a potent vasodilator [253] [268]. Notably, the vascular hyperaemia increased at 24h and 48h in the 20mg group, and this raised the question whether the 20mg dose of JBT-101 is causing a rebound inflammation. While the volunteers in the 20mg group did not report of increased pain over the forearm site at these later time points, to definitively answer this question a separate study was conducted (by Dr Frances Bennett and Ms Alice Henderson) to ask this question. Briefly, they recruited five volunteers in the placebo group and the JBT-20mg group and put them on the same dosing regimen as for the original study (described in Figure 6.1). However, blisters were raised at 24h and 48h after UVkEC injection, and the level of inflammation was assessed by neutrophil numbers in the blister. The results of this study showed that the neutrophil count was not different between the placebo and JBT-101 group at 24h or 48h (Appendix Figure 8.5), suggesting that the vasodilation at 24h and 48h in JBT-101 arm might not be associated with rebound inflammation. To confirm this, measurement of inflammatory cytokines in the 24h and 48h blister fluid are ongoing in our laboratory. An interesting observation made during this follow up study was

that vascular hyperaemia in the JBT-101 20 mg group was lower at 10hr and 24hr compared to the original study, where blisters were raised at 4hr and 10hr. It could be that JBT-101 induces formation of endogenous factors, not currently known, between 4h and 10h and removal of these factors by the process of suction blister, leads to increased vascular hyperaemia. In summary, JBT-101 induced vasodilation seen in this model at the later time points is unlikely to be associated with increased inflammation.

In addition to exerting a potent inhibitory effect on neutrophil trafficking at 4h, JBT-101 also showed a dose-dependent decreasing trend in levels of endotoxin. This observation is consistent with the results in murine studies which showed that JBT-101 decreases bacterial load while also reducing neutrophilic inflammation in a model of *P. aeruginosa* induced lung inflammation [248]. One of the mechanisms that could underlie this effect of JBT-101 may be through increased production of nitric oxide via PPARγ (as described above), which in addition to being a potent vasodilator can also enhance bacterial clearance as shown previously in a murine model of *E. coli* triggered peritonitis [269]. Measurement of NO levels in the blister fluid could provide further evidence into the role of this mechanism in reducing endotoxin. On a related note, another observation made in this model was that JBT-101 did not decrease the circulating CRP levels. CRP is produced by the liver in response to inflammatory stress and has been shown to directly participate in bacterial clearance by activating complement, opsonisation and promoting neutrophil phagocytosis [252][270]. This could imply that the JBT-101 might not have systemic immunosuppressive effects. Also, compared to JBT-101, prednisone showed an increasing trend for endotoxin levels at both the time

points and strongly inhibited the rise of circulating CRP. Bearing in mind that corticosteroids increase risk of local and systemic infections [271], together these observations provide a clue that JBT might be acting as a local anti-inflammatory without compromising the host's antimicrobial defence at local and systemic levels.

In this model, the anti-inflammatory effect of JBT-101, evidenced by its effect on inhibition of neutrophil migration was to the same extent as naproxen and prednisone. In addition, studies in mice have shown that JBT-101 lacks the potential for gastrointestinal ulceration, a common side effect of NSAIDs. [272]. Moreover, the effect of JBT-101 on enhancing endotoxin clearance in this model provide the preliminary evidence that JBT-101 does not interfere with antimicrobial defence systems like corticosteroids. Taken together, these observations suggest that JBT-101 could be a novel anti-inflammatory agent for treatment of chronic inflammatory drugs with a better risk-benefit ratio. The promise of JBT-101 in this regard is further supported by results from the recently concluded Phase II clinical trials. In cystic fibrosis patients, JBT-101 reduced the number of neutrophils and levels of IL-8 in the patient's sputum and lowered the frequency of acute pulmonary exacerbations [273]. In another phase II trial in scleroderma patients, JBT-101 offered a clinical benefit as evidenced by significantly lowering scleroderma clinical disease scores called CRISS, Combined Response Index in diffuse cutaneous Systemic Sclerosis (CRISS) [274]. In summary, these results support future clinical development for JBT-101 and also the expansion of its indications to other chronic inflammatory disorders, e.g. rheumatoid arthritis, where disease management

is difficult due to side effects associated with long-term use of NSAIDs and corticosteroids.

In conclusion, this study shows that JBT-101, at doses currently being investigated in Phase II clinical trials, exerts a profound anti-inflammatory in UVkEc triggered self-resolving dermal inflammation model. This effect is most likely due to its effect on inhibition of pro-inflammatory lipids than the rise in levels of SPMs. Further investigations are required to understand the contribution of SPMs in explaining the effect of JBT-101 on resolution indices.

Chapter 7

Summary of findings and future directions

7.1 Summary of findings

My PhD aim was to develop a human model of acute resolving inflammation and use it as a tool to investigate the local generation of SPMs and also test their effect on resolution indices. In chapter 3, I performed a detailed characterisation of the cantharidin skin blister to validate its use for investigating resolution biomarkers. However, I found that the cantharidin blister model was associated with incomplete clearance of apoptotic neutrophils during the resolution, an important hallmark of resolution. In chapter 4, I describe a novel model where inflammation was triggered by injecting UVkEc in the dermis, and the inflammatory exudate was collected in a suction blister raised at different time points of the inflammatory spectrum. The UVkEc triggered dermal inflammation model allowed me to appreciate a clear temporal profile of inflammatory cells, pro-inflammatory cytokines and vascular hyperaemia during onset and resolution. In Chapter 5, using the UVkEc triggered self-resolving dermal inflammation model, I identified the presence of SPMs at the inflamed site and the key receptors through which they act. I then utilised this model as the first in human proof of concept platform to investigate the effect of two different types of SPM based therapies. Using a local route of administration, I demonstrated that therapeutic supplementation of SPMs (LXB_4, RvE1, RvD2, AT-RvD1) reduced neutrophil numbers during the resolution phase, but had an insignificant effect on other indices of resolution including clearance of inflammatory stimulus, decrease in levels of pro-inflammatory cytokines or switching pro-resolving macrophage phenotype. In chapter 6, I tested the pro-resolution effect of orally active SPM inducing small molecule JBT-101, CB2 receptor agonist (Corbus Pharmaceuticals) using this

novel model. Indeed, in this model JBT-101 inhibited neutrophil infiltration at onset coincident with the reduction of inflammatory mediators including LTB_4, PGE_2, $PGF_{2\alpha}$, IL-8 and also enhanced endotoxin clearance. It is also triggered the biosynthesis of SPMs including LXB_4, RvD1 and RvD3 during the resolution phase but the neither the levels of these SPMs nor the time point when their synthesis increased correlated with the response of JBT-101 on resolution biomarkers. In totality, this thesis demonstrates a novel human model of self-resolving dermal inflammation that allows determination of quantifiable indices of resolution. Using this model as a tool to investigate resolution in humans, I found SPMs and expression of their receptors at the inflamed site, but the therapeutic addition of SPMs at endogenous levels resulted only in the reduction of neutrophils and modest effects on other resolution indices. And while JBT-101 exhibited anti-inflammatory effects comparable to prednisone, convincing evidence is lacking to place SPMs as a key mechanism of action of JBT-101.

7.2 Implications of the detailed characterisation of cantharidin skin blister

Detailed investigation of cantharidin skin blister revealed incomplete clearance of neutrophils during resolution. This observation discouraged me to use it further for investigation of SPMs, as one of the main effects of SPMs is on neutrophil clearance. However, the same observation provided the clue that stromal scaffold around the inflammatory cells could be important for their clearance, and this led me to develop the UVkEc triggered dermal inflammation model. Another important insight I derived from this observation

was that cantharidin blister can be used as a model to study neutrophil apoptosis in humans. This additional use of cantharidin model has now been exploited in our laboratory to show that neutrophil apoptosis is defective in aged volunteers (> 65 years) compared to young volunteers (< 45 years) (Roel De Maeyer, personal communication). In addition to allowing investigation of defects in neutrophil apoptosis, the cantharidin blister model can also serve as a proof of concept platform in humans to study the drugs modulating neutrophil apoptosis, e.g. cyclin dependent kinase inhibitors [275].

7.3 The potential use of UVkEc triggered self-resolving dermal inflammation model to solve the controversy around role of fish oils in inducing SPM formation in humans

The beneficial effects of supplementation of n-3 fish oils, e.g. EPA and DHA in inflammatory disorders including arthritis and asthma triggered the research to identify the molecular mechanisms of their anti-inflammatory effect [276]. This led to the identification and characterisation of SPMs including resolvins, maresins and protectins [219]. Supplementation of n-3 fish oils is becoming a conventional approach to increase the SPM levels. However, this approach has yielded conflicting results in clinical studies conducted by different groups. On one hand, a study by Barden et al. in healthy volunteers observed a significant increase in plasma levels of RvE1 [277]. The same group has also observed increased plasma levels of SPMs including RvD1, AT-RvD1, RvD2 in clinical populations, e.g. arthritis [278] and chronic kidney disease [279]. Contrastingly, studies by Skarke et al. showed that fish oil supplements failed to increase SPM levels in healthy volunteer plasma either in a steady state or

after systemic endotoxin challenge [280]. Fischer et al. also failed to detect D- or E- series resolvins in healthy volunteers after fish oil supplementation despite seeing a rise in the levels of its precursor 17-HDHA and 18-HEPE respectively [281]. While the exact reasons for this discrepancy are unclear at this stage, it has been speculated that they could be due to differences in analytical techniques including the use of deuterated internal standards and other inherent challenges, e.g. low levels of these mediators, sample extraction from a complex biological matrix such as plasma [282]. In summary, the consensus is lacking on whether fish oils can increase SPM levels in humans.

I speculate whether the choice of tissue can influence the detection of SPMs. SPMs are a product of transcellular metabolism, a process which involves coordinated action between multiple cell types, each contributing the enzymes necessary for the specific steps in SPM biosynthesis, e.g. neutrophil 5-LO and platelet 12-LO interaction in LXA_4 formation [283], neutrophil 5-LO and endothelial acetylated COX-2 interaction in formation of RvE1/E2 [284]. It is likely that the site of local tissue inflammation facilitates interaction between these cell types which could increase SPM generation unlike in plasma where immune cells are in circulation. The validity of this argument gains some support from a recent study investigating the effect of fish oil supplementation on SPM levels in arthritis patients. Here it was shown that the conversion of SPM precursors 18-HEPE and 17-HDHA into the corresponding E-series and D-series resolvins was greater in synovial fluid compartment compared to plasma [278].

I propose to test the effect of fish oil supplementation using UVkEc triggered dermal inflammation model to address whether the use of local tissue instead of plasma can enhance SPM detection. This model would allow temporal analysis and comparison of local tissue inflammatory exudate and plasma in the same person. Importantly, this study could be conducted in healthy volunteers, and thus it would preclude the interactions of fish oils with other medications and co-morbidities that are observed in clinical populations.

7.4 Potential applicability of UVkEc triggered self-resolving dermal inflammation model to guide the clinical development of stable synthetic SPM analogues

Although research demonstrating the effect of fish oils on inducing SPM formation in humans is still controversial, the discovery of SPMs as endogenous mediators of resolution of inflammation has led to the development of an alternative approach that involves direct supplementation with SPMs. Synthetic stable SPM analogues which resist metabolic inactivation by eicosanoid reductase, the main enzyme involved in SPM degradation, and those that can be delivered orally or intravenously have been developed to advance this approach, e.g. 3-oxo-15-epi-LXA_4 analogues which can be delivered orally or intravenously and have been shown to retain biological activity similar to native LXA_4 as evidenced by their effect on reducing leucocyte infiltration in multiple murine models of inflammation such as zymosan-induced peritonitis and ischaemia reperfusion injury in lung [285]. Another example is of benzo-diacetylenic-17*R*-RvD1-methyl ester (BDA-RvD1)

which like the native RvD1 has been shown to reduce neutrophil infiltration and hasten bacteria clearance in *E. coli* induced peritonitis model [286].

Clinical development of these stable SPM analogues will be a very promising and reliable approach to test the direct effect of SPMs in humans on resolution biomarkers. It can also help us understand whether effects of SPMs on different resolution indices is dose dependent in humans. After establishing the safety of these analogues in Phase I clinical trials, I propose that the use of UVkEc induced self-resolving dermal inflammation model would be helpful to obtain information about their pharmacokinetics and preliminary evidence of its pharmacodynamic activity in humans. For instance, after oral or intravenous delivery, the tissue bioavailability and stability of these synthetic SPMs at steady state and during inflammation can be obtained by measuring their levels in the inflammatory exudate obtained at different time points. In addition, the model can allow to investigate the effect of SPMs at different doses on the resolution biomarkers. Such proof of concept studies would not only guide dose optimization of these SPMs for use in future studies in patients but would also help in choosing an appropriate biomarker for future clinical trials for different types of inflammatory conditions, e.g. neutrophil clearance for autoimmune conditions, endotoxin clearance for infectious diseases or assessment of local pain for their analgesic use.

7.5 Conclusion

In this thesis, I developed a novel human model of resolution of acute inflammation triggered by intradermal injection of UV-killed *E. coli*. Using this model, I demonstrated that supplementation with SPMs, at physiological doses, hastened resolution as noticeable from increased neutrophil clearance. I also showed that JBT-101, a CB2 receptor agonist, had a potent anti-inflammatory effect which is likely due to its effect on inhibition of pro-inflammatory lipid mediators than enhancing SPM biosynthesis. Clinical development of synthetic SPM analogues can confirm and extend these observations to accomplish the objective of harnessing SPMs for therapeutic gain.

Chapter 8

Appendix

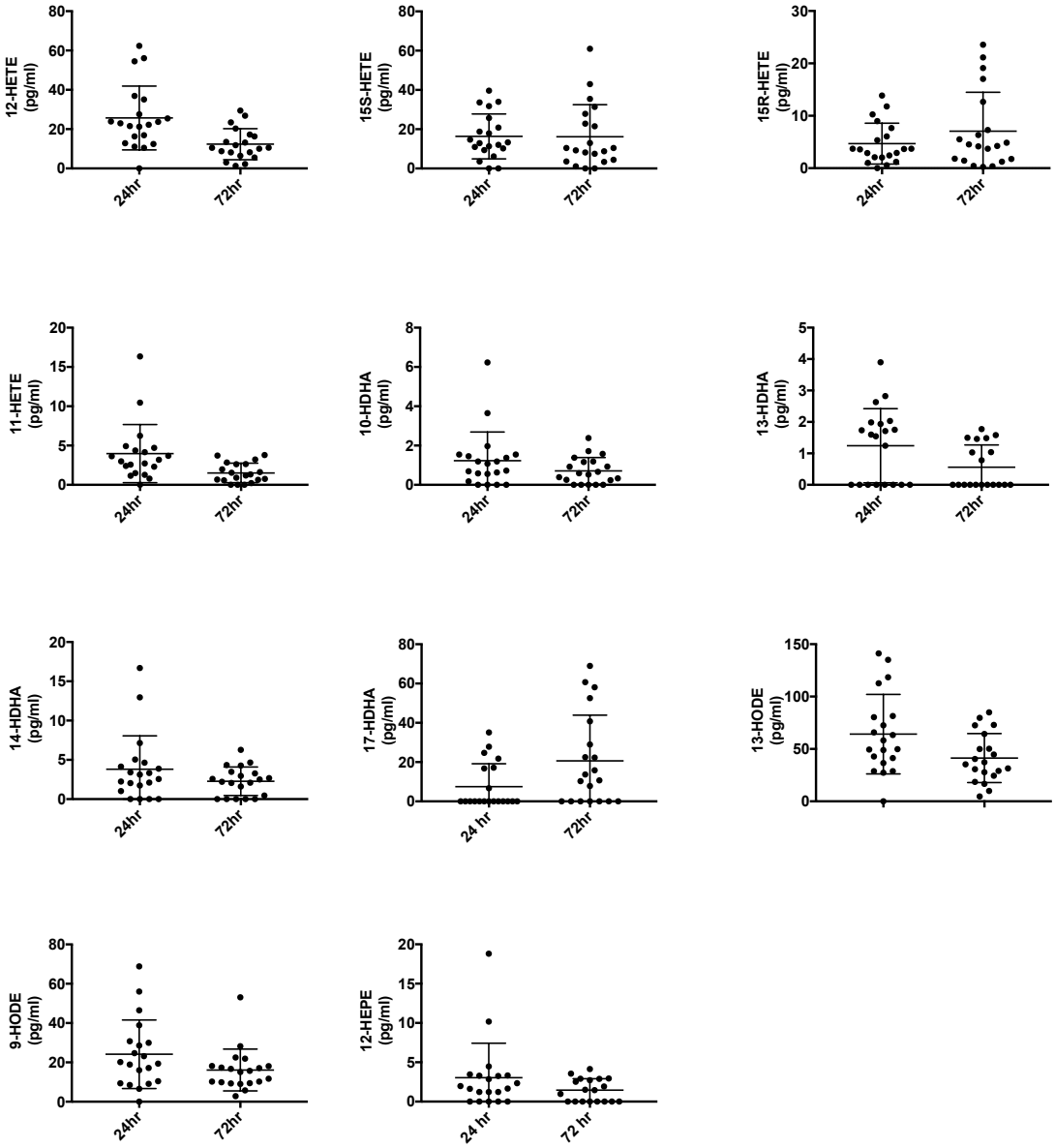

Figure 8.1: Additional lipid mediators in cantharidin skin blister at 24hr and 72hr

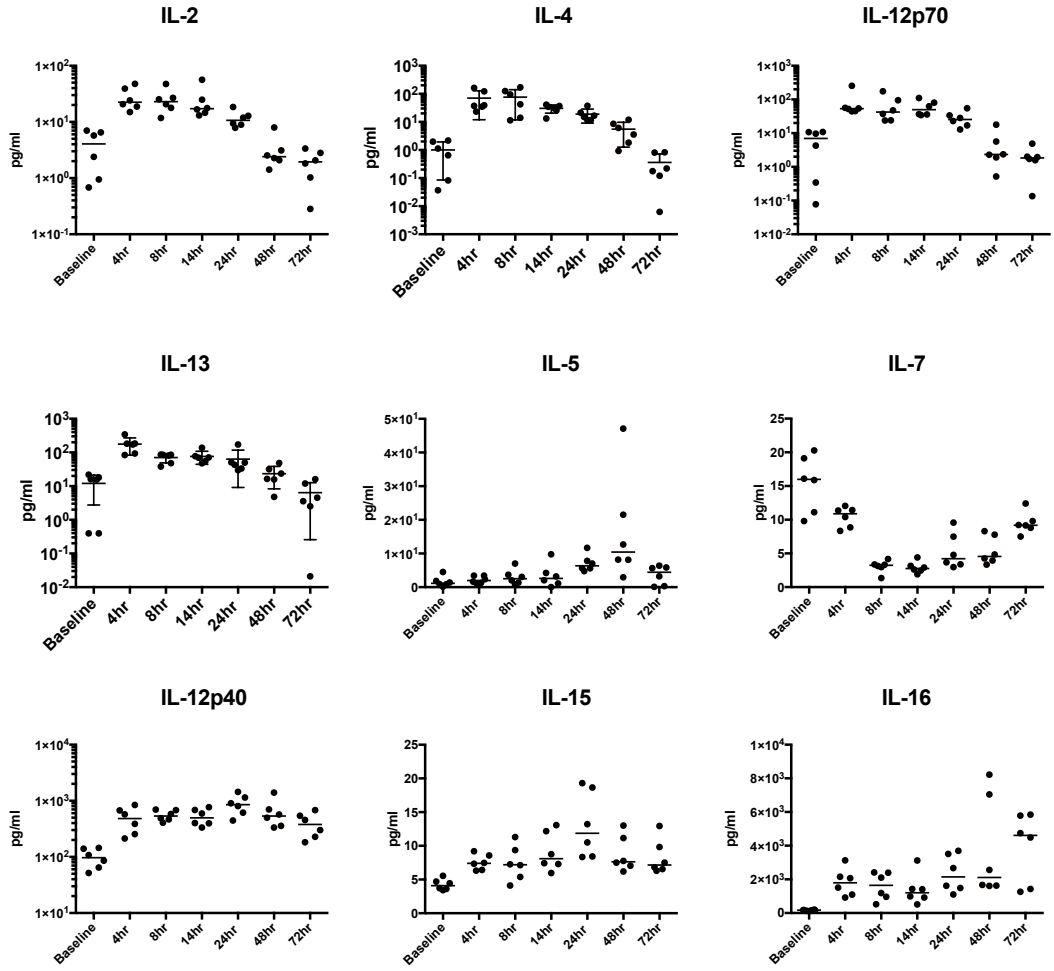

Figure 8.2 : Additional cytokines and chemokines measured at the site of UVkEc triggereed acute resolving inflammation.

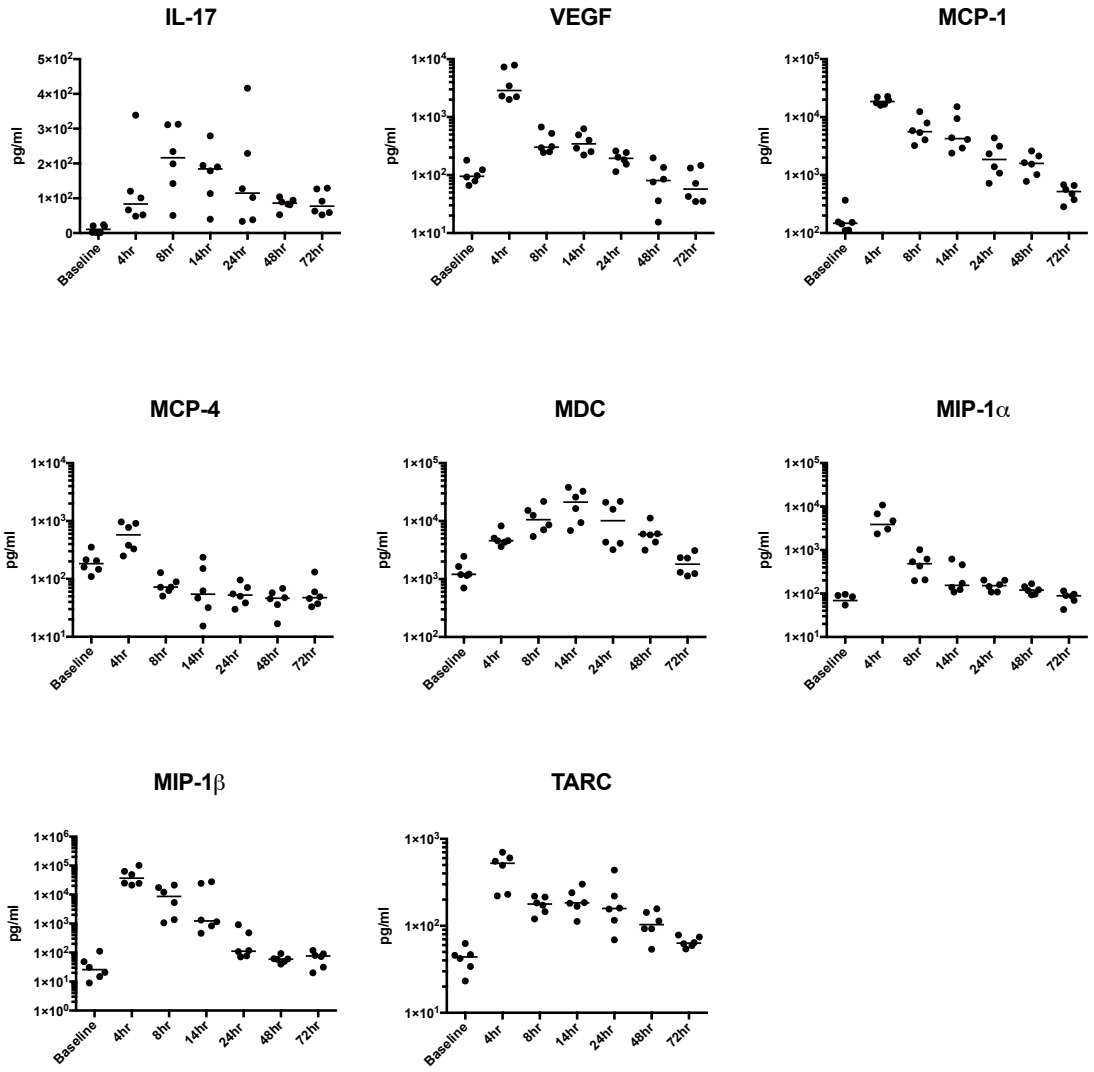

Figure 8.3: Additional cytokines and chemokines measured at the site of UVkEc triggereed acute resolving inflammation.

A

B

Figure 8.4: Demonstration of measurement of pain threshold using algometer (A) and temperature using infrared thermometer (B) at the site of UVkEc triggered acute inflammation

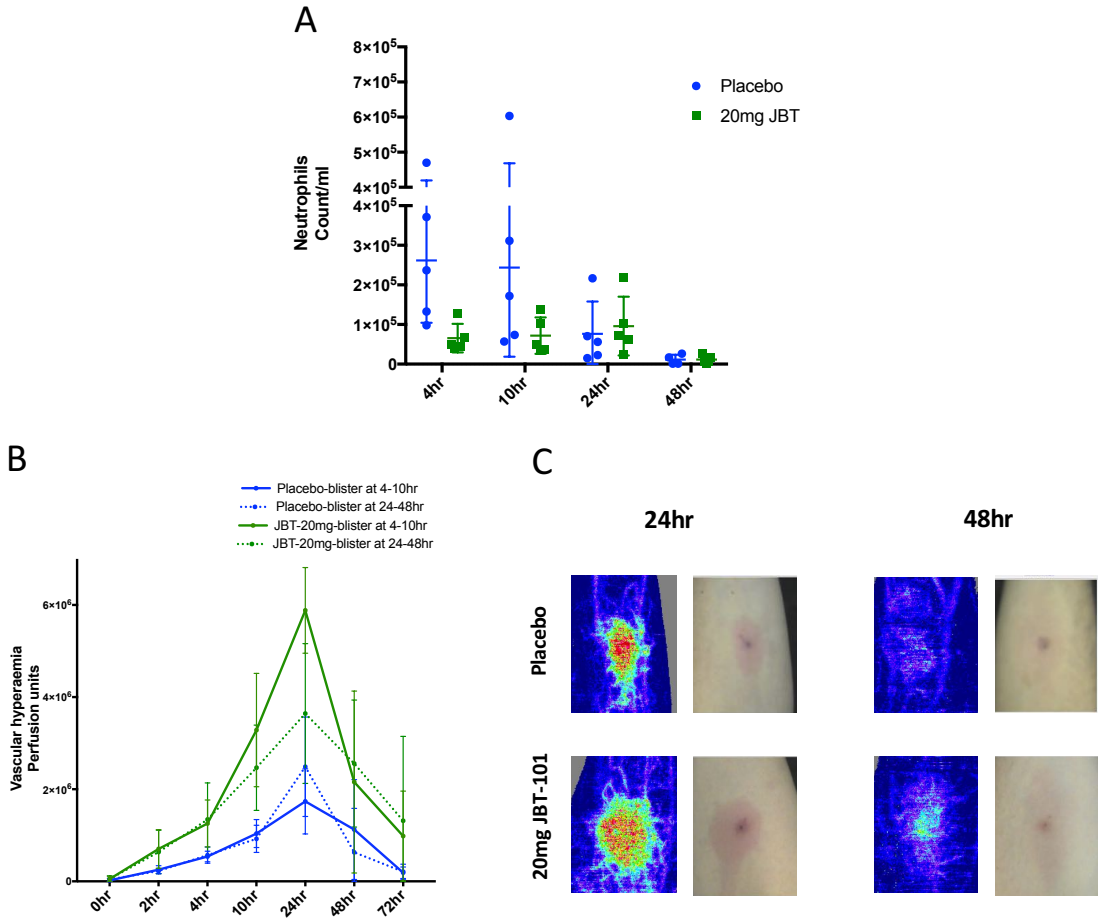

Figure 8.5 : The effect of 20mg JBT-101 vs. placebo on neutrophil numbers and vascular hyperaemia when blister was raised at 24hr and 48hr time point at the site of UVkEc triggered self resolving dermal inflammation

Healthy male volunteers were randomized to receive either Placebo, or JBT-101^{20mg}, twice daily for four days. On fourth day, acute inflammation was triggered by intradermal injection of UV killed *E. coli* on both the forearms. Inflammatory exudate at the injection site was acquired into a suction blister raised at 24hr on one forearm and at 48hr on the contralateral forearm. Vascular hyperaemia at the injection site was assessed by a laser Doppler imager (moorLDI-HIR).

Figure 8.4 A shows the neutrophil count at 24hr and 48hr vs the neutrophil count at 4hr and 10hr blister. **Figure 8.4 B** shows vascular hyperaemia over the inflammation site when blister was raised at 24hr and 48hr (dotted line) vs the vascular hyperaemia over the inflammation site when blister was raised at 4hr and 10hr (solid line). **Figure 8.4 C** shows the representative laser Doppler and camera images at 24hr and 48hr. Data expressed as mean ± SD. n=5.

References

1. Lawrence T. Inflammation and cancer: a failure of resolution? Trends Pharmacol. Sci. 2007;28:162–5.

2. Cash JL, Norling LV, Perretti M. Resolution of inflammation: targeting GPCRs that interact with lipids and peptides. Drug Discov. Today. 2014;19:1186–92.

3. Nestle FO, Di Meglio P, Qin J-Z, Nickoloff BJ. Skin immune sentinels in health and disease. Nat. Rev. Immunol. 2009;9:679–91.

4. Takeuchi O, Akira S. Pattern Recognition Receptors and Inflammation. Cell. 2010;140:805–20.

5. Kupper TS, Fuhlbrigge RC. Immune surveillance in the skin: mechanisms and clinical consequences. Nat. Rev. Immunol. 2004;4:211–22.

6. Abraham SN, St John AL. Mast cell-orchestrated immunity to pathogens. Nat. Rev. Immunol. 2010;10:440–52.

7. Pober JS, Cotran RS. The role of endothelial cells in inflammation. Transplantation. 1990;50:537–44.

8. Gainetdinov RR, Premont RT, Bohn LM, Lefkowitz RJ, Caron MG. Desensitization of G protein-coupled receptors and neuronal functions. Annu. Rev. Neurosci. 2004;27:107–44.

9. Tran Q-K, Ohashi K, Watanabe H. Calcium signalling in endothelial cells. Cardiovasc. Res. 2000;48:13–22.

10. Mitchell JA, Ali F, Bailey L, Moreno L, Harrington LS. Role of nitric oxide and prostacyclin as vasoactive hormones released by the endothelium. Exp. Physiol. 2008;93:141–7.

11. Shen Q, Rigor RR, Pivetti CD, Wu MH, Yuan SY. Myosin light chain kinase in microvascular endothelial barrier function. Cardiovasc. Res. 2010;87:272–80.

12. Birch KA, Ewenstein BM, Golan DE, Pober JS. Prolonged peak elevations in cytoplasmic free calcium ions, derived from intracellular stores, correlate with the extent of thrombin-stimulated exocytosis in single human umbilical vein endothelial cells. J. Cell. Physiol. 1994;160:545–54.

13. Prescott SM, Zimmerman GA, McIntyre TM. Human endothelial cells in culture produce platelet-activating factor (1-alkyl-2-acetyl-sn-glycero-3-phosphocholine) when stimulated with thrombin. Proc. Natl. Acad. Sci. U. S. A. 1984;81:3534–8.

14. Cotran RS, Pober JS. Cytokine-endothelial interactions in inflammation, immunity, and vascular injury. J. Am. Soc. Nephrol. 1990;1:225–35.

15. Félétou M, Huang Y, Vanhoutte PM. Endothelium-mediated control of vascular tone: COX-1 and COX-2 products. Br. J. Pharmacol. 2011;164:894–912.

16. Zarbock A, Ley K, McEver RP, Hidalgo A. Leukocyte ligands for endothelial selectins: specialized glycoconjugates that mediate rolling and signaling under flow. Blood. 2011;118:6743–51.

17. Bargatze RF, Kurk S, Butcher EC, Jutila MA. Neutrophils roll on adherent neutrophils bound to cytokine-induced endothelial cells via L-selectin on the rolling cells. J. Exp. Med. 1994;180:1785–92.

18. Ding ZM, Babensee JE, Simon SI, Lu H, Perrard JL, Bullard DC, et al. Relative contribution of LFA-1 and Mac-1 to neutrophil adhesion and migration. J. Immunol. Baltim. Md 1950. 1999;163:5029–38.

19. Coelho FM, Pinho V, Amaral FA, Sachs D, Costa VV, Rodrigues DH, et al. The chemokine receptors CXCR1/CXCR2 modulate antigen-induced arthritis by regulating adhesion of neutrophils to the synovial microvasculature. Arthritis Rheum. 2008;58:2329–37.

20. Phillipson M, Heit B, Colarusso P, Liu L, Ballantyne CM, Kubes P. Intraluminal crawling of neutrophils to emigration sites: a molecularly distinct process from adhesion in the recruitment cascade. J. Exp. Med. 2006;203:2569–75.

21. Ley K, Laudanna C, Cybulsky MI, Nourshargh S. Getting to the site of inflammation: the leukocyte adhesion cascade updated. Nat. Rev. Immunol. 2007;7:678–89.

22. Foxman EF, Campbell JJ, Butcher EC. Multistep Navigation and the Combinatorial Control of Leukocyte Chemotaxis. J. Cell Biol. 1997;139:1349–60.

23. Lin AM, Rubin CJ, Khandpur R, Wang JY, Riblett M, Yalavarthi S, et al. Mast cells and neutrophils release IL-17 through extracellular trap formation in psoriasis. J. Immunol. Baltim. Md 1950. 2011;187:490–500.

24. Afonso PV, Janka-Junttila M, Lee YJ, McCann CP, Oliver CM, Aamer KA, et al. LTB4 IS A SIGNAL RELAY MOLECULE DURING NEUTROPHIL CHEMOTAXIS. Dev. Cell. 2012;22:1079–91.

25. Shi C, Pamer EG. Monocyte recruitment during infection and inflammation. Nat. Rev. Immunol. 2011;11:762–74.

26. Soehnlein O, Lindbom L. Phagocyte partnership during the onset and resolution of inflammation. Nat Rev Immunol. 2010;10:427–39.

27. Hurst SM, Wilkinson TS, McLoughlin RM, Jones S, Horiuchi S, Yamamoto N, et al. Il-6 and its soluble receptor orchestrate a temporal switch in the pattern of leukocyte recruitment seen during acute inflammation. Immunity. 2001;14:705–14.

28. Soehnlein O, Zernecke A, Eriksson EE, Rothfuchs AG, Pham CT, Herwald H, et al. Neutrophil secretion products pave the way for inflammatory monocytes. Blood. 2008;112:1461–71.

29. Gombart AF, Koeffler HP. Neutrophil specific granule deficiency and mutations in the gene encoding transcription factor C/EBP(epsilon). Curr. Opin. Hematol. 2002;9:36–42.

30. Berahovich RD, Miao Z, Wang Y, Premack B, Howard MC, Schall TJ. Proteolytic activation of alternative CCR1 ligands in inflammation. J. Immunol. Baltim. Md 1950. 2005;174:7341–51.

31. Segal AW. How Neutrophils Kill Microbes. Annu. Rev. Immunol. 2005;23:197–223.

32. Brinkmann V, Reichard U, Goosmann C, Fauler B, Uhlemann Y, Weiss DS, et al. Neutrophil extracellular traps kill bacteria. Science. 2004;303:1532–5.

33. Rajakariar R, Newson J, Jackson EK, Sawmynaden P, Smith A, Rahman F, et al. Nonresolving Inflammation in gp91phox-/- Mice, a Model of Human Chronic Granulomatous Disease, Has Lower Adenosine and Cyclic Adenosine 5'-Monophoshate. J. Immunol. Baltim. Md 1950. 2009;182:3262–9.

34. Buckley CD, Gilroy DW, Serhan CN, Stockinger B, Tak PP. The resolution of inflammation. Nat. Rev. Immunol. 2013;13:59–66.

35. Mantovani A, Bonecchi R, Locati M. Tuning inflammation and immunity by chemokine sequestration: decoys and more. Nat. Rev. Immunol. 2006;6:907–18.

36. Nibbs RJ, Kriehuber E, Ponath PD, Parent D, Qin S, Campbell JD, et al. The beta-chemokine receptor D6 is expressed by lymphatic endothelium and a subset of vascular tumors. Am. J. Pathol. 2001;158:867–77.

37. Bonecchi R, Locati M, Galliera E, Vulcano M, Sironi M, Fra AM, et al. Differential recognition and scavenging of native and truncated macrophage-derived chemokine (macrophage-derived chemokine/CC chemokine ligand 22) by the D6 decoy receptor. J. Immunol. Baltim. Md 1950. 2004;172:4972–6.

38. Fra AM, Locati M, Otero K, Sironi M, Signorelli P, Massardi ML, et al. Cutting Edge: Scavenging of Inflammatory CC Chemokines by the Promiscuous Putatively Silent Chemokine Receptor D6. J. Immunol. 2003;170:2279–82.

39. Gardner L, Patterson AM, Ashton BA, Stone MA, Middleton J. The human Duffy antigen binds selected inflammatory but not homeostatic chemokines. Biochem. Biophys. Res. Commun. 2004;321:306–12.

40. Darbonne WC, Rice GC, Mohler MA, Apple T, Hébert CA, Valente AJ, et al. Red blood cells are a sink for interleukin 8, a leukocyte chemotaxin. J. Clin. Invest. 1991;88:1362–9.

41. Martinez de la Torre Y, Locati M, Buracchi C, Dupor J, Cook DN, Bonecchi R, et al. Increased inflammation in mice deficient for the chemokine decoy receptor D6. Eur. J. Immunol. 2005;35:1342–6.

42. Dawson TC, Lentsch AB, Wang Z, Cowhig JE, Rot A, Maeda N, et al. Exaggerated response to endotoxin in mice lacking the Duffy antigen/receptor for chemokines (DARC). Blood. 2000;96:1681–4.

43. Ariel A, Fredman G, Sun Y-P, Kantarci A, Van Dyke TE, Luster AD, et al. Apoptotic neutrophils and T cells sequester chemokines during immune response resolution through modulation of CCR5 expression. Nat. Immunol. 2006;7:1209–16.

44. D'Amico G, Frascaroli G, Bianchi G, Transidico P, Doni A, Vecchi A, et al. Uncoupling of inflammatory chemokine receptors by IL-10: generation of functional decoys. Nat. Immunol. 2000;1:387–91.

45. Ortega-Gómez A, Perretti M, Soehnlein O. Resolution of inflammation: an integrated view. EMBO Mol. Med. 2013;5:661–74.

46. Dean RA, Cox JH, Bellac CL, Doucet A, Starr AE, Overall CM. Macrophage-specific metalloelastase (MMP-12) truncates and inactivates ELR+ CXC chemokines and generates CCL2, -7, -8, and -13 antagonists: potential role of the macrophage in terminating polymorphonuclear leukocyte influx. Blood. 2008;112:3455–64.

47. McQuibban GA, Gong J-H, Tam EM, McCulloch CAG, Clark-Lewis I, Overall CM. Inflammation Dampened by Gelatinase A Cleavage of Monocyte Chemoattractant Protein-3. Science. 2000;289:1202–6.

48. Fullerton JN, Gilroy DW. Resolution of inflammation: a new therapeutic frontier. Nat. Rev. Drug Discov. 2016;15:551–67.

49. Nakahira K, Haspel JA, Rathinam VAK, Lee S-J, Dolinay T, Lam HC, et al. Autophagy proteins regulate innate immune responses by inhibiting the release of mitochondrial DNA mediated by the NALP3 inflammasome. Nat. Immunol. 2011;12:222–30.

50. Fuchs TA, Abed U, Goosmann C, Hurwitz R, Schulze I, Wahn V, et al. Novel cell death program leads to neutrophil extracellular traps. J. Cell Biol. 2007;176:231–41.

51. Yousefi S, Simon H-U. NETosis – Does It Really Represent Nature's 'Suicide Bomber'? Front. Immunol. [Internet]. 2016 [cited 2017 Apr 13];7. Available from: http://www.ncbi.nlm.nih.gov/pmc/articles/PMC4999959/

52. Yipp BG, Kubes P. NETosis: how vital is it? Blood. 2013;122:2784–94.

53. Chan FK-M. Fueling the Flames: Mammalian Programmed Necrosis in Inflammatory Diseases. Cold Spring Harb. Perspect. Biol. [Internet]. 2012 [cited 2017 Apr 13];4. Available from: http://www.ncbi.nlm.nih.gov/pmc/articles/PMC3536335/

54. Silva MT. Secondary necrosis: The natural outcome of the complete apoptotic program. FEBS Lett. 2010;584:4491–9.

55. Fox S, Leitch AE, Duffin R, Haslett C, Rossi AG. Neutrophil Apoptosis: Relevance to the Innate Immune Response and Inflammatory Disease. J. Innate Immun. 2010;2:216–27.

56. Renshaw SA, Timmons SJ, Eaton V, Usher LR, Akil M, Bingle CD, et al. Inflammatory neutrophils retain susceptibility to apoptosis mediated via the Fas death receptor. J. Leukoc. Biol. 2000;67:662–8.

57. Brown SB, Savill J. Phagocytosis triggers macrophage release of Fas ligand and induces apoptosis of bystander leukocytes. J. Immunol. Baltim. Md 1950. 1999;162:480–5.

58. Cross A, Moots RJ, Edwards SW. The dual effects of TNFalpha on neutrophil apoptosis are mediated via differential effects on expression of Mcl-1 and Bfl-1. Blood. 2008;111:878–84.

59. Conus S, Perozzo R, Reinheckel T, Peters C, Scapozza L, Yousefi S, et al. Caspase-8 is activated by cathepsin D initiating neutrophil apoptosis during the resolution of inflammation. J. Exp. Med. 2008;205:685–98.

60. Watson RW, Redmond HP, Wang JH, Condron C, Bouchier-Hayes D. Neutrophils undergo apoptosis following ingestion of Escherichia coli. J. Immunol. 1996;156:3986–92.

61. Kasahara Y, Iwai K, Yachie A, Ohta K, Konno A, Seki H, et al. Involvement of Reactive Oxygen Intermediates in Spontaneous and CD95(Fas/APO-1)–Mediated Apoptosis of Neutrophils. Blood. 1997;89:1748–53.

62. Solito E, Kamal A, Russo-Marie F, Buckingham JC, Marullo S, Perretti M. A novel calcium-dependent proapoptotic effect of annexin 1 on human neutrophils. FASEB J. 2003;17:1544–6.

63. Scannell M, Flanagan MB, deStefani A, Wynne KJ, Cagney G, Godson C, et al. Annexin-1 and peptide derivatives are released by apoptotic cells and stimulate phagocytosis of apoptotic neutrophils by macrophages. J. Immunol. Baltim. Md 1950. 2007;178:4595–605.

64. Ren Y, Xie Y, Jiang G, Fan J, Yeung J, Li W, et al. Apoptotic cells protect mice against lipopolysaccharide-induced shock. J. Immunol. Baltim. Md 1950. 2008;180:4978–85.

65. Hall SE, Savill JS, Henson PM, Haslett C. Apoptotic neutrophils are phagocytosed by fibroblasts with participation of the fibroblast vitronectin receptor and involvement of a mannose/fucose-specific lectin. J. Immunol. Baltim. Md 1950. 1994;153:3218–27.

66. Han CZ, Juncadella IJ, Kinchen JM, Buckley MW, Klibanov AL, Dryden K, et al. Macrophages redirect phagocytosis by non-professional phagocytes and influence inflammation. Nature. 2016;539:570–4.

67. Martin CJ, Peters KN, Behar SM. Macrophages Clean Up: Efferocytosis and Microbial Control. Curr. Opin. Microbiol. 2014;0:17–23.

68. Elliott MR, Ravichandran KS. Clearance of apoptotic cells: implications in health and disease. J. Cell Biol. 2010;189:1059–70.

69. Ravichandran KS, Lorenz U. Engulfment of apoptotic cells: signals for a good meal. Nat. Rev. Immunol. 2007;7:964–74.

70. Poon IKH, Lucas CD, Rossi AG, Ravichandran KS. Apoptotic cell clearance: basic biology and therapeutic potential. Nat. Rev. Immunol. 2014;14:166–80.

71. Hoffmann PR, deCathelineau AM, Ogden CA, Leverrier Y, Bratton DL, Daleke DL, et al. Phosphatidylserine (PS) induces PS receptor-mediated macropinocytosis and promotes clearance of apoptotic cells. J. Cell Biol. 2001;155:649–59.

72. Hochreiter-Hufford A, Ravichandran KS. Clearing the Dead: Apoptotic Cell Sensing, Recognition, Engulfment, and Digestion. Cold Spring Harb. Perspect. Biol. [Internet]. 2013 [cited 2017 Feb 4];5. Available from: http://www.ncbi.nlm.nih.gov/pmc/articles/PMC3579390/

73. Rodriguez-Manzanet R, Sanjuan MA, Wu HY, Quintana FJ, Xiao S, Anderson AC, et al. T and B cell hyperactivity and autoimmunity associated with niche-specific defects in apoptotic body clearance in TIM-4-deficient mice. Proc. Natl. Acad. Sci. U. S. A. 2010;107:8706–11.

74. Fadok VA, Bratton DL, Konowal A, Freed PW, Westcott JY, Henson PM. Macrophages that have ingested apoptotic cells in vitro inhibit proinflammatory cytokine production through autocrine/paracrine mechanisms involving TGF-beta, PGE2, and PAF. J. Clin. Invest. 1998;101:890–8.

75. Golpon HA, Fadok VA, Taraseviciene-Stewart L, Scerbavicius R, Sauer C, Welte T, et al. Life after corpse engulfment: phagocytosis of apoptotic cells leads to VEGF secretion and cell growth. FASEB J. Off. Publ. Fed. Am. Soc. Exp. Biol. 2004;18:1716–8.

76. Morimoto K, Amano H, Sonoda F, Baba M, Senba M, Yoshimine H, et al. Alveolar macrophages that phagocytose apoptotic neutrophils produce hepatocyte growth factor during bacterial pneumonia in mice. Am. J. Respir. Cell Mol. Biol. 2001;24:608–15.

77. Bellingan GJ, Caldwell H, Howie SE, Dransfield I, Haslett C. In vivo fate of the inflammatory macrophage during the resolution of inflammation: inflammatory macrophages do not die locally, but emigrate to the draining lymph nodes. J. Immunol. 1996;157:2577–85.

78. Angsana J, Chen J, Liu L, Haller CA, Chaikof EL. Efferocytosis as a regulator of macrophage chemokine receptor expression and polarization. Eur. J. Immunol. 2016;46:1592–9.

79. Weichand B, Weis N, Weigert A, Grossmann N, Levkau B, Brüne B. Apoptotic cells enhance sphingosine-1-phosphate receptor 1 dependent macrophage migration. Eur. J. Immunol. 2013;43:3306–13.

80. Hampton HR, Bailey J, Tomura M, Brink R, Chtanova T. Microbe-dependent lymphatic migration of neutrophils modulates lymphocyte proliferation in lymph nodes. Nat. Commun. 2015;6:7139.

81. Beauvillain C, Cunin P, Doni A, Scotet M, Jaillon S, Loiry M-L, et al. CCR7 is involved in the migration of neutrophils to lymph nodes. Blood. 2011;117:1196–204.

82. Eruslanov EB, Lyadova IV, Kondratieva TK, Majorov KB, Scheglov IV, Orlova MO, et al. Neutrophil Responses to Mycobacterium tuberculosis Infection in Genetically Susceptible and Resistant Mice. Infect. Immun. 2005;73:1744–53.

83. Abadie V, Badell E, Douillard P, Ensergueix D, Leenen PJM, Tanguy M, et al. Neutrophils rapidly migrate via lymphatics after Mycobacterium bovis BCG intradermal vaccination and shuttle live bacilli to the draining lymph nodes. Blood. 2005;106:1843–50.

84. Nourshargh S, Renshaw SA, Imhof BA. Reverse Migration of Neutrophils: Where, When, How, and Why? Trends Immunol. 2016;37:273–86.

85. Mathias JR, Perrin BJ, Liu T-X, Kanki J, Look AT, Huttenlocher A. Resolution of inflammation by retrograde chemotaxis of neutrophils in transgenic zebrafish. J. Leukoc. Biol. 2006;80:1281–8.

86. Woodfin A, Voisin M-B, Beyrau M, Colom B, Caille D, Diapouli F-M, et al. The junctional adhesion molecule JAM-C regulates polarized transendothelial migration of neutrophils in vivo. Nat. Immunol. 2011;12:761–9.

87. Buckley CD, Ross EA, McGettrick HM, Osborne CE, Haworth O, Schmutz C, et al. Identification of a phenotypically and functionally distinct population of long-lived neutrophils in a model of reverse endothelial migration. J. Leukoc. Biol. 2006;79:303–11.

88. Newson J, Stables M, Karra E, Arce-Vargas F, Quezada S, Motwani M, et al. Resolution of acute inflammation bridges the gap between innate and adaptive immunity. Blood [Internet]. 2014 [cited 2014 Aug 24]; Available from: http://www.bloodjournal.org/content/early/2014/07/08/blood-2014-03-562710

89. Rajakariar R, Lawrence T, Bystrom J, Hilliard M, Colville-Nash P, Bellingan G, et al. Novel biphasic role for lymphocytes revealed during resolving inflammation. Blood. 2008;111:4184–92.

90. Jarnicki AG, Lysaght J, Todryk S, Mills KHG. Suppression of antitumor immunity by IL-10 and TGF-beta-producing T cells infiltrating the growing tumor: influence of tumor environment on the induction of CD4+ and CD8+ regulatory T cells. J. Immunol. Baltim. Md 1950. 2006;177:896–904.

91. Huang B, Pan P-Y, Li Q, Sato AI, Levy DE, Bromberg J, et al. Gr-1+CD115+ immature myeloid suppressor cells mediate the development of tumor-induced T regulatory cells and T-cell anergy in tumor-bearing host. Cancer Res. 2006;66:1123–31.

92. Lesokhin AM, Hohl TM, Kitano S, Cortez C, Hirschhorn-Cymerman D, Avogadri F, et al. Monocytic CCR2+ Myeloid-Derived Suppressor Cells Promote Immune Escape by Limiting Activated CD8 T-cell Infiltration into the Tumor Microenvironment. Cancer Res. 2012;72:876–86.

93. Romano M, Serhan CN. Lipoxin generation by permeabilized human platelets. Biochemistry (Mosc.). 1992;31:8269–77.

94. Serhan CN. Lipoxin biosynthesis and its impact in inflammatory and vascular events. Biochim. Biophys. Acta BBA - Lipids Lipid Metab. 1994;1212:1–25.

95. Clària J, Serhan CN. Aspirin triggers previously undescribed bioactive eicosanoids by human endothelial cell-leukocyte interactions. Proc. Natl. Acad. Sci. 1995;92:9475–9.

96. Clària J, Lee MH, Serhan CN. Aspirin-triggered lipoxins (15-epi-LX) are generated by the human lung adenocarcinoma cell line (A549)-neutrophil interactions and are potent inhibitors of cell proliferation. Mol. Med. Camb. Mass. 1996;2:583–96.

97. Fiore S, Ryeom SW, Weller PF, Serhan CN. Lipoxin recognition sites. Specific binding of labeled lipoxin A4 with human neutrophils. J. Biol. Chem. 1992;267:16168–76.

98. Chiang N, Serhan CN, Dahlén S-E, Drazen JM, Hay DWP, Rovati GE, et al. The Lipoxin Receptor ALX: Potent Ligand-Specific and Stereoselective Actions in Vivo. Pharmacol. Rev. 2006;58:463–87.

99. Serhan CN, Chiang N, Van Dyke TE. Resolving inflammation: dual anti-inflammatory and pro-resolution lipid mediators. Nat. Rev. Immunol. 2008;8:349–61.

100. Serhan CN, Chiang N. Endogenous pro-resolving and anti-inflammatory lipid mediators: a new pharmacologic genus. Br. J. Pharmacol. 2008;153:S200–15.

101. Isobe Y, Arita M, Matsueda S, Iwamoto R, Fujihara T, Nakanishi H, et al. Identification and Structure Determination of Novel Anti-inflammatory Mediator Resolvin E3, 17,18-Dihydroxyeicosapentaenoic Acid. J. Biol. Chem. 2012;287:10525–34.

102. Levy BD, Serhan CN. Resolution and Regulation of Inflammation. In: McManus LM, Mitchell RN, editors. Pathobiol. Hum. Dis. [Internet]. San Diego: Academic Press; 2014 [cited 2017 Feb 7]. p. 332–48. Available from: https://www.sciencedirect.com/science/article/pii/B9780123864567018116

103. Serhan CN, Gotlinger K, Hong S, Lu Y, Siegelman J, Baer T, et al. Anti-Inflammatory Actions of Neuroprotectin D1/Protectin D1 and Its Natural Stereoisomers: Assignments of Dihydroxy-Containing Docosatrienes. J. Immunol. 2006;176:1848–59.

104. Serhan CN, Yang R, Martinod K, Kasuga K, Pillai PS, Porter TF, et al. Maresins: Novel macrophage mediators with potent antiinflammatory and proresolving actions. J. Exp. Med. 2009;206:15–23.

105. Arita M, Ohira T, Sun Y-P, Elangovan S, Chiang N, Serhan CN. Resolvin E1 selectively interacts with leukotriene B4 receptor BLT1 and ChemR23 to regulate inflammation. J. Immunol. Baltim. Md 1950. 2007;178:3912–7.

106. Wittamer V, Franssen J-D, Vulcano M, Mirjolet J-F, Le Poul E, Migeotte I, et al. Specific recruitment of antigen-presenting cells by chemerin, a novel processed ligand from human inflammatory fluids. J. Exp. Med. 2003;198:977–85.

107. Kaur J, Adya R, Tan BK, Chen J, Randeva HS. Identification of chemerin receptor (ChemR23) in human endothelial cells: chemerin-induced endothelial angiogenesis. Biochem. Biophys. Res. Commun. 2010;391:1762–8.

108. Bäck M, Dahlén S-E, Drazen JM, Evans JF, Serhan CN, Shimizu T, et al. International Union of Basic and Clinical Pharmacology. LXXXIV: Leukotriene Receptor Nomenclature, Distribution, and Pathophysiological Functions. Pharmacol. Rev. 2011;63:539–84.

109. Krishnamoorthy S, Recchiuti A, Chiang N, Fredman G, Serhan CN. Resolvin D1 receptor stereoselectivity and regulation of inflammation and proresolving microRNAs. Am. J. Pathol. 2012;180:2018–27.

110. Chiang N, Dalli J, Colas RA, Serhan CN. Identification of resolvin D2 receptor mediating resolution of infections and organ protection. J. Exp. Med. 2015;212:1203–17.

111. Filep JG, Zouki C, Petasis NA, Hachicha M, Serhan CN. Anti-inflammatory actions of lipoxin A(4) stable analogs are demonstrable in human whole blood: modulation of leukocyte adhesion molecules and inhibition of neutrophil-endothelial interactions. Blood. 1999;94:4132–42.

112. Papayianni A, Serhan CN, Brady HR. Lipoxin A4 and B4 inhibit leukotriene-stimulated interactions of human neutrophils and endothelial cells. J. Immunol. Baltim. Md 1950. 1996;156:2264–72.

113. Arita M, Ohira T, Sun Y-P, Elangovan S, Chiang N, Serhan CN. Resolvin E1 selectively interacts with leukotriene B4 receptor BLT1 and ChemR23 to regulate inflammation. J. Immunol. Baltim. Md 1950. 2007;178:3912–7.

114. Norling LV, Dalli J, Flower RJ, Serhan CN, Perretti M. Resolvin D1 limits PMN recruitment to inflammatory loci: receptor dependent actions. Arterioscler. Thromb. Vasc. Biol. 2012;32:1970–8.

115. Sun Y-P, Oh SF, Uddin J, Yang R, Gotlinger K, Campbell E, et al. Resolvin D1 and its aspirin-triggered 17R epimer. Stereochemical assignments, anti-inflammatory properties, and enzymatic inactivation. J. Biol. Chem. 2007;282:9323–34.

116. El Kebir D, József L, Pan W, Wang L, Petasis NA, Serhan CN, et al. 15-epi-lipoxin A4 inhibits myeloperoxidase signaling and enhances resolution of acute lung injury. Am. J. Respir. Crit. Care Med. 2009;180:311–9.

117. El Kebir D, Gjorstrup P, Filep JG. Resolvin E1 promotes phagocytosis-induced neutrophil apoptosis and accelerates resolution of pulmonary inflammation. Proc. Natl. Acad. Sci. U. S. A. 2012;109:14983–8.

118. Maddox JF, Serhan CN. Lipoxin A4 and B4 are potent stimuli for human monocyte migration and adhesion: selective inactivation by dehydrogenation and reduction. J. Exp. Med. 1996;183:137–46.

119. Godson C, Mitchell S, Harvey K, Petasis NA, Hogg N, Brady HR. Cutting edge: lipoxins rapidly stimulate nonphlogistic phagocytosis of apoptotic neutrophils by monocyte-derived macrophages. J. Immunol. Baltim. Md 1950. 2000;164:1663–7.

120. Schwab JM, Chiang N, Arita M, Serhan CN. Resolvin E1 and protectin D1 activate inflammation-resolution programmes. Nature. 2007;447:869–74.

121. Gewirtz AT, McCormick B, Neish AS, Petasis NA, Gronert K, Serhan CN, et al. Pathogen-induced chemokine secretion for model intestinal epithelium is inhibited by lipoxin A4 analogs. J. Clin. Invest. 1998;101:1860–9.

122. Qiu FH, Devchand PR, Wada K, Serhan CN. Aspirin-triggered lipoxin A4 and lipoxin A4 up-regulate transcriptional corepressor NAB1 in human neutrophils. FASEB J. Off. Publ. Fed. Am. Soc. Exp. Biol. 2001;15:2736–8.

123. Recchiuti A, Krishnamoorthy S, Fredman G, Chiang N, Serhan CN. MicroRNAs in resolution of acute inflammation: identification of novel resolvin D1-miRNA circuits. FASEB J. Off. Publ. Fed. Am. Soc. Exp. Biol. 2011;25:544–60.

124. Ariel A, Fredman G, Sun Y-P, Kantarci A, Van Dyke TE, Luster AD, et al. Apoptotic neutrophils and T cells sequester chemokines during immune response resolution through modulation of CCR5 expression. Nat. Immunol. 2006;7:1209–16.

125. Sodin-Semrl S, Taddeo B, Tseng D, Varga J, Fiore S. Lipoxin A4 Inhibits IL-1β-Induced IL-6, IL-8, and Matrix Metalloproteinase-3 Production in Human Synovial Fibroblasts and Enhances Synthesis of Tissue Inhibitors of Metalloproteinases. J. Immunol. 2000;164:2660–6.

126. Zhang MJ, Sansbury BE, Hellmann J, Baker JF, Guo L, Parmer CM, et al. Resolvin D2 Enhances Postischemic Revascularization While Resolving Inflammation. Circulation. 2016;134:666–80.

127. Li N, He J, Schwartz CE, Gjorstrup P, Bazan HEP. Resolvin E1 Improves Tear Production and Decreases Inflammation in a Dry Eye Mouse Model. J. Ocul. Pharmacol. Ther. 2010;26:431–9.

128. Campbell EL, MacManus CF, Kominsky DJ, Keely S, Glover LE, Bowers BE, et al. Resolvin E1-induced intestinal alkaline phosphatase promotes resolution of inflammation through LPS detoxification. Proc. Natl. Acad. Sci. U. S. A. 2010;107:14298–303.

129. Karp CL, Flick LM, Park KW, Softic S, Greer TM, Keledjian R, et al. Defective lipoxin-mediated anti-inflammatory activity in the cystic fibrosis airway. Nat. Immunol. 2004;5:388–92.

130. Seki H, Fukunaga K, Arita M, Arai H, Nakanishi H, Taguchi R, et al. The Anti-Inflammatory and Proresolving Mediator Resolvin E1 Protects Mice from Bacterial Pneumonia and Acute Lung Injury. J. Immunol. Baltim. Md 1950. 2010;184:836–43.

131. Ueda T, Fukunaga K, Seki H, Miyata J, Arita M, Miyasho T, et al. Combination therapy of 15-epi-lipoxin A4 with antibiotics protects mice from Escherichia coli-induced sepsis*. Crit. Care Med. 2014;42:e288-295.

132. Chiang N, Fredman G, Backhed F, Oh SF, Vickery T, Schmidt BA, et al. Infection regulates pro-resolving mediators that lower antibiotic requirements. Nature. 2012;484:524–8.

133. Vane JR. Inhibition of prostaglandin synthesis as a mechanism of action for aspirin-like drugs. Nature. New Biol. 1971;231:232–5.

134. Barnes PJ. How corticosteroids control inflammation: Quintiles Prize Lecture 2005. Br J Pharmacol. 2006;148:245–54.

135. Tabas I, Glass CK. Anti-inflammatory therapy in chronic disease: challenges and opportunities. Science. 2013;339:166–72.

136. Schäcke H, Döcke W-D, Asadullah K. Mechanisms involved in the side effects of glucocorticoids. Pharmacol. Ther. 2002;96:23–43.

137. Ong CKS, Lirk P, Tan CH, Seymour RA. An Evidence-Based Update on Nonsteroidal Anti-Inflammatory Drugs. Clin. Med. Res. 2007;5:19–34.

138. Gilroy DW, Colville-Nash PR, Willis D, Chivers J, Paul-Clark MJ, Willoughby DA. Inducible cyclooxygenase may have anti-inflammatory properties. Nat. Med. 1999;5:698–701.

139. Chan MM-Y, Moore AR. Resolution of inflammation in murine autoimmune arthritis is disrupted by cyclooxygenase-2 inhibition and restored by prostaglandin E2-mediated lipoxin A4 production. J. Immunol. Baltim. Md 1950. 2010;184:6418–26.

140. Ali T, Kaitha S, Mahmood S, Ftesi A, Stone J, Bronze MS. Clinical use of anti-TNF therapy and increased risk of infections. Drug Healthc. Patient Saf. 2013;5:79–99.

141. Lawrence T, Gilroy DW. Chronic inflammation: a failure of resolution? Int. J. Exp. Pathol. 2007;88:85–94.

142. Krönke G, Katzenbeisser J, Uderhardt S, Zaiss MM, Scholtysek C, Schabbauer G, et al. 12/15-lipoxygenase counteracts inflammation and tissue damage in arthritis. J. Immunol. Baltim. Md 1950. 2009;183:3383–9.

143. Kazani S, Planaguma A, Ono E, Bonini M, Zahid M, Marigowda G, et al. Exhaled breath condensate eicosanoid levels associate with asthma and its severity. J. Allergy Clin. Immunol. 2013;132:547–53.

144. Gilroy DW, Colville-Nash PR, McMaster S, Sawatzky DA, Willoughby DA, Lawrence T. Inducible cyclooxygenase-derived 15-deoxy(Delta)12-14PGJ2 brings

about acute inflammatory resolution in rat pleurisy by inducing neutrophil and macrophage apoptosis. FASEB J. Off. Publ. Fed. Am. Soc. Exp. Biol. 2003;17:2269–71.

145. Gilroy DW, Edin ML, Maeyer RPHD, Bystrom J, Newson J, Lih FB, et al. CYP450-derived oxylipins mediate inflammatory resolution. Proc. Natl. Acad. Sci. 2016;113:E3240–9.

146. Wallace JL, Vong L, McKnight W, Dicay M, Martin GR. Endogenous and exogenous hydrogen sulfide promotes resolution of colitis in rats. Gastroenterology. 2009;137:569–578, 578.e1.

147. Schingnitz U, Hartmann K, Macmanus CF, Eckle T, Zug S, Colgan SP, et al. Signaling through the A2B adenosine receptor dampens endotoxin-induced acute lung injury. J. Immunol. Baltim. Md 1950. 2010;184:5271–9.

148. Dalli J, Consalvo AP, Ray V, Filippo CD, D'Amico M, Mehta N, et al. Proresolving and Tissue-Protective Actions of Annexin A1–Based Cleavage-Resistant Peptides Are Mediated by Formyl Peptide Receptor 2/Lipoxin A4 Receptor. J. Immunol. 2013;190:6478–87.

149. Cash JL, Hart R, Russ A, Dixon JPC, Colledge WH, Doran J, et al. Synthetic chemerin-derived peptides suppress inflammation through ChemR23. J. Exp. Med. 2008;205:767–75.

150. Getting SJ, Gibbs L, Clark AJL, Flower RJ, Perretti M. POMC Gene-Derived Peptides Activate Melanocortin Type 3 Receptor on Murine Macrophages, Suppress Cytokine Release, and Inhibit Neutrophil Migration in Acute Experimental Inflammation. J. Immunol. 1999;162:7446–53.

151. Dufton N, Hannon R, Brancaleone V, Dalli J, Patel HB, Gray M, et al. Anti-Inflammatory Role of the Murine Formyl-Peptide Receptor 2: Ligand-Specific Effects on Leukocyte Responses and Experimental Inflammation. J. Immunol. Baltim. Md 1950. 2010;184:2611–9.

152. Levy BD, Lukacs NW, Berlin AA, Schmidt B, Guilford WJ, Serhan CN, et al. Lipoxin A4 stable analogs reduce allergic airway responses via mechanisms distinct from CysLT1 receptor antagonism. FASEB J. Off. Publ. Fed. Am. Soc. Exp. Biol. 2007;21:3877–84.

153. Gewirtz AT, Collier-Hyams LS, Young AN, Kucharzik T, Guilford WJ, Parkinson JF, et al. Lipoxin a4 analogs attenuate induction of intestinal epithelial proinflammatory gene expression and reduce the severity of dextran sodium sulfate-induced colitis. J. Immunol. Baltim. Md 1950. 2002;168:5260–7.

154. Spite M, Norling LV, Summers L, Yang R, Cooper D, Petasis NA, et al. Resolvin D2 is a potent regulator of leukocytes and controls microbial sepsis. Nature. 2009;461:1287–91.

155. Spite M, Norling LV, Summers L, Yang R, Cooper D, Petasis NA, et al. Resolvin D2 is a potent regulator of leukocytes and controls microbial sepsis. Nature. 2009;461:1287–91.

156. Xu Z-Z, Zhang L, Liu T, Park JY, Berta T, Yang R, et al. Resolvins RvE1 and RvD1 attenuate inflammatory pain via central and peripheral actions. Nat. Med. 2010;16:592–7.

157. Webb DR. Animal models of human disease: Inflammation. Biochem. Pharmacol. 2014;87:121–30.

158. Pound P, Ebrahim S, Sandercock P, Bracken MB, Roberts I. Where is the evidence that animal research benefits humans? BMJ. 2004;328:514–7.

159. Marshall JC. Why have clinical trials in sepsis failed? Trends Mol. Med. 2014;20:195–203.

160. Doeing DC, Borowicz JL, Crockett ET. Gender dimorphism in differential peripheral blood leukocyte counts in mice using cardiac, tail, foot, and saphenous vein puncture methods. BMC Clin. Pathol. 2003;3:3.

161. Eisenhauer PB, Lehrer RI. Mouse neutrophils lack defensins. Infect. Immun. 1992;60:3446–7.

162. Bogdan C. Nitric oxide and the immune response. Nat. Immunol. 2001;2:907–16.

163. Mestas J, Hughes CCW. Of Mice and Not Men: Differences between Mouse and Human Immunology. J. Immunol. 2004;172:2731–8.

164. Liu Z, Miner JJ, Yago T, Yao L, Lupu F, Xia L, et al. Differential regulation of human and murine P-selectin expression and function in vivo. J. Exp. Med. 2010;207:2975–87.

165. Seok J, Warren HS, Cuenca AG, Mindrinos MN, Baker HV, Xu W, et al. Genomic responses in mouse models poorly mimic human inflammatory diseases. Proc. Natl. Acad. Sci. 2013;110:3507–12.

166. Warren HS, Fitting C, Hoff E, Adib-Conquy M, Beasley-Topliffe L, Tesini B, et al. Resilience to Bacterial Infection: Difference between Species Could Be Due to Proteins in Serum. J. Infect. Dis. 2010;201:223–32.

167. Munford RS. Murine responses to endotoxin: another dirty little secret? J. Infect. Dis. 2010;201:175–7.

168. Hayday AC, Peakman M. The habitual, diverse and surmountable obstacles to human immunology research. Nat. Immunol. 2008;9:575–80.

169. van der Merwe R, Molfino NA. Challenge models to assess new therapies in chronic obstructive pulmonary disease. Int. J. Chron. Obstruct. Pulmon. Dis. 2012;7:597–605.

170. Calvano SE, Coyle SM. Experimental human endotoxemia: a model of the systemic inflammatory response syndrome? Surg. Infect. 2012;13:293–9.

171. Fiuza C, Suffredini AF. Human models of innate immunity: local and systemic inflammatory responses. J. Endotoxin Res. 2001;7:385–8.

172. Moed L, Shwayder TA, Chang MW. Cantharidin Revisited: A Blistering Defense of an Ancient Medicine. Arch. Dermatol. 2001;137:1357–60.

173. Bertaux B, Prost C, Heslan M, Dubertret L. Cantharide acantholysis: endogenous protease activation leading to desmosomal plaque dissolution. Br. J. Dermatol. 1988;118:157–65.

174. Funt TR, Mehr KA. Cantharidin: A Valuable Office Treatment of Molluscum Contagiosum. ET J. 1979;72.

175. Day RM, Harbord M, Forbes A, Segal AW. Cantharidin blisters: a technique for investigating leukocyte trafficking and cytokine production at sites of inflammation in humans. J. Immunol. Methods. 2001;257:213–20.

176. Morris T, Stables M, Hobbs A, de Souza P, Colville-Nash P, Warner T, et al. Effects of low-dose aspirin on acute inflammatory responses in humans. J. Immunol. 2009;183:2089–96.

177. Dinh PH, Corraza F, Mestdagh K, Kassengera Z, Doyen V, Michel O. Validation of the cantharidin-induced skin blister as an in vivo model of inflammation. Br. J. Clin. Pharmacol. 2011;72:912–20.

178. Evans BJ, Haskard DO, Finch JR, Hambleton IR, Landis RC, Taylor KM. The inflammatory effect of cardiopulmonary bypass on leukocyte extravasation in vivo. J. Thorac. Cardiovasc. Surg. 2008;135:999–1006.

179. Fiuza C, Salcedo M, Clemente G, Tellado JM. In vivo Neutrophil Dysfunction in Cirrhotic Patients with Advanced Liver Disease. J. Infect. Dis. 2000;182:526–33.

180. Dadfar E, Lundahl J, Jacobson SH. Granulocyte extravasation and recruitment to sites of interstitial inflammation in patients with renal failure. Am. J. Nephrol. 2004;24:330–9.

181. Senn H, Holland JF, Banerjee T. Kinetic and comparative studies on localized leukocyte mobilization in normal man. J. Lab. Clin. Med. 1969;74:742–56.

182. Mass MF, Dean PB, Weston WL, Humbert JR. Leukocyte migration in vivo: a new method of study. J. Lab. Clin. Med. 1975;86:1040–6.

183. Marks DJB, Radulovic M, McCartney S, Bloom S, Segal AW. Modified skin window technique for the extended characterisation of acute inflammation in humans. Inflamm. Res. Off. J. Eur. Histamine Res. Soc. Al. 2007;56:168–74.

184. Laser Doppler Monitoring and Imaging Theory [Internet]. [cited 2017 Mar 13]. Available from: https://gb.moor.co.uk/page/support-pages/theory/11

185. Essex TJ, Byrne PO. A laser Doppler scanner for imaging blood flow in skin. J. Biomed. Eng. 1991;13:189–94.

186. Saez AMO, Mosel F, Nürnberger J, Rushentsova U, Gössl M, Mitchell A, et al. Laser Doppler imager (LDI) scanner and intradermal injection for in vivo

pharmacology in human skin microcirculation: responses to acetylcholine, endothelin-1 and their repeatability. Br. J. Clin. Pharmacol. 2005;59:511–9.

187. Vukmanovic-Stejic M, Agius E, Booth N, Dunne PJ, Lacy KE, Reed JR, et al. The kinetics of CD4+Foxp3+ T cell accumulation during a human cutaneous antigen-specific memory response in vivo. J. Clin. Invest. 2008;118:3639–50.

188. MSD ELISA [Internet]. [cited 2017 Mar 14]. Available from: https://www.mesoscale.com/en/products/k15049d-1/

189. Iwanaga S. Biochemical principle of Limulus test for detecting bacterial endotoxins. Proc. Jpn. Acad. Ser. B Phys. Biol. Sci. 2007;83:110–9.

190. Wong J, Jeraj H, Vilar E, Viljoen A, Farrington K. Endotoxin detection in end-stage kidney disease. J. Clin. Pathol. 2015;68:73–8.

191. Abeles RD, McPhail MJ, Sowter D, Antoniades CG, Vergis N, Vijay GK, et al. CD14, CD16 and HLA-DR reliably identifies human monocytes and their subsets in the context of pathologically reduced HLA-DR expression by CD14(hi) /CD16(neg) monocytes: Expansion of CD14(hi) /CD16(pos) and contraction of CD14(lo) /CD16(pos) monocytes in acute liver failure. Cytom. Part J. Int. Soc. Anal. Cytol. 2012;81:823–34.

192. Tippett E, Cheng W-J, Westhorpe C, Cameron PU, Brew BJ, Lewin SR, et al. Differential Expression of CD163 on Monocyte Subsets in Healthy and HIV-1 Infected Individuals. PLOS ONE. 2011;6:e19968.

193. Dransfield I, Buckle AM, Savill JS, McDowall A, Haslett C, Hogg N. Neutrophil apoptosis is associated with a reduction in CD16 (Fc gamma RIII) expression. J. Immunol. 1994;153:1254–63.

194. Smith CW. Structure and Composition of Neutrophils, Eosinophils, and Basophils. In: Kaushansky K, Lichtman MA, Prchal JT, Levi MM, Press OW, Burns LJ, et al., editors. Williams Hematol. [Internet]. 9th ed. New York, NY: McGraw-Hill Education; 2015 [cited 2017 Mar 14]. Available from: accessmedicine.mhmedical.com/content.aspx?aid=1121095474

195. Zizzo G, Hilliard BA, Monestier M, Cohen PL. Efficient clearance of early apoptotic cells by human macrophages requires 'M2c' polarization and MerTK induction. J. Immunol. Baltim. Md 1950. 2012;189:3508–20.

196. Schaljo B, Kratochvill F, Gratz N, Sadzak I, Sauer I, Hammer M, et al. Tristetraprolin is required for full anti-inflammatory response of murine macrophages to IL-10. J. Immunol. Baltim. Md 1950. 2009;183:1197–206.

197. Fullerton JN, Gilroy DW. Resolution of inflammation: a new therapeutic frontier. Nat. Rev. Drug Discov. [Internet]. 2016 [cited 2016 Apr 27];advance online publication. Available from: http://www.nature.com/nrd/journal/vaop/ncurrent/full/nrd.2016.39.html

198. Bedner E, Halicka HD, Cheng W, Salomon T, Deptala A, Gorczyca W, et al. High affinity binding of fluorescein isothiocyanate to eosinophils detected by laser scanning cytometry: a potential source of error in analysis of blood samples utilizing fluorescein-conjugated reagents in flow cytometry. Cytometry. 1999;36:77–82.

199. Floyd H, Ni J, Cornish AL, Zeng Z, Liu D, Carter KC, et al. Siglec-8 A NOVEL EOSINOPHIL-SPECIFIC MEMBER OF THE IMMUNOGLOBULIN SUPERFAMILY. J. Biol. Chem. 2000;275:861–6.

200. Yamada T, Tani Y, Nakanishi H, Taguchi R, Arita M, Arai H. Eosinophils promote resolution of acute peritonitis by producing proresolving mediators in mice. FASEB J. Off. Publ. Fed. Am. Soc. Exp. Biol. 2011;25:561–8.

201. Gleich GJ, Frigas E, Loegering DA, Wassom DL, Steinmuller D. Cytotoxic Properties of the Eosinophil Major Basic Protein. J. Immunol. 1979;123:2925–7.

202. Fulkerson PC, Rothenberg ME. Targeting eosinophils in allergy, inflammation and beyond. Nat Rev Drug Discov. 2013;12:117–29.

203. Day RM, Harbord M, Forbes A, Segal AW. Cantharidin blisters: a technique for investigating leukocyte trafficking and cytokine production at sites of inflammation in humans. J. Immunol. Methods. 2001;257:213–20.

204. Maini AA, George MJ, Motwani MP, Day RM, Gilroy DW, O'Brien AJ. A Comparison of Human Neutrophils Acquired from Four Experimental Models of Inflammation. PLOS ONE. 2016;11:e0165502.

205. Smith AM, Rahman FZ, Hayee B, Graham SJ, Marks DJ, Sewell GW, et al. Disordered macrophage cytokine secretion underlies impaired acute inflammation and bacterial clearance in Crohn's disease. J. Exp. Med. 2009;206:1883–97.

206. Vukmanovic-Stejic M, Agius E, Booth N, Dunne PJ, Lacy KE, Reed JR, et al. The kinetics of CD4+Foxp3+ T cell accumulation during a human cutaneous antigen-specific memory response in vivo. J. Clin. Invest. 2008;118:3639–50.

207. Serhan CN, Brain SD, Buckley CD, Gilroy DW, Haslett C, O'Neill LA, et al. Resolution of inflammation: state of the art, definitions and terms. FASEB J. Off. Publ. Fed. Am. Soc. Exp. Biol. 2007;21:325–32.

208. Pillay J, Kamp VM, van Hoffen E, Visser T, Tak T, Lammers J-W, et al. A subset of neutrophils in human systemic inflammation inhibits T cell responses through Mac-1. J. Clin. Invest. 2012;122:327–36.

209. Pillay J, Tak T, Kamp VM, Koenderman L. Immune suppression by neutrophils and granulocytic myeloid-derived suppressor cells: similarities and differences. Cell. Mol. Life Sci. CMLS. 2013;70:3813–27.

210. Greenlee-Wacker MC. Clearance of apoptotic neutrophils and resolution of inflammation. Immunol. Rev. 2016;273:357–70.

211. Hall SE, Savill JS, Henson PM, Haslett C. Apoptotic neutrophils are phagocytosed by fibroblasts with participation of the fibroblast vitronectin receptor and involvement of a mannose/fucose-specific lectin. J. Immunol. Baltim. Md 1950. 1994;153:3218–27.

212. Mathias JR, Perrin BJ, Liu T-X, Kanki J, Look AT, Huttenlocher A. Resolution of inflammation by retrograde chemotaxis of neutrophils in transgenic zebrafish. J. Leukoc. Biol. 2006;80:1281–8.

213. Hampton HR, Bailey J, Tomura M, Brink R, Chtanova T. Microbe-dependent lymphatic migration of neutrophils modulates lymphocyte proliferation in lymph nodes. Nat. Commun. 2015;6:7139.

214. Ziegler-Heitbrock L, Ancuta P, Crowe S, Dalod M, Grau V, Hart DN, et al. Nomenclature of monocytes and dendritic cells in blood. Blood. 2010;116:e74-80.

215. Cros J, Cagnard N, Woollard K, Patey N, Zhang SY, Senechal B, et al. Human CD14dim monocytes patrol and sense nucleic acids and viruses via TLR7 and TLR8 receptors. Immunity. 2010;33:375–86.

216. Uderhardt S, Herrmann M, Oskolkova OV, Aschermann S, Bicker W, Ipseiz N, et al. 12/15-Lipoxygenase Orchestrates the Clearance of Apoptotic Cells and Maintains Immunologic Tolerance. Immunity. 2012;36:834–46.

217. Thurlings RM, Wijbrandts CA, Bennink RJ, Dohmen SE, Voermans C, Wouters D, et al. Monocyte scintigraphy in rheumatoid arthritis: the dynamics of monocyte migration in immune-mediated inflammatory disease. PloS One. 2009;4:e7865.

218. Kinser AM, Sands WA, Stone MH. Reliability and validity of a pressure algometer. J. Strength Cond. Res. 2009;23:312–4.

219. Serhan CN, Clish CB, Brannon J, Colgan SP, Chiang N, Gronert K. Novel Functional Sets of Lipid-Derived Mediators with Antiinflammatory Actions Generated from Omega-3 Fatty Acids via Cyclooxygenase 2–Nonsteroidal Antiinflammatory Drugs and Transcellular Processing. J. Exp. Med. 2000;192:1197–204.

220. Krishnamoorthy S, Recchiuti A, Chiang N, Yacoubian S, Lee CH, Yang R, et al. Resolvin D1 binds human phagocytes with evidence for proresolving receptors. Proc. Natl. Acad. Sci. U. S. A. 2010;107:1660–5.

221. Colas RA, Shinohara M, Dalli J, Chiang N, Serhan CN. Identification and signature profiles for pro-resolving and inflammatory lipid mediators in human tissue. Am. J. Physiol. Cell Physiol. 2014;307:C39-54.

222. Norling LV, Headland SE, Dalli J, Arnardottir HH, Haworth O, Jones HR, et al. Proresolving and cartilage-protective actions of resolvin D1 in inflammatory arthritis. JCI Insight. 1.

223. Planagumà A, Kazani S, Marigowda G, Haworth O, Mariani TJ, Israel E, et al. Airway lipoxin A4 generation and lipoxin A4 receptor expression are decreased in severe asthma. Am. J. Respir. Crit. Care Med. 2008;178:574–82.

224. Dalli J, Colas RA, Quintana C, Barragan-Bradford D, Hurwitz S, Levy BD, et al. Human Sepsis Eicosanoid and Proresolving Lipid Mediator Temporal Profiles: Correlations With Survival and Clinical Outcomes. Crit. Care Med. 2017;45:58–68.

225. Kubes P, Suzuki M, Granger DN. Nitric oxide: an endogenous modulator of leukocyte adhesion. Proc. Natl. Acad. Sci. U. S. A. 1991;88:4651–5.

226. Maekawa T, Hosur K, Abe T, Kantarci A, Ziogas A, Wang B, et al. Antagonistic effects of IL-17 and D-resolvins on endothelial Del-1 expression through a GSK-3β-C/EBPβ pathway. Nat. Commun. 2015;6:8272.

227. Song E, Jaishankar GB, Saleh H, Jithpratuck W, Sahni R, Krishnaswamy G. Chronic granulomatous disease: a review of the infectious and inflammatory complications. Clin. Mol. Allergy CMA. 2011;9:10.

228. Seki H, Fukunaga K, Arita M, Arai H, Nakanishi H, Taguchi R, et al. The Anti-Inflammatory and Proresolving Mediator Resolvin E1 Protects Mice from Bacterial Pneumonia and Acute Lung Injury. J. Immunol. Baltim. Md 1950. 2010;184:836–43.

229. Levy BD, Clish CB, Schmidt B, Gronert K, Serhan CN. Lipid mediator class switching during acute inflammation: signals in resolution. Nat. Immunol. 2001;2:612–9.

230. Homann J, Suo J, Schmidt M, Bruin N de, Scholich K, Geisslinger G, et al. In Vivo Availability of Pro-Resolving Lipid Mediators in Oxazolone Induced Dermal Inflammation in the Mouse. PLOS ONE. 2015;10:e0143141.

231. Norling LV, Spite M, Yang R, Flower RJ, Perretti M, Serhan CN. Humanized nano pro-resolving medicines mimic inflammation-resolution and enhance wound healing. J. Immunol. Baltim. Md 1950. 2011;186:5543–7.

232. Serhan CN, Chiang N. Resolution Phase Lipid Mediators of Inflammation: Agonists of Resolution. Curr. Opin. Pharmacol. 2013;13:632–40.

233. Chiang N, Rosa X de la, Libreros S, Serhan CN. Novel Resolvin D2 Receptor Axis in Infectious Inflammation. J. Immunol. 2016;1601650.

234. Gobbetti T, Coldewey SM, Chen J, McArthur S, le Faouder P, Cenac N, et al. Nonredundant protective properties of FPR2/ALX in polymicrobial murine sepsis. Proc. Natl. Acad. Sci. U. S. A. 2014;111:18685–90.

235. Mou H, Li Z, Kong Y, Deng B, Qian L, Wang JM, et al. Proinflammatory stimulants promote the expression of a promiscuous G protein-coupled receptor, mFPR2, in microvascular endothelial cells. Inflammation. 2012;35:656–64.

236. Herová M, Schmid M, Gemperle C, Hersberger M. ChemR23, the receptor for chemerin and resolvin E1, is expressed and functional on M1 but not on M2 macrophages. J. Immunol. Baltim. Md 1950. 2015;194:2330–7.

237. Dimitris Tousoulis A-MK. The Role of Nitric Oxide on Endothelial Function [Internet]. http://www.eurekaselect.com. [cited 2017 May 21]. Available from: http://www.eurekaselect.com/89263/article

238. Davignon J, Ganz P. Role of endothelial dysfunction in atherosclerosis. Circulation. 2004;109:III27-32.

239. Arita M, Bianchini F, Aliberti J, Sher A, Chiang N, Hong S, et al. Stereochemical assignment, antiinflammatory properties, and receptor for the omega-3 lipid mediator resolvin E1. J. Exp. Med. 2005;201:713–22.

240. Chiang N, Dalli J, Colas RA, Serhan CN. Identification of resolvin D2 receptor mediating resolution of infections and organ protection. J. Exp. Med. 2015;212:1203–17.

241. Mas E, Barden A, Burke V, Beilin LJ, Watts GF, Huang R-C, et al. A randomized controlled trial of the effects of n-3 fatty acids on resolvins in chronic kidney disease. Clin. Nutr. Edinb. Scotl. 2015;

242. Auven Therapeutics USA. Safety and Efficacy Study of RX-10045 on the Signs and Symptoms of Dry Eye. Clinical trial number: NCT00799552 [Internet]. Clin. Identifier NCT00799552. [cited 2017 Mar 6]. Available from: https://clinicaltrials.gov/show/NCT00799552

243. The Forsyth Insititute. Safety and Preliminary Efficacy of Lipoxin Analog BLXA4-ME Oral Rinse for the Treatment of Gingivitis (BLXA4). Clinical trial number NCT02342691 [Internet]. [cited 2017 Apr 20]. Available from: https://clinicaltrials.gov/ct2/show/NCT02342691

244. Morris T, Stables M, Colville-Nash P, Newson J, Bellingan G, de Souza PM, et al. Dichotomy in duration and severity of acute inflammatory responses in humans arising from differentially expressed proresolution pathways. Proc. Natl. Acad. Sci. U. S. A. 2010;107:8842–7.

245. Dalli J, Chiang N, Serhan CN. Elucidation of novel 13-series resolvins that increase with atorvastatin and clear infections. Nat. Med. 2015;21:1071–5.

246. Corbus Pharmaceutical, USA. Corbus Pharmaceutical Drug Pipeline [Internet]. [cited 2017 Apr 18]. Available from: http://www.corbuspharma.com/pipeline/overview

247. Zurier RB, Sun Y-P, George KL, Stebulis JA, Rossetti RG, Skulas A, et al. Ajulemic acid, a synthetic cannabinoid, increases formation of the endogenous proresolving and anti-inflammatory eicosanoid, lipoxin A4. FASEB J. Off. Publ. Fed. Am. Soc. Exp. Biol. 2009;23:1503–9.

248. Tracey Bonfield, Tepper, Mark. RESUNAB, A CB2 AGONIST FOR THE TREATMENT OF CF, Abstract 194. Poster Number 194 Pediatr. Pulmonol. [Internet]. 2015 [cited 2017 Mar 6]. p. S193–453. Available from: http://onlinelibrary.wiley.com/doi/10.1002/ppul.23297/abstract

249. Pinto AT, Pinto ML, Cardoso AP, Monteiro C, Pinto MT, Maia AF, et al. Ionizing radiation modulates human macrophages towards a pro-inflammatory phenotype preserving their pro-invasive and pro-angiogenic capacities. Sci. Rep. 2016;6:18765.

250. Martinez FO, Sica A, Mantovani A, Locati M. Macrophage activation and polarization. Front. Biosci. 2008;13:453–61.

251. Wong J, Jeraj H, Vilar E, Viljoen A, Farrington K. Endotoxin detection in end-stage kidney disease. J. Clin. Pathol. 2015;68:73–8.

252. Pepys MB, Hirschfield GM. C-reactive protein: a critical update. J. Clin. Invest. 2003;111:1805–12.

253. Stebulis JA, Johnson DR, Rossetti RG, Burstein SH, Zurier RB. Ajulemic acid, a synthetic cannabinoid acid, induces an antiinflammatory profile of eicosanoids in human synovial cells. Life Sci. 2008;83:666–70.

254. Weylandt KH, Krause LF, Gomolka B, Chiu C-Y, Bilal S, Nadolny A, et al. Suppressed liver tumorigenesis in fat-1 mice with elevated omega-3 fatty acids is associated with increased omega-3 derived lipid mediators and reduced TNF-α. Carcinogenesis. 2011;32:897–903.

255. Brancaleone V, Gobbetti T, Cenac N, Faouder P le, Colom B, Flower RJ, et al. A vasculo-protective circuit centered on lipoxin A_4 and aspirin-triggered 15-epi-lipoxin A_4 operative in murine microcirculation. Blood. 2013;122:608–17.

256. Camp RD, Coutts AA, Greaves MW, Kay AB, Walport MJ. Responses of human skin to intradermal injection of leukotrienes C4, D4 and B4. Br. J. Pharmacol. 1983;80:497–502.

257. Neuschäfer-Rube F, Pathe-Neuschäfer-Rube A, Hippenstiel S, Kracht M, Püschel GP. NF-κB-dependent IL-8 induction by prostaglandin E(2) receptors EP(1) and EP(4). Br. J. Pharmacol. 2013;168:704–17.

258. Wallace AE, Sales KJ, Catalano RD, Anderson RA, Williams ARW, Wilson MR, et al. Prostaglandin F2α-F-Prostanoid Receptor Signaling Promotes Neutrophil Chemotaxis via Chemokine (C-X-C Motif) Ligand 1 in Endometrial Adenocarcinoma. Cancer Res. 2009;69:5726–33.

259. Liu J, Li H, Burstein SH, Zurier RB, Chen JD. Activation and binding of peroxisome proliferator-activated receptor gamma by synthetic cannabinoid ajulemic acid. Mol. Pharmacol. 2003;63:983–92.

260. Ribeiro RA, Cunha FQ, Ferreira SH. Recombinant gamma interferon causes neutrophil migration mediated by the release of a macrophage neutrophil chemotactic factor. Int. J. Exp. Pathol. 1990;71:717–25.

261. Murata T, Aritake K, Tsubosaka Y, Maruyama T, Nakagawa T, Hori M, et al. Anti-inflammatory role of PGD2 in acute lung inflammation and therapeutic application of its signal enhancement. Proc. Natl. Acad. Sci. U. S. A. 2013;110:5205–10.

262. Sarashina H, Tsubosaka Y, Omori K, Aritake K, Nakagawa T, Hori M, et al. Opposing immunomodulatory roles of prostaglandin D2 during the progression of skin inflammation. J. Immunol. Baltim. Md 1950. 2014;192:459–65.

263. Napimoga MH, Vieira SM, Dal-Secco D, Freitas A, Souto FO, Mestriner FL, et al. Peroxisome proliferator-activated receptor-gamma ligand, 15-deoxy-Delta12,14-prostaglandin J2, reduces neutrophil migration via a nitric oxide pathway. J. Immunol. Baltim. Md 1950. 2008;180:609–17.

264. Gonzalez EG, Selvi E, Balistreri E, Akhmetshina A, Palumbo K, Lorenzini S, et al. Synthetic cannabinoid ajulemic acid exerts potent antifibrotic effects in experimental models of systemic sclerosis. Ann. Rheum. Dis. 2012;annrheumdis-2011-200314.

265. Zurier RB, Rossetti RG, Burstein SH, Bidinger B. Suppression of human monocyte interleukin-1β production by ajulemic acid, a nonpsychoactive cannabinoid. Biochem. Pharmacol. 2003;65:649–55.

266. Gasperi V, Evangelista D, Chiurchiù V, Florenzano F, Savini I, Oddi S, et al. 2-Arachidonoylglycerol modulates human endothelial cell/leukocyte interactions by controlling selectin expression through CB1 and CB2 receptors. Int. J. Biochem. Cell Biol. 2014;51:79–88.

267. Findlay L, Sharp G, Fox B, Ball C, Robinson CJ, Bird C, et al. Endothelial cells co-stimulate peripheral blood mononuclear cell responses to monoclonal antibody TGN1412 in culture. Cytokine. 2011;55:141–51.

268. Polikandriotis JA, Mazzella LJ, Rupnow HL, Hart CM. Peroxisome proliferator-activated receptor gamma ligands stimulate endothelial nitric oxide production through distinct peroxisome proliferator-activated receptor gamma-dependent mechanisms. Arterioscler. Thromb. Vasc. Biol. 2005;25:1810–6.

269. Gomes RN, Teixeira-Cunha MGA, Figueiredo RT, Almeida PE, Alves SC, Bozza PT, et al. BACTERIAL CLEARANCE IN SEPTIC MICE IS MODULATED BY MCP-1/CCL2 AND NITRIC OXIDE. Shock Augusta Ga. 2013;39:63–9.

270. Szalai AJ, Briles DE, Volanakis JE. Human C-reactive protein is protective against fatal Streptococcus pneumoniae infection in transgenic mice. J. Immunol. 1995;155:2557–63.

271. Rostaing L, Malvezzi P. Steroid-Based Therapy and Risk of Infectious Complications. PLOS Med. 2016;13:e1002025.

272. Dajani EZ, Larsen KR, Taylor J, Dajani NE, Shahwan TG, Neeleman SD, et al. 1',1'-Dimethylheptyl-Δ-8-tetrahydrocannabinol-11-oic Acid: A Novel, Orally Effective Cannabinoid with Analgesic and Anti-inflammatory Properties. J. Pharmacol. Exp. Ther. 1999;291:31–8.

273. Press Release Corbus Pharmaceuticals, November 2016. Corbus Pharmaceuticals Reports Positive Topline Results Showing Clear Signal of Clinical Benefit with Resunab (JBT-101) in Phase 2 Study in Systemic Sclerosis [Internet]. [cited 2017 Apr 20].

Available from: http://www.corbuspharma.com/news/press-releases/detail/221/corbus-pharmaceuticals-reports-positive-topline-results

274. Press Release Corbus Pharmaceuticals, March 2017. Corbus Pharmaceuticals Reports Positive Topline Data Demonstrating Anabasum Reduces Acute Pulmonary Exacerbations and Multiple Inflammatory Biomarkers in Phase 2 Study in Patients with Cystic Fibrosis [Internet]. Available from: http://www.corbuspharma.com/news/press-releases/detail/233/corbus-pharmaceuticals-reports-positive-topline-data

275. Rossi AG, Sawatzky DA, Walker A, Ward C, Sheldrake TA, Riley NA, et al. Cyclin-dependent kinase inhibitors enhance the resolution of inflammation by promoting inflammatory cell apoptosis. Nat. Med. 2006;12:1056–64.

276. Endres S, Caterina RD, Schmidt EB, Kristensenj SD. n-3 Polyunsaturated fatty acids: update 1995. Eur. J. Clin. Invest. 1995;25:629–38.

277. Barden A, Mas E, Croft KD, Phillips M, Mori TA. Short-term n-3 fatty acid supplementation but not aspirin increases plasma proresolving mediators of inflammation. J. Lipid Res. 2014;55:2401–7.

278. Barden AE, Moghaddami M, Mas E, Phillips M, Cleland LG, Mori TA. Specialised pro-resolving mediators of inflammation in inflammatory arthritis. Prostaglandins Leukot. Essent. Fatty Acids. 2016;107:24–9.

279. Mas E, Barden A, Burke V, Beilin LJ, Watts GF, Huang R-C, et al. A randomized controlled trial of the effects of n-3 fatty acids on resolvins in chronic kidney disease. Clin. Nutr. 2016;35:331–6.

280. Skarke C, Alamuddin N, Lawson JA, Li X, Ferguson JF, Reilly MP, et al. Bioactive products formed in humans from fish oils. J. Lipid Res. 2015;56:1808–20.

281. Fischer R, Konkel A, Mehling H, Blossey K, Gapelyuk A, Wessel N, et al. Dietary omega-3 fatty acids modulate the eicosanoid profile in man primarily via the CYP-epoxygenase pathway. J. Lipid Res. 2014;55:1150–64.

282. Murphy RC. Specialized pro-resolving mediators: do they circulate in plasma?1. J. Lipid Res. 2015;56:1641–2.

283. Serhan CN, Sheppard KA. Lipoxin formation during human neutrophil-platelet interactions. Evidence for the transformation of leukotriene A4 by platelet 12-lipoxygenase in vitro. J. Clin. Invest. 1990;85:772–80.

284. Serhan CN, Clish CB, Brannon J, Colgan SP, Chiang N, Gronert K. Novel Functional Sets of Lipid-Derived Mediators with Antiinflammatory Actions Generated from Omega-3 Fatty Acids via Cyclooxygenase 2–Nonsteroidal Antiinflammatory Drugs and Transcellular Processing. J. Exp. Med. 2000;192:1197–204.

285. Bannenberg G, Moussignac RL, Gronert K, Devchand PR, Schmidt BA, Guilford WJ, et al. Lipoxins and novel 15-epi-lipoxin analogs display potent anti-inflammatory actions after oral administration. Br. J. Pharmacol. 2004;143:43–52.

286. Orr SK, Colas RA, Dalli J, Chiang N, Serhan CN. Proresolving actions of a new resolvin D1 analog mimetic qualifies as an immunoresolvent. Am. J. Physiol. - Lung Cell. Mol. Physiol. 2015;308:L904–11.